DOCTORAL THESIS

MACHINE LEARNING-AIDED DESIGN METHODOLOGY FOR A MARS HABITATION

by Gokhan Dede

POLITECNICO MILANO

POLITECNICO DI MILANO

Department of Architecture, Built Environment, and Construction Engineering

Doctoral Programme In 2023

Machine Learning-Aided Generative Design Methodology for A Mars Habitation

By

Gokhan Dede

Student Number: 948469

35th Cycle

B.Sc. in Architecture

Izmir Institute of Technology, 2014

M.Sc. in Construction and Project Management

Mimar Sinan Fine Arts University, 2018

Submitted to the Department of ABC

in Fulfillment of the Requirements for the Degree of

Doctor of Philosophy in Architecture

at the Politecnico di Milano

Dissertation Committee

Supervisor: Massimiliano Nastri
Associate Professor of Architectural Technology
Politecnico di Milano

Co-Supervisor: Ingrid Maria Paoletti
Associate Professor of Architectural Technology
Politecnico di Milano

Tutor: Paola Caputo
Associate Professor of Building Physics and Building Energy Systems
Politecnico di Milano

Coordinator: Marco Scaioni
The Chair of the Doctoral Program
Professor of Surveying and Mapping
Politecnico di Milano

Acknowledgments

"This dissertation is dedicated to my wife, Esra, as well as my mother and father, Hatice and Abdullah, and my sisters, Perihan and Reyhan."

To begin, I would like to express my gratitude to the ABC Department at Politecnico di Milano for providing me with the chance and support I needed. I sincerely thank the Chair of the Doctoral Program, Professor Marco Scaioni, for supporting me and chairing my thesis committee.

In particular, I would like to express my sincere gratitude to my supervisor, Professor Massimiliano Nastri, for his guidance and unconditional support. Under his supervision, I had as much freedom as I desired, but he was always available for discussion and, when necessary, for bringing me back on track from my constant wandering among disparate research topics.

The first idea for this thesis work came from my co-supervisor, Professor Ingrid Paoletti, the founder of Material Balance Research Lab, who allowed me to join her research group and supported my innovative research efforts.

Also, I would like to express my deepest gratitude to my tutor, Professor Paola Caputo, for her constructive support throughout the process and for mentoring me both as a student and colleague.

I am particularly grateful for the incisive evaluations and suggestions of Profs. Nerantzia (Julia) Tzortzi, Poli Tiziana, and Salvalai Graziano. Without a doubt, I could not complete my research studies without their instructive comments. Lastly, I would like to express my gratitude to Turkey's Ministry of National Education for encouraging and assisting me throughout the research.

Sincere gratitude for everything!

Gokhan

Machine Learning-Aided Generative Design Methodology for A Mars Habitation

By

Gokhan Dede

Submitted to the Department of ABC in Politecnico di Milano

in Fulfillment of the Requirements for

the Doctor of Philosophy in Architecture

Abstract

A Novel Design Strategy for a Self-generated Mars Habitation

"A research of advanced design methodology paved the foundation for the long-term Mars exploration."

NASA has prioritized sending robots and vehicles to Mars to research the natural characteristics of the Martian environment since the 1960s, with plans to send humans to Mars by 2040 after conducting a mission to the Moon. How architects, engineers, and other professionals will assist humanity in adapting to these dynamic and unpredictable surroundings is crucial for ensuring human habitability in such severe situations.

With research into the severe environments of the Moon and Mars, humanity may be able to prepare for and address future environmental concerns on Earth. It also highlights how architecture may adapt to hostile settings where people cannot exist. NASA and other universities have been developing various Mars analog simulations in preparation for a future mission. These simulations evaluate astronauts' and developed systems' habitability performance to aid humans in surviving in the hostile Martian environment.

The thesis provides a systematic design approach for developing habitation concepts that can be realized in remote places when construction materials cannot be transported to the site.

The research study theorized that merging generative design approaches with augmented intelligent algorithms is necessary to execute a design and construction process autonomously, overcoming distance limits, communication delays, and harsh environmental circumstances. A novel methodology for designing habitations for extreme environments was developed to give a strong foundation for this idea.

Initially, the historical context of Mars explorations was established to depict humanity's future vision and provide an overview of the chronological history of Mars investigations to identify the public and private visionaries' desired exploration milestones.

Following that, a detailed assessment of the findings of the exploration missions was conducted to analyze Mars' environmental conditions and establish an appropriate background for a crewed Mars exploration mission. The defined environmental forces were evaluated to transform them into habitation design parameters. In addition, potential landing sites for a crewed Mars mission were analyzed to give a comparative analysis highlighting the benefits and hazards of each site. In addition, the results of three distinct landing site selection methodologies were combined to determine the optimal landing site for a future Mars mission.

After extensive evaluations of the Mars environment and potential landing sites, attempts were made to define habitability and human factors by adopting graph-data science approaches to analyze Mars analog missions' habitation projects. Illustrating the findings was a direction for the designer's future research.

Habitation technologies and advancement studies were provided to establish the design criteria for a fully operational and sustainable Mars surface habitation. In addition, the winning Mars habitation designs for NASA's 3-D Printed Habitat Challenge were examined to identify the design requirements and technologies required to construct a Mars habitat.

After defining design criteria, human considerations, and environmental conditions on Mars, a novel design process was developed to address each design problem for Mars habitation. The tools and approaches to defining the novel design methodology based on autonomous processes were established and extensively addressed. As a subsequent step, the established design methodology was applied to three habitation projects to evaluate its viability and validity.

The conclusion of the dissertation includes an explanation of the dissertation's contributions to the literature and questions for future research. For the purpose of evaluating the thesis's results, the future applications and implications of architectural design approaches are examined critically.

Keywords

Mars; Extreme Environment Habitation; Generative Design; Parametric Analysis; Artificial Intelligence

List Of Figures

List Of Tables

Table of Contents

01st Chapter
INTRODUCTION TO A NOUEL DESIGN METHODOLOGY

The introductory chapter examines briefly the motivations for space exploration and the space agencies' future vision of human colonization of Mars. The chapter subsequently summarizes the necessary technology advancements as a problem statement for developing a surface habitation system and describes the research objectives. Lastly, the chapter outlines the structure of the thesis, which is defined in order to identify a solution to the presented problem.

1.1. Research Context and Problem Statement

Researchers revealed that extreme environments would emerge in unexpected places due to global warming and environmental problems (Masson-Delmotte, V., P. Zhai, A. Pirani, et al., 2021). While extreme environments have already occurred on Earth, other environments will also experience extreme climate situations resulting from climate change. Since the 1960s, space organizations have been attempting to discover other planets to teach about planetary science, comprehend the nature of climate change, and predict Earth's evolution. For example, according to Wordsworth (R. Wordsworth et al., 2015; R. D. Wordsworth, 2016) and Forget (Forget, 2009), Munderwent a dramatic transformation during Martian evolution. According to Milliken et al. (Milliken et al., 2010), some data suggest that Mars has experienced periods of drastic climate change during its evolutionary history. Mars has geological features that make us think that liquid water flowed on Mars once. Even recent research studies have confirmed the presence of underground water. Following the announcement of incentive explorations, as part of the Artemis program, NASA and its partners scheduled robot and human missions to the Moon in the 2020s to ensure safer human missions to Mars, even in the 2030s (Dunbar, 2021b).

These technologically mediated explorations of the Moon and Mars have given humanity tremendous knowledge. Mars once had liquid oceans and a much denser atmosphere (Potter, 2018). Given what we know about Mars today, the planet could have held the keystones for the existence of life forms. However, according to the data, something happened to the planet, and it is uninhabitable for life. We are unsure if Mars ever held life and if life has arisen outside the safe environment of Earth, but given how we know the simplest forms of life can come to exist (Lazcano & Bada, 2008), Mars should at one time have had all the ingredients for life (Potter, 2018).

Nevertheless, other, and maybe more relevant, questions could lead to knowledge of grave importance for the future of humanity. Questions such as whether there was ever life on Mars, and if so,

what happened for the planet to turn dead, when it happened, what can we learn from it, and will the same thing happen to the Earth? Some of these questions are what NASA and other space agencies aim to answer, but human intuition is needed in-situ to do so thoroughly and within a short timeframe.

However, what could compel any human being to leave its breathable atmosphere and life-giving environment on Earth, place itself in a small spacecraft, travel almost 60 million kilometers, and then live in a slightly bigger enclosed habitat on Mars in an environment that - if the habitat's technology fails - will destroy every cell in the human body. Another consideration is the voyage's total duration of 3 years. Several factors could be the deciding ones. One reason for popular belief is to find the answer to the question, "Are we alone?" hence, is there or has there been life, maybe even intelligent life, on Mars? However, not the only reason for traveling to Mars, and those brave men and women who will encompass the voyage could, if history will have it, in the future, be seen as pioneers much like the Conquistadors of Spain or the Vikings of Scandinavia.

The beginning steps are always time and resource-consuming, and a mission to Mars is no exception. It could potentially be the most expensive venture in the history of civilization, but at the same time, it could have the most incredible feedback on the civilization of all time. We have several examples of everyday objects: direct derivatives of space exploration (Bogdahn et al., 2019), battery-powered tools (power tools), or battery power. While NASA did not invent this technology, it helped advance development immensely. Without this necessity for the specific technology, the industry, and society as we know it, might not have advanced to the point we are today, as the battery technology probably would not have advanced as far as it has. The first crewed exploration mission to Mars could pave the way for making a permanent colony and maybe even expand or renew our civilization in an otherwise hostile environment; Mars. The success of the first missions to Mars is crucial to ensure the possible future of a colonized Mars. The science learned, the archaeological and geologic history uncovered, the experiments performed, and the technological spinoffs to civilization on Earth from the technologies developed to facilitate missions to Mars could have life-changing implications. Today approximately 2000 NASA technologies have contributed to all aspects of civilization (NASA, 2021d). With a mission or several to Mars, new technologies will undoubtedly evolve. Humanity must create an entire system that can sustain life in an alien and dangerous environment. Advances in robotics, rocketry, and habitation will be required to perform a mission such as the one to Mars.

Exploring a design and construction methodology to develop an inhabitable space with a habitation concept is required for future human developments to adapt to the most extreme conditions, such as Moon and Mars, and existing and future extreme locations on Earth.

1.2. Research Motivation

The research is established at the intersection of three technical innovations that contribute to the stimulation of novel architectural design implementations and the work presented in the thesis:

1. Environmental Design | Modern buildings are expected to perform efficiently regarding the health and well-being of their tenants and the surrounding conditions. Designers are better at understanding and designing for human requirements thanks to the collection and use of data. As a result, the methodology should incorporate these concerns into the workflow. Because structures contribute considerable global carbon emissions, the performance-driven design methodology is also driven by the recognition that buildings influence the environment. Future architecture must be designed to reduce its influence on the environment by incorporating low operational energy, efficient use of materials, durability, and resiliency, among other goals. Although in addition to what can be measured or simulated, design professionals consider a broader, more holistic set of design implications and results.

2. Performance-driven Design | Architects and engineers have used computers in the design phase for years. More and more design professionals, including architects, are becoming aware of the usage of performance simulations. Researchers have devised novel approaches to handle massive datasets associated with architectural design and construction, including incorporating geometry straight from modeling environments into validated simulation engines. Many firms also look for parametric design, coding, and simulation skills. It is open to discussing whether all simulated data can be used successfully for guidance or why one design is better than all other conceptual alternatives. In what ways may simulation be utilized to explore these possibilities?

3. Artificial Intelligence | Machine learning and artificial intelligence (AI) have recently proven a remarkable ability to find patterns and trends that may be used to benefit humans. Applying these approaches to forecasting outcomes and assisting decision-making has sparked revolutions across various professions. It is possible to analyze these theoretical datasets using parametric design and associated approaches that automatically create design choices with numerical representations and immediately simulatable performance, notably through interactive optimization.

At the intersection of these three knowledge areas, a representation of a potential novel design process that may be implemented without the assistance of humans may be established. Eventually, using the emerging novel methodology for the needed Mars habitation model may guide future habitation design research in space architecture.

1.3. Research Questions and Objectives

The intersection of emerging environmental and performance-driven design methodologies and artificial intelligence generates two essential research questions.

"How can architects identify, acquire, and utilize environmental data, such as that revealed by Mars missions, to manage overlapping quantitative objectives in a computational design process? How can architects transform a data-driven process into a data-driven, autonomous computational design methodology to develop a Mars habitation that can resist the severe climate of the planet?"

It is a multidisciplinary research area that necessitates a comprehensive examination of the design process and the required data as design parameters. This dissertation's context chapters include a review of space missions, revealed environmental data of Mars, analog investigations for Mars to understand human factors under extreme conditions of a Mars mission and habitation technologies, and advanced habitation design practices to provide design data for space exploration literature. In the scope of architectural design literature, this dissertation's methodology chapter discusses performance-based and data-driven design methodologies and conceptual mapping of conventional parametric processes. It also contains a discussion of research objectives directly related to advances in Artificial Intelligence and contemporary computational design approaches. The subsequent chapters raise and respond to more particular questions regarding space formulation, form-finding, interactive optimization, diversity-driven design, and efficient digital design environments.

The main objective of this dissertation is to develop methodological approaches that lead to a high-performing habitation concept in the extreme conditions of the Mars environment, while still being responsive to human-based design requirements and defined data, and simulated through an organic creative process involving collaboration between environmental data and computers. It is more concerned with comparative design decisions at an early stage than with absolute measurements or benchmark comparisons of other alternatives. The dissertation focuses on navigation design decisions that interact in meaningful ways, especially evaluating performance measurements affected by international geometries in the following chapters.

The another objective of the dissertation is to direct space architects to use the quantitative methodologies described in the dissertation or develop new ones based on those described in the dissertation to create new forms of habitation based on planetary data, insights derived from previously designed Mars habitation proposals, and human-centered requirements derived from analog missions designed following NASA's standards. Yet, it is probable that some designers will employ these methodologies to modify form-driven architecture, resulting in relative efficiency improvements and heightened design knowledge of the consequences of their decisions. This dissertation examines how designers should analyze the process of designing an extraterrestrial habitation and the conceptual

possibilities within all parametric datasets, and how they respond when quantitative information leads or pushes them toward specific design realms.

1.4. Organization of Dissertation

The dissertation consists of eight chapters. The problem statement and research topic that motivates the subsequent chapters are introduced in the first chapter.

The second chapter presents a complete literature study of past and present space exploration missions and efforts to outline technological advancements in space explorations. The historical review of Mars explorations aimed to outline humanity's future goals and provide a broad overview of the Mars expeditions' chronological history to identify the upcoming exploration milestones that both public and private visionaries had set as their goals.

The environment of Mars is the topic of discussion in the third chapter, which focuses on the findings of many planetary exploration missions. For each environmental component that serves as a design parameter for the Mars settings, specific instructions are supplied for simulating that component. This chapter discusses three distinct strategies for identifying the criteria for selecting a landing and research site on the surface of Mars for a future crewed expedition. These strategies aim to determine where humans might land and conduct research.

In the fourth chapter, habitability, and human factors were determined by employing graph-data science approaches to examine habitation projects for Mars analog missions after thorough evaluations of the Martian environment and the conditions of potential landing locations. The results were illustrated to provide the designer with a visual reference for future research.

The fifth chapter outlined the prerequisites for a fully functional and sustainable surface habitat design for a Mars mission, together with the latest research on habitat technologies. Furthermore, the winning projects of NASA's 3-D Printed Habitat Challenge were analyzed to evaluate the design requirements and construction technologies needed to develop a habitation on Mars.

The sixth chapter attempts to develop a new habitation design approach by integrating Social Network Analysis (SNA) measurements and the Label Propagation Approach (LPA) into the generative design process. The novel design process was developed to address each design problem for a Mars habitat after the needs for such a habitat were defined, together with the human factors involved and the Martian environment.

The seventh chapter presents design implementations of the developed machine learning-assisted generative design approach and the outcomes of three design projects completed to show the effects of Mars's environmental conditions on a habitation shell.

The eighth chapter contains a summary of contributions, an assessment and impact analysis, a discussion of future research, and concluding remarks.

02 nd Chapter
THE MISSION TO EXPLORE MARS: A Space-Resilient Habitat

In the second chapter, a critical literature analysis addresses the research activities presented in this dissertation within the perspective of previous Mars missions and space agency aspirations for the future. In order to better understand the necessity for a new habitation architecture for crewed Mars missions, this section explores the technical advancements of Mars missions over the past decades.

2.1. Mars Observations: The Origins and Historical Relevance

Humanity has a documented history of observing the planet Mars' activities dating back to the Ancient Egyptians around 2000 B.C. (NASA, 2021c). Mars has been associated with Roman and Greek mythology as the god of battle, Mars in Roman mythology, and Ares in Greek mythology. Mars could only be seen as a red dot, appearing more significant than the stars in the sky, until the invention of the telescope, and that is what inspired the Egyptian name 'Her Desher,' which translates as 'the red one or 'the red planet' in common usage.

Mars was a mystery to ancient astronomers, who were confused by its seemingly arbitrary movement across the sky—sometimes in the same direction as the Sun and other celestial objects (direct, or prograde, motion), and occasionally in the opposite way (Belton, Michael J.S., Malin, Michael C., and Carr, Michael H., 2022). In 1609, Johannes Kepler utilized his Danish colleague Tycho Brahe's better naked-eye observations of the planet to empirically establish its laws of motion, paving the path for the contemporary gravitational theory of the Solar system (Myers & Myers, 2006). Kepler discovered that Mars' orbit was an ellipse along which the planet moved in an unpredictable yet nonuniform manner (Myers & Myers, 2006).

Galileo, an Italian astronomer, made the first telescopic views of Mars in 1610 (van Helden, 1994). Although Galileo's modest telescope could only see the planet's reddish-orange disk in 1609 (van Helden, 1994), larger telescopes steadily revealed more details. Galileo stated in 1610 that Mars had a gibbous phase, which observers confirmed—first reported in 1659 by Christiaan Huygens, whose chart showed a dark speck, possibly Syrtis Major (Tanaka et al., 2019). Detecting surface albedo marks allowed astronomers to calculate Mars' rotation period. Giovanni Cassini noted the dazzling polar caps in 1666. Visual observers produced several important discoveries. Huygens detected the planet's rotation in 1659, and Cassini timed it in 1666 at 24 hours 40 minutes, 3 minutes off (van Helden, 1994). Giacomo Maraldi,

Cassini's nephew, observed the polar caps during numerous favorable oppositions, including 1719 (P. Moore, 1997).

Sir William Herschel examined Mars from 1777 to 1783 and was the first to discover that its rotation axis was inclined 30° from perpendicular to its orbit (N. Barlow, 2014). This research proved that Mars had four seasons like Earth. Herschel also found the planet's rotation period to be 24 hours 39 minutes 21.67 seconds. Herschel concluded that a thin atmosphere surrounding Mars was based on variations in the planet's appearance, which he ascribed to clouds (N. Barlow, 2014). These were the white clouds, now known to contain ice particles. Honoré Flaugergues noted the yellow dust clouds in 1809 (N. Barlow, 2014).

In 1830, significant developments in Mars research occurred during Mars' closest approach to Earth. Johan von Mädler and Wilhelm Beer released the first complete map of Mars in 1840, based on observations made during this period, with the zero longitude line indicated by a small, extremely dark point (N. Barlow, 2014). Mars' rotation is now 24 hours 37 minutes 22.6 seconds (with 0.1 seconds of the currently accepted value) (N. Barlow, 2014). Richard Proctor (1867), Nicolas Flammarion (1876), and E.M. Antoniadi (1876) all drew maps of Mars between 1830 and the early twentieth century (between 1901 and 1930) (N. Barlow, 2014). While Proctor and Flammarion identified features on their maps, the current nomenclature scheme for martian features is based on Giovanni Schiaparelli's 1877 map proposal (N. Barlow, 2014).

There were many unexpected discoveries in 1877 since Mars was so close to Earth. Asaph Hall discovered Mars' two minor moons, Phobos and Deimos (English, 2018). Nathaniel Green discovered high-altitude clouds as white dots on the planet's morning and evening limbs, and M. Gould attempted to picture it first this year (D. Strauss, 1997). However, Schiaparelli's discoveries of thin black lines traversing the Martian surface, which he dubbed Canali, drew much attention to Mars for many years to come (D. Strauss, 1997). It is unclear where Schiaparelli saw thin black streaks traversing the Martian surface. So he called these traits “channels.” A channel is a natural feature created by liquid/ice movement, tectonics, or wind (D. Strauss, 1997). The Italian term for a channel is “canali,” which has been mistranslated into English as “canal,” which indicates a human-made watercourse.

The finding of these “canali” on Mars just strengthened existing evidence for life on Mars (N. Barlow, 2014). Mars has several Earth-like properties that have been recognized since the eighteenth century. Mars has a rotating period 37 minutes longer than Earth's and, like Earth, has four seasons due to the tilt of its spin axis (N. Barlow, 2014). Polar caps and an atmosphere were visible, but their compositions remained unknown. The “wave of darkening” was an intriguing observation of hypothetical Martian life (N. Barlow, 2014). A telescopic study found that when one hemisphere's polar cap retreated in the spring, the area around it got darker (N. Barlow, 2014). The darkening expanded toward the equator

as the arctic cap receded during summer. After summer, the "wave of darkening" reversed, and a "wave of brightening" was observed from the equator to the poles. Most observers associated the wave of darkening with the polar caps melting water ice and the surface plants absorbing this water (N. Barlow, 2014).

Schiaparelli's “canali” were readily recognized as proof of Martian vegetation and intelligent life. Percival Lowell constructed the Lowell Observatory in Flagstaff, AZ, in 1894 to explore martian canals. Lowell spotted hundreds of single and double canals using the Observatory's 0.6-m Clark refracting telescope and published numerous books on their formation (Schindler, 2016). Lowell claims that ancient Mars had a thicker atmosphere, allowing for more moderate temperatures on the surface, including liquid water. In these conditions, Martians arose and colonized the entire planet. Because Mars is only 52% the size of Earth, the atmosphere began to escape into space, cooling the surface and decreasing liquid water availability (N. Barlow, 2014). The Martians went to the planet's warm equatorial zone and built a complex network of canals to convey water from the arctic regions to the equator's parched masses. Lowell claimed that the dark lines he saw were vegetation around the canals because Earth-based telescopes could not discern the canals themselves (N. Barlow, 2014). As a result of this conversation, several science fictions works about Martians have been written (e.g., The Martian Chronicles and The War of the Worlds).

Most astronomers, however, doubted the existence of Martian canals. Larger telescopes revealed black blotches on the surface rather than dark lines. The linear canals were thought to be optical illusions generated by the human mind “connecting the dots” while looking with a telescope. The turbulent atmospheres of both Earth and Mars worsen these situations. Spacecraft research allowed astronomers to conclusively prove that there are no canals on Mars and that the “wave of darkening” is caused by seasonal winds moving dust and sand across the planet.

In recent years, telescope size and technological advancement have improved astronomical observations' quality and type, including Mars investigations. Infrared scans of Mars from Earth-based observatories and the Hubble Space Telescope revealed differences in mineralogical composition, including hydrated minerals (N. Barlow, 2014). Adaptive optics and Hubble views have dramatically improved resolution and allowed the study of martian characteristics previously only observed by circling spacecraft at Mars (N. Barlow, 2014).

On December 25, 2021, NASA's James Webb Space Telescope, the agency's successor to the famed Hubble telescope, launched a mission to study the universe's history (The European Space Agency, 2022). Webb is a joint venture between NASA, the European Space Agency, and the Canadian Space Agency. The telescope was launched from Europe's Spaceport in French Guiana aboard an Ariane 5 (The European Space Agency, 2022). Following Hubble, the James Webb Space Telescope (Webb) has been

the next major space research observatory to answer outstanding questions about the Universe and make groundbreaking discoveries in all disciplines of astronomy (NASA, 2022). On July 12, 2022, NASA's Goddard Space Flight Center in Greenbelt, Maryland, published the first full-color photos and spectroscopic data from the telescope. One of the newly revealed photos (seen in Figure 1) depicts the Southern Ring Nebula, a planetary nebula representing the brilliant remnant of a sun-like star (Dunbar, 2022).

The James Webb Space Telescope does not orbit the Earth as the Hubble Space Telescope does; it orbits the Sun 1.5 million kilometers from the Earth at the second Lagrange point, or L2 (NASA, 2022; The European Space Agency, 2021). This orbit is unique because it allows the telescope to remain aligned with the Earth while it orbits the Sun. The telescope can function at a temperature of around 225 degrees below zero Celsius (NASA, 2022). The temperature differential between the hot and cold sides of the telescope is enormous; on the hot side, water would boil, while nitrogen would freeze on the cold side!

Webb will view the whole disk of Mars every two years after it reaches its destination. If a global dust storm envelops the Martian Surface during a period when Webb can observe it, the massive space telescope will be able to collect data on the storm, supplementing data from spacecraft on or near the planet's surface (Landau, 2019). Monitoring the Martian climate is only one way that Webb, built to see into deep space and unravel cosmic mysteries, might collaborate with other NASA missions to investigate Mars. Webb can see Mars in the infrared, a wavelength of light invisible to the human eye, and is particularly valuable for analyzing specific compounds in planetary atmospheres (Landau, 2019). While Webb's primary mission will be to search for chemical fingerprints on distant planets circling other stars, known as exoplanets, it will also apply the same capabilities to neighboring Mars.

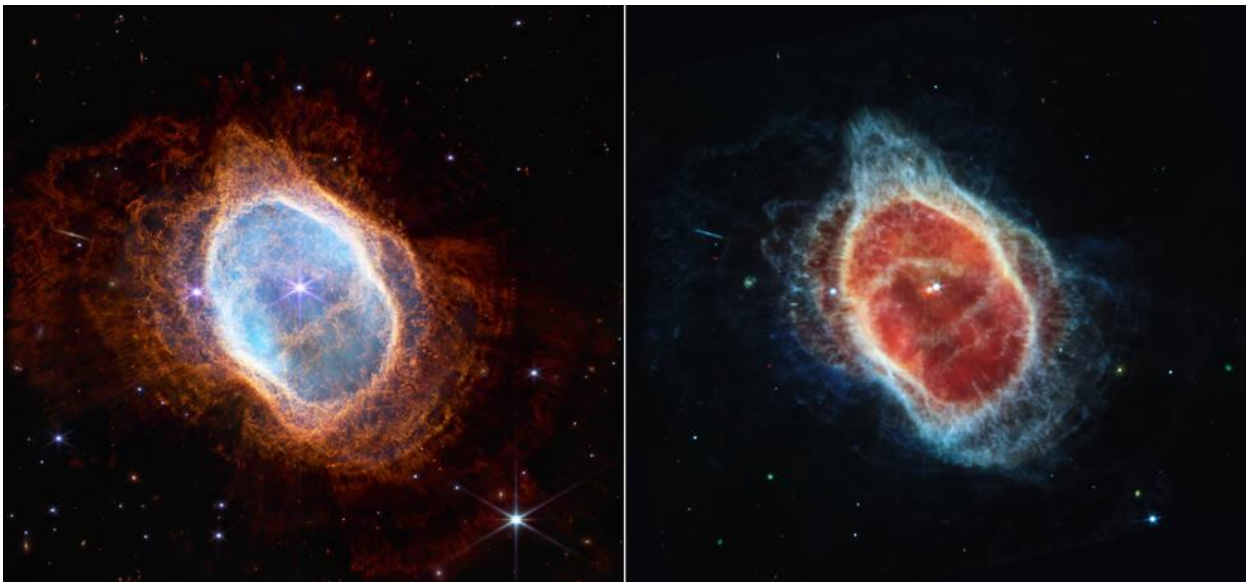

Figure 1. Southern ring nebula images from the James Webb Space Telescope.

2.2. A Chronology Of Mars Exploration Missions

Mars has intrigued humanity since we first saw it as a star-like object in the night sky. Its ruddy tint set it apart from its dazzling siblings, each captivating in its way, but none following a ruddy arc across Earth's skies. Then, in the late 1800s, telescopes showed a surface full of exciting features—patterns and landforms that scientists initially misattributed to a busy Martian civilization. Scientists currently know that Mars has no artificial structures. However, we have also learned that today's arid, the poisonous planet may have once been as hospitable as Earth.

Humanity has been exploring Mars since the 1960s to learn more about how planets develop and change and whether or not it has ever been home to creatures. Only uncrewed spacecraft have traveled to Mars thus far, but that might change soon. In the 2030s, NASA plans to send the first humans to Mars, and numerous more missions will be launched to accelerate the process (M. Smith et al., 2020). A glimpse at what humans have discovered about Mars through decades of investigation is presented in this chapter. The primary motivation for Mars research is the question of whether or not the planet has hosted life in the past or even today. "Follow the water" is a NASA motto emphasizing water's role in Earth's geological and atmospheric development and its implications for biological activity (Hubbard et al., 2002). Regarding research on Mars, around two-thirds of all planetary missions have had some success, although not all. The following sections explain these missions in further detail according to reference publications for space explorations. (Biswal M & Annavarapu, 2019; Lele, 2014; NASA, 2021a; Portree, 2001).

2.2.1. Flybys and first photographs of Mars

Mars is relatively close to Earth, and humans have long dreamt of colonizing another planet. Mars missions are intended to expand our understanding of the planet. Long-term orbiters were launched to Mars and stayed for an extended time, and scientists additionally took use of the flyby, which allowed for data collection in small increments.

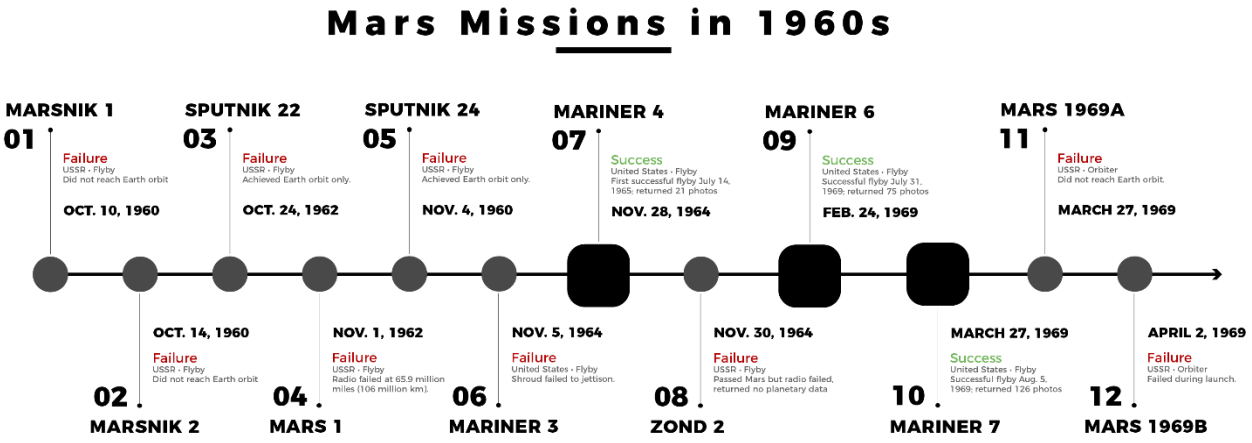

Figure 2. Timeline illustration of Mars missions in the 1960s.

Figure 2 shows the timeline of Mars missions in the 1960s, including failed ones, to illustrate the space race between the powerful countries. The earliest attempts to reach Mars happened shortly after the advent of space flight. Given that the first satellite, the Soviet Union's Sputnik, was launched in 1957, it is astonishing that the Soviet Union's space program sought to broaden its range to Mars only three years later. In the 1960s, the Soviet Union, technically known as the Union of Soviet Socialist Republics (USSR), made numerous attempts to reach Mars, and NASA promptly responded with the Mariner 3 spacecraft. These earliest efforts failed even to come close to Mars. The chronology is as follows:

• The Soviet Union launched Marsnik 1 on October 10, 1960, preparing for a scheduled flyby to Mars. The spacecraft suffered damage during the launch and could not reach Earth's orbit.

• The Soviet Union launched Marsnik 2 on October 14, 1960, preparing for a flyby of Mars. However, similar to Marsnik 1, the spacecraft was destroyed during launch and never made it into Earth's orbit.

• On October 24, 1962, the Soviet Union launched Sputnik 22 to conduct a flyby to Mars. The spacecraft was destroyed shortly after reaching Earth's orbit due to a catastrophic failure.

• Mars 1 (USSR) was launched on November 1, 1962, to conduct a flyby to Mars. The spacecraft has completed its voyage to and beyond Earth's orbit. However, more than five months later, on March 21, 1963, the spacecraft was 106 million kilometers from Earth when its radio failed, thereby cutting off communication with the spacecraft.

• On November 4, 1962, the Soviet Union launched Sputnik 24 to conduct a flyby to Mars. The spacecraft entered Earth's orbit but encountered a fatal flaw when it deviated toward Mars, eventually crashing back to Earth in pieces.

• Mariner 3 (US) was launched on November 5, 1964, to fly to Mars. Around an hour after launch, there was a problem with the solar panels. Ground personnel could not fix the problem before the spacecraft's batteries ran out, ending the mission.

Several primary missions failed to accomplish their goals, but NASA's Mariner 4 succeeded. On November 28, 1964, the spacecraft was launched and became the first to circle Mars on July 14, 1965. It returned to Earth with a total of twenty-one photos of Mars. Two days after Mariner 4, the Soviet Union tried another launch with Zond 2. The spacecraft passed close to Mars, but the radio failed, and no data from the planet were returned. NASA also launched Mariners 6 and 7 in 1969, landing on Mars and returning several images. All of these spacecraft flew across cratered regions of Mars. These images first gave astronomers the notion that Mars resembled the moon.

Between 1969 and 1971, many further attempts were undertaken, most of which were unsuccessful. Just for a decade, the number of intentions of observing Mars was tremendous, and these attempts triggered a new era based on technological development.

2.2.2. First Mars satellite and lander

After obtaining knowledge and experience from several mainly unsuccessful missions in the 1960s, space agencies made significant strides forward to study Mars for long-term objectives. The next decade saw the successful launch of a Mars satellite and landing mission. The missions carried out in the 1970s are depicted in Figure 3 in chronological order.

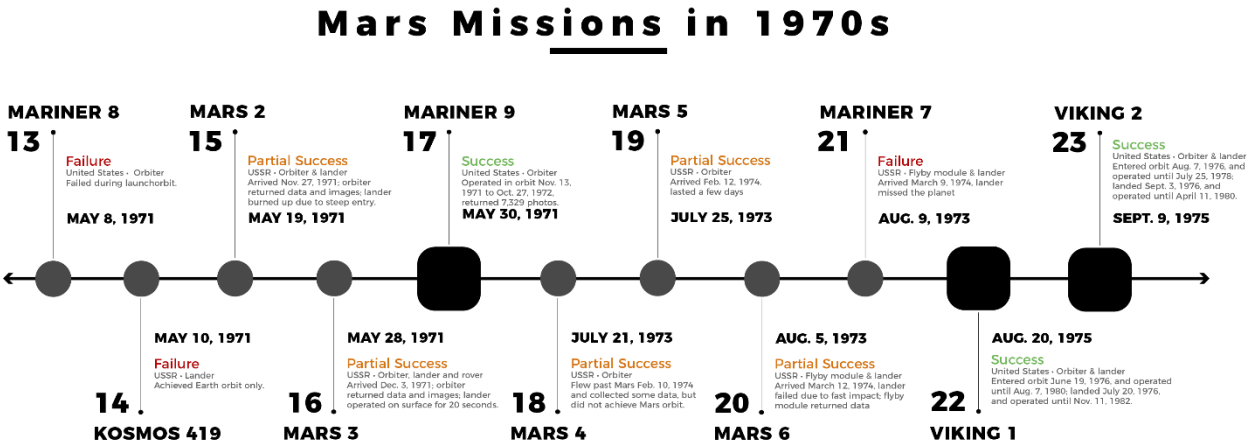

Figure 3. Timeline illustration of Mars missions in the 1970s.

In the 1970s, a certain amount of attempts were undertaken. Mariner 8 by the US and Kosmos 419 by the USSR were failed missions in 1971. Mariner 8 (U.S.) likewise failed during its launch attempt on May 8, 1971. Kosmos 419 (USSR) launched and reached Earth's orbit before collapsing on May 10, 1971.

After multiple failed efforts, the Soviet Union ultimately succeeded in its mission to the Red Planet in 1971. The Mars 2 orbiter, launched on May 19, 1971, arrived in November. The Mars 2 lander, on the other hand, fell to the planet's surface and was rendered un-operational. A lander and orbiter mission to Mars, Mars 3, was launched on May 28, 1971, and landed on the Red Planet on December 3. The lander failed a few seconds after landing on the surface, while the orbiter continued to function well.

The arrival of NASA's Mariner 9 in November 1971 altered the perception of Mars. Mariner 9 became the first satellite to orbit Mars in November 1971, generating a precise photographic picture of the planet's surface that reveals evidence of volcanism and river erosion. On May 30, 1971, the spacecraft reached Mars during a dust storm that blanketed the whole planet. Additionally, something strange protruded above the dust clouds. When the debris dropped to the surface, scientists realized that the strange structures were the summits of dormant volcanoes. Mariner 9 also detected a massive rift across the Martian surface, eventually named Valles Marineris in honor of the spacecraft that discovered it. Mariner 9 orbited the Red Planet for over a year, returning 7,329 images.

The Soviet Union had limited success with its Mars series of spacecraft; of four spacecraft headed to Mars, only one orbiter and one lander returned data briefly in 1974:

• July 21, 1973: Mars 4 (USSR) launched and then flew by Mars on Feb. 10, 1974; however that was not the intention; the mission's objective was to circle the planet, not continue.

• July 25, 1973: Mars 5 (USSR) launched on July 25, 1973, and entered orbit above Mars on February 12, 1974. However, the mission lasted just a few days.

• Aug. 5, 1973: Mars 6 (USSR) launched with a flyby module and lander on March 3, 1974; however, the lander was destroyed on impact.

• Aug. 9, 1973: Mars 7 (USSR) launched again with a flyby module and lander on March 3, 1974; however, the lander failed to reach the Red Planet.

In 1975, NASA launched two pairs of orbiters and landers toward Mars. Viking 1 and Viking 2 landed on Mars in 1976, sending their lander to the surface while the orbiter stayed above. The Viking mission was the first comprehensive investigation of Mars since each spacecraft lasted years and returned massive data to Earth. The information aided scientists in their quest to learn more about Mars. Another advancement made by the Viking expedition was the transmission of measurements of the Martian atmosphere.

Consequently, the components of meteorites were determined to be comparable to those found on Earth. According to the scientists who presented their findings, certain meteorites discovered on Earth originated on Mars. By the late 1970s, researchers had made significant progress in understanding Mars, owing to the Viking Missions, Marine 9, and other spacecraft. Advancement was thanks to these spacecraft successfully transmitting their data to Earth.

However, hopes of discovering life on Mars were disappointed when the probes could not conclusively demonstrate the presence of microorganisms. The findings continue to be debated as more information on microbial activity becomes available.

2.2.3. Better, faster, and cheaper technological advancements

Following a series of successful and partially successful missions to Mars in the 1970s, space agencies did not attempt to reach Mars until the 1980s. In 1982, the Soviet Union attempted to reach Phobos, one of Mars's moons, but both flights failed, and the Soviet Union was obliged to stop the missions. On the other hand, the 1990s was the decade of lander missions to Mars's surface to analyze its nature. Figure 4 depicts a chronological representation of the Mars missions carried out throughout the 1980s and 1990s.

NASA's subsequent effort to reach Mars occurred in the 1990s, with the launch of Mars Observer on September 25, 1992. On August 21, 1993, the spacecraft disappeared before it was scheduled to enter Mars orbit. Whereas the communication breakdown has never been thoroughly explained, the most plausible explanation is that a fuel tank rupture led the spacecraft to spin out of control and lose contact with Earth. According to NASA's Jet Propulsion Laboratory, the spacecraft cost

an estimated $813 million, about four times the initial project budget, making the loss heartbreaking. Spacecraft failure spurred fresh efforts by NASA to develop better, faster, and cheaper missions that could use sophisticated computer electronics and team management approaches. NASA started the Faster, Better, and Cheaper (abbreviated FBC) program to make space missions more feasible and sustainable.

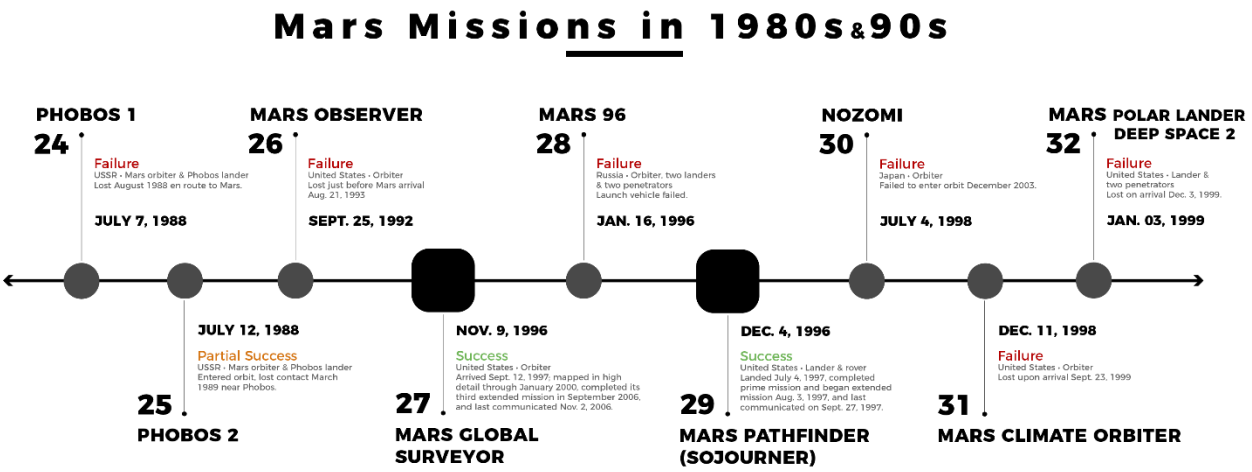

Figure 4. Timeline illustration of Mars missions in the 1980s and 1990s.

NASA's Mars Global Surveyor (MGS) spacecraft was the first FBC program. On November 7, 1996, it was launched from Earth and arrived on Mars on September 12, 1997. NASA extended its mission until 2006 when it lost contact with NASA. MGS examined the whole surface of Mars from pole to pole, revealing several ancient signs of water, such as gullies and hematite (a mineral that forms in water). NASA used MGS data to help choose the best landing locations for its future Mars rovers.

The Soviet Union was dissolved in 1991. The Russian space agency resumed the Soviet journey to Mars with the launch of the Mars 96 mission on November 16, 1996. Nevertheless, the orbiter, two landers, and two penetrators were lost after the rocket failed. On the opposite side of the world, the first mission of the FBC program was a remarkable success. In July 1997, NASA's Pathfinder lander and Sojourner rover arrived at Mars. The lander was the first to land with airbags, while Sojourner was the first rover to trundle on Mars. Pathfinder was planned to operate for one month and Sojourner for one week, but both stayed operational until September 1997, when Pathfinder lost communication. Two more FBC missions were unable to reach the Red Planet. The Mars Climate Orbiter was launched on December 11, 1998, and after arriving at Mars in September 1999, it vanished due to a measuring mistake. The Mars Polar Lander (MPL) and two space probes that went with it were launched by NASA on January 3, 1999, but all were lost before completing their voyage.

Japan was the following country to enter the Mars mission arena, with the launch of Nozomi on July 4, 1998. The spacecraft arrived on Mars in December 2003 but could not enter orbit.

2.2.4. Discovery of ancient water evidence

The 2000s was the decade of successful Mars missions conducted by NASA, and thanks to these missions, scientific communities revealed, discussed, and wrote a massive amount of data on Mars missions. Revealed data boosted the intention and plans of crewed Mars missions. Figure 5 shows the launch and landing information of missions in the 2000s.

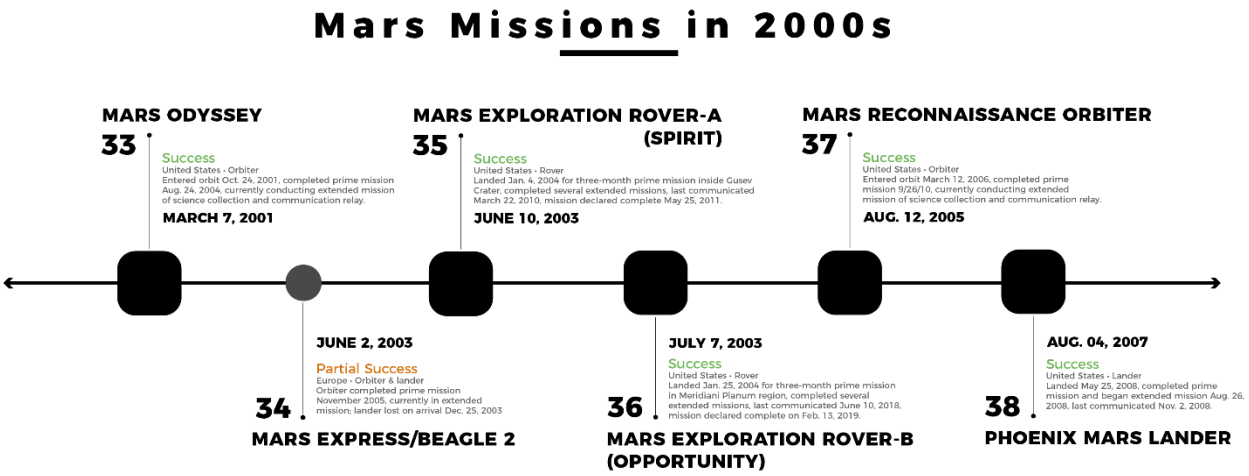

Figure 5. Timeline illustration of Mars missions in the 2000s.

NASA launched Mars Odyssey on March 7, 2001, and landed on the Red Planet on October 24, 2001. The orbiter continues to conduct scientific experiments as part of its extended research mission. It surpassed the record for the longest-serving spacecraft on Mars on December 15, 2010. The spacecraft returned almost 350,000 images, mapped the planetary distributions of several elements, and transmitted more than 95% of the data collected by the Spirit and Opportunity rovers.

The European Space Agency launched Mars Express/Beagle 2 on June 2, 2003. While the lander was destroyed upon arrival, the orbiter completed its primary mission and continued on an extended mission in November 2005.

In 2004, NASA launched the Spirit and Opportunity rovers to the surface of Mars. Each provided compelling evidence that water flowed on Mars in the past. Spirit was destroyed in March 2010 after it crashed with a dune, while Opportunity continued to run for nearly another decade. Due to a sandstorm in 2018, the Opportunity was missed, and NASA declared the missions accomplished. NASA launched another orbiter, the Mars Reconnaissance Orbiter, on August 12, 2005. It began circling the globe on March 12, 2006. The mission returned more data than all previous Mars missions combined and sent high-resolution photos of Mars's landscape and climate. On August 4, 2007, NASA also launched Mars Phoenix, a stationary lander. It landed on Mars on May 25, 2008, and detected subsurface water ice. Phoenix's solar panels received considerable damage during the harsh Martian winter, and in November 2008, communication with the lander was lost. Phoenix was confirmed dead by NASA in May 2010 following many efforts to re-establish communication.

2.2.5. Fundamental discoveries for future long-term Mars missions

After a comprehensive Mars environment analysis and possible evidence of water existence, the focus of space missions was shifted to the preparation for human missions. While space crafts were launching for the Mars explorations, in-situ resource utilization technologies gained importance for future crewed mission plans. Figure 6 illustrates the missions conducted for deep analysis of Mars conditions.

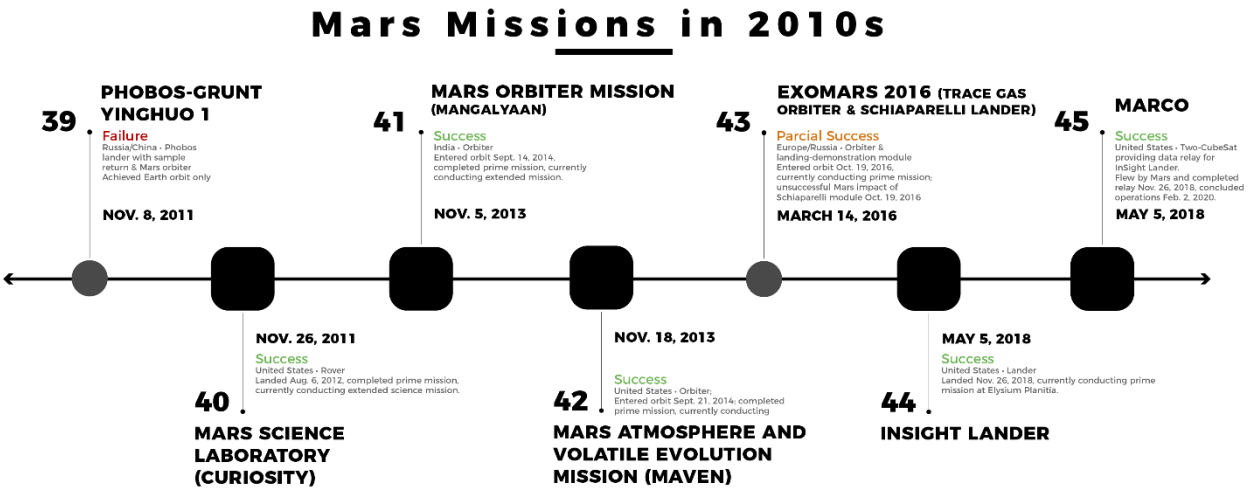

Figure 6. Timeline illustration of Mars missions in the 2010s.

The Russian space agency, Roscosmos, attempted to reach Phobos again with the Phobos-Grunt mission, which launched in 2011 but crashed on January 15, 2012, after failing to leave Earth orbit. Phobos-Grunt also carried China's first effort at a Mars orbiter and an experiment by the Planetary Society in the United States to explore how extended journeys through deep space affect microorganisms. The mission of China's orbiter was likewise a failure.

NASA's powerful rover, Curiosity, landed at Gale Crater in 2012 to look for evidence of ancient habitable conditions. It made several significant discoveries, including the discovery of previous floodwaters, the detection of methane on the surface, and the discovery of organic compounds. In 2021, it is still operating at total capacity.

ExoMars, a partnership between the European Space Agency and Russia, launched an orbiter named the Trace Gas Orbiter (TGO) and a demonstration lander Schiaparelli in 2016. Although Schiaparelli crashed on Mars, TGO is still working and delivering information about the Martian atmosphere's composition.

Other countries are amassing Martian experience to get a close look at at least one of the planet's moons. In 2013, India's MOM (Mars Orbiter Mission) successfully attained orbit, giving a unique perspective on the planet's weather and surface characteristics.

MAVEN (Mars Atmosphere and Volatile Evolution) was launched by NASA in November 2013 and reached orbit on September 21, 2014. It continues to monitor changes in the Martian atmosphere to understand better how it thinned over billions of years.

NASA sent Mars InSight to the planet's surface in 2018 to conduct the first detailed examination of Mars' inner structure. InSight's mission was extended in 2021 based on its preliminary discoveries on Martian history, while plans to dig a heat-seeking probe (or "mole") into the Martian surface failed due to the regolith being harder than planned. Additionally, InSight transported the first Martian CubeSats.

Besides the big rover and orbiter missions, NASA's other spacecraft examines various aspects of Mars' evolution and current environment to further our understanding of rocky planets and prepare for future landing missions.

2.2.6. Active spacecraft for Mars exploration

By the beginning of 2022, Mars will host eleven functioning spacecraft: eight in orbit and three on the surface, and the landing sites of Mars rovers are also presented in Table 1 (The Planeraty Society, 2021).

Table 1. List of active spacecraft for Mars Exploration (The Planetary Society, 2021).

Name	Location	Nationality	Launch Date	Status
Mars Odyssey	In orbit	United States	07.04.2001	Operational
Mars Express	In orbit	ESA	02.06.2003	Operational
Mars Reconnaissance Orbiter	In orbit	United States	12.08.2005	Operational
Mars Science Laboratory Curiosity	Surface	United States	26.11.2011	Operational
Mars Orbiter Mission	In orbit	India	05.11.2013	Operational
MAVEN	In orbit	United States	18.11.2013	Operational
ExoMars Trace	In orbit	ESA/Russia	14.03.2016	Operational
InSight	Surface	United States	05.05.2018	Operational
Al-Amal	In orbit	United Arab Emirates	20.07.2020	Operational
Tianwen-1	In orbit	China	23.07.2020	Operational
Perseverance rover	Surface	United States	30.07.2020	Operational

NASA's Mars Odyssey mission launched in 2001 (NASA Science, 2022a). Its objective is to map the Martian surface's chemical components and minerals. From February 2002 through August 2004, it performed its primary science mission. Extended orbiter operations resume today. Odyssey's measurements have helped scientists map minerals and chemical components and locate underlying water ice. Images of Martian topography taken by measuring surface temperature are stunning. Odyssey discovered early in the mission that radiation in low-Mars orbit is double that in low-Earth orbit, an important finding for future human exploration. In addition to the Mars Exploration Rovers Spirit and Opportunity, the Odyssey orbiter also relays communications for the Mars Science Laboratory's Curiosity rover. Images and data from Mars Odyssey assist probable rover and lander landing locations.

Mars Express is a collaborative project between NASA and the European Space Agency. Since landing on Mars in 2003, the spacecraft has been conducting remote observations of the planet's atmosphere and surface (NASA Science, 2022e). In order to explore undiscovered territory on Mars, the Mars Express carried the Beagle 2 lander, which had been lost on the planet since 2003 but was spotted by a NASA orbiter over a decade later. The mission's primary goal is to look for subsurface water from space. Seven scientific instruments on the orbiting spacecraft have investigated the geology, atmosphere, surface environment, history of water, and the possibility of life on Mars. Recent glacial activity, explosive volcanism, and methane gas discovered by Mars Express are contested by scientists today. Mars Surface Information System (MARSIS) has already revealed hidden impact craters, layers, and signs of water ice deep underground.

The 2005-launched Mars Reconnaissance Orbiter is equipped with the most advanced camera yet used on a planetary exploration mission, granting it the highest capacity for virtual observation (NASA Science, 2022f). Unlike previous Mars orbiter cameras, this camera can detect targets as small as a plate. The technology offers a detailed understanding of Mars' geology and structure and assists in the recognition of possible threats for prospective rovers and landers. The Mars Reconnaissance Orbiter is also equipped with a sounder for the detection of subsurface water, which is essential for determining potential landing locations. Additional instruments on this dependable spacecraft detect surface minerals and track atmospheric dust and water on Mars. The secondary camera collects medium-resolution images that help contextualize high-resolution observational data. In addition, the Mars Reconnaissance Orbiter serves as the initial element of a "interplanetary internet," a crucial service for future missions. Several spacecraft utilize the Mars Reconnaissance Orbiter as a communication channel to Earth.

As part of NASA's Mars Science Laboratory project, the largest and most advanced rover to date, Curiosity, has been deployed to the red planet (NASA Science, 2022g). The rover arrived on Mars on August 5, 2012, after its first launch on November 26, 2011. The spacecraft descended using a parachute and ignited rockets in the last seconds before landing, allowing it to dangle in the air as Curiosity was brought to the surface using a rope. Depending on the instrument's activity, the terrain, and the visibility of the way ahead in its cameras, it can overcome knee-high obstacles and travel at a speed of approximately 30 meters per hour. The objective of the Curiosity expedition was to determine whether or not microorganisms, could survive in the Mars environment. Early in the mission, Curiosity's science equipment detected chemical and geological indications of a habitable environment on Mars. It travels to Gale Crater to conduct research and gather samples of the region's rocks, soil, and atmosphere for further research into Mars' climate and geological history. In addition, the chemical fingerprints of samples are analyzed to learn more about their previous interactions with water.

The Mars Orbiter Mission (MOM), also known as Mangalyaan ("Mars-craft," from Mangala, "Mars" and yāna, "craft, vehicle"), is a space probe that has been circling Mars since September 24, 2014 (NASA Science, 2018). The Indian Space Research Organization launched it on November 5, 2013. (ISRO). MOM is the country's first mission to Mars. The mission aims to test essential technologies for interplanetary exploration and employ its five research equipment to explore the Martian surface and environment from orbit. MOM's orbit also provides multiple opportunities to examine the Martian moon Phobos. The expedition arrived successfully in Mars orbit, completing the technical test. The core science mission is currently underway.

MAVEN (Mars Atmospheric and Volatile Evolution) is NASA's second Mars Scout mission, a competition for smaller, low-cost missions led by a principal scientist (NASA Science, 2022d). MAVEN is acquiring essential observations of the Martian atmosphere to aid in understanding the red planet's remarkable climatic change during its history in response to high-priority research goals identified in the National Academy of Science's 2003 decadal review on planetary exploration. MAVEN provides information on atmospheric gas loss to space and infers what happened in the past from those extensive investigations. Examining how the Martian atmosphere was lost to space can provide insight into the influence of change on the Martian temperature, geology, and geochemical conditions across time, which are critical for determining if Mars ever had a habitable environment. MAVEN is the first spacecraft to conduct direct measurements of the Martian atmosphere. It is equipped with eight research instruments that measure the Martian upper atmosphere. MAVEN can also dip to an altitude of roughly 129 kilometers above the globe to sample the whole upper atmosphere of Mars. The spacecraft can act as a communications relay for Martian landers and rovers.

ExoMars (Exobiology on Mars) is a European Space Agency (ESA) initiative that consists of a series of missions aimed at determining whether life has existed on Mars (NASA Science, 2022b). NASA provides scientific, engineering, and technological skills to assist other nations in exploring Mars. The Trace Gas Orbiter (TGO) is the first mission in the ExoMars program, a collaboration between ESA and Russia's Federal Space Agency, Roscosmos. The Trace Gas Orbiter of the European Space Agency monitors the Martian atmosphere for methane and other gases in trace amounts. NASA's contribution to the 2016 ExoMars Trace Gas Orbiter includes the "Electra" radio telemetry system. As an Electra-carrying spacecraft, ESA's 2016 orbiter can interact with approaching spacecraft carrying identical Electra payloads to establish their location and speed to Mars as they approach. Electra can also give ultra-high frequency (UHF) coverage to Mars landers and rovers on the surface, lacking the radio strength necessary to connect directly with Earth.

InSight (Interior Exploration using Seismic Investigations, Geodesy, and Heat Transport) is a NASA Discovery Program project that will land a single geophysical lander on Mars to research the planet's

deep interior (NASA Science, 2019). However, InSight is more than a Mars mission; it is a terrestrial planet explorer that will answer one of the most fundamental questions in planetary and solar system science: how the rocky planets of the inner solar system (including Earth) formed over four billion years ago. Through the use of robust geophysical sensors, InSight will explore deep into the surface of Mars, finding the fingerprints of terrestrial planet formation processes and monitoring the planet's "vital signs": its "pulse" (seismology), "temperature" (heat flow probe), and "reflexes" (precision tracking).

The Emirates Mars Mission is an uncrewed space exploration mission to Mars launched by the United Arab Emirates Space Agency (UAE Space Agency, 2022). On 19 July 2020, the Hope orbiter (Al-Amal) was launched and entered orbit around Mars on 9 February 2021. The Mohammed bin Rashid Space Centre controls mission planning, development, and operations (MBRSC). The spacecraft was built in the United States at the Laboratory for Atmospheric and Space Physics (LASP) at the University of Colorado Boulder, with Arizona State University (ASU) and the University of California, Berkeley. The space probe investigates daily and seasonal weather cycles, weather phenomena in the lower atmosphere, such as dust storms, and how weather differs around the globe. Additionally, it contributes to understanding Mars' atmospheric hydrogen and oxygen depletion and other plausible explanations for its dramatic climatic fluctuations.

Tianwen-1 ("questions to heaven" or "questioning the heavens") is China's first Mars mission, including an orbiter and the Zhurong rover (The Planetary Society, 2022). Zhurong was launched into Mars orbit in February 2021 and landed on May 14, 2021. Zhurong can connect directly with Earth or via a high-speed data relay via its Tianwen-1 orbiter. The orbiter is equipped with science equipment for researching Mars, including a high-resolution camera capable of producing breathtaking photos. Zhurong is equipped with cameras, tools for researching Mars' temperature and geology, and even a device for zapping rocks and recording their chemical signatures—much like NASA's Curiosity and Perseverance rovers. The rover radar works by firing radio waves into the surface and measuring the time it takes to reflect, allowing scientists on Earth to build a three-dimensional image of what lies underground.

Mars 2020 Perseverance Rover is a NASA mission that is part of NASA's Mars Exploration Program, a long-term attempt to explore Mars robotically (NASA Science, 2019). Perseverance was slated to launch between July 30 and August 15, 2020, when Earth and Mars were in favorable orbital alignments for landing on Mars. That is, it requires less energy to get to Mars at that moment than at other times when Earth and Mars are in different orbital locations. Mars 2020's design is based on NASA's successful Mars Science Laboratory mission architecture, including the Curiosity rover and proven landing technology. The mission covers Mars exploration's highest-priority research objectives, including critical concerns concerning the possibility of life on Mars. Perseverance goes the next step by looking for previous livable circumstances on Mars and past microbial life. The rover incorporates a drill capable of

collecting core samples of Mars's most promising rocks and soils and storing them in a "cache" on the planet's surface. A future expedition may bring these samples back to Earth, and thanks to this, scientists would enable to analyze the samples in laboratories equipped with specialized laboratory equipment that would be too bulky to transport to Mars. Additionally, the mission gives possibilities to collect data and showcase technology that addresses the obstacles of future human Mars journeys. These include developing a method for producing oxygen from the Martian atmosphere, identifying additional resources (such as subsurface water), optimizing landing techniques, and characterizing weather, dust, and other potential environmental conditions that may affect future astronauts living and working on Mars.

2.3. Crewed Mission Plans for Mars Exploration

Since 1880, science fiction authors and, since the late 1940s, the engineering and scientific communities have envisioned a human mission to Mars. National space organizations have been pursuing the exploration of Mars for several decades. Since the 1950s, there has been ongoing conceptual work on missions involving human explorers, with planned missions frequently saying that they will take place between 10 and 30 years after they are conceived. It is possible to see the many different mission concepts proposed by various organizations and space agencies in the crewed Mars mission plans database. It is possible to plan anything from short-term scientific missions (a small group of two to eight astronauts may spend a few weeks or a year on Mars) to long-term expeditions that would maintain a permanent presence on Mars (e.g., through research stations, colonization, or other continuous humanization). Haptic improvements have also been proposed to simulate space flight to Mars.

There have been more than 70 human Mars mission proposals suggested since 1952 by space enthusiasts and experts. Examining hundreds of pages of documentation, comparing it to currently available technology, and putting the mission plan into action with an adequate budget all look like complicated undertakings. Because of this, it is desirable to develop clear, durable, economically sound, and feasible techniques.

Over the previous seven decades, many mission concepts for human-manned space missions to Mars have been proposed or researched. Chemical, radioactive, and electric propulsion have all been suggested, as well as a diverse spectrum of landing, living, and return choices for spacecraft. A chronological explanation of each of the proposed crewed Mars missions is presented in this section.

2.3.1. Mars mission plans in the 20th century

Numerous mission proposals for an expedition to Mars were presented throughout the 20th century. David Portree's Humans to Mars: Fifty Years of Mission Planning, 1950–2000 discusses a number of these proposals (Portree, 2001). Human missions to Mars seem forthcoming, and each of the proposals mentioned below represented a significant step in the right direction.

Wernher von Braun proposal (1947 through the 1950s): Wernher von Braun conducted the first technical analysis of a Mars mission. Details were included in his 1953 book Das Marsprojekt (von Braun & White, 1953) (translated as The Mars Project in 1962) and several publications (Ward, 2013). Von Braun's Mars project envisaged roughly a thousand three-stage vehicles taken from Earth to transport components for the Mars mission, built in an Earth-orbiting space station (Platoff, 1999). The mission consisted of a fleet of 10 spacecraft carrying a combined crew of 70 to Mars, where they would deliver three-winged surface excursion ships that would land horizontally on Mars's surface.

The 1956 updated version of the Mars Project concept, described in Wernher Von Braun and Willy Ley's book The Exploration of Mars (Black, 1956), reduced the mission's size, requiring only 400 launches to assemble two ships still carrying a winged landing vehicle. Later iterations of the mission proposal, as depicted in the Disney film series "Man In Space," included nuclear-powered ion-propulsion vehicles for interplanetary travel (Crowley & Trudeau, 2011).

U.S. proposals (the 1950s to 1970s): Project Orion, a nuclear pulse propulsion spacecraft proposal, was developed by General Atomics between 1957 and 1965 (Dyson, 2002). Compared to chemical rocketry, Orion was designed to transport extraordinarily massive payloads, allowing crewed expeditions to Mars and the outer planets. One of the early vehicle concepts was to launch an 800-ton payload into Mars orbit. Further development became unfeasible after the 1963 Partial Nuclear Test Ban Treaty, and work was stopped in 1965.

As part of NASA's Marshall Spaceflight Center's "Project EMPIRE" in 1962, Aeronutronic Ford, General Dynamics, and Lockheed Missiles and Space Company researched Mars mission ideas (Platoff, 1999). According to these studies, a Mars journey (potentially including a Venus flyby) may be accomplished by launching eight Saturn V boosters and assembling them in low Earth orbit or launching a single "post-Saturn" heavy-lift vehicle. Even though the EMPIRE missions were never funded, they were the first detailed analyses of what it would take to complete a human journey to Mars utilizing data from real NASA spaceflight, laying the groundwork for subsequent studies (Platoff, 1999).

After the Apollo Program's success, von Braun argued for NASA's crewed space program to concentrate on a crewed mission to Mars. In the early 1980s, Von Braun proposed launching two six-crew spacecraft on a twin mission using Saturn V boosters and NERVA-powered upper stages (Powers, 2017). President Richard Nixon considered the plan, but the Space Shuttle was chosen instead.

Soviet mission proposals (1956 through 1969): From 1956 to 1962, Mikhail Tikhonravov of the Soviet Union proposed the Martian Piloted Complex (MPK) as a concept for a crewed Mars mission aboard the N1 rocket (Harvey, 2007a). The Soviet Union's program to explore Mars had a low success rate.

For a crewed flight to Mars and Venus (TMK-MAVR design) without landing, the Soviet Union developed the Heavy Interplanetary Spacecraft (known by the Russian acronym TMK) in the 1960s (Lai et al., 2018). Probes were to be dropped from the TMK spacecraft during a 3-year mission to Mars in 1971, including a flyby. The project was never finished due to the failure of the N1 rocket, which was essential for its completion. Russia's 1969 Mars Expeditionary Complex (known as "MEK") proposed a 630-day journey to the red planet, which would send a crew of three or six to Mars and back (Harvey, 2007b).

Case for Mars (1981–1996): Between 1981 and 1996, the University of Colorado in Boulder hosted a series of conferences called the Case for Mars, in which scientists discussed the possibility of sending humans to Mars in the future. A series of workshops were organized at these conferences to build a baseline idea for the mission, which promoted human exploration of Mars and proposed concepts and technologies. The return trip's rocket propellant was suggested to be made using in-situ resource usage. In a series of proceedings volumes, the mission study was published. Robert Zubrin and David Baker's "Mars Direct" plan (R. Zubrin et al., 1991) was followed by the "Footsteps to Mars" proposal of Geoffrey A. Landis (Landis, n.d.) and the "Great Exploration" proposal from Lawrence Livermore National Laboratory (Hyde et al., 1990), among others.

NASA Space Exploration Initiative (1989): For the first time since the International Space Station was launched, NASA is considering a plan for human lunar and Mars exploration as a possible follow-up. Following this, NASA issued a 90-day study (DRAKE, 1990), which recommended a long-term strategy to complete the Space Station as "a key next step in all our space operations," return to the Moon and construct a permanent base on Mars. In response to this study, Congress canceled all funding for human exploration beyond the Earth's orbit (Day, 2004).

Mars Direct (the early 1990s): Mars missions would be significantly riskier and more expensive than previous Moon missions due to the enormous distance. Supplies and fuel would need to be provided for a two- to three-year round journey, and the spacecraft would require some protection from ionizing radiation. Robert Zubrin and David A. Baker, then of Martin Marietta, argued in 1990 that the mission's mass (and thus its cost) could be reduced by utilizing in situ resources to produce fuel from the Martian atmosphere (R. Zubrin et al., 1991). This proposal was based on the concepts generated during the previous "Case for Mars" conference series. Zubrin refined the proposal over the next decade, resulting in the Mars Direct mission concept presented in The Case for Mars (1996) (R. M. Zubrin & Baker, 1992). The Mars Society, created by Zubrin in 1998, advocates for the expedition as a feasible and economic endeavor.

International Space University (1991): In 1991, the International Space University in Toulouse, France, examined the feasibility of an international human Mars trip (MENDEL, 1993). They envisioned an eight-person crew flying to Mars in a nuclear-powered vehicle that rotated to create artificial gravity. On the surface, a 40 kW photovoltaic array supplied power to 40-tonne habitats pressurized to 69 kPa.

NASA Design reference missions (the 1990s): In the 1990s, NASA conducted a study for a crewed space mission to Mars called NASA Design Reference Mission 3.0 (Drake, 1998). It was a plan for a crewed exploration framework for Mars published in 1998 as an addendum to the 1994 design plans. The goal is for numerous launches to transport diverse space technology, surface exploration devices, and a human crew to Mars in the early twenty-first century, with the crew returning to Earth. Various technologies, like nuclear, solar, aerobraking, and in-situ resource utilization, are being investigated to launch the payloads into space, send them to Mars, and minimize the overall weight of the mission.

2.3.2. Mars mission plans in the 21st century

Marpost (2000–2005): The Mars Piloted Orbital Station (Marpost) is a proposed crewed orbital mission to Mars that would use a nuclear reactor to power an electric rocket engine. Russia suggested the mission proposed in October 2000 as the next step for Russia in space after participation in the International Space Station, and a 30-volume draft project for MARPOST was confirmed by the Russian government as early as 2005 (Harvey, 2007b). It was proposed that the design for the ship would be completed in 2012 and the construction in 2021.

ESA Aurora program (2001+): In 2001, the European Space Agency (ESA) set out a long-term program to send a crewed mission to Mars by 2033 (Messina et al., 2005). The suggested timeframe for the project would begin with robotic exploration, progress through a proof-of-concept simulation of supporting humans on Mars, and conclude with a crewed journey to Mars.

Objections from ESA participating states and other delay save called the timeframe into question (Gibney, 2016). The program's first phase is a 2016 mission that launched the Trace Gas Orbiter into Mars orbit and released the Schiaparelli EDM lander (Karatekin et al., 2018). The orbiter is operating, but the lander has crashed on the planet's surface.

The second rover was supposed to launch in 2018 and land on Mars in early 2019; in May 2016, ESA confirmed that the launch would occur in 2020 due to delays in European and Russian industrial operations and scientific payload deliveries.

The second mission was postponed until 2022 March 12 due to the vehicle not being ready for launch in 2020, with delays aggravated by travel restrictions during the COVID-19 epidemic.

USA Vision for Space Exploration (2004): On the 14th of January, 2004, President George W. Bush introduced the Vision for Space Exploration, a program aimed at crewed space exploration (Tatarewicz, 2009). It involved developing essential planning for a return to the Moon by 2012 and

constructing an outpost on the Moon by 2020. By 2005, preliminary plans had been developed for predecessor missions that would aid in developing necessary technology during the 2010s (Andringa et al., 2005). On September 24, 2007, NASA Administrator Michael Griffin stated that the agency would launch a crewed mission to Mars by 2037. The necessary finances were to be raised by shifting $11 billion from space science missions to the vision of human exploration (Tatarewicz, 2009). NASA has also discussed the possibility of launching Mars missions from the Moon to cut travel expenses.

Mars Society Germany – European Mars Mission (EMM) (2005): The Mars Society Germany has proposed an enhanced heavy-lift version of the Ariane 5 for a crewed Mars mission (Griebel et al., 2002). One hundred twenty thousand kilograms of the payload was necessary for a five crew to travel for 1200-days. The entire project was expected to cost between ten and fifteen billion euros.

China National Space Administration (CNSA) (2006): For the Eleventh Five-Year Plan (2006–2010), China's National Space Administration Administrator Sun Laiyan stated that China would begin deep-space exploration focusing on Mars within the next five years (Xinhua, 2006). The first uncrewed Mars missions could occur between 2014 and 2033, followed by crewed missions in 2040–2060, sending astronauts to Mars and bringing them back to Earth. This crewed mission was prepared for by the Mars 500 study of 2011.

Mars to Stay (2006): Numerous times, the idea of a one-way journey to Mars has been discussed. Bruce Mackenzie, a space activist, advocated a one-way mission to Mars in 1988 during a presentation at the International Space Development Conference, saying that the trip might be accomplished with less trouble and expense without returning to Earth (MACKENZIE, 1989). In 2006, former NASA engineer James C. McLane III suggested the initial colonization of Mars by a single human on a one-way trip (McLane III, 2006).

NASA Design Reference Mission 5.0 (2007 and 2009): ASA provided an overview of human Mars mission architecture (Drake et al., 2010). The study expanded on concepts explored in past NASA DRMs and brought them up to speed with more modern launchers and technology. NASA updated NASA DRM 5.0 in early 2009 to include the Ares V launcher and the Orion CEV and improved mission planning.

Martian Frontier (2007–2011): Russian experts have proposed several ideas for a Mars mission. Between 2016 and 2020 were the stated launch dates. Four or five cosmonauts would be on board the Mars probe, spending about two years in space. Mars 500, the world's most extended high-fidelity spaceflight simulation, was conducted in Russia from 2007 to 2011 as a feasibility study for crewed trips to Mars (Tafforin, 2013). The ground-based MARS-500 was completed in late 2011 by Russian and European space agencies. In July 2000, Russia accomplished a biological experiment mimicking a crewed mission to Mars.

NASA Austere Human Missions to Mars (2009): Extracted from the DRMA 5.0, proposals for a crewed Mars mission using chemical propulsion (Price et al., 2009). The simple approach is motivated by limiting high-risk or high-cost technology development and emphasizing development and production commonality to maintain a program in a flat-funded budget environment. The following vital features would enable a lower technology implementation: using a blunt-body entry vehicle without deployable decelerators; utilizing aerobraking rather than aerocapture to place the crewed element into low Mars orbit; avoiding the use of liquid hydrogen due to its low temperature and significant volume issues; using standard bipropellant propulsion for the landers and ascent vehicle, and utilizing radioisotope surface power systems rather than a nuclear fusion reactor.

2-4-2 concept (2011–2012): Jean-Marc Salotti made new proposals for crewed Mars missions in 2012 (Salotti, 2011). Just two astronauts are needed for the '2-4-2' concept, based on the repetition of the complete mission. Each spacecraft has two astronauts on board; four are on the surface of Mars, and two are returning. The other astronauts are ready to assist if a part of the hardware fails (two for two). By lowering the size of the landing vehicles, this architecture makes it easier to enter, descend, and land the spacecraft. For one thing, it avoids the construction of enormous spacecraft in LEO. According to the author, his plan is cheaper and risk-free than NASA's reference mission and may be implemented as early as 2030.

Boeing Conceptual Space Vehicle Architecture (2012): In 2012, Boeing, United Launch Alliance, and RAL Space in Britain presented a conceptual architecture that laid out a possible design for a crewed Mars mission (Benton et al., 2012). Spacecraft for the travel to Mars, landing, and time on the surface are all included in the design. Several uncrewed cargo landers have been assembled into a base on the surface of Mars, among other things. The "Mars Personnel Lander" would bring the crew to this base, and it could also transport them back into orbit around Mars. The crewed interplanetary spacecraft design included an artificial magnetic field and artificial gravity. As a whole, the design was modular to facilitate iterative research and development.

Inspiration Mars Foundation (2013): Inspiration The Mars Foundation was a non-profit corporation created by Dennis Tito in 2013 to launch a crewed trip to Mars in January 2018 or 2021 if they missed the first synodic chance in 2018 (Nikle et al., n.d.). The mission system comprised a modified capsule launched from Earth orbit in a single propulsive maneuver to reach Mars. After launch, an inflatable housing module will be deployed and detachable before re-entry. Closed-loop life support and operational components will be integrated into the vehicle, simplifying maintenance and repair and allowing for "hands-on" repair. There was no NASA support for the mission.

Evolvable Mars Campaign (2014): NASA has listed bringing humans to the surface of Mars as one of its primary objectives in order to advance exploration, science, technology, human benefits, and

international cooperation. To attain this objective, in 2014, NASA announced a three-pronged strategy for expansion into space titled the Evolvable Mars Campaign (Rojdev et al., 2015). As part of this plan, several initiatives will concentrate on perfecting human long-duration spaceflight on the International Space Station (ISS) and cooperating with commercial companies to open up low-Earth orbit (LEO). These initiatives are crucial to the "Earth Reliant" development phase. During the "Proving Ground" phase, multiple human and robotic missions will be sent to cis-lunar and lunar space to test the technology required for human habitation on Mars. The "Earth Independent" phase of the campaign will be devoted to human and robotic exploration of Mars.

Boeing Affordable Mission (2014): Deputy Associate Administrator for Programs James Reuther and Advanced Human Exploration Systems and Operations Mission Director Jason Crusan announced tentative support for the Boeing "Affordable Mars Mission Design," which includes radiation shielding, centrifugal artificial gravity, in-transit consumable resupply, and a landing that can return (Raftery et al., 2013). According to Reuther, the projected mission may be completed in the early 2030s if appropriate funds could be obtained.

Mars Semi-Direct Revisited (2016): Due to the perceived weight of the Earth Return Vehicle, Robert Zubrin proposed a "semi-direct" scenario in 1993 (R. Zubrin & Weaver, 1993), in which the outbound trip remains direct to the surface, but the return is split into two steps, with the first returning to Mars orbit via a relatively small ascent vehicle to join a return vehicle that has been sent there months in advance. Since the return is no longer direct, the circumstance is "semi-direct." In 2016, Jean-Marc Salotti reassessed the mission's design and determined that four heavy launches of the NASA Space Launch System's heaviest version would be adequate to complete the mission (Jean-Marc & Richard, n.d.).

NASA's Journey to Mars and Moon to Mars Programs (2015–present): NASA presented its roadmap for human exploration and sustainable human presence on Mars on October 8, 2015 (NASA, 2015). The concept is divided into three phases that result in a sustainable human presence.

The first stage, which is already underway, is the "Earth Reliant" phase, which will maintain using the International Space Station until 2024 to validate deep space technologies and research the effects of long-duration space trips on the human body.

The second stage, "Proving Ground," deviates from Earth-based operations and performs most of its functions in cislunar space. The projected Lunar Gateway would verify deep-space habitation facilities and the capabilities required for human Mars colonization.

Finally, phase three involves the shift to self-sufficiency in Earth's resources. The "Earth Independent" phase entails long-term missions on Mars' surface with self-sustaining habitats and collecting Martian resources for fuel, water, and building materials. NASA is still planning human missions to Mars in the 2030s, though it may take decades to achieve Earth's independence.

In November 2015, NASA Administrator Chris Bolden reaffirmed the agency's mission to send humans to Mars. According to him, a crewed landing on Mars will occur in 2030, and the 2021 Mars rover Perseverance will support the mission.

Pence said in March 2019 that "American astronauts will walk on the Moon again by the end of 2024, 'by whatever means necessary." By 2024, NASA is planning a return to the Moon's surface. "To take the next huge leap - sending men to Mars," NASA says it will use the Artemis lunar program with the Lunar Gateway (M. Smith et al., 2020).

SpaceX Mars transportation infrastructure (2016–present): SpaceX announced in 2016 that it intended to deliver a Red Dragon capsule to Mars for a soft landing by 2018 (J. L. Heldmann et al., 2017); however, the mission was postponed by mid-2017 to devote engineering resources to the effort that would become known as "Starship." SpaceX publicly proposed to colonize Mars by creating a high-capacity transportation system. As previously stated in 2016, the ITS launch vehicle's initial design called for a big reusable rocket, a spaceship, or a tanker for in-orbit refueling. The aspirational goal was to progress technology and infrastructure so that the first humans on Mars may depart as early as 2024.

Elon Musk has continued to describe idealistic ambitions for early Mars trips as one of the program's objectives, while SpaceX's top development goal after 2018 became constructing a larger and more capable launch vehicle. Musk presented an improved vehicle concept for the Mars mission during the International Astronautical Congress in September 2017. Until 2018, this mission's vehicle was known as BFR (Big Falcon Rocket). In 2018, it was renamed "Starship." Starship could allow on-orbit activities such as satellite delivery, servicing the International Space Station, and Moon and Mars missions. Cargo missions to Mars would occur before crewed missions. Pathfinder Starship transport ships could be launched to Mars as early as 2024. Crewed Starship vehicles would follow two years after the first cargo flights in 2026.

Mars Base Camp (2016): Mars Base Camp is a plan developed by Lockheed Martin for a US spaceship that would carry astronauts to Mars orbit as early as 2028 (Cichan et al., 2016). Lockheed Martin designed the vehicle concept, incorporating future and legacy technologies and NASA's Orion spacecraft.

Deep Space Transport (2017): NASA's Deep Space Transport (DST), also known as the Mars Transit Vehicle, is a design for a crewed interplanetary spacecraft capable of supporting up to 1,000-day Mars science exploration missions (Crusan et al., 2018). It would consist of an Orion capsule and a self-sustaining habitation module. Since April 2018, the DST has remained a concept under study, and NASA has not made an official proposal to the US federal government during the annual budget cycle. The DST vehicle would travel from and return to the Lunar Gateway, where it would be maintained and repurposed for a future Mars journey.

2.3.3. The Future of Mars Missions: What is Next?

Once every 26 months, Earth and Mars align to minimize travel durations and costs, allowing spacecraft to complete the interplanetary voyage in around half a year (NASA, 2015). Earth's space agencies frequently launch probes during these alignments, which occurred in the summer of 2020. During this period, three countries launched spacecraft to Mars: The United Arab Emirates launched its Hope spacecraft on July 20 to examine Mars' atmosphere and weather patterns; China launched its Tianwen-1 on July 23, and the United States launched its Perseverance rover on July 30.

An enormous, six-wheeled rover called Perseverance is outfitted with sophisticated instruments. It aims to reach Jezero Crater, a historic river delta and prospective home for ancient living forms. Research into the Martian climate and weather, as well as technology that may help humans survive on the planet, will be conducted with Perseverance. One of the primary goals of this project is to help determine whether or not Mars was ever inhabited, making it an actual Mars life-finding expedition. Indeed, all labor robots lay the groundwork for human colonization of the next planet. NASA has been working on the Orion spacecraft, taking humans to the moon and beyond. According to the plan, the first people will land on the surface of Mars in the 2030s.

The Rosalind Franklin rover and its accompanying lander are expected to depart Earth in 2022 as the second phase of ExoMars (following a two-year delay due to technical problems and the coronavirus pandemic.) Japan also wants to return to the Martian system in 2024 with the Mars Moons Exploration (MMX) mission, which will conduct a sample return mission from Phobos, one of Mars's two moons. Additionally, private spaceflight businesses such as SpaceX are entering the Mars race. Elon Musk, CEO of SpaceX, has often stated that humanity must evolve into a "multi-planetary species" to survive, and he is now working on a plan to establish a million people on Mars by the end of this century. Soon, humankind will learn if our neighboring planet has ever supported life—and whether our species has a future on another Earth.

Numerous countries and groups have long-term goals of sending humans to Mars. The United States is researching Mars with multiple robotic missions, with a sample return mission planned in the future. The Orion Multi-Purpose Crew Vehicle (MPCV) will serve as the launch/splashdown crew delivery vehicle, with a Deep Space Habitat module providing additional living space during the 16-month mission. The first crewed Mars mission, projected for the 2030s, would comprise sending astronauts to Mars, orbiting Mars, and returning to Earth. While technology development for US government missions to Mars is underway, there is currently no well-funded strategy for completing the notional project with human landings on Mars by the mid-2030s. The president has directed NASA to land humans on Mars by 2033, and NASA-funded engineers are investigating a method for constructing prospective human dwellings on Mars using bricks made from compressed Martian soil.

The ESA's long-term goal is to carry humans into space, but the agency has not developed a crewed spaceship. It has already launched robotic probes such as ExoMars in 2016 and intends to launch another in 2022. Russia intends to launch humans between 2040 and 2045. In 2033, China intends to send humans. Among these plans, SpaceX's Mars mission, Mars One, and NASA's Design reference mission possess the technology necessary to try a human-manned journey to Mars between 2040 and 2060. Additionally, these tactics were judged to be realistic and affordable compared to alternative mission concepts based on the current state of mature technology.

The Artemis program, headed by NASA, is a new generation of lunar exploration missions to take humans farther into space than ever before (Canadian Space Agency, 2021). The Artemis missions are exceedingly challenging, but they will set the foundation for the long-term human and robotic investigation of Earth's only natural satellite, the Moon. Planned missions include (Canadian Space Agency, 2021):

- Space Launch System (SLS) is scheduled to launch Artemis I, an uncrewed test flight of the Orion spacecraft in 2022;
- Artemis II, a crewed test flight of Orion, is scheduled to launch in May 2024;
- Artemis III, a mission that will put the first woman and the first person of color on the Moon, is scheduled to launch in May 2025.

Artemis will begin with missions around the Moon (Artemis I and II) before a mission that settles on the lunar surface (Artemis III) (Artemis III) (Canadian Space Agency, 2021). On subsequent trips, NASA astronauts will attach Orion to the Lunar Gateway, a small space station to which Canada supplies the sophisticated robotic system Canadarm3 for use in the station. The Gateway is essential to long-term lunar exploration and will serve as a model for future Mars missions.

For the long-term objective of the Artemis Program, NASA collaborates with commercial companies and universities to design and develop human landers that will take astronauts there (Dunbar, 2021a). NASA planned to create human landers that are larger and more capable, allowing them to transport more cargo and land with greater precision. NASA has also presented a strategy for establishing infrastructure for a long-term sustainable presence on the Moon by robotic and human explorers. According to NASA, to get astronauts around their landing zone, there is a lunar terrain vehicle (LTV), a habitable mobility platform (HMP), and a surface habitat (SH) that could house up to four people for short-term stays on the Moon's surface (Dunbar, 2021a).

In addition, NASA continues to collaborate with companies to address the issues of living in space, such as how to use available resources, dispose of waste, and more (Dunbar, 2021a). On the Moon, the distance from the Earth is nearly 1,000 times greater, necessitating technologies that can consistently operate far from home, meet the necessities of human existence, and be light enough to launch. These

technologies will be increasingly critical during the mission to Mars. Human habitats and life support systems can be tested on the Moon to see if they are suitable for Mars (Dunbar, 2021a). NASA aims to test new technologies to create self-sustaining outposts distant from Earth.

2.4. The Key of Crewed Mars Missions: Space-resilient Habitation

A hurricane, earthquake, typhoon, drought, tsunami, or tropical storm are just a few examples of the many natural disasters that may happen on Earth. Furthermore, extreme weather conditions, such as heat or cold, are commonplace in some parts of the earth, such as the desert or the poles. Through trial and error, humans have learned a great deal about how to design our habitats on Earth to withstand these extreme conditions. Even though it took thousands of years to discover the Moon and Mars, the harsh conditions under the Earth's protective atmosphere are not as severe as these. The Moon and Mars, two of the most desirable possibilities for near-term exploration and habitation, are not only devoid of atmospheres and 'normal' gravitational fields but also undergo chaotic temperature changes and other dangers such as meteorite impacts and severe radiation. The most advanced engineering and technology will be required to overcome these obstacles and create habitable living circumstances on the surface of planets (Dyke et al., 2021). To develop the required technologies to survive on the Moon and Mars, NASA and other space agencies have been trying to answer the following essential questions (Mahoney, 2016):

- Where will future astronauts spend their days and nights on long-term expeditions to Mars and other planets?
- How will habitats be constructed or installed on another planet’s surface, and what systems will be installed inside?

NASA has conducted space habitation experiments for a long time, and the International Space Station has been proven successful (Brady et al., 2018). By the end of April 2022, more than 250 astronauts have lived on the space station, which has helped to sustain a dynamic economy in low-Earth orbit by bringing supplies such as food and water from Earth (Garcia, 2022). On the other hand, deep space habitation systems will not receive supplies as frequently as those on Earth. Research, concept studies, prototyping, and validation are required to ensure that our next-generation space technologies maximize efficiency while minimizing waste, which is not all that different from our efforts to maintain our environment on "spaceship Earth."

In order to keep humans safe, healthy, and productive for extended periods in deep space, human habitats must have a variety of habitation systems for sustaining life, controlling the environment, protecting against fire and radiation, and promoting physical activity and health. For a crew of four on a Mars class mission, the mission equates to around 1,100 days (Mahoney, 2016). These technologies are currently being developed and can be tested and proven aboard the International Space Station (ISS).

Habitation modules are the structures that contain the habitation systems and symbolize the homes of future deep space explorers (Mahoney, 2016). NASA is working with the U.S. industry to refine concepts further and produce prototypes for testing in cislunar space as part of an ongoing set of transactions. Extreme temperature variations, micrometeoroids, and solar and galactic cosmic radiation threaten astronauts in the habitat modules (Mahoney, 2016). Increasing human presence in the solar system is a worldwide undertaking that necessitates the participation of other space agencies, private enterprises, and academic institutions.

X-Hab challenges were introduced in 2011 by NASA for university students who designed answers to our most challenging habitation difficulties – from growing food on the voyage to properly recycling breathable air to maximizing every single resource available (Mahoney, 2016). A series of NASA-standard assessments, including a System Definition Review (SDR), a Preliminary Design Review (PDR), and a Critical Design Review (CDR), is required of teams. The pupils are expected to take on much responsibility in this approach by NASA. As a result, the students have a more significant stake in developing space technologies that are anticipated to form the basis for future space systems and technologies.

In 2014, NASA released an announcement on the NextSTEP BAA model for public-private partnerships aimed at commercializing deep space exploration capabilities to support more extensive human spaceflight missions on the Moon is proving ground, referred to as "cislunar space," and to allow transit to Mars (Mahoney, 2016). This collaboration strategy enables NASA to gain new ideas and promote industry commercialization goals for low-Earth orbit through this model. In April 2016, NASA had a new NextSTEP BAA, referred to as "NextSTEP-2," in its sights (Mahoney, 2016).

Since its inception in 2015, NASA's 3D-Printed Habitat Challenge has sought to enhance the additive construction technology needed to create sustainable homes on Earth, the Moon, Mars, and beyond (M. C. Roman et al., 2016). Sustainable habitation modules could be constructed where traditional building materials and skills are scarce, and these capabilities could be used. To build semi-permanent shelters for human occupancy, local indigenous materials (soil, clay, sand, etc.) could be blended with readily available recyclable materials and utilized. An evaluation of potential procedures, materials, and designs for planetary construction was made possible by the challenge's completion in May 2019.

As NASA prepares for exploration missions to the Moon and Mars, it will need to explore automated habitat maintenance technologies. The Space Technology Mission Directorate (STMD) creates revolutionary space technology to enable future NASA missions. STMD has selected two Space Technology Research Institutes (STRIs) to assist in reaching habitation module design objectives by developing resilient and autonomous technologies for constructing space habitats.

To construct durable, autonomous, and self-maintained homes for human explorers in deep space, the HOME (Habitats Optimized for Missions of Exploration) Institution employs known engineering procedures and risk assessment methods as cutting-edge technologies in its design process. The institute's mission is to advance state-of-the-art in autonomous systems, human and automation teaming, data science, machine learning, mechanical maintenance, onboard manufacturing, and more (Rollock & Klaus, 2022).

The Resilient ExtraTerrestrial Habitats Institute (RETHi) aims to create, test, and deploy deep space habitats that can swiftly and efficiently recover from and adapt to a wide range of stressors (Dyke et al., 2021). The center seeks to integrate expertise in civil infrastructure with cutting-edge technical disciplines such as hybrid simulation and modular, autonomous robots. RETHi aims to construct deep space habitats that can operate in either a manned or unmanned mode through a concerted effort. The institute also intends to design, implement, and validate various capabilities by establishing a cyber-physical prototype testbed comprised of physical and virtual models. Resilience is essential; thus, we must develop and run deep space habitat systems that can withstand the stresses of space exploration, said Dyke et al. (2021). In the field of structural design, resilience refers to the capacity of buildings and structures to resume their intended use promptly following a shock incidence or disaster. Resilience, on the other hand, is more than just robustness or redundancy. As an alternative, it is a multifaceted strategy that considers potential problems up front and adjusts to them as they arise. We do not have the new frameworks and technologies for deep space habitat design required to attain this level of robustness and operate independently under various unmanned and manned operating modes (and transition between them) (Dyke et al., 2021).

Numerous studies have highlighted the likelihood of sustaining human existence without the requirement for terraforming on Mars and the Moon due to their proximity to Earth (Benaroya et al., 2002; Fogg, 1998). These studies also concur that, in addition to being able to endure the harsh conditions of space, habitats (bases) must also be adequately constructed, preferably using resources found in the natural space environment, to offer a safe environment for humans. Interestingly, research on lunar and Maritain soils has revealed a wealth of components that might be used to make building materials (Alexiadis et al., 2017; Lin, 1985). In-situ materials are crucial, which has been highlighted by numerous research (C. C. Allen, 1998; Johnson-Freese, 2017; Lin, 1985). This emphasis is necessary because it can cost up to $20,000 to ship one kilogram of supplies from Earth to the Moon; on Mars, the price may increase exponentially (Johnson-Freese, 2017). Due to this, over the past 50 years, parallel research has been done to increase our understanding of structural design and material science, enabling the creation of habitats that are resilient to space and can be built with space-native building materials (Davis et al., 2017; Johnson et al., 1971; Lin et al., 1992; Meek et al., 1987). Human habitats, like Earth-based

structures, must defend their occupants and offer a secure environment where they can live and work, regardless of whether they are constructed using conventional, cutting-edge, or space-native construction materials. Despite recent developments in structural engineering, almost no space habitat designs or constructions have been done before (Sumini & Mueller, 2017).

Skylab, the Space Shuttle, and the International Space Station (ISS) are the only three spacecraft ever constructed and flown with permanent or temporary crew quarters (Litaker & Howard, 2022). Each of the three implementations was different. NASA, commercial partners, and international partners are collaborating to design spacecraft for the forthcoming Artemis and Mars human exploration missions, some of which may have private crew quarters for up to six people. In the next decade, the agency may be responsible for the construction of twice as many crew quarters than it has in the preceding fifty years.

NASA has issued two reference documents for designers, engineers, and scientists on the design and engineering issues of crewed space habitats. The Human Integration Design Handbook (HIDH), NASA/SP-2010-3407, is a resource for most of the aforementioned NASA human space flight programs and projects, which were completed by 2014, and it includes guidelines for the crew's health, habitability, environment, and human factors design. The manual also serves as a reference for NASA-STD-3001, the Space Flight Human Systems Standard, which outlines human-system guidelines for guiding and prioritizing the development of crew health needs to overcome extraterrestrial circumstances and complete space missions (Lim & Herrmann, n.d.). However, NASA and other public and private organizations are still working to develop or enhance design and construction solutions for in-situ applications. For a long-term crewed mission, standards for major challenges such as additive manufacturing and construction, in-situ materials, transportation, communication delay of up to 24 minutes, and protection against hazards in extraterrestrial environments are still under development, but a Mars mission is becoming more and more likely every day.

Due to the harsh and hostile environmental conditions associated with the Moon and Mars, the development of safe, space-resilient structures appears to be a unique problem that demands in-depth research and collaborative efforts. One of the primary motivations for this research, without developing or proposing a new material, is to develop a space-resilient habitation design methodology by using the harsh conditions of Mars as design parameters to simulate the structural behaviors of design proposals under extreme environmental events. The other key objective is to research design automation without human interaction to develop a design solution for unanticipated environmental phenomena and communication delays.

The next chapters explore the unique design criteria for a crewed Mars mission in an effort to define a novel design approach, utilizing the outcomes of space missions, analog Mars missions, and some advanced design proposals submitted to NASA's 3D-Printed Habitat Challenge.

03 rd Chapter
MARS'S ENVIRONMENTAL FACTS AND EFFECTS ON A MISSION

The third chapter addresses the environmental conditions on Mars as revealed by missions to the planet. Defined data provides context information for a hypothetical site on Mars in order to represent extreme environmental events and clarify which environmental forces must be simulated in order to create a space-resilient habitation. In order to maximize design parameters from the beginning, all potential site options for robotic Mars expeditions are afterwards analyzed based on their in-situ resources.

Mars is the solar system's fourth planet in terms of distance from the Sun and seventh in size and mass. It is a reddish phenomenon that periodically appears in the night sky (N. Barlow, 2014). Mars, also referred to as the Red Planet, has a long history of war and death. It is called after the Roman god of war, Mars. Phobos ("Fear") and Deimos ("Terror"), the planet's two moons, were named after two of Ares and Aphrodite's sons (the counterparts of Mars and Venus, respectively) (N. Barlow, 2014).

Aside from its scary aspect, Mars has received much global attention. People can see it in the night sky because it is the second nearest planet after Venus (N. Barlow, 2014). In addition, it is the only planet where the solid surface and the atmosphere can be observed simultaneously (N. Barlow, 2014). People on Earth have noticed how similar Mars is to our planet for ages. Clouds, winds, a 24-hour day, seasonal weather, polar ice caps, volcanoes, canyons, and other distinctive traits are all present on Mars. Mars may have had a thick, warm atmosphere similar to Earth's billions of years ago and a large amount of water—rivers, lakes, floodways, and perhaps oceans—in the past (Catling, 2014). A possible lake under the South Polar Cap has been detected by radar, implying that liquid water may persist in isolated areas of the planet's surface, as evidenced by images of dark streaks on the edges of several craters throughout the spring and summer months (Lauro et al., 2021). The existence of life as we know it is impossible without water on Mars. It is a significant possibility that if life ever existed on Mars, it would hide in these watery environments. However, a group of researchers claimed in 1996 to have found signs of ancient microbial life in a Mars meteorite, although most experts disagree (Becker, 2021).

Mars has long been considered the most favorable solar planet for indigenous life, human exploration, and settlement. A further claim of biological activity was supported by seasonal changes in the planet's appearance. Although the seasonal changes were geological rather than biological, scientific popularity interest in Mars exploration has not diminished.

3.1. Planetary Data For Mars

Mars is the fourth planet from the Sun, 2.279108 km away (1.5237 AU) (N. Barlow, 2014). Mars' orbit has a 1.851° inclination to the ecliptic plane (N. Barlow, 2014). Its eccentricity is 0.0934, making it one of the most elliptical planetary orbits. Mars' orbit is relatively long (N. Barlow, 2014). Therefore the distance between Mars and the Sun varies from 206.6 million to 249.2 million km (N. Barlow, 2014). Mars orbits the Sun once every 687 Earth days (N. Barlow, 2014). That is why its year is nearly twice as long. Mars is less than 56 million km from Earth during its closest approach, but it recedes to approximately 400 million km when the two planets are on different parts of the Solar System (N. Barlow, 2014).

Mars is clearest to notice whenever it and the Sun are in opposite directions in the sky since it is directly overhead and has a wholly illuminated surface. Every 26 months, there is a series of oppositions (Beish, 2002). Mars is at its brightest and most prominent when it is nearest to the Sun. Every 15 years lasted for approximately; there is close opposition.

Planetary data for Mars	
mean distance from Sun	227,943,824 km (1.5 AU)
eccentricity of orbit	0.093
the inclination of the orbit to the ecliptic	1.85°
Martian year	686.98 Earth days
mean synodic period*	779.94 Earth days
mean orbital velocity	24.1 km/sec
equatorial radius	3,396.2 km
north polar radius	3,376.2 km
south polar radius	3,382.6 km
surface area	1.44×10^8 km^2
mass	6.417×10^{23} kg
mean density	3.93 g/cm^3
mean surface gravity	371 cm/sec^2
escape velocity	5.03 km/sec
rotation period (sidereal day)	24 hr 37 min 22.663 sec
Martian mean solar day (sol)	24 hr 39 min 36 sec
the inclination of the equator to orbit	25.2°
mean surface temperature	210 K (-82 °F, -63 °C)
typical surface pressure	0.006 bar
number of known moons	2
*Time required for the planet to return to the same position in the sky relative to the Sun as seen from Earth	

Table 2. Planetary data of Mars

Since Mars rotates once every 24 hours and 37 minutes, a day on Mars is similar to Earth(Stooke, 2012). Mars' rotation axis is inclined by about 25° to its orbital plane, giving way to seasons like Earth's. The Martian year has 668.6 sols. In the south, summers are shorter (154 Martian days) and warmer than in the north (178 Martian days) (Stooke, 2012). However, in 25,000 years, the northern summers will be shorter and warmer (Stooke, 2012). Also, the axis obliquity (tilt) has been shifting for over a million years (Stooke, 2012). It can range from near zero, when Mars has no seasons,

to 45°, when extreme seasonal changes. Over billions of years, obliquity can approach 80° (Stooke, 2012).

Mars is a tiny planet, bigger than Mercury and half the size of Earth. It has an equatorial radius of 3,396 km and a polar radius of 3,379 km (N. Barlow, 2014). Mars' mass is one-tenth that of Earth, and its surface gravitational acceleration of 3,71 m/sec^2 means that objects weigh about a third of what they do on Earth (N. Barlow, 2014). Mars has only 28% of Earth's surface area, yet because Earth is mostly water, the land areas of the two planets are comparable (Belton, Michael J.S., Malin, Michael C. and Carr, Michael H., 2022).

During the 1877 perihelic opposition, the two tiny moons of Mars were identified (D. Strauss, 1997). The outermost moon (Deimos) was spotted by Asaph Hall of the US Naval Observatory on August 12, 1877, while the inner moon (Phobos) was discovered six nights later. Ares' sons Phobos and Deimos were given names by Hall, who referred to them as "fear or fright" and "dread or terror" (D. Strauss, 1997).

The Olympus Mons volcanic peak is the highest point on Mars, at 21.287 kilometers, while the Hellas impact basin is the lowest, at 8.180 kilometers (N. G. Barlow, 2013). More information on orbital and physical parameters can be found in Table 2.

3.2. Atmospheric Conditions Of Mars

Long-term studies by orbiting spacecraft utilizing radio occultation measurements and infrared sounding reveal data about atmospheric structure across broader areas and periods. The martian atmosphere is divided into layers according to their composition, temperature, isotopic composition, and physical nature. Multiple spacecraft and ground-based observations have discovered this structure. The five lander missions collected pressure, density, and temperature (VL1, VL2, MPF, and MER). As a result of these findings, the martian atmosphere is classified into three layers: lower, middle, and upper.

The lower atmosphere exists from the Martian surface to 40 kilometers. Within the first 10 kilometers of the lower atmosphere, pressure and temperature fall as altitude increases, and energy transmission is dominated by convection (Leovy, 2001). At night, convection pauses, and a significant temperature anomaly near the surface forms. Temperatures and pressures are comparable to those seen in the Earth's stratosphere in the lower atmosphere. The lower atmosphere's density is mainly determined by periodic CO_2 and H_2O cycles associated with the sublimation and condensation of the polar caps, which result in annual fluctuations in surface pressure. Two processes heat the Martian lower atmosphere. The lower atmosphere warms slightly due to atmospheric CO_2, which prevents infrared radiation from the surface from escaping to space. The martian lower atmosphere is densely packed with dust, absorbing solar radiation and reemitting thermal infrared energy. Atmospheric dust

contributes significantly to lower atmosphere heating and must be considered in this region's circulation simulations.

The middle atmosphere, or mesosphere, is 40 and 100 kilometers above the Martian surface. The profiles of the middle atmosphere produced by VL1, VL2, and MPF demonstrate that temperatures can shift significantly over time. These temperature changes are caused by CO_2's near-infrared absorption and emission of solar radiation and waves generated in the lower atmosphere and exacerbated by thermal tides between the day and night hemispheres (J. T. Schofield et al., 1997).

The thermosphere, or upper atmosphere, extends over 110 kilometers in altitude. Solar EUV radiation, with energy ranging from 10 to 100 eV and wavelengths ranging from 10 to 100 nm, heats the thermosphere. Solar EUV output varies with the solar activity cycle, dramatically changing thermospheric temperatures above 120 kilometers altitude. Temperatures are colder during low solar activity times and rise as the sunspot cycle reaches its maximum. The ionosphere is above 130 kilometers, where solar energy ionizes the atmospheric gases.

Mars' atmosphere is highly thin in comparison to Earth's. On Mars's surface, the atmosphere has a density of approximately 0,020 kg/m^3 (NASA, 2021b). Currently, atmospheric pressure on the surface varies between 30 Pa (0.030 kPa) on Olympus Mons and over 1,155 Pa (1.155 kPa) in Hellas Planitia, with a mean pressure of 600 Pa near the surface (0.60 kPa) (Bolonkin, 2009). On Mars, the greatest air density is equivalent to 35 kilometers above the Earth's surface. As a result, the mean surface pressure is only 0.6 percent of Earth's (101.3 kPa). The scale height of Mars' atmosphere is around 10.8 kilometers, which is higher than Earth's (6 kilometers) due to Mars' surface gravity being only about 38% that of Earth, an effect compensated by the lower temperature and 50% higher average molecular weight of Mars' atmosphere.

The Sample Analysis at Mars (SAM) small chemistry lab inside NASA's Curiosity rover core exhaled Gale Crater's air and analyzed its structure. SAM's measurements showed the Martian atmosphere's surface composition as seen in Table 3: 95% carbon dioxide (CO_2), 2% molecular nitrogen (N_2), 1.6% argon (Ar), 0.13 molecular oxygen (O_2), and 0.08 carbon monoxide (CO) (Shekhtman, 2019). Carbon dioxide makes up 95.3% of the atmosphere, nine times the amount in Earth's considerably larger atmosphere. The amount of carbon dioxide in the Martian atmosphere is less than a thousandth of Earth.

Table 3. Composition of Mars's atmosphere

Constituents of the martian atmosphere	Volume
Carbon dioxide (CO_2)	95.32%
Nitrogen (N_2)	2.70%
Argon (Ar)	1.60%
Oxygen (O_2)	0.13%
Carbon monoxide (CO)	0.08%
Water (H_2O)	210 ppm
Nitrogen oxide (NO)	100 ppm
Neon (Ne)	2.5 ppm
Hydrogen–deuterium–oxygen	0.85 ppm
Krypton (Kr)	0.3 ppm
Xenon (Xe)	0.08 ppm

3.3.Surface Environment Conditions Of Mars

Spacecraft photos and altitude measurements have well-documented the nature of the Martian landscape. Mars has been photographed from orbit at a resolution of 20 meters, and selected locations have been imaged at a resolution of 30 centimeters or better (NASA, 2010). Mars Global Surveyor also had a laser altimeter on board, which measured all of Mars' surface elevations, averaged over a circle of 300 meters across to a vertical precision of 1 meter (D. E. Smith et al., 2001). This chapter discusses Mars's surface environment, including its radiation level, wind and dust storms, temperature, surface composition, seismic activities, and water existence.

3.3.1. Landscape conditions on Mars

Mars, despite its diminutive size, contains some enormous landscape features. Its most incredible impact basins, volcanoes, and canyons surpass anything on Earth, as seen in Figure 7 (National Air and Space Museum, 2021). In certain regions, the elevation difference between the southern highlands and northern lowlands surpasses six kilometers, equal to the distance between Earth's continents and ocean floors. How such a substantial northern plain evolved amid a ring of ancient cratered hills remains a mystery.

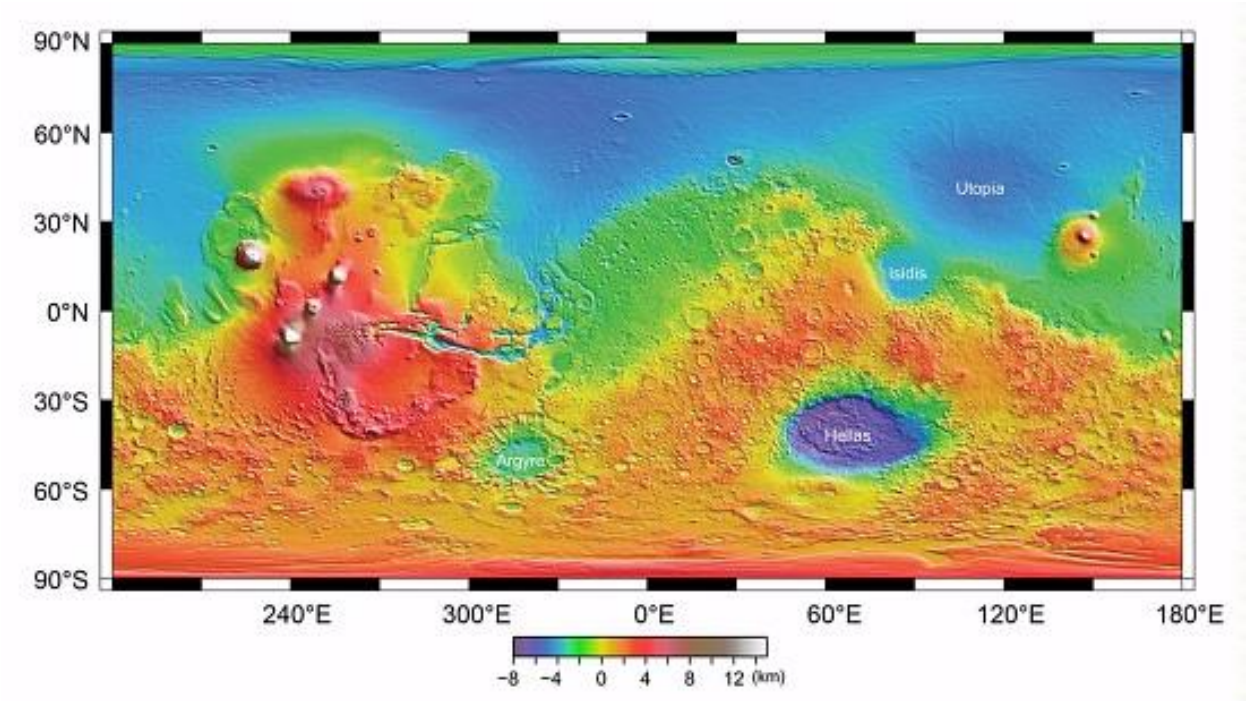

Figure 7. Topographic map of Mars (National Air and Space Museum, 2021).

Mars is home to some of the solar system's most significant impact basins. They were created when asteroids impacted Mars, ejecting material across many globes. The Hellas Basin is nearly 9 kilometers deep and 2,300 kilometers broad, making it Mars' largest exposed impact site. Utopia and Isidis Planitia are smooth-floored remnants of other vast ancient basins. Tharsis Rise is Mars's most massive volcanic and tectonic feature. Here, crustal elements have been dragged apart and forced

together to produce troughs and pushed together and buckled to form ridges. The largest of the solar system is certain Tharsis formations, such as the 26-kilometer-high Olympus Mons volcano and the Valles Marineris canyon system. Valles Marineris, named after the Mariner 9 spacecraft that first imaged it, reaches a depth of up to 8 kilometers and a length of 4,500 kilometers. The Grand Canyon might readily be squeezed into one of its tributaries.

3.3.2. Radiation level on the surface

Radiation is energy transmission through particles traveling through space at extremely high velocities. There are two types of radiation: ionizing and non-ionizing (Holmberg, 2010).

Radiation having enough energy to displace electrons from their orbits within atoms and produce charged particles is known as "ionizing radiation," which is considered for radiation protection (Holmberg, 2010). Gamma rays, protons, and neutrons are examples of ionization-capable radiation.

The definition of non-ionizing radiation is radiation that lacks the necessary energy to expel electrons from their orbits; for example, electromagnetic radiation encompasses radio waves, light, and microwaves. Unlike ionizing radiation, ion creation during typical chemical processes, such as salt generation from sodium and chlorine, is harmless and non-ionizing, whereas ionizing radiation is exceedingly hazardous (Holmberg, 2010).

Electromagnetic waves and other non-ionizing sources of radiation are mostly unrelated to the topic of radiation shielding in space; thus, we will not explore them further. The three most prominent sources of natural particle radiation in space are solar particle events (SPE), galactic cosmic radiation (GCR), and trapped radiation.

Numerous space agencies have conducted feasibility studies on human deep space exploration missions to our neighboring planet Mars. Since August 2012, the Mars Science Laboratory (Grotzinger et al., 2012) - Radiation Assessment Detector (MSL-RAD) onboard the Curiosity rover (Hassler et al., 2014) has been measuring the radiation environment on Mars. The Radiation Assessment Detector (RAD) is a Mars Science Laboratory equipment placed on the Curiosity rover. RAD is one of the first instruments to be deployed to Mars to prepare for human exploration in the future. RAD, about the size of a small toaster or a six-pack of soda, detects and characterizes all high-energy radiation on the Martian surface, including protons, energetic ions of various elements, neutrons, and gamma rays. This comprises direct radiation from the sun and space and secondary radiation from interaction with the Martian atmosphere, surface rocks, and soils. RAD has measured radiation exposure, its diurnal variation, heliospheric modulation, charged and neutral particle spectra, and zenith angle dependence on the Martian surface (Ehresmann et al., 2014; Guo, Zeitlin, Wimmer-Schweingruber, Rafkin, et al., 2015; Hassler et al., 2014; Köhler et al., 2014). It was the first instrument to provide particle spectrum and dose rate observations during a trip to Mars (Guo, Zeitlin, Wimmer-

Schweingruber, Hassler, et al., 2015; Zeitlin et al., 2013) and the surface measurements (Ehresmann et al., 2016). Rad collects data that can be used to compute the equivalent radiation dosage (a measure of the effect radiation has on humans) that would be present on the surface of Mars for future human exploration. As seen in Table 4, Hassler et al. (2014) published and discussed measurements of the absorbed dose and dose equivalent from galactic cosmic rays and solar energetic particles on the Martian surface for 300 sols (1 martian sol = 24 hours 39 min.) at the current solar maximum (Hassler et al., 2014). These data shed light on the radiation risks of a human mission to Mars' surface.

Table 4. Galactic cosmic rays and solar energetic particles on Mars's surface (Hassler et al., 2014).

	GCR dose rate (mGy/day)	GCR dose-equivalent rate (mSv/day)	SEP dose (mGy/event)	SEP dose equivalent (mSv/event)
MSL Cruise	0.464	1.84	1.2 to 19.5	1.2 to 19.5
Mars Surface	0.210	0.64	0.025	0.025

Based on Feynman and Gabriel (Feynman & Gabriel, 2000), the following table summarizes some of the most significant radiation effects caused by these particles of varying types and intensities. As illustrated in Table 5, high-energy GCR and SEP-induced radiation impacts are the primary issues for distant space missions outside Earth's magnetosphere and radiation belts, such as the Moon and Mars.

Table 5. Radiation levels from different sources and their effects on crewed Mars mission

Particle energy and type	Radiation effects	Sources
10–100 keV electrons	Spacecraft surface charging	Magnetospheric substorms and trapped particles
>100 keV electrons	Deep dielectric charging, and background counting in sensors and solar cell damage	Trapped magnetospheric particles
>1 MeV electrons	Ionization radiation damage	Trapped magnetospheric particles and SEPs
0.1–1 MeV protons	Surface damage to materials	Radiation belt and SEPs
1–10 MeV protons	Displacement damage in solar cells	Radiation belts and SEPs accelerated in shocks
>10 MeV protons	Ionization and displacement damage, background counting in sensors	Radiation belts and SEPs and GCRs
≳30 MeV protons	Biological damage to humans in deep space	Radiation belts and SEPs and GCRs
>50 MeV protons	Single-event effects	Radiation belts and SEPs and GCRs
>10 MeV/nuc ions	Single-event effects	SEPs and GCRs
≳150 MeV/nuc ions	Biological damage to humans on Mars	SEPs and GCRs

3.3.3. Wind and dust storms on the surface

Ground-based observers noted that albedo markings on Mars are often obscured and correctly attributed these changes to clouds within the martian atmosphere. Martian clouds are divided into yellow, white, and polar hoods (N. Barlow, 2014). Hazes, optically thin while clouds are optically thick, are often seen along the terminator, particularly along the sunrise limb, and observed from the surface landers (N. Barlow, 2014). These result from vapor condensation during the low nighttime temperatures. Early morning fog also is seen in low-lying areas such as the Valles Marineris canyon and inside impact craters.

Yellow clouds have been observed since 1877 and are now recognized as dust storms (N. Barlow, 2014). Dust is prevalent across the Martian surface because of the lack of liquid water and the range of geologic processes which have eroded surface rocks. Longitudinal differences in atmospheric pressure and temperature can produce strong winds capable of dust storms. Dust devil activity, which is more common in the southern hemisphere and extends from late spring to early fall (Fisher et al., 2005; Greeley et al., 2006), helps lift dust into the atmosphere (Basu et al., 2004; Kahre et al., 2006). Martian dust storms can be local, regional, or global, depending on the atmospheric conditions. Global dust storms typically occur near the perihelion in summer in the southern hemisphere. The more robust daytime heating associated with Mars' proximity to the Sun produces strong winds and dust devil activity which initiate dust storms. Cooling the surface under the dust storm leads to further temperature gradients and more wind, causing the dust storm to expand. According to NASA's Viking Lander data, the wind speed was measured between 2-7 m/s in summer, 5-10 m/s in fall, and 17-30 m/s during a dust storm (Miscio, 2018).

White clouds and hazes have been observed since the seventeenth century and are primarily composed of H_2O, although some CO_2 clouds have also been detected (Szantai et al., 2021). The white clouds clearly show on UV and blue filter images of Mars. Many white clouds are orographic clouds produced as the atmosphere is forced to higher altitudes where the lower temperatures allow condensation of the H_2O vapor. Ground-based observers in the seventeenth century often reported the presence of a W-shaped cloud in the western hemisphere of Mars (Szantai et al., 2021). Today we know that the W-shape cloud is an orographic cloud associated with the Tharsis volcanoes.

3.3.4. Temperature on surface

Gradients in pressure and temperature resulting from solar heating produce winds to reduce these gradients. Atmospheric pressure and temperature gradients result from three major factors: seasonal changes, dust storms, and diurnal variations (Wu et al., 2020). The seasonal changes result from the condensation and sublimation of CO_2 and H_2O from the polar caps. As noted above, dust storms can enhance the temperature gradient leading to stronger winds. The diurnal variations result from the temperature differences between the day and night sides of the planet and the presence of passing storm systems. The average temperature on Mars's surface environment is -63°C (NASA, 2021b). The temperature on Mars can be as high as 20°C in the equatorial zone or as low as about minus 153°C on the planet's pole (Park et al., 2020). However, the seasonal temperature change is critical. The temperature differential between day and night is also significant. The temperature can fluctuate at about +27°C and -133°C throughout the day and night (Royal Belgian Institute for Space Aeronomy, 2021).

3.3.5. Surface structure and analysis of the material composition

In 1963, the first radar echoes from Mars were received, and the method has since been employed during most following oppositions (Simpson et al., 1992). The round-trip echo flight time reveals the distance between Earth and Mars and the surface's topographic changes. The dispersion of the returned echo can be used to estimate surface roughness, and the strength of the echo can be used to constrain the surface's reflectivity. Radar observations can determine heights, slopes, textures, and materials.

The MARSIS (Mars Advanced Radar for Subsurface and Ionosphere Sounding) ground-penetrating radar reveals the underlying characteristics and structure of a 3–5km (Picardi et al., 2005; Watters et al., 2006). The dielectric constant of the underlying materials is constrained by the radar return's attenuation, allowing compositional differences to be mapped. According to preliminary results from the north polar cap, the summer (remnant) cap and much of the polar layered deposits are made of H_2O-ice. With a strong contrast in radar reflectivity matching the base of the layer of approximately 1.8km, MARSIS has revealed the thickness of the polar deposits. (Seu et al., 2004).

The ice character of the polar caps, extensive portions covered in dust mantles, abrasive lava flows, and indications that lava flows have infilled at least some channels were all shown by ground-based radar measurements (Harmon et al., 1999; Simpson et al., 1992). A region southwest of Tharsis that roughly corresponds to the Medusae Fossae formation shows little radar return (Harmon et al., 1999; Muhleman et al., 1995). The presence of large layers of fine-grained material in this "Stealth" zone is evidenced by radar data (Edgett et al., 1997). Radar data has been used to constrain surface

material qualities at potential landing locations and supplement information from circling spacecraft on surface roughness, rock abundances, and dust coatings (Golombek et al., 2003).

In-situ investigations can restrict individual landing locations' elemental and mineralogical compositions. The Viking 1 lander (VL1) in Chryse Planitia, the Viking 2 lander (VL2) in Utopia Planitia, the Mars Pathfinder (MPF) in the outwash zone of Ares Valles, the MER Spirit rover in Gusev Crater, and MER Opportunity rover in Meridiani Planum have all returned compositional data from the surface of Mars (N. Barlow, 2014). Spirit and Opportunity explored older portions of the planet, while VL1, VL2, and MPF landed in the younger, lower-elevation northern plains. Using X-ray fluorescence spectrometers, VL1 and VL2 studied the soil within reach of their robotic arms (N. Barlow, 2014). These findings revealed that the soil had higher Fe, S, and Cl concentrations than terrestrial continental soils. Despite the 4500-kilometer range between the two landers, the soil composition was very similar, owing to dust deposition. The dust collected by MPF, Spirit, and Opportunity was similar to that found at VL1 and VL2, implying that global dust storms homogenize the planet's soil (N. Barlow, 2014).

MPF was the first to examine rocks and find elements below VL1 and VL2 detection limits. The rocks were covered with Fe^{3+} dust coats and weathering rinds, making accurate rock compositions impossible to ascertain (R. v Morris et al., 2000). The MPF rocks appear andesitic in composition, having been generated by fractionating tholeiitic basaltic magmas during early mantle melting. Because the soil composition does not precisely match the nearby rocks, it is possible that the soils were formed by hydrous alteration of basalt combined with material coming from the andesitic rocks at the landing site (J. F. Bell et al., 2000).

Spirit and Opportunity have delivered the most comprehensive mineralogical investigation of surface minerals. The Mini-TES, APXS, and Mössbauer instruments and the Rock Abrasion Tool (RAT) for removing surface alteration rinds and the Microscopic Imager (MI) for examining rock and soil textures have provided substantial insight into the geologic development of the surface structure. The Spirit landing location was chosen for Gusev Crater based on a geomorphic study indicating that its bottom was covered by paleolake deposits (Golombek et al., 2003). Spirit spent 157 sols of its mission operating in its landing site's plains. The rocks and soils of the Gusev plains have been discovered to be not sedimentary in origin but instead formed from olivine-rich basaltic lava flows (Christensen et al., 2004; McSween et al., 2006; R. Morris et al., 2006). The composition is comparable to that of olivine-phyric shergottites but differs from that of basaltic and andesite-rich shergottites. Spirit moved out of the volcanic plains on sol 157 of the mission and into the elevated terrain known as Columbia Hills. The Columbia Hills are basalts, ultramafic sedimentary rocks cemented with sulfates, and other clastic rocks. The Columbia Hills rocks exhibit varying degrees of water modification, and several appear to be altered impact crater ejecta deposits.

Mars' color and albedo variations are dictated not only by composition but also by grain size. Terrestrial materials are classified based on size, ranging from dust to rocks. Martian materials are subdivided into rocks (pebbles, cobbles, and more considerable material), drift material (fine-grained and cohesive material, primarily composed of clay-sized particles), crusty-to-cloddy material (clay-sized grains weakly cemented by salts), and blocky material (composed of sand-sized and smaller grains which are firmly cemented by salts) (H. J. Moore & Jakosky, 1989). The sizes of surface materials at a specific location depending on that region's geologic processes. The uppermost layer of the surface, composed of the fragments produced by weathering processes, is called the regolith. The terms "regolith" and "soil" are often used interchangeably in planetary applications, although terrestrial geologists argue that biologic activity is an essential component of the composition and mixing processes of "soil." The martian regolith likely contains mixtures of soil and ice, particularly at the higher latitudes. The color of the martian regolith ranges from bright red dust to darker red and gray material. The color differences are primarily due to variations in iron mineralogy, degree of alteration, and particle sizes and shapes. The surface composition of Mars is shown in Tables 6 and 7, which indicate the analysis of the Mars Pathfinder lander (Rieder et al., 1997).

Table 6. Preliminary Results of Mars Pathfinder for Elements (Rieder et al., 1997).

Element	A-2, Soil weight %	A-4, Soil weight %	A-5, Soil weight %	A-3, Rock weight %	A-7, Rock weight %
Carbon [C]	-	-	-	-	-
Oxygen [O]	42.5	43.9	43.2	45.0	44.6
Sodium [Na]	3.2	3.8	2.6	3.1	1.9
Magnesium [Mg]	5.3	5.5	5.2	1.9	3.8
Aluminum [Al]	4.2	5.5	5.4	6.6	6.0
Silicon [Si]	21.6	20.2	20.5	25.7	23.8
Phosphorus [P]	-	1.5	1.0	0.9	0.9
Sulphur [S]	1.7	2.5	2.2	0.9	1.7
Chlorine [Cl]	-	0.6	0.6	0.5	0.6
Potassium [K]	0.5	0.6	0.6	1.2	0.9
Calcium [Ca]	4.5	3.4	3.8	3.3	4.2
Titanium [Ti]	0.6	0.7	0.4	0.4	0.5
Chromium [Cr]	0.2	0.3	0.3	0.1	0.0
Manganese [Mn]	0.4	0.4	0.5	0.7	0.4
Iron [Fe]	15.2	11.2	13.6	9.9	10.7
Nickel [Ni]	-	-	0.1	-	-
Sum	100.0	100.0	100.0	100.0	100.0

Table 7. Preliminary Results of Mars Pathfinder for Oxides (Rieder et al., 1997).

Oxide	A-2, Soil weight %	A-4, Soil weight %	A-5, Soil weight %	A-3, Rock weight %	A-7, Rock weight %
Na_2O	4.3	5.1	3.6	4.2	2.5
MgO	8.7	9.0	8.6	3.1	6.3
Al_2O_3	8.0	10.4	10.1	12.4	11.4
SiO_2	46.1	43.3	43.8	55.0	50.9
SO_3	4.3	6.2	5.4	2.2	4.2
K_2O	0.6	0.7	0.7	1.4	1.1
CaO	6.3	4.8	5.3	4.6	5.8
TiO_2	1.1	1.1	0.7	0.7	0.8
MnO	0.5	0.5	0.6	0.9	0.5
FeO	19.5	14.5	17.5	12.7	13.8

The regolith at the Spirit landing site in Gusev Crater generally consists of five components (Greeley et al., 2006). The topmost layer is a thin deposit (<1mm) of dust that has settled out of the atmosphere. This layer is underlain by a lag deposit of coarse sand and granules, a layer of subangular fragments more significant than a few millimeters in size. A cohesive crust ("duricrust") several millimeters thick is next, with a layer of dark soil forming the bottom of the regolith. Gusev Crater regolith displays many general characteristics as regolith at the MPF (McSween, H. Y. et al., 1998) and Viking landing sites (H. J. Moore & Jakosky, 1989), although the VL1 and MPF sites display more fine-grained drifts than either VL2 or Gusev. Martian soil-like deposits are similar to moderately dense soils on Earth. Table 8 lists some of the mechanical properties of soils at the three rover sites.

Table 8. Soil properties at the three rover sites.

	MPF (McSween et al., 1998)	Spirit (Squyres et al., 2004)	Opportunity (Squyres et al., 2004)
Friction angle	30°–40°	~20°	~20°
Soil bearing strength		5–200 kPa	~80 kPa
Cohesion	0–0.42 kPa	~1–15 kPa	~1–15 kPa
Angle of repose	32.4°–38.3°	up to 65°	>30°
Soil bulk density	1285–1581kg m^{-3}	1200–1500kg m^{-3}	~1300kg m^{-3}
Grind energy density		11–166 Jmm^{-3}	0.45–7.3 Jmm^{-3}

Analyzed average values of regolith's chemical compositions taken from various landers are shown in Table 9 (Ramkissoon et al., 2019). Martian regolith is primarily silicon dioxide (43.19 % by weight). Significantly differing, though, is the high content of metallic inorganic compounds; iron oxides are the next most abundant mineral at 18.09 wt%, followed by aluminum oxide at 9.12 wt%. The remaining composition comprises calcium oxide, magnesium oxide, sulfur trioxide, sodium oxide, and trace minerals.

Table 9. Martian Regolith Chemical Compositions (Ramkissoon et al., 2019).

Martian chemistries		Na_2O	MgO	Al_2O3	SiO_2	P_2O_5	SO_3	Cl	K_2O	CaO	TiO_2	Cr_2O_3	MnO	FeO	Total
Viking 1	The landing site, undisturbed fines	-	5.67	7.33	43.30	–	6.57	0.65	0.00	5.93	0.66	–	–	16.62	86.76
	the landing site, deep fines	-	6.00	7.25	44.00	–	6.70	0.80	0.04	5.70	0.63	–	–	15.74	86.86
Viking 2	the landing site, undisturbed fines	-	–	–	43.00	–	8.00	0.30	0.03	5.88	0.62	–	–	16.73	74.56
	the landing site, deep fines	-	–	–	42.00	–	7.75	0.35	0.00	5.50	0.51	–	–	15.56	71.66
Pathfinder	the landing site, Ares Vallis	1.09	8.69	7.98	42.30	0.98	6.79	0.55	0.61	6.53	1.01	0.30	0.52	20.06	97.41
	the soil next to yogi	3.20	8.00	10.60	41.00	1.20	6.90	0.80	0.50	5.60	1.00	0.40	0.40	18.35	97.95
	next to yogi	3.20	7.10	10.40	40.70	0.60	5.70	0.80	0.50	6.10	0.40	0.50	0.20	21.32	97.52
	disturbed soil next to scooby	2.60	6.40	10.20	41.70	0.80	6.60	1.20	0.70	6.40	0.80	0.20	0.10	19.97	97.67
Spirit	Gusev Crater	3.20	9.10	10.00	46.50	0.93	6.36	0.51	0.45	6.03	0.80	0.29	0.31	15.80	100.2
Opportunity	Meridiani Planum bright soils	2.31	7.62	9.21	45.33	0.91	7.23	0.81	0.50	6.66	0.99	0.34	0.36	17.59	99.86
	Meridiani Planum, Eagle crater	1.40	7.20	8.80	45.50	0.82	4.93	0.43	0.48	7.52	1.09	0.52	0.40	20.10	99.79
MSL	Rocknest Gale crater soil	2.72	8.69	9.43	42.88	0.94	5.45	0.69	0.49	7.28	1.19	0.49	0.41	19.19	99.85
Average of the global chemistry		2.47	7.45	9.12	43.19	0.90	6.58	0.66	0.36	6.26	0.81	0.38	0.34	18.09	94.86

Regolith is the principal construction material 3D printers will employ to create habitats on the Moon or Mars (M. Morris et al., 2016c). The material, which makes up most of both planetary bodies' surfaces, is called Lunar Regolith or Martian Regolith, depending on which astronomical body is discussed. Regolith comprises sands, powdered basalt, small rocks, and other loose surface particles. Their regolith structures resemble Earth's soil but lack nearly all water and known biological components. The lack of a hydrological cycle and an active climate has kept the Moon's and Mars's surfaces unchanged for millions, if not billions, of years. Covering habitats with regolith is a cheap and straightforward approach to ensure that habitats in harsh settings on the Moon or Mars are secure from radiation (M. Morris et al., 2016c). Radiation protection will be a critical step in assuring the physical safety of people living in extreme space environments. Many research studies have been conducted on creating a construction material based on regolith composition.

3.3.6. Seismic data of Mars

Unlike all previous Mars missions that explored Mars's geology, chemistry, and atmosphere in great detail, the task of Interior Exploration using Seismic Experiments, Geodesy, and Heat Transport (InSight) focuses on Mars' internal structure and processes (Giardini et al., 2020). At the end of 2018, InSight landed in a degraded crater at Elysium Planitia on a smooth, sandy, granular-and pebble-rich surface with few rocks. Elysium Planitia is Mars' second-largest volcanic zone. It is 1,700 by 2,400 km in size and is situated on an inverted dome. The InSight research aims to assess the evolution of terrestrial planets by studying Mars' internal structure and processes and establishing the present degree of geological movements and influence intensity on Mars. In a short time following its landing, NASA's InSight Mission installed a seismic instrument SEIS (Seismic Experiment for Internal Structure), a seismometer on the Mars surface, fitted with a long-period three-axes Very Broad Band (VBB) instrument and a three-axis short-term (SP) instrument. Since SEIS's seismometer records accelerations traveling into the shallow subsurface.

On Earth, tectonic plate movement causes earthquakes. However, there are no tectonic plates on Mars, and the planet's crust is a massive plate (Andrew et al., 2021). NASA notes that 'marsquakes' are created by forces that result in rock fractures or crustal faults (Andrew et al., 2021).

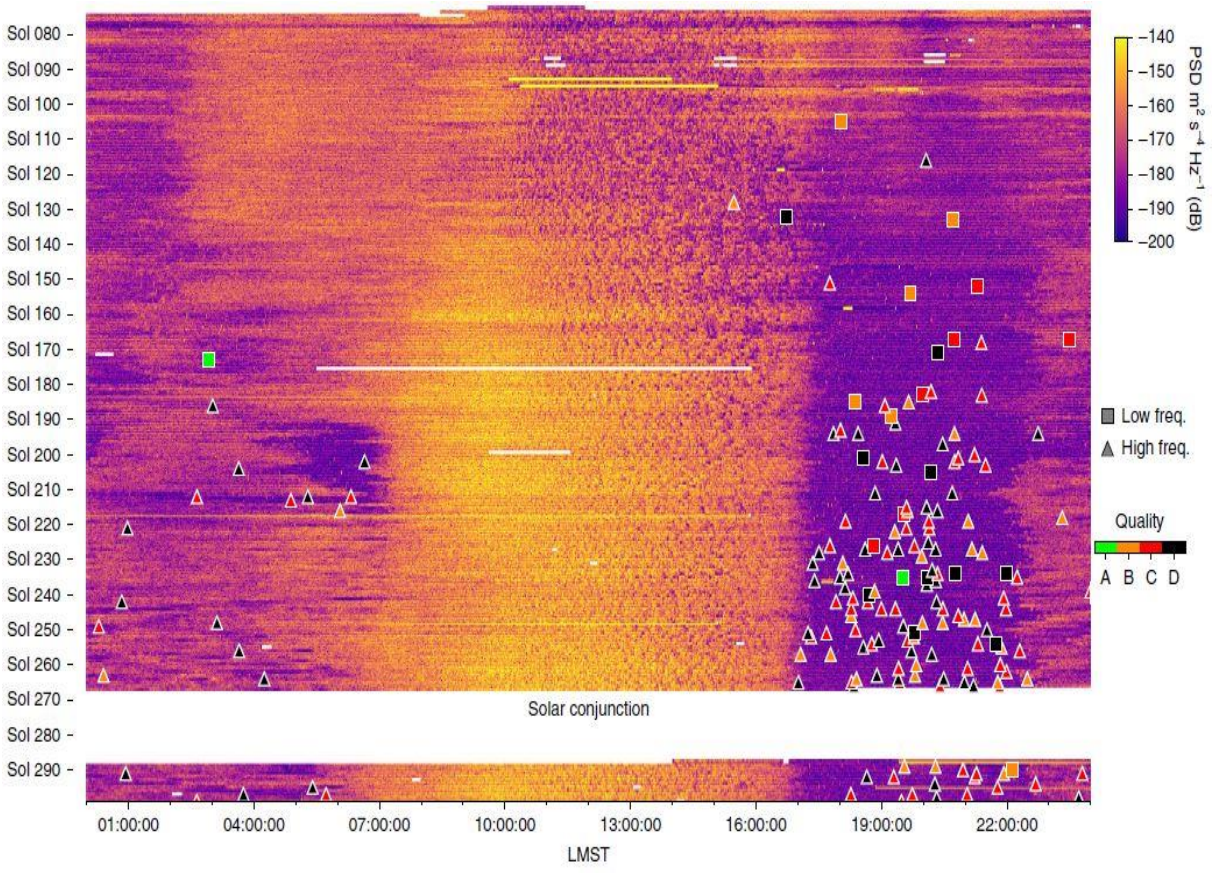

Figure 8. Seismic activities on Mars between Sol 72 and 299 (Giardini et al., 2020).

In the first ten months since its research operations began in February 2019, 174 possible Martian quakes have been identified by the seismometer of SEIS from InSight. In 2020, Giardini, D., Lognonné, P., Banerdt, W.B. et al. published an article to represent the seismicity of Mars's surface by analyzing recorded data from the Insight mission (Giardini et al., 2020). In Figure 8, 174 events were identified as Marsquake between Sols 72 and 299 and were categorized into two major categories: (1) low-frequency (LF) events with an energy content generally below 1 Hz; (2) high-frequency (HF) events with an energy content above 1 Hz, up to 612 Hz. 24 LF and 150 HF events are included in the 174 events recorded up until Sol 299. In the spectrogram stack, each horizontal line corresponds to a sol-long acceleration spectrogram from 20 s to 4 Hz for the vertical VBB component. White spaces indicate data gaps (Giardini et al., 2020). The results released by researchers from the Max Planck Institute for Solar System Science (MPS) in Germany provide the first detailed confirmation that Mars is seismically active, like Earth and Moon. However, Mars lags far below Earth in terms of the magnitude and intensity of the quakes. No quakes reached a magnitude of 4. More than 1,313 seismic activities have been recorded by InSight since its landing on Mars in November 2018 (NASA Jet Propulsion Laboratory, 2022). As of August 25, 2021, the most significant quake recorded was 4.2.

On May 4, 2022, the 1,222nd Martian day, or sol, the InSight Mars lander recorded the strongest quake with an estimated magnitude of 5.0, as shown in Figure 9, ever observed on Cerberus Fossae is distinguished by its fractured surface and frequent rockfalls (NASA Jet Propulsion Laboratory, 2022).

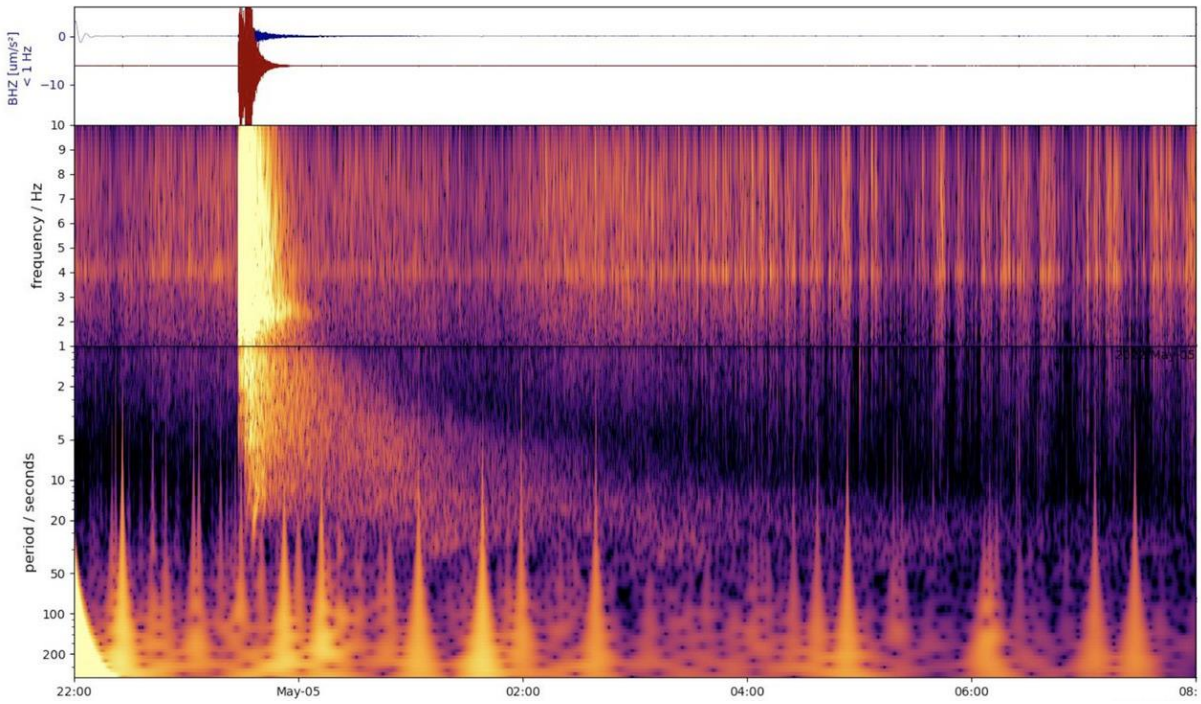

Figure 9. The spectrogram of the biggest Marsquake (NASA Jet Propulsion Laboratory, 2022).

An earthquake with a magnitude of 5.0 is considered a large earthquake on Earth, but it is very close to the upper limit of what scientists expected to experience during the InSight mission on Mars (NASA Jet Propulsion Laboratory, 2022). The seismogram depicted in Figure 10 indicates that the highest ground velocity of seismic events is around 1.2 x 10^{-5} meters per second, which is a shallow velocity for audibility by humans.

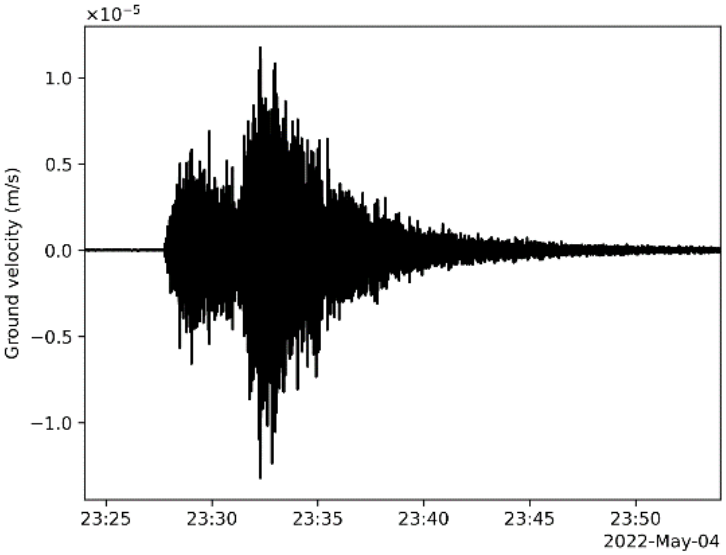

Figure 10. The seismogram of the biggest Marsquake (NASA Jet Propulsion Laboratory, 2022).

3.3.7. Existence of water

A stable form of pure liquid water cannot exist on Mars due to the planet's low temperature and pressure (Martínez & Renno, 2013). However, short periods may see water at the lowest elevations (Nazari-Sharabian et al., 2020). Geological mysteries began to emerge in 2006 when the Mars Reconnaissance Orbiter observed the presence of gully deposits that had not been seen for ten years (Nazari-Sharabian et al., 2020). Gullies on the surface of Mars may be the result of liquid brine flowing on the surface during the hottest months of the year.

Five locations have been identified where pressure and temperature conditions may allow liquid water to exist for short periods (37 to 70 sols): between 0° and 30°N in Amazonis, Arabia, and Elysium Planitia, and in the Hellas and Argyre impact basins (Haberle et al., 2001). Whether liquid water occurs in these regions is uncertain, mainly since there is only a weak correlation between these areas and the distribution of near-surface H_2O from GRS. However, the salt-rich nature of the martian soils, as determined by the surface landers and rovers, suggests that H_2O brines may exist on the surface for short periods.

Scientists debate whether liquid water can form gullies (Head et al., 2008; J. Heldmann et al., 2005; Malin et al., 2006). There is also a possibility that the flow carving gullies are composed of dry grains or that they have been lubricated by carbon dioxide. According to certain studies, gullies are generated by melting carbon dioxide throughout the summer. Although it is believed that water moving across the planet's surface created gullies, the source of the water and the mechanics by which it moved remain unexplained. Certain studies assert that unfavorable conditions preclude gullies'

creation by water in the southern highlands. While the non-geothermal low-pressure cooler zones would be excellent for solid carbon, they would never provide suitable conditions for liquid water.

Mars's surface features deep channels, which appear to be cut into various slopes and are referred to as dry gullies. However, some of them fluctuate according to the season. NASA announced in August 2011 the present seasonal fluctuations in Mars' southern hemisphere, on the steep slopes beneath the rocky outcrops along the rims of craters (Garcia-Chevesich, P., Bendek, E., Pizarro, R., Valdes-Pineda, R., Gonzalez, D., Bown, H., Martínez, E. and Gonzalez, 2017). Increased temperatures on certain summer days cause these black streaks, dubbed recurrent slope lineae (RSL), to flow downslope; subsequently, as the temperature drops during the year, they gradually fade away; this process recurs cyclically between years. Scientists hypothesized that these marks were caused by salty water flowing downslope (brines) and deposited by evaporation. In 2015, researchers established that these lineae are formed by liquid brines running through shallow soils (Hoffman, 2002; Kolb et al., 2010; Malin & Edgett, 2000; Mcewen et al., 2011; Musselwhite et al., 2001). They reported that they detected hydrous salts forming concurrently with the formation of repeated slope lineae using the CRISM spectroscopic equipment. The lineae are perchlorate salts, hydrated chlorate (ClO_4^-), and liquid water molecules. When the temperature on Mars exceeds -23°C, the lineae descend. However, the source of the water remains unknown. Nonetheless, over ten years, the Mars Odyssey orbiter's neutron spectrometer data revealed no evidence of water (hydrogenated regolith) at the active spots; however, two plausible explanations are advanced: first, short-lived atmospheric water vapor deliquescence; and second, dry granular flows. Even if evidence of liquid water exists on Mars today, it is merely a thin coating and traces of moisture that have dissolved from the atmosphere, rendering the climate unsuitable for life as we know it.

Mariner 9, 1971: The earliest clear evidence that Mars formerly had water comes from dried river beds and canyons discovered in photos taken by the Mariner 9 Mars probe following its launch in 1971 (Hanel et al., 1972). These photos comprise around 4020 kilometers of canyons in the Valles Marineris system. Mariner 9 discovered weather frons, fogs, water erosion, and water deposits (Hanel et al., 1972). The vast Valles Marineris canyon system was named in honor of Mariner 9's accomplishments, and the following Viking program was based on the Mariner 9 mission’s discoveries.

Viking Program, 1976: The investigators discovered extensive outflow canals in various locations (Farmer et al., 1977). These were evidence of dams being breached by floodwaters, which etched grooves into the bedrock, created deep valleys, and traveled thousands of kilometers. The rainfall on Mars's surface can be inferred from valley networks that branch out across extensive sections of the planet's southern hemisphere. When the two landers and two Viking orbiters identified several geological formations that require substantial amounts of water to develop, a paradigm shift in our understanding of water on Mars occurred. Craters typically resemble mud shapes after being

struck by impactors. During their development, soil ice most likely melted, converting the soil to mud and causing mud to flow across the surface. Downstream, "Chaotic Terrain" was formed when a vast amount of water was quickly lost.

Additionally, Chaotic terrains are irregular to circular fractured areas made of jumbles of blocks ranging in size and shape from knobs and irregular conical mounds to angular mesas with preserved remnants of the upland plateau; they are frequently found in enclosed to semi-closed depressions surrounded by fractured highlands. The predicted flow rates of some channels exceed 10 thousand times that of the Mississippi River. One explanation is that subterranean volcanism thawed the ice, causing water to flow away and crumble the ground, resulting in a chaotic environment. Additionally, the two Viking landers, using comprehensive chemical analyses, have revealed that the planet has been exposed to water on its surface or submerged in water.

Mars Global Surveyor, 1996: The Thermal Emission Spectrometer (TES) on the Mars Global Surveyor could allow us to figure out better what kind of minerals are on the surface of Mars (Nelson, 2015). This data can help us figure out how much water has been on Mars in the past and how much water is still there. It also examined how Nili Fossae, made up of the mineral olivine, formed. Between 60 degrees south and 60 degrees north, scientists have found olivine in a few small places on Earth (Nelson, 2015). The probe also shows that there may have been steady liquid flows in the past, two of which could be in Nanedi Valles and Nirgal Vallis (Nelson, 2015).

Mars Pathfinder, 1996: The mission of Mars Pathfinder was to document the thermal changes that happen during the day and night on Mars (J. Schofield et al., 1998). The coldest period in the cycle was before sunrise, with a temperature of about -78 °C. The warmest period was just after noon on Mars, at about -8 °C. The highest temperature was always lower than the water's freezing point, so it would be too cold for a pure liquid to exist on the surface at that temperature. Pressure on Mars was found to be very low by the Pathfinder lander. It found that it was only about 0.6 percent of that on Earth. This pressure is insufficient for pure, liquid water to exist on the planet's surface.

Several observations support the historical presence of water on Mars. For example, several of the rocks in the locations investigated by the Mars Pathfinder were imbricated, implying the presence of water in the past. The researchers hypothesized that significant flooding pushed rocks aside from the water flow in the past. Additionally, rounded stones were discovered that were possibly tumbled in a stream. Additionally, the ground regions were crusty, possibly due to cementing from a mineral-containing fluid. Additionally, the Pathfinder discovered cloud and possibly fog evidence.

Mars Odyssey, 2001: The 2001 Mars Odyssey's images revealed numerous indicators of water on Mars, and its neutron spectrometer detected considerable amounts of water ice on the ground (Nazari-Sharabian et al., 2020). Mars's surface is covered in enough ice to fill Lake Michigan twice. Ice with a high density can be found in both hemispheres of the planet, near the ground, from

latitudes of 55° to the poles. One kilogram of soil contains about 500 grams of water ice. However, only 2%–10% of soil contains water near the equator. According to researchers, a large quantity of this water gets trapped in the chemical structure of minerals such as clay and sulfates. The planet's upper surface contains just a minimal quantity of chemically bound water, but ice can be found just a few meters underground; for example, the Arabia Terra, Amazonis, and Elysium quadrangles have significant amounts of water ice.

The orbiter near the planet's surface revealed enormous bulk water ice in equatorial regions. The Medusae Fossae formation and the Tharsis Montes both have equatorial hydration morphological and compositional levels. There are hints of a layered structure in the southern hemisphere based on data analysis of stratified deposits located beneath a massive water mass that has since vanished. The top meter of soil information was gathered using the Mars Odyssey's instruments. Calculations based on existing data in 2002 indicated that a layer of water covering all soil surfaces would be similar to a 0.5–1.5 km deep global layer of water (GLW).

Calculations based on existing data in 2002 indicated that a layer of water covering all soil surfaces would be similar to a 0.5–1.5 km deep global layer of water (GLW). Numerous photos taken by the Odyssey spacecraft reveal that significant volumes of water formerly flowed across the surface of Mars. Layers formed under lakes can be identified from the photos, as can patterns of branching valleys and river and lake deltas. Scientists assume glaciers existed for many years under an insulating rock layer. Lineated valley fill, which occurs on the floors of some channels, is an excellent example of rock-covered glaciers. These surfaces are ridged and grooved, deflecting material away from impediments. Orbiting radar has revealed a potential connection between lineated floor deposits and lobate debris aprons containing significant amounts of ice.

Phoenix, 2007: The Phoenix lander discovered indications of significant water ice on Mars's northern polar regions. On June 19, 2008, NASA stated that small fragments of bright materials in the "Dodo-Goldilocks" trench, an area excavated by the lander's robotic arm, had vaporized (Nazari-Sharabian et al., 2020). Since the substance melted over four days, it was determined that the fragments were most likely made of ice and sublimated due to exposure. While solid CO_2 (dry ice) is also sublime under identical conditions, the assertion of water ice sublimation cannot be ignored, as the former sublime faster than the bright substance. On July 31 of the same year, NASA stated that more confirmation of water ice at the Phoenix landing site had been made. The lander took a sample, and when the material temperature reached 0°C., vaporization happened. Due to Mars's low temperature and air pressure, liquid water can only survive briefly at the lowest elevations.

Because of the retrorockets, soil and melted ice were splattered into the vehicle during the Phoenix's landing. The exposed material expanded, reminiscent of deliquescence, becoming darker before disappearing, as happens when something liquefies and drops. The thermodynamic data and

these observations showed that the substance was likely liquid brine droplets. Other scientists referred to this substance as "clumps of frost."

The landing site appeared to be flat from the camera's perspective. However, several polygons looked to be bordered by 20–50 cm deep troughs. Polygons are primarily generated due to the expansion and contraction of ice in the soil caused by significant temperature fluctuations. On top of the polygons, which can be considered a type of clay, rounded and flat particles can be observed in a microscope as the main components of the soil. A thin layer of ice exists in the center of the polygons and beneath their surface, but the ice thickness along the polygons' edges exceeds 200 mm.

Additionally, Cirrus clouds originated in the atmosphere at a temperature of approximately -65°C and are believed to be the origin of snowfall. As a result, water ice made up most clouds rather than carbon dioxide ice (CO_2 or dry ice), requiring a temperature of less than -120 ° C to develop. Researchers now suspect that water ice (snow) may have collected at this site later in the year due to the mission data. The most extraordinary temperature recorded on Mars throughout the mission was -19.6 ℃, while the lowest was -97.7 ℃. As a result, this region's temperature never surpassed the freezing point of water (0 ℃). Recent research indicates that shallow transitory liquid water, likely abundant on today's Mars, may be capable of supporting life. Additionally, areas of the shallow subsurface of Mars can sustain microbial life.

Mars Exploration Rovers, 2003: Spirit (June 10, 2003) and Opportunity (July 8, 2003) of the Mars Exploration Rovers uncovered substantial evidence of water on Mars in the past (Nazari-Sharabian et al., 2020). The area where the Spirit rover landed is believed to have been a large lake bed in the past. It was initially challenging to discover indications of water in the past due to the lake's concealment by lava flows. On March 5, 2004, NASA announced that the Spirit had uncovered evidence of Mars' water history in a rock named "Humphrey." An investigation of the rock thoroughly revealed a brilliant material filling internal fissures. Such material may have crystallized due to water seeping through the volcanic basalt. The amount of ancient water that covered Mars in the past is unknown, as both rovers landed in previously regarded aquatic zones. In December 2007, the rover's wheels gradually scraped the top layer of soil, revealing some white silica-rich terrain. Scientists are aware of only two possible mechanisms for producing white silica-rich ground: dissolving silica in one location and transferring it to another (i.e., a geyser) or silica being left behind after acidic streams depleted mineral components in rock cracks. The Spirit rover may indicate water in the Columbia Hills of the Gusev Crater. The Mössbauer spectrometer (MB) identified many components in Clovis rocks, including goethite, which can only form in water; an oxidized form of iron (Fe^{3+}); and carbonate-rich rocks, which indicate the presence of water in some regions of the planet.

A considerable amount of hematite was visible from orbit at a location where the Opportunity rover was headed. The rover also discovered hematite concretions and marbleized

layered rocks. Opportunity explored aeolian dune stratigraphy on its traverse in the Burns Cliff area of Endurance Crater. Opportunity operators recognized that shallow groundwater was critical in preserving and cementing the outcrops. The rover's years of continuous operation revealed that the area on Mars had been submerged in liquid water.

The MER rovers confirmed the presence of highly acidic ancient wet conditions. Opportunity uncovered sulfuric acid evidence, indicating that the planet's climate is harsh for life. However, NASA revealed on 17 May 2013 that the discovery was made in clay deposits that typically form in moist conditions with neutral acidity. The revelation provided additional evidence for an ancient wet environment, which probably created a suitable environment for life.

Mars Reconnaissance Orbiter, 2005: The Mars Reconnaissance Orbiter's HiRISE instrument acquired many photos showing that water-related activities have occurred on Mars in the past (Nazari-Sharabian et al., 2020). Its first discovery was an indication of ancient hot springs. If Mars once supported microbial life, detecting their biosignatures is a possibility. In January 2010, researchers discovered significant evidence for continuous precipitation at Valles Marineris. They established a link between minerals and water.

Additionally, significant precipitation is forecast due to small branching channels with a high density in that location. On Mars, rocks are often arranged in layers, referred to as strata, in various locations. These strata can be generated in various ways, including through wind, volcanoes, or water. The majority of the light-toned rocks on Mars are composed of hydrated minerals such as clay and sulfates. The orbiter confirmed that Mars' surface is covered by a thick, smooth mantle composed of ice and dust.

Climate change on a large scale is thought to be one of the primary causes for Mars' shallow subsurface having an ice mantle. As one descends from the polar regions to latitudes comparable to Texas on Earth, significant changes in the water ice distribution can be seen, induced by changes in the planet's tilt and orbit. Water vapor rises from polar ice during particular climates and returns to the ground as snow or frost mixed with dust at lower latitudes. Researchers discovered evidence in 2008 that the lobate debris aprons (LDA) in Hellas Planitia and mid-northern latitudes are glaciers covered in a fine layer of rocks.

A strong reflection was detected by its radar from the top and bottom of the LDAs, implying that most of the formation is composed of pure water. Given the discovery of water ice in the LDAs, it is believed that water can also be found in lower latitudes. In September 2009, it was reported that several fresh craters on Mars had revealed pure water ice. After a while, the ice vanishes and melts into the atmosphere. The Mars Reconnaissance Orbiter's Compact Imaging Spectrometer (CRISM) confirmed the presence of ice.

In 2019, researchers determined the amount of water ice at the north pole. In one study, scientists incorporated data from the MRO's SHARAD (SHAllow RADar sounder) probes. SHARAD can scan up to about two kilometers beneath the surface at intervals of 15 meters. When previous SHARAD runs were studied, clues about the water ice strata and sand beneath the Planum Boreum were acquired. The Planum Boreum's volume contains around 60% to 88 % water ice. The findings corroborated the theory of Mars' long-term global weather, which includes cycles of global warming and cooling; during cooling periods, ice layers formed at the poles as a result of accumulating water; and during global warming, dust and dirt from Mars' recurrent dust storms coated the unthawed water ice. According to this study, the ice volume was around 2.2 x 105 cubic kilometers, required to cover Mars' surface entirely with 1.5 m of water. A subsequent study that used gravity data to assess the density of Planum Boreum confirmed this work, revealing that up to 55% of the volume was made up of water ice on average.

Curiosity Rover, 2011: At the start of its mission, NASA's Curiosity rover found unmistakable sediments washed away by water (Nazari-Sharabian et al., 2020). A streambed with water between the waist and ankle-deep was expected to have a strong flow at some point in the past because of the characteristics of the pebbles in these outcrops. These rocks were found at the bottom of an alluvial fan system from a crater wall, even though they were already seen from space. The soil in the tested sample was like the basaltic soil found on Hawaiian volcanoes after it had been eroded. NASA announced that sulfur, chlorine, and water molecules were found in the soil of Mars in December 2012, when Curiosity began its first long-term soil analysis. Also, from the broken pieces of "Tintina" rock and "Sutton Inlier" rock, as well as the nodules and veins in other rocks like "Knorr" rock and "Wernicke," NASA said in March 2013 that they had found clues about mineral hydration, which was most likely hydrated calcium sulfate.

The DAN instrument on the rover was used to see if water was below the surface. In the analysis, researchers found water below the surface around the rover, from the Bradbury Landing site to the Yellowknife Bay area, down to 60 cm. The Curiosity rover took soil samples from the Aeolis Palus in the Rocknest region of the Gale Crater and found a lot of chemically-bound water (1.5 to 3 weight %). NASA scientists announced this on September 26, 2013. NASA also found two main types of soil: a coarse-grained felsic type and a fine-grained mafic type. Like other soils and dust on Mars, the basaltic type was caused by water in the soil's formless parts. Scientists found perchlorates near where the Curiosity rover landed, making it harder to find organic molecules that could be linked to life.

According to a NASA report from December 9, 2013, a large freshwater lake was once inside Gale Crater, so it may have made microbial life possible. On December 16, 2014, NASA reported that methane levels in Mars' atmosphere had changed unusually. The Curiosity rover also found organic chemicals in a sample drilled from a rock. Before the lakebed in Gale Crater on Mars was formed, much

water was lost at Gale Crater on Mars. According to studies into the deuterium-to-hydrogen ratio, the water loss persisted over time. Researchers analyzed the ground temperature and humidity data returned by Curiosity. They discovered that liquid brine water formed layers in the upper five centimeters of Mars' subsurface during the night. As a result, temperature and water activity continued to be lower than the minimum values that microorganisms need to reproduce or break down food for their bodies.

Additionally, based on the deuterium to hydrogen ratio measurements, it was determined that a significant amount of water was lost at Gale Crater on Mars in ancient periods; before the formation of the lakebed in the crater, loss of vast amounts of water persisted over time. Researchers reviewed Curiosity's ground temperature and humidity data and discovered evidence for producing layers of liquid brine water in the upper five centimeters of Mars' subsurface throughout the night. However, temperature and water activity remained below the minimum values required for reproducing or metabolizing Earth's microbes. On October 8, 2015, NASA confirmed that the Gale crater existed approximately 3.3–3.8 billion years ago. This crater shaped Mount Sharp's lower levels by transporting sediments. Geologists presented abundant water on early Mars on November 4, 2018, following Curiosity rover investigations in Gale Crater.

Mars Express, 2003: The European Space Agency launched the Mars Express Orbiter to look for signs of subsurface water (Nazari-Sharabian et al., 2020). The orbiter employs radar equipment to survey Mars' surface. Between 2012 and 2015, the Orbiter investigated the area under Palnum's ice caps for signs of subsurface water. According to the data, before 2018, experts have proved the existence of an approximately 20-kilometer-wide underground lake containing water. While the lake's upper location, approximately 1.5 kilometers beneath the planet's surface, is known, its depth is unknown.

3.4.Analysis of landing sites for a future Mars habitation

This section explains different approaches from the literature to select a landing and research site on Mars surface for a future crewed mission to outline the site selection criteria from different perspectives. The section includes an overview of NASA's site selection workshop series for the 2020 Mars rover landing, a plant-based site selection research study conducted at Wageningen University & Research (WUR), an ice mapping methodology conducted by a team of Subsurface Water Ice Mapping (SWIM) at The Planetary Science Institute (PSI) to define optimum site selection and a research study at MIT for developing software tools that can assimilate large amounts of geologic and other data of Mars to more quickly assess site feasibilities all over the planet.

3.4.1. NASA: 2020 Mars rover landing site workshop

The Mars 2020 Perseverance Rover mission used intensive scientific criteria to evaluate prospective landing locations over four workshops (NASA Science, 2022c). This workshop series aims to identify and discuss potential landing sites for humans to land, work, and live on Mars for a future crewed mission and select a final landing site for The Mars 2020 Perseverance Rover mission (NASA Science, 2022c). The exploration zone's scientific value and resource base are essential to the success and viability of the crewed mission on Mars. The research location should meet all crew requirements and have valuable locally available resources that can be exploited to maintain the crew during extended surface stays. NASA has identified 46 possible landing sites for robots and humans (Grant et al., 2018).

Between May 14-16, 2014, the first landing site workshop was held to narrow the field of possible landing sites down to 27 candidates (Grant et al., 2018). Following that, a second workshop was organized from August 4-6, 2015, during which participants defined eight advanced landing location candidates (NASA Science, 2022i). They focused on two fundamental issues:

- Which locations will allow scientists to learn the most about Mars's previous life?
- Which locations provide the best opportunity for engineers to land safely and move the rover?

According to scientists, the optimal location for the rover is one where water has saturated the ground for an extended period throughout Mars' ancient history. Scientists and engineers assessed eight landing sites(NASA Science, 2022i). Several of these previously waterlogged areas were formed by bubbling subsurface springs. Others were formed as rain-fed rivers filled craters. The following described eight locations on Mars that had been chosen for detailed analysis to limit the list to three alternate destinations in the 2017 workshop (Grant et al., 2018).

Gusev Crater's Columbia Hills: Home to the Mars Rover Spirit: Mineral springs previously gushed forth from the Columbia Hills' rocky formations (NASA Science, 2022i). The discovery of flowing

hot springs was a significant accomplishment of the Mars Exploration Rover Spirit. Spirit's discovery was a pleasant surprise, as Spirit had previously discovered no evidence of water anyplace else in the crater's 100-mile-wide (160-kilometer-wide) Gusev Crater. Following the rover's deactivation in 2010, analyses of its earlier data revealed indications of previous floods that may have generated a shallow lake in Gusev.

A Delta Within a Delta, Eberswalde: This crater was formed by a large body of water, which left dry lake bottom deposits (NASA Science, 2022i). The crater was a top choice for the Mars Exploration Rovers' landing site. Scientists continue to choose this area due to an ancient delta at the mouth of a Martian river. Deltas form only in areas with water for an extended length of time. A network of well-preserved water-flow features, including twisting stream channels and riverbeds, remains here. In these streambeds, water-deposited sediments have solidified and have resisted wind erosion. As a result, some streambeds in this area are elevated above the surrounding landscape. The clays discovered here were formed by water reacting with volcanic rock. Clay minerals are a critical indicator of a wet history and can preserve any indications of life for an extended period.

Shaking and Stirring the Holden Crater: Holden Crater was formed and shaped by violent impacts and fluid flows (NASA Science, 2022i). Scientists have identified the ancient impact crater as a possible location for microbial life to have existed. At some point, perhaps during a significant flood, the rim of the water-swollen crater collapsed. Water rushing out of the shattered crater rim eroded layers of material, exposing even older clay strata from an earlier lakebed. That older lake may have lasted for thousands of years, long enough for microorganisms to establish a foothold. The clays may include traces of life.

Jezero Crater: Wet, Dry, and Wet Once More: Jezero Crater provides insight into Mars' wet past's on-again, off-again character (NASA Science, 2022i). River channels burst over the crater wall and formed a lake more than 3.5 billion years ago. After the lake dried up, scientists believed that water carried clay minerals into the crater. Microbial life may have existed in Jezero during one or more rainy periods. If this is the case, evidence of their existence may be discovered in lakebed sediments.

Mawrth Vallis: A Mysterious Source of Water: Orbiting spacecraft take images of the Martian river channels' sources (NASA Science, 2022i). The images provide valuable insight into how ancient lakes were initially filled with water. The valley contains numerous minerals that have been altered by water; however, the minerals do not reveal the water source, but a strange channel appears. The channel excavated the clay deposits regardless of the source of the water. These clay deposits may include traces of microbial life from the distant past.

NE Syrtis: Once Warm and Wet: Underground heat sources were responsible for the flow of hot springs and the melting of surface ice (NASA Science, 2022i). Microbes could have thrived in this

environment due to minerals in the liquid water. The stratified surface of NE Syrtis has a wealth of information on the interactions between water and minerals during early Mars's history.

Nili Fossae: A Profusion of Minerals and a Small Quantity of Methane: Enormous natural forces sculpted Nili Fossae (NASA Science, 2022i). Collisions pounded its surface. Shifting tectonic faults resulted in the collapse of large surface sections, resulting in valley formation. The water affected the chemical and mineral composition of the rocks in this area, resulting in clays and rocks with high silica content. Geologists are interested in determining whether these changes contain evidence of previous life. Telescopes on Earth have identified signs of potential methane in the atmosphere around Nili Fossae. Methane can be produced naturally (e.g., through volcanic eruptions) or by living organisms. The source of that methane is unknown to scientists.

SW Melas: A Section of the Solar System's Largest Canyon: What is concealed behind the layers of ancient SW Melas's lakebed and shores? Previously, this basin was home to a lake or delta (NASA Science, 2022i). Its water reacted with a diverse array of minerals found on the surface. Volcanic ash layers are interlaced with layers of clay. Water deposited the clays, which were created from eroded rock fragments. This historically wet, volcanic environment may include traces of previous microbial life.

The third workshop, held in Monrovia, California, on February 8-10, 2017, gathered 240 attendees and up to 60 online participants (NASA Science, 2022c). Attendees in the workshop selected three areas for future examination. Northeast Syrtis (a very ancient region of Mars' surface), Jezero crater (formerly the site of an ancient Martian lake), and Columbia Hills (possibly the site of an ancient hot spring investigated by NASA's Spirit rover) were the three proposed landing sites for NASA's Mars rover.

In Glendale, California, the fourth and last Mars 2020 rover landing site workshop took place between 16 to 18 October 2018 (NASA Science, 2022c). After a five-year assessment of alternative locations, each with distinctive traits and attractions, Jezero emerged as the winner (NASA Science, 2022c). Jezero Crater is 45 kilometers wide and is located on the western margin of Isidis Planitia, a flat plain lying slightly north of the Martian equator (NASA Science, 2022h). The landing spot is approximately 3,700 kilometers from Curiosity's Gale Crater landing site (NASA Science, 2022h).

Jezero Crater, as seen in Figure 11, reveals the on-again, off-again dynamic of Mars' wet past. River channels burst over the crater wall more than 3.5 billion years ago, forming a lake (NASA Science, 2022h). Thus, Jezero Crater was likely livable in the distant past. The CRISM sensor onboard the Mars Reconnaissance Orbiter discovered that the crater contains clays, which develop only in water (NASA Science, 2022h). Jezero Crater is an excellent location for the Mars 2020 mission's science objective of researching a potentially livable environment that may still contain evidence of previous life (NASA Science, 2022h).

Figure 11. Jezero Crater as Seen by ESA's Mars Express Orbiter (NASA Science, 2022h).

3.4.2. WUR: Plant-friendly Mars landing locations

Choosing the optimal landing site is critical to the success of the first Mars settlement. One of the astronauts' primary responsibilities will be to grow food for a sustainable solution. Wageningen University & Research scientists have identified locations on Mars where plant species can thrive (Wamelink, 2018). Although plants will be cultivated indoors, regolith and ice will be employed. Wieger Wamelink and his student Line Schug created a three-dimensional map of Mars from the standpoint of plants (Wamelink, 2018).

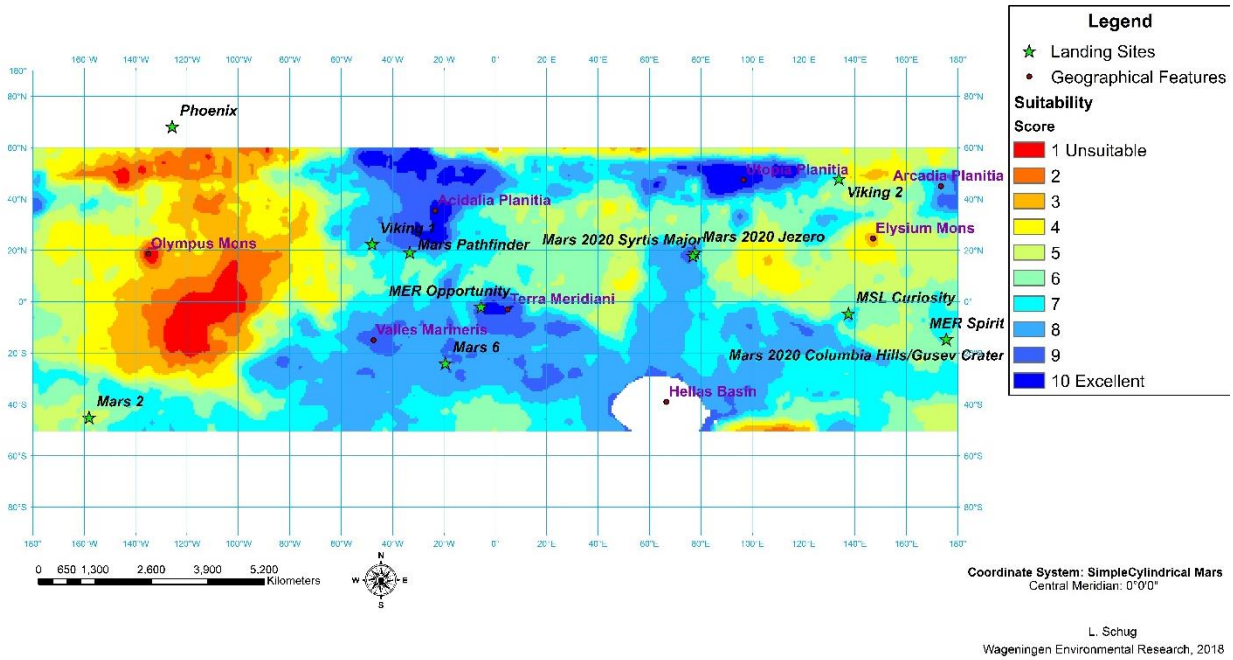

Figure 12. The map of the ideal landing sites on Mars from a plant perspective (Wamelink, 2018).

The researchers estimated the ideal landing sites on Mars using numerous Martian maps made publicly available by NASA Jet Propulsion Laboratory (JPL) and Arizona State University (Wamelink, 2018). The maps include mineral composition knowledge, such as calcium and heavy metal concentrations. Also, element maps for potassium, chloride, iron, and silicon and maps for radiation, temperature, topography, altitude, and cosmic radiation were included. The research study requirements are as follows: high levels of heavy metals in the soil and intense radiation make a location unsuitable for the establishment, but high temperatures or calcium levels and relatively flat terrain are considered positive to evaluate a region as acceptable for establishment.

The maps were combined, and an average score was calculated, with higher values indicating better landing spots from the standpoint of the plant (Wamelink, 2018). Due to a paucity of data, the poles and the Hellas Basin are not covered. Moreover, the poles are primarily composed of CO_2 and ice. On Mars, a few prominent landmarks are denoted with stars. Additionally, the locations of past and future Mars landers are indicated. In the resulting map, as seen in Figure 12, blue colors denote strong potentials, with the darkest blue representing the best locations, red denoting less desirable locations, and dark red representing the worst (Wamelink, 2018).

3.4.3. SWIM: Subsurface water ice mapping and optimal landing site

Research released in Nature Astronomy in February 2021 shows a detailed picture of Mars's northern hemisphere showing where water ice is most and least likely to be found. The report results from a project called Subsurface Water Ice Mapping, or SWIM, which included data from NASA's Mars Odyssey, Mars Reconnaissance Orbiter, and the now-inactive Mars Global Surveyor. The NASA Jet Propulsion Laboratory in Southern California oversees the SWIM project conducted by the Planetary Science Institute in Tucson, Arizona.

The SWIM project's outputs help Mars Human Landing Sites Studies and planning for future resource assessment needs (N. Putzig, 2020). Scientists focused on the southern hemisphere after completing phase one in 2019(N. Putzig, 2020). In the second phase, completed in 2020, they broadened their study to cover the southern and northern (N. Putzig, 2020). The SWIM project aims to produce mapping products based on existing data from spacecraft to identify subsurface ice on Mars in the middle latitudes. Using a combination of all data sets, scientists can determine the possibility of underlying ice in both shallow (less than 5 meters) and deep (more than 5 meters) zones (N. Putzig, 2020). The implemented methodology uses five remote sensing techniques: neutron spectroscopy, thermal analysis, radar surface analysis, radar subsurface compositional (dielectric) analysis, and geomorphic mapping of periglacial features (The Planetary Science Institute, 2021).

Not all existing ice could be recognized due to lateral and vertical resolution limitations and detecting depth imposed by current data sets. In general, the available data sets examine four zones:

1) the surface itself (i.e., to a few microns depth) for imagery and elevation data, 2) the upper ~1 m for thermal and neutron spectrometers, 3) the upper ~5 m for radar reflections from the surface, and 4) between ~15 m and several hundred meters depths for radar reflections from subsurface interfaces (N. Putzig, 2020). Ice-related geomorphological indications exist in all four zones. Except for transient ice caused by a previous impact, there was no ice at the surface in the study areas (0 to 60° latitude).

These data sets' interpretation of ice presence is subjective and does not lend themselves to the exact probability estimation. However, quantifying confidence in identifying and mapping ice is warranted and highly desirable for planning future landing locations that rely on ice for resources or scientific purposes. Figures 13, 14, and 15 illustrate the existence of ice across a combined sensing depth of 1 m, between 1 and 5 m, and more than 5 m, respectively, indicating the presence or absence of ice in that location.

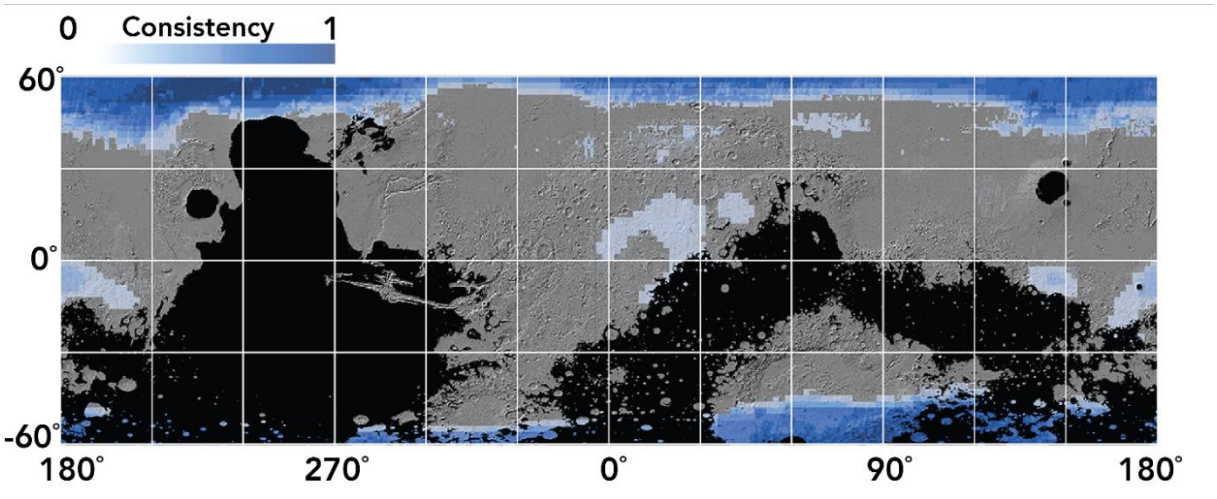

Figure 13. Combined Ice Consistency for the depth between 0-1 meters (The Planetary Science Institute, 2021).

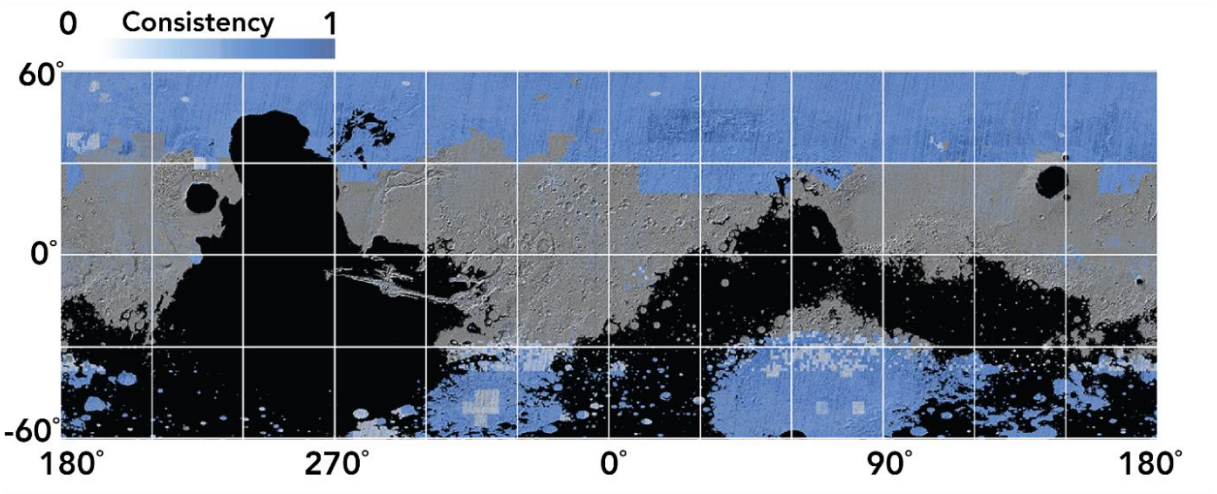

Figure 14. Combined Ice Consistency for the depth between 1-5 meters (The Planetary Science Institute, 2021).

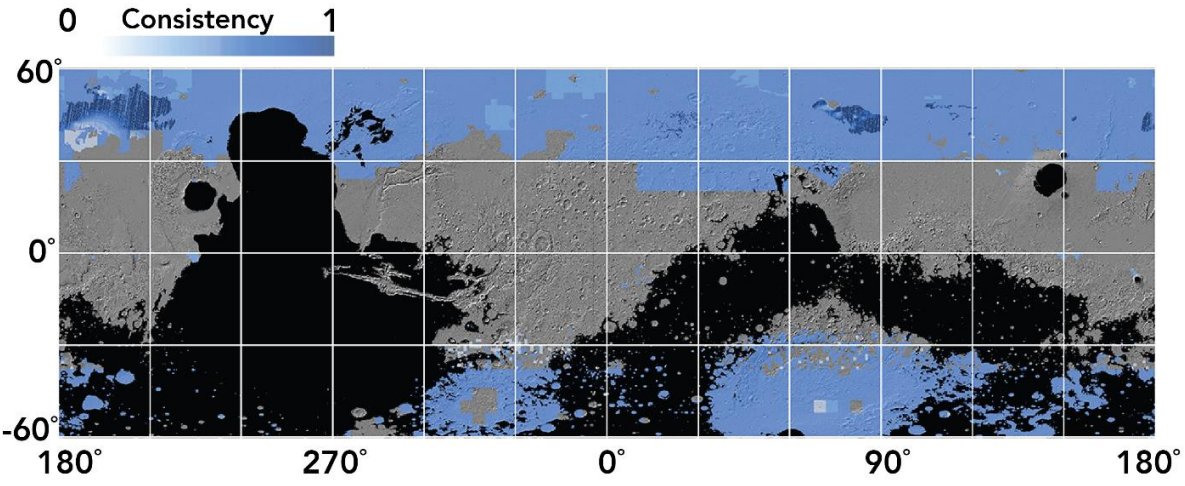

Figure 15. Combined Ice Consistency for a depth of more than 5 meters (The Planetary Science Institute, 2021).

SWIM summarizes the findings at the 2021 Fall AGU Conference, from December 13th to December 17th, 2021, in New Orleans, Louisiana (N. E. Putzig et al., 2021). The revealed data map comprises values of ice consistency ranging from -1 to +1 for hydrogen detections using a neutron spectrometer, thermal behavior using a variety of thermal spectrometers, multiscale geomorphology using imagery, and surface and subsurface echoes using a radar sounder. Positive ice consistency (blue tones) is depicted in Figure 16 at all depths within the SWIM study area. Red crosses indicate locations of recent, ice-exposing impacts, which are highly correlated with areas of positive ice consistency. Hillshade and topography in greyscale are generated from MOLA data. Elevations greater than +1 km (in black) were excluded. The highest ice consistency values are found poleward of ~40º latitude, where ice is relatively shallow, although positive values continue into the ~20º–30º latitude zones, which are recommended for a human landing site.

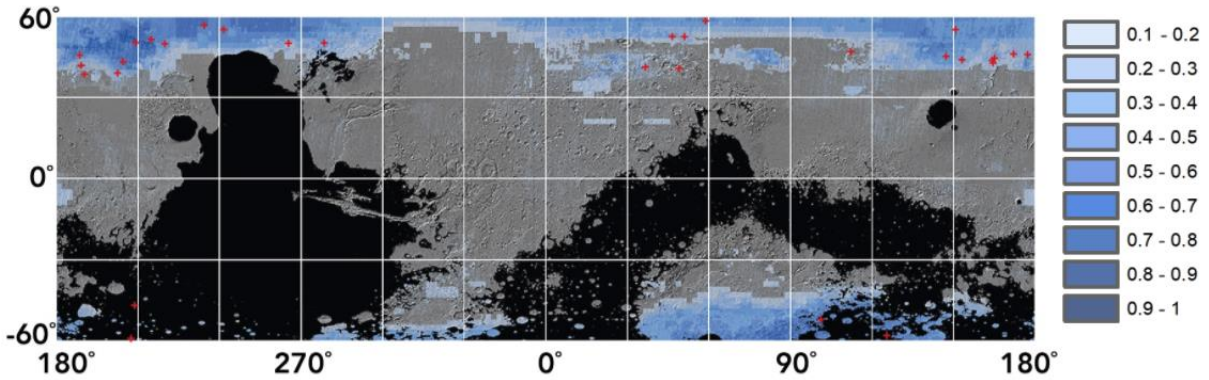

Figure 16. Positive ice consistency (blue shades) for all depths in the SWIM study area (N. E. Putzig et al., 2021).

3.5.An Assessment of Mars for Space-Resilient Design

The environmental variables of Mars have been studied, and we must next assess them to discover what barriers stand in the way of constructing a space-resilient settlement capable of surviving the challenges of extraterrestrial life. To begin, we must analyze how the Martian environment—gravity, temperature, atmospheric pressure, wind, radiation, seismic activity, and meteorites—would affect construction on the planet. We also need to figure out which areas of Mars provide the best prospects for carrying out surface activities, having access to water, growing plants, and obtaining local resources for construction.

3.5.1. Site selection for a long-term crewed Mars mission

During a NASA-hosted workshop, an expert panel chose the eight best probable landing sites for the Mars 2020 Perseverance Rover. Experts selected landing places in the middle latitudes due to the higher average yearly temperatures and low heights so the rover would produce more significant atmospheric drag upon touchdown. Jezero Crater was determined to be the optimal location for the long-term landing and operation of the rover after considerable analysis.

SWIM has conducted a comparison study to assess surface locations to disclose ice resources, their depth levels, and distribution because underneath ice resources are essential for long-term crewed missions as the resource to sustain life and ensure operations on the Martian surface. The illustration Figure 17 depicts a topographical map of Mars superimposed with the combined ice consistency maps for 0-1 meters and 1-5 meters and the eight landing alternatives for NASA's Mars 2020 Perseverance Rover to show how the two studies can be comparable in each other. According to the maps, the sixth point in the SW Melas Basin is the worst place to set down if explorers want to get to the underground ice resources nearby. However, the terrain, altitude, and distance from other ice deposits make landing sites 4 and 5 in Holden Crater and Eberswalde less feasible. The map shows us that the second landing spot on Columbia Hills provides the best access to the ice reserves (0-1 meters deep). Despite being situated in the middle latitudes, its high altitude makes it less desirable for long-term surface operations and more atmospheric drag for landing. All three of the 1, 3, and 7 numbered landing sites (Jezero Crater, NE Syrtis Major, and Nili Fossae) are relatively close to each other. However, Nili Fossae is located at a greater height than the other two locations, and the surrounding terrain is another disadvantage for surface activities when compared with the other two. Because of their proximity to ice reserves 1-5 meters underground, desired latitudes, lower altitudes, and suitable landscape forms for surface operations, the first, third, and eighth (Mawrth Vallis) locations have the highest potential to settle a human colony and have surface operations for a long-term mission, as shown by the superimposing study.

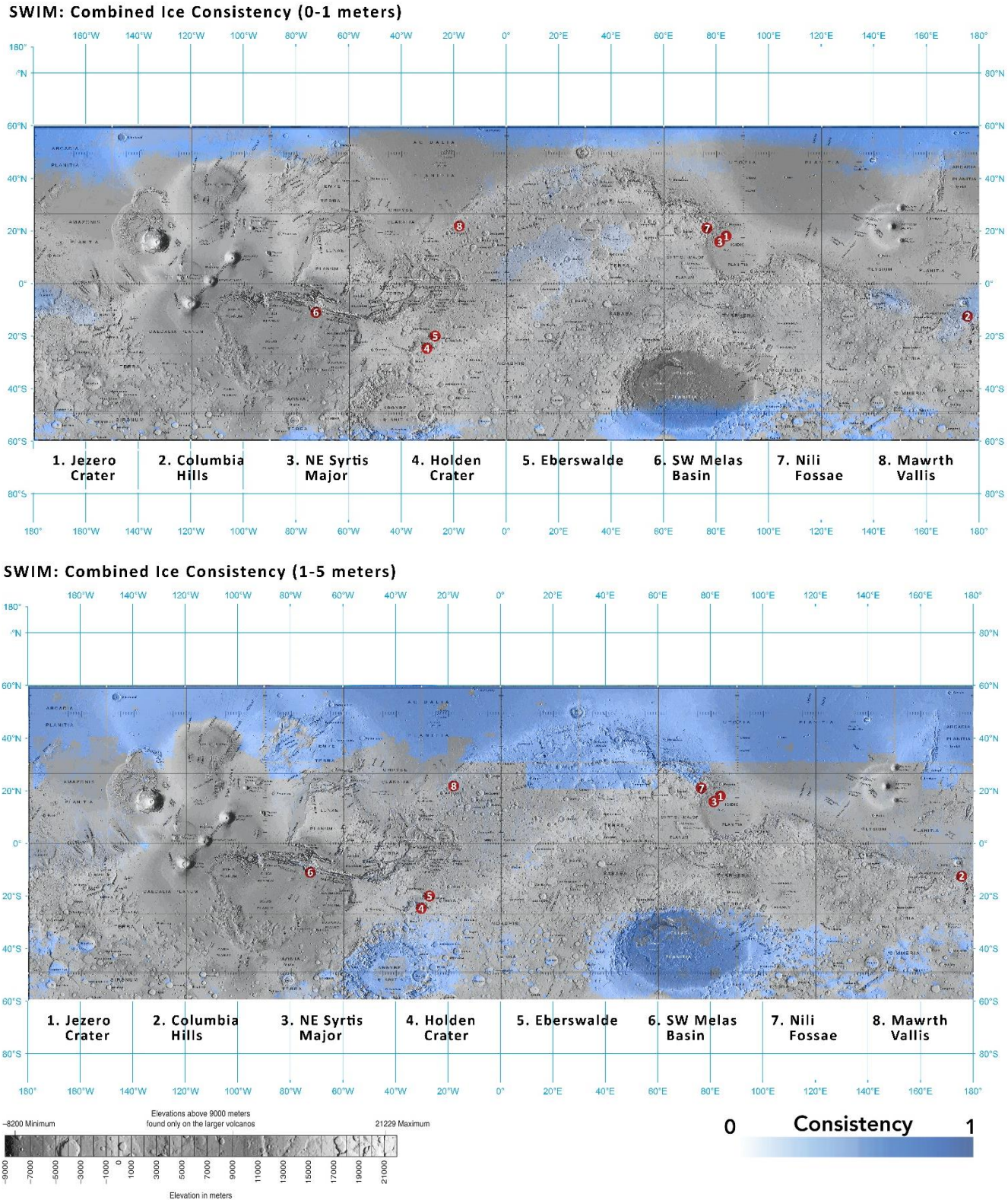

Figure 17. The superimposed topographical map of NASA's workshop findings and SWIM's maps.

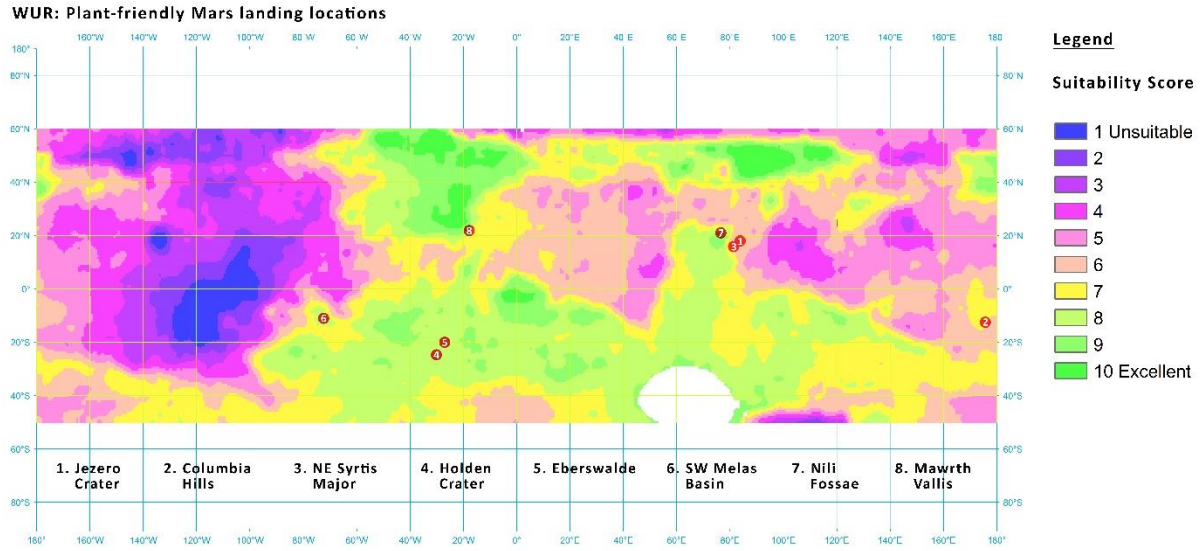

Figure 18. The superimposition of Mars's plant-friendly locations and NASA's landing site workshop findings

Similarly, WUR conducted a study looking at the Martian surface through the perspective of plants to identify potential settlement locations. The study's final map of suitable plant-growing locations featured a suitability score to help visualize the findings. Future crewed missions to Mars interested in the possibility of growing food there will find these results extremely useful. Mawrth Vallis, the eighth landing site on this map, is the best landing location for a long-term crewed surface mission in terms of latitude, altitude, landforms, distance from ice reserves, and plant-friendliness to grow local foods when compared with the findings of previous superimposition analysis as can be seen in Figure 18.

3.5.2. In-situ materials on Mars as a construction material

The benefits of 3D printing when designing and constructing within extreme environments range from the economical, due to the immensely reduced costs of certain kinds of construction, to the practical, such as the ability to print objects as needed (Bassingthwaighte, 2017). Another advantage of 3D printing technologies is that once the essential habitat is built, the 3D printers remain on-site, enabling habitat growth and manufacturing other essential structures without requiring them to be delivered from Earth (Mueller et al., 2014). 3D printers only require solar power or another energy source and printing material. Renewable energy and locally produced resources give a habitat or colony more resource independence from Earth than achievable. This construction would be less expensive than transporting habitat modules and would be completed considerably faster once printers were installed on location, thanks to the simplicity of printed designs. It is also possible to construct structures beyond the transport capability of launch vehicles. Printed designs would include a complex of modules that could be expanded upon as needed instead of a single, pressurized habitat that would need to be brought up from Earth at a high cost.

Several studies have explored utilizing Martian in-situ materials as 3D-printing material (M. Morris et al., 2016c; Mueller et al., 2014). Primary in-situ materials' mechanical characteristics and structural capabilities are therefore examined.

Characteristics of Martian regolith

The third chapter describes the average chemical compositions of Martian regolith analyzed by many landers. Silicon dioxide (43.19 wt%) dominates the Martian regolith. Iron oxides are the second most prevalent mineral, with 18.09 wt%, followed by aluminum oxide, which comprises 9.12 wt%. The remaining content comprises calcium oxide, magnesium oxide, sulfur trioxide, sodium oxide, and trace minerals.

Using Martian soil to build a Mars project is better than sending all the building materials from Earth at an astronomically high expense. There are many research studies for developing a construction material by using Martian surface data. For instance, since Mars has always been a "sulfur-rich planet," Wan, Wendner, and Cusatis (2016) developed Martian concrete in Figure 19 as a novel material for construction on-site composed mainly of synthetic material Martian soil and molten sulfur (Wan et al., 2016). Its mechanical properties can be seen in Table 10, and easy curing, low-temperature durability, acid and salt environment tolerance, and 100 percent reusability are all promising properties of the manufactured Martian Concrete. The optimum Martian Concrete composition comprises 50% sulfur and 50% regolith.

Figure 19. A simulant from Martian Concrete (Wan et al., 2016).

Table 10. Properties of Martian concrete (Wan et al., 2016)

Normal modulus [GPa]	10
Densification ratio [–]	1
Tensile strength [–] [MPa]	3.7
Yielding compressive Stress [MPa]	300
Shear Strength Ratio [–]	4
Tensile characteristic length [mm]	55
Softening exponent [–]	0.2
Initial hardening modulus ratio [–]	0.12
Transitional strain ratio [–]	4
Initial friction [–]	0.1

Sulfur, abundant on the Moon and Mars, is another resource used in buildings on the Moon or Mars (Anyszka et al., 2016). Sulfur melts at 112.8°C (orthorhombic) or 119°C (monoclinic) depending on its crystal structure, becomes viscous at about 160°C, and boils at 444.6°C. These properties of sulfur enable its processing in lunar and Martian conditions and incorporation into the binding of non-hydraulic construction materials and the creation of sulfuric acid, commonly used in metal extraction. Sulfur is common on Mars, reaching a minimum of 1–3 percent by soil/regolith weight. Table 11 illustrates a comparison study of cement and sulfur concrete materials.

Table 11. Comparison of mechanical properties of cement and sulfur concrete (Wan et al., 2016).

Property	Cement Concrete	Sulfur concrete	Unit
Density	2.2	2.4	g/cm^3
Compression strength	15-60	40-115	MPa
Flexural strength	6-7	10-16	MPa
Tensile strength	-	5-7.5	MPa
Modulus	25-28	35-50	GPa
Porosity	9-15	1-4	%
Corrosion resistance	medium	high	-
Frost resistance	medium	high	-
Material recycling	difficult	easy	-
Resistance to fire and high temperature	medium/high	low	-

Characteristics of Basalt

Mars is rich in basalt. Magma extrusions during lava flows generate this igneous rock (Kading & Straub, 2015). Density measurements for basaltic rocks (such as Bathurst in Gale crater) show a range from 3100 to 3600 kg/m^3, with most measurements being in the 3200 to 3300 kg/m^3 range (Baratoux et al., 2014). It is made up primarily of SiO_2 (but also some other gases) and has a low percentage of other elements (Kading & Straub, 2015). The material's tensile strength is 14 MPa, while the modulus of elasticity is 73 GPa (Schultz, 1993). Based on these values, basalt is more elastic than steel (i.e., 205 GPa for 1018 low-carbon steel and is on par with aluminum in terms of elasticity (i.e., 70 GPa for 7075 aluminum) (Kading & Straub, 2015). Its stress threshold is also in the same range as certain plastics, such as low (11.6 MPa) and high (26.3 MPa) polyethylene (Kading & Straub, 2015).

As a form of stone, basalt is resistant to radiation (Kim et al., 2000). Moreover, it appears excellent for making pressured structures due to its high specific heat and low permeability constant (Turner & Verhoogen, 1960). Furthermore, basalt can be re-heated and rapidly cooled in different ways, resulting in crystals with different structural features. If the magma that produces basalt is allowed to cool very slowly, it transforms into gabbro, poorly graded magma intruding rock with allotriomorphic texture (Turner & Verhoogen, 1960). Depending on its specific composition, basalt has a melting point between 900 and 1100 ℃ (Kading & Straub, 2015).

Characteristics of ice

Water primarily exists on Mars as enormous ice caps at the poles, as permafrost at mid- and high-latitudes, and as frost patches and old glaciers distributed across the planet's surface (Janssen & Houben, 2013). At a temperature of 0°C and atmospheric pressure, pure liquid water transforms into its solid state, ice. A peculiar attribute of water is that its highest density occurs just beyond the freezing point (+4°C) (Janssen & Houben, 2013). This characteristic is uncommon in liquids, although it is not unique. Intriguingly, the density of liquid water at the freezing point is not 0.99984 g/cm^3 but reduces to 0.91668 g/cm^3 when that water crystallizes at 0°C (Petrenko & Whitworth, 1999). This density differential is caused by the ice crystal lattice's vast free gaps. On freezing, the increased volume of the solid lattice causes pure water to expand by around 9 percent (Petrenko & Whitworth, 1999). At –30 degrees Celsius, ice has a density of around 920,6 kilograms per cubic meter, similar to most other substances.

Ice's strength is highly varied due to its inhomogeneity. Nevertheless, ice is more resistant to compression than tension. The dispersion of ice tensile strength is relatively large, ranging from 0.70 MPa to 3.10 MPa (Petrovic, 2003). According to published research, the specific tensile strength of ice at temperatures between -10 and -20 degrees Celsius is 1.43 megapascals (Petrovic, 2003). The flexural strength of ice diminishes as the grain size increases; for temperatures below –5°C, measurements on freshwater ice range from 0.5 to 3 MPa, with an average of 1.73 MPa (Veritas, 2010). Between -10°C and -20°C, the compressive strength of ice fluctuates between 5 and 25 MPa (Petrovic, 2003). Ice's tensile and compressive strengths generally increase with decreasing temperature (Petrovic, 2003). Depending on the loading rate, ice can exhibit either brittle or ductile behavior. Under strain, ice fractures after increasing in length by 0.01–0.1% by transgranular cleavage (Schulson, 1999). Typically, the fracture toughness of ice falls between 50 and 150 kPa √m (Petrovic, 2003). Comparatively, the fracture toughness of glass is typically between 700 and 1000 kPa √m (Petrovic, 2003). At temperatures close to the melting point (-5 to -10°C), Young's modulus of single crystals changes by less than 30 percent, from 12 GPa in the least compliant direction to 8.6 GPa in the most compliant direction. Typical values of Young's modulus and Poisson's ratio for ice are 9.0-11.2 MPa and 0.29-0, respectively (Petrenko & Whitworth, 1999; Petrovic, 2003; Schulson, 1999).

Thermal conductivity is the ability of ice to carry heat under a temperature gradient of one degree Celsius (Petrenko & Whitworth, 1999). Numerous experiments have been conducted to measure the thermal conductivity of ice. At 0°C, the thermal conductivity of ice (2,18 W/(m. K) is nearly four times that of water (0,58 W/(m. K) (Petrenko & Whitworth, 1999). Ice has a higher thermal conductivity than construction materials such as concrete and wood but a far lower thermal conductivity than metal (Petrenko & Whitworth, 1999).

3.5.3. Mars's gravitational effect

According to Einstein's Theory of General Relativity, gravity is caused by the curvature of space-time, and gravitational acceleration is perceived as gravity (T. W. Hall, 1999). This acceleration is approximately 9,81 m^2/s on Earth's surface and is 1 G (van Ellen, 2018). While this is about 0,16 G on the surface of the Moon, the surface of Mars has a gravity of around 0.38 G, causing an acceleration of about 3.71 m/s^2. (van Ellen, 2018).

Consequently, the "weights" and downward actions that Martian structures must withstand are much lighter than they would be on Earth. The minimum load-bearing capacity for a European residential floor is 200 kg/m^2, while on Mars, it is only 57 kg/m^2.

3.5.4. The extreme thermal fluctuation on Mars

On average, Mars is about 1.5 times further away from the Sun than the Earth, making it a much colder place. On average, Mars is estimated to have -63 °C, with the lowest at -153 °C and the highest at 20 °C (Park et al., 2020). These values indicate an average of 14 °C for Earth, with the lowest at -88 °C and the highest at 58 °C (van Ellen, 2018). It should be noted that diurnal temperature variances on the Mars surface are more significant than on Earth (van Ellen, 2018). The temperature can fluctuate between +27°C and -133°C throughout the day and night. The temperature fluctuation mainly results from Mars's weak greenhouse effect and the Martian soil's low energy storage capacity. Temperatures also vary according to the amount of dust in Mars's atmosphere.

Extreme thermal fluctuations on Mars will make it challenging to construct and sustain life there. The temperature fluctuations on Mars's surface threaten the mission's components and living quarters because of the mechanical and material stress they induce. Also, if the buildings on Mars are made from materials that are already there, the mechanical properties of the materials must be able to handle the daily temperature changes.

3.5.5. Atmospheric pressure on Mars and its correlation factors

Mars has an average atmospheric pressure of 600 Pa or approximately 0.6% of Earth's. As the internal pressure of the habitat must match or be close to that of Earth's atmosphere, a pressure difference will constantly exist, causing the structure to expand. The building material must therefore be able to sustain this amount of force.

The average atmospheric pressure on Mars is approximately 0.6 kPa, whereas the average atmospheric pressure on Earth is 101.325 kPa or 10332.27237 kg per square meter. Due to a pressure difference of 100.725 kPa between its interior and external surfaces, the inner surface of a Mars structure will be subjected to a force of 10271.08941 kg per square meter. The most effective method for addressing the discrepancy between exterior and interior pressure is to specify a material and

building system that can withstand the extreme circumstances imposed by the pressure differentiation. Establishing a lower internal habitation pressure at which people can continue to live without endangering their health is one way to make the system more resilient. NASA recommends a minimum internal pressure of 52.67 kPa, which is lower than that on Earth but still within the safe range for human inhabitants, for routine activities on Mars (Park et al., 2020). Consequently, the tolerable pressure difference for habitation on Mars is 48.655 kPa which means the designed system must be resistant to 4961.429234244 kg per square meter.

The NASA Glenn Research Center's definition of Mars' atmosphere includes two distinct zones, each with its own set of curve fits (N. Hall, 2021). As the altitude increases, the atmosphere's density falls due to the effects of temperature and pressure, as described by the equation of state. We can measure the gas's volume (V), pressure (p), temperature (T), and mass (m). Equation of state calculations allows us to determine the density across different zones. Density (ρ) is measured in kilograms per cubic meter, while pressure (p) is given in kilopascals. T equals the current temperature In Celsius. The equation of state can be expressed in terms of the specific volume or the air density as follows:

$p * v = R * T$ where $v = V/m$ corresponds to $1/\rho$

$\rho = p / [0.1921 * (T + 273.1)]$

Up to 7,000 meters above the surface of Mars is the lower atmosphere. The temperature drops linearly, and the pressure drops exponentially in the lower atmosphere. The lower atmosphere's temperature and pressure are expressed in metric units as follows:

$T = -31 - 0.000998 * h$, and $p = 0.699 * \exp(-0.00009 * h)$,

Where h is the altitude in meters and T and p are the temperature in Celcius degrees and pressure in kilo-Pascals, respectively. The lower atmosphere curve shown in Figure 20 fits in metric units for density (ρ) and altitude (h) as follows:

$\rho = 0.669 * \exp(-0.00009 * h)/(0.1921*((-31 - 0.000998 * h) + 273.1))$

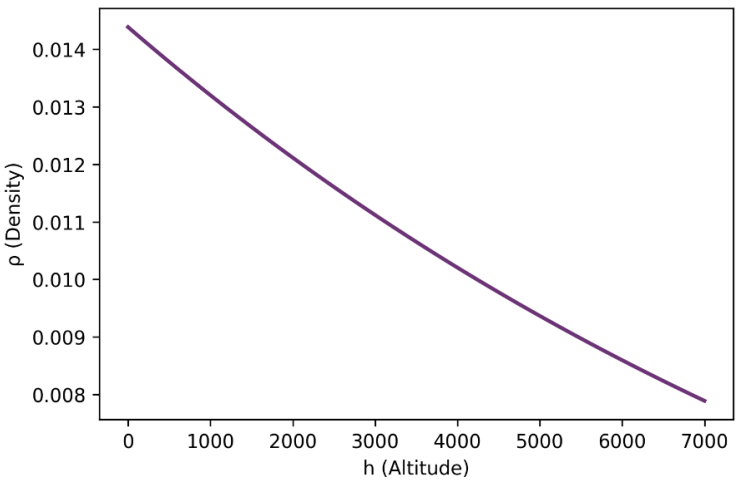

Figure 20. The density-altitude relationship in Mars' lower atmosphere

3.5.6. Wind pressure on Mars

When scientists investigated the influence of Mars' wind on the planet, it is plausible to believe that this component posed a significant challenge to the planning process. However, an analysis of Martian wind speed records finds numbers much lower than anticipated. On Mars, wind speeds of up to 30 meters per second have been reported (Miscio, 2018), which is considerably slower than the fastest wind speeds ever recorded on Earth. The following dynamic pressure formula was used to determine the wind pressure on Mars's surface:

$$q = 0.5 \; x \; \rho \; x \; v^{2}$$

Where q represents the pressure, ρ indicates the atmosphere's density, and v is the wind velocity. On the surface of Mars, the atmosphere has a density of around 0,020 kg/m^3 (NASA, 2021b). As a result, the most extraordinary wind pressure on the surface of Mars is 9 Pa (9 N/m^2).

3.5.7. Radiation impacts and shielding capability of Martian regolith

The radiation exposure on Mars' surface is much harsher than on Earth's surface for two reasons: Mars lacks a global magnetic field to deflect energetic charged particles, and the Martian atmosphere is much thinner (<1%) than Earth's, providing little shielding against high-energy particles that are incident at the top of its atmosphere (Hassler et al., 2014). This climatic component, which has not comparable to Earth, provides a challenge for future human exploration of Mars and is crucial in comprehending geological and prospective biological evolution on the Martian Surface (Hassler et al., 2014).

Astronauts are exposed to a high risk of galactic and solar cosmic rays (GCR and SCR), as well as solar particle events (SPE) (Biswal M & Annavarapu, 2021). NASA has classified the significant health risks of GCR and SCR exposure into four distinct human diseases. Their effects cause carcinogenesis, a cardiovascular disease resulting from cell degeneration, the risk to the central nervous system throughout a person's lifetime, and acute radiation syndromes (Chancellor et al., 2014). Thus, the crew's health consciousness is critical to the success of a human mission.

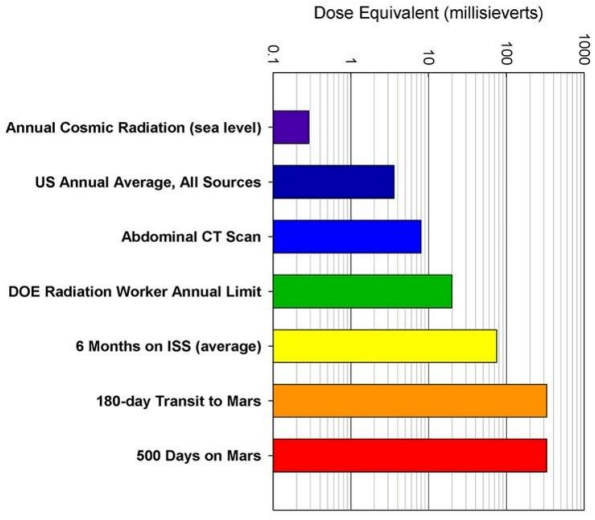

Figure 21. Radiation dose comparison (Hassler et al., 2014).

Figure 21 shows a dose-equivalent comparison of a 500-day surface stay to a 180-day transit to Mars, a 6-month stay on the International Space Station (ISS) at 420 km altitude at the 2013 solar

maximum multiple earth-based radiation sources (Hassler et al., 2014). The term "dose" refers to a physical quantity measured in gray or milligray.

For the estimated solar cycle, Hassler, Donald M. et al. (2014) projected a total mission dose equivalent of ~1.01 Sv (1010 mSv) for a round trip Mars surface mission with 180 days (each way) cruise and 500 days on the Martian surface based on their observations and those collected during the cruise phase (Hassler et al., 2014). These mission phase lengths are based on one hypothetical NASA design reference mission; alternative mission designs and windows at various periods in the solar cycle or a different solar cycle would result in somewhat varying radiation exposures. Age and gender define the precise organ and occupational exposure limitations, as seen in Table 12. A person's annual average exposure is around 3.6 mSv, a meager amount (Rask et al., 2008). International Standards, on the other hand, enable those who operate with and near radioactive material to be exposed to as much as 50 mSv per year (Rask et al., 2008). The limit is greater in spaceflight. In low-Earth orbit, the NASA limit for radiation exposure is 50 mSv/year (Rask et al., 2008). Notably, the number of younger astronauts is lower than that of older astronauts. Because it is anticipated that, even though they may survive longer than older astronauts, their early exposure to higher radiation levels may create more severe health issues.

Table 12. NASA radiation exposure limits according to gender and age (Rask et al., 2008).

Career Exposure Limits for NASA Astronauts by Age and Gender				
Age (years)	25	35	45	55
Male	1500 mSv	2500 mSv	3250 mSv	4000 mSv
Female	1000 mSv	1750 mSv	2500 mSv	3000 mSv

The average annual natural radiation dose on Marss 600 mSv (Hassler et al., 2014; McKenna-Lawlor et al., 2012). According to NASA Standards, one astronaut is only expected to get 50 mSv of radiation annually, so a minimum protection factor of 91,67% is required to build structures and life bases that can shield people from radiation.

The linear attenuation coefficient (μ) indicates the amount of an x-ray or gamma-ray beam absorbed or scattered per unit of absorber thickness (Center for Nondestructive Evaluation, 2022). This measurement depends on the number of atoms per cubic centimeter and the probability that a photon will be scattered or absorbed by the nucleus or an electron of one of these atoms (Center for Nondestructive Evaluation, 2022). Since the density of a material influences its linear attenuation coefficient, the mass attenuation coefficient is frequently used instead (Center for Nondestructive Evaluation, 2022). In the case of water, water vapor has a significantly lower linear attenuation than ice because its molecules are more dispersed, so the possibility that a photon will collide with a water particle is lower (Center for Nondestructive Evaluation, 2022). By dividing the linear attenuation

coefficient (μ) by the element's or compound's density (ρ), we can obtain an identical value for each element or compound. This constant is known as the mass attenuation coefficient and has the units cm^2/g. When the mass attenuation coefficient is substituted for the linear attenuation coefficient, the basic shielding equation to determine the thickness of the shielding material when the radiation rates with and without the shield and the material density are known (The U.S. Nuclear Regulatory Commission, 2011)

$$x = -\frac{ln\left(\frac{\dot{x}}{\dot{x}_0}\right)}{\left(\frac{\mu}{\rho}\right)\rho}$$

x = required shield thickness (cm)

$\dot{x}_0$ = the exposure rate without the shield (R/hr)

$\dot{x}$ = the exposure rate with the shield in place (R/hr)

μ = Linear attenuation coefficient (cm^{-1})

ρ = density of shielding material (g/cm^3)

μ / ρ = mass attenuation coefficients (cm^2/g)

On average, SEP events generate ~11 MeV to the radiation environment of Mars, whereas GCR adds between 122 and 153 MeV (Hassler et al., 2014). In addition, the 1.2-1.7 MeV comes from photons in Mars's atmosphere (Hassler et al., 2014). As a result, the average cumulative radiation intensity on the surface of Mars is around 150 MeV, with a range of 134 to 166 MeV for the total radiation environment on Mars (Hassler et al., 2014).

At 150 MeV, the regolith of Mars, with an average soil density of 1.52 g/cm^3, has a linear attenuation coefficient 'μ' (cm^{-1}) of 0.0407 and a mass attenuation coefficient 'μ/ρ' (cm^2/g) of 0.0268 (Shunk et al., 2020). Using the radiation shield formula and assuming a protection factor of 91,67 percent, we estimate that a minimum shield thickness of 60.99 centimeters composed of Martian regolith is required.

If we want to provide a daily life for Mars explorers as they have on Earth, we need to estimate the required shell thickness against average annual radiation of 3.6 mSv during Mars' solar cycle, which means a protection factor of 99.4 percent against 600 mSv for a Mars surface mission during Mars' solar cycle. Based on the calculations, a regolith shell thickness of 125.59 centimeters is sufficient for daily Earth-like radiation protection.

3.5.8. Effects of seismicity on Mars

The Insight lander successfully detected quakes on Mars at the end of 2018 (Giardini et al., 2020).; however, the strongest earthquake previously recorded was an estimated magnitude of 4.2 quakes identified on August 25, 2021. The lander has detected the strongest earthquake ever recorded on another planet: a magnitude five seismic activity on May 4, 2022. A magnitude five quake is recognized as a strong earthquake on Earth, while it is close to the maximum limit of what researchers anticipated to encounter during the InSight mission on Mars (NASA Jet Propulsion Laboratory, 2022).

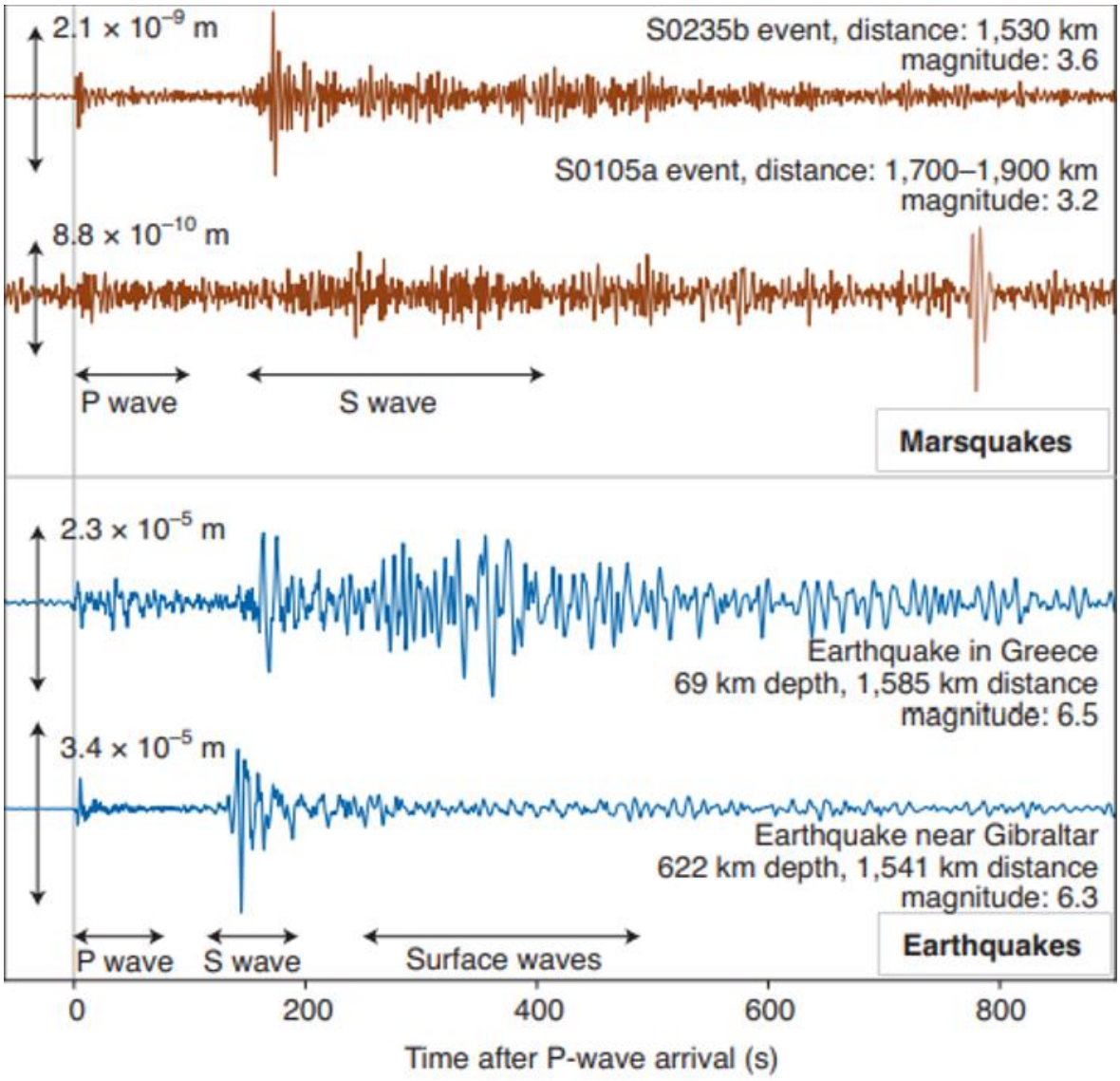

Figure 22. Comparison of Marsquake and Earthquake for similar distances (Banerdt et al., 2020).

According to NASA, the stresses that cause rock fractures or crustal faults on Mars are responsible for causing "marsquakes" (Andrew et al., 2021). For a regular quake on Mars to be audible to a human, the signal must be multiplied by roughly 10 million times. Since the surface accelerations induced by such forces are of the order of magnitude, the structures' response times and influence are negligible (Banerdt et al., 2020). As shown in Figure 22, according to the data gathered by the probe,

vertical accelerations, oscillations, and magnitudes are far smaller than those of Earth at the same distance from the epicenter (Banerdt et al., 2020). In addition, as indicated previously, the maximum ground velocity of seismic events is approximately 1.2 x 10^{-5} meters per second, which is a relatively low velocity for audibility by humans.

Earthquakes are caused by the movement of tectonic plates, as was previously mentioned. On the other hand, Mars has no tectonic plates, and its crust is one giant plate (Andrew et al., 2021). The Earth's active plate tectonics regularly increase stress to extensive plate boundary fractures, which results in earthquakes that are both more frequent and more powerful than those we would expect on Mars. Without plate tectonics, seismic activity on Mars is expected to be extremely rare.

3.5.9. Impact of Micrometeoroids on Mars

Mars has a far smaller mass than Earth, which results in much lower gravitational acceleration. The atmospheric constituents depart the planet as a result of insufficient gravitational acceleration. Mars' magnetic field has a weaker repelling effect than Earth's, and its atmosphere is noticeably less dense. In other words, Mars lacks physical defenses against meteorites, which could jeopardize the success of the mission on the planet. Therefore, the effect of micrometeorites on Mars was investigated to understand its effects on surface habitation.

In 2010, Rubin and Grossman provided the following definitions for the word "meteoroid" and related terms: A meteoroid is a natural solid object traveling through space between 10 µm and 1 meter in size. A micrometeoroid is any meteoroid between 10 µm and 2 mm in size (Rubin & Grossman, 2010).

Micrometeoroids with enough momentum can shred cables, tethers, springs, pressurized vessels (manned habitats, propulsion tanks), batteries, coolant lines, or spacesuits (Rodmann et al., 2019). Penetration or spallation by grains as small as a millimeter can cause severe structural damage to a spacecraft, resulting in anything from a failure of a single component to the loss of the entire spacecraft and its crew (Rodmann et al., 2019).

A micrometeoroid's destructive potential is determined by its size, speed, density, and impact orientation (M. Bell, 1999). The physical response of an impacting structure is determined by its material, thickness, temperature, stress level, and the number and spacing of the plates (including shielding) making up the structure (M. Bell, 1999). For Mars, the estimated entry velocity ranges from 5.7 to 8 km/s, with most particles entering under 15 km/s (Tomkins et al., 2019). The mass density of a meteoroid can be preassumed as 2.5 g/cm^3 (M. Bell, 1999). To learn about the resilience of regolith surface structures on Mars, we need to simulate an impact test simulation on a single surface structure. The interiors of structures need shielding from these cosmic bullets.

04th Chapter
HABITABILITY ON MARS :
ASSESSMENT OF MARS ANALOG MISSIONS

To contextualize previously reported environmental conditions with habitation's functional requirements, Chapter 4 discusses a review and assessment of Mars analog missions to explore habitability on Mars. The chapter provides a concise description of the data science approaches utilized in the assessment study. The chapter ends with the research findings of data science approaches, which provide a layout design guideline for a space-resilient habitation.

The ability of an environment to maintain life has been broadly characterized by its habitability. A high habitability is the best possible state for life, whereas a low level is merely good enough for survival. Time is the essential variable in habitability; in fact, "habitability criteria for space missions are determined by mission duration" (Woolford & Mount, 2006). According to Connors (1985), long-term conditions must support individuals' physical and psychological well-being (Connors et al., 2005). Sending uncrewed spacecraft was a physics issue; sending crewed flights was a physiological difficulty, and sending people to stay in space was a psychological challenge.

The space environment is unique and requires specific consideration. As described in the preceding chapter, gravity, temperature changes, atmospheric composition and pressure, wind forces, radiation, marsquakes, and micrometeoroid impact separate the Martian environment from typical Earth conditions. In addition to extreme environmental conditions, a space exploration mission is an example of an isolated and confined environment in which the crew is physically separated from various support systems, such as friends and family, and is limited within a habitat. Space agencies and other institutions have researched analog habitats to comprehend and mimic the impacts of living in an extraterrestrial environment. In this chapter, the risks of space hazards on the human body will be described, and a review study of Mars analog missions on Mars-like sites will be undertaken to demonstrate prior research performed to comprehend the human factors of a long-term Mars expedition. Next, an architectural evaluation of analog missions' habitation instances will be conducted to understand the criteria of habitation design for a crewed-Mars mission to safeguard the crew from the risks of living in an isolated and confined system.

4.1. Impacts of the Mars Mission on Human Health

The search for solutions to the risks of space travel and settlement is a primary motivation for analog missions. NASA classified the dangers of exploring Mars into five broad categories based on the stresses they would create on an astronaut: Radiation, confinement, distance from Earth, gravity fields, and hostile, isolated environments are all issues that astronauts must contend with (Whiting, Melanie; Abadie, 2019). This section explains the effects of specified stressors for a long-term exploration mission.

4.1.1. Effect of space radiation on human

Space radiation is hazardous, yet the Earth's magnetic field and atmosphere protect humans from its most significant effects. There is evidence that radiation exposure increases the risk of developing cancer (Whiting, Melanie; Abadie, 2019). It can have immediate and long-term effects on the central nervous system, resulting in symptoms such as memory loss, motor function difficulties, and behavioral problems (Whiting, Melanie; Abadie, 2019). Symptoms of radiation sickness include feeling ill and then vomiting, not wanting to eat, and being overly fatigued.

Holubec and Connolly (2010), who are NASA's researchers, suggest that the highest recommended limit for radiation exposure is for astronauts-250 mSv per Space Shuttle mission, principally from cosmic rays (Holubec & Connolly, 2010). This amount exceeds the average of three mSv of natural radiation sources and any medical radiation a person has received (Holubec & Connolly, 2010).

Table 13. Important thresholds for deterministic radiation effects (Fincher & Boduch, 2009).

Dose	
100 mSv	The lower estimate for the threshold for damage to the unborn child.
500 mSv	In the case of acute exposure, reddening of the skin occurs from this— threshold.
1,000 mSv	In the case of acute exposure, acute radiation effects (e.g., nausea, vomiting) occur from this threshold upwards.
3,000–4,000 mSv	Without medical intervention, this dose results in the death of 50 percent of exposed individuals within 3–6 weeks if the radiation exposure was experienced over a short period.
>8,000 mSv	Without appropriate medical treatment, there is only a tiny chance of survival if the radiation exposure is experienced over a short period.

Since space radiation is virtually undetectable, the first risk of a human mission to Mars is also the most difficult to perceive. Table 13 explains critical radiation dose levels for the human body. Radiation induces behavioral changes, affects the central nervous system, alters cognitive function, reduces physical performance, and raises cancer risk (Chancellor et al., 2014). The space station is placed just outside the Earth's magnet field of protection, and the astronauts are exposed to ten times greater radiation than they have on Earth.

4.1.2. Isolation and spatial confinement

Astronauts spend 2.5 to 3 years in isolation/containment on a human journey to Mars, impacting their mental and behavioral processes. Regardless of how well-trained a group is, behavioral challenges are inevitable when they share a limited location for an extended period. Anxiety, depression, digestive problems, loneliness, low blood pressure, and hypo- or hypertension are all possible side effects of long-term space travel for astronauts (Whiting, Melanie; Abadie, 2019). Moods and relationships with other crew members improve due to these psychological changes.

The spacecraft has a limited amount of accessible space. In the case of an EVA, astronauts will be allowed to move around the station for a limited time, but only with significant technological support in the radiation danger. Under these conditions, space addition must be studied about group, individual, private, and public needs, separating areas with zoning study. Messerschmidt's and Bertrand’s book Space Stations explains this: Aboard a space station, a wide range of activities are carried out concurrently in a relatively constrained work and residential environment (Messerschmid & Bertrand, 2013). The various activities are classified as private/public and individual/group in a coordinate system. Similarly, the greater the distance between two activities, the greater their potential incompatibility (Messerschmid & Bertrand, 2013).

4.1.3. Distance from Earth

"We do not know what will happen" on a Mars expedition, Kanas says (Kanas & Manzey, 2008). However, according to Kanas, the big unknown is not who astronauts would be unable to communicate with or what presents they will be unable to obtain, but rather what they will be unable to see on planet Earth (Kanas & Manzey, 2008). This element is only available for space missions such as orbiting the moon. The consequences are equivalent to losing one's home view in an unknown desert. Indeed, as described by the author in the 2010 mission simulation on the Mars Desert Research Station, at least two of the six crew members experienced high earth rate disorientation, making it difficult to proceed with the extravehicular activity (EVA). Prof. Dietrich Manzey, a former ESA psychologist, co-discovered the "Earth out of view" effect with Nick Kanas, a space psychologist

professor at the University of California, San Francisco. More research is needed in preparation for a long-duration, long-distance mission to Mars (Kanas & Manzey, 2008).

International Space Station (ISS) crew experiences are inconsistent due to the ISS crew experiencing disrupted connectivity with base and family members while en route to Mars. Instead, they must wait 40 minutes to transmit and receive a single message, leading to stressful situations and social problems (Schlacht, 2012). They are completely unprepared for these shifts, no matter how well-trained or experienced they are. Because of this, it is essential to identify astronauts who are physically and psychologically healthy and who can also demonstrate their ability to work in different disciplines. In addition, they must cope with stressful events in a limited space.

4.1.4. Different gravity fields

On an expedition to Mars, an astronaut would encounter three different types of gravity: zero gravity in space, one-third of the gravity of Earth on Mars, and full Earth gravity upon your return (Whiting, Melanie; Abadie, 2019). Risks cause motion nausea and problems with spatial awareness, visual tracking, hand-eye coordination, balance, and the ability to move about (Whiting, Melanie; Abadie, 2019). Movement, coordination, balance, and bone and muscle strength can all suffer from repeated exposure to different gravity fields and transitions (Whiting, Melanie; Abadie, 2019). A mission-critical assignment can be made significantly more complicated when an individual suffers from physical limitations or is distracted by the symptoms of changing gravity fields.

Many physiological changes occur in microgravity. Since blood and cerebrospinal fluid float around the body without being affected by gravity, the head swells up while the lower half loses mass, giving the impression of a "puffy" face and skinny legs. Space motion sickness, headaches, and vision problems are all made possible by this fluid shift. Vision distortion, known as Spaceflight Associate Neuro-ocular Syndrome, is a side effect of the increased blood flow to the brain seen during space travel (Lee et al., 2017; Marshall-Goebel et al., 2019). When astronauts return to Earth, they often report feeling dizzy and having trouble regaining their motor coordination. The inner ear's vestibular system uses gravity to calculate the orientation and keep the body in equilibrium. It takes astronauts a couple of weeks to become used to both the lack of gravity in space and the return to Earth's gravity. During this shift, astronauts may experience nausea and deterioration in spatial orientation, hand-eye coordination, balance, and movement (Bloomberg et al., 2015).

As a person ages, their bone density decreases due to mineral loss. Muscles weaken and tire more easily. A person's heart and lungs lose endurance. It is possible that alterations in fluid pressure could impinge on the eyes, resulting in impaired vision, and being dehydrated increases the risk of developing kidney stones.

4.1.5. A hostile and closed environment

It is considerably easier for microorganisms to spread and grow in the closed environment of a spacecraft, whether they come from the crew's microbiomes, materials and supplies from Earth, or the onboard waste management and recycling systems. A person's immune system may transform space flight. As a result, they may be more susceptible to allergies and illnesses, which could hamper their performance.

Although the habitat is not a natural setting, it must be constructed safely. The air on the spacecraft is regularly monitored since it is essential to human survival. Gases, including formaldehyde, carbon monoxide, carbon dioxide, and ammonia, can be especially hazardous in confined spaces. Some chemicals, like ammonia, can alter the firing potential of brain cells and cause issues with cognition, including memory, attention, and sleep (Bosoi & Rose, 2009). By decreasing hippocampus stress hormone receptors, formaldehyde can negatively impact memory and exacerbate depressive symptoms (Y. Li et al., 2016).

4.2.A Review Study of Analog Mars Missions

Space habitats and subsystems are tested on Earth before launch to ensure a successful space mission. When space habitats are tested on Earth, they are often tested via simulations, which means that the habitats are tested with inhabitants in environments that resemble the target environment. These tests are conducted to ensure the overall functioning of the technological soft and hardware and examine how the human psyche and sociocultural differences affect humans in isolated, confined spaces.

Since the beginning of the space age, researchers have utilized space simulations to understand better how humans react in similar situations to those in space. For instance, they have used simulators of the space shuttle and the space station, neutral buoyancy chambers, aircraft that fly in a parabolic pattern to imitate microgravity for short periods, and computer programs that generate virtual space stations. The realism of the simulations depends on the knowledge of interest, funding, and ingenuity (Harrison, 2010).

Prior generations practiced "analog missions" before actually orbiting Earth or departing Earth's atmosphere. Following a similar thought, NASA is conducting analog trips to prepare for destinations as far out in space as Mars and the Moon. NASA and other space agencies have been conducting space simulations on analog environments to understand the habitability conditions of space environments better. By examining these analogs, NASA can learn more about its crewed space plans' feasibility, effectiveness, and limitations. Using analogies, we can also see how integrating humans and machines into scientific inquiry might yield better results.

NASA has always used space simulations to prepare astronauts for different situations and conditions. The ‘Sonny Carter training facility is a neutral buoyancy laboratory where NASA’s astronauts practice spacewalks in a massive pool (S. Strauss, 2004).

An analog mission is a fully integrated set of activities supporting and/or imitating future exploration missions to the Moon or Mars (Williamson et al., 2007). Analog missions are typically conducted in analog habitats, which share one or more significant characteristics (such as temperature, remoteness, topography, mineralogy, and so on) with the environment the mission intends to study (K. Binsted et al., 2010). The mission's analog structure has the potential to yield valuable insights into how humans react to a variety of challenges, including hazards and isolation.

The term "analog mission" refers to the testing carried out in environments that are physically analogous to those encountered in space. Before being dispatched to space, mission components are put through extensive testing on Earth. Engineers and scientists from NASA work with professionals from other government agencies, educational institutions, and private organizations to decide the specifics of these tests. During these testing, a wide variety of technological and robotics instruments, as well as vehicles, habitats, communications, power production, mobility, infrastructure, and storage systems, are put through tests. Isolation and confinement, social dynamics within the group, and other behavioral effects of a similar nature can also be observed.

Space analog environments are environments on Earth that simulate aspects of space missions with varying degrees of fidelity. Over the years, researchers have used multiple analogs for space habitats and flights, such as caves, supertankers, submarines, mines, mountains, and national parks. Fidelity, affordability, and accessibility learned through analogs are factors that can be leveraged and used in other extreme environments (Harrison, 2010). As seen in Figure 23, the literature was reviewed to analyze conducted habitability research from the beginning of space exploration. However, the established habitat review exhibits a diversity of aspects that might perplex newcomers and insiders. Some, for example, are freely available and need more than just a completed application form to become a regular crew member (e.g., MDRS).

In contrast, others determine their crews based on strict requirements such as nationality or certain personality qualities (e.g., most analog bases are run directly by national space agencies). Some habitats (such as HMP) are designed to research the ecosystem in which they are located, while others focus on technological development and testing planned mission steps (e.g., Bios-3, Lunar Palace 1). Although some are specifically designed for this purpose, human factors and habitability research may be conducted in almost all (e.g., HI-SEAS, NEK).

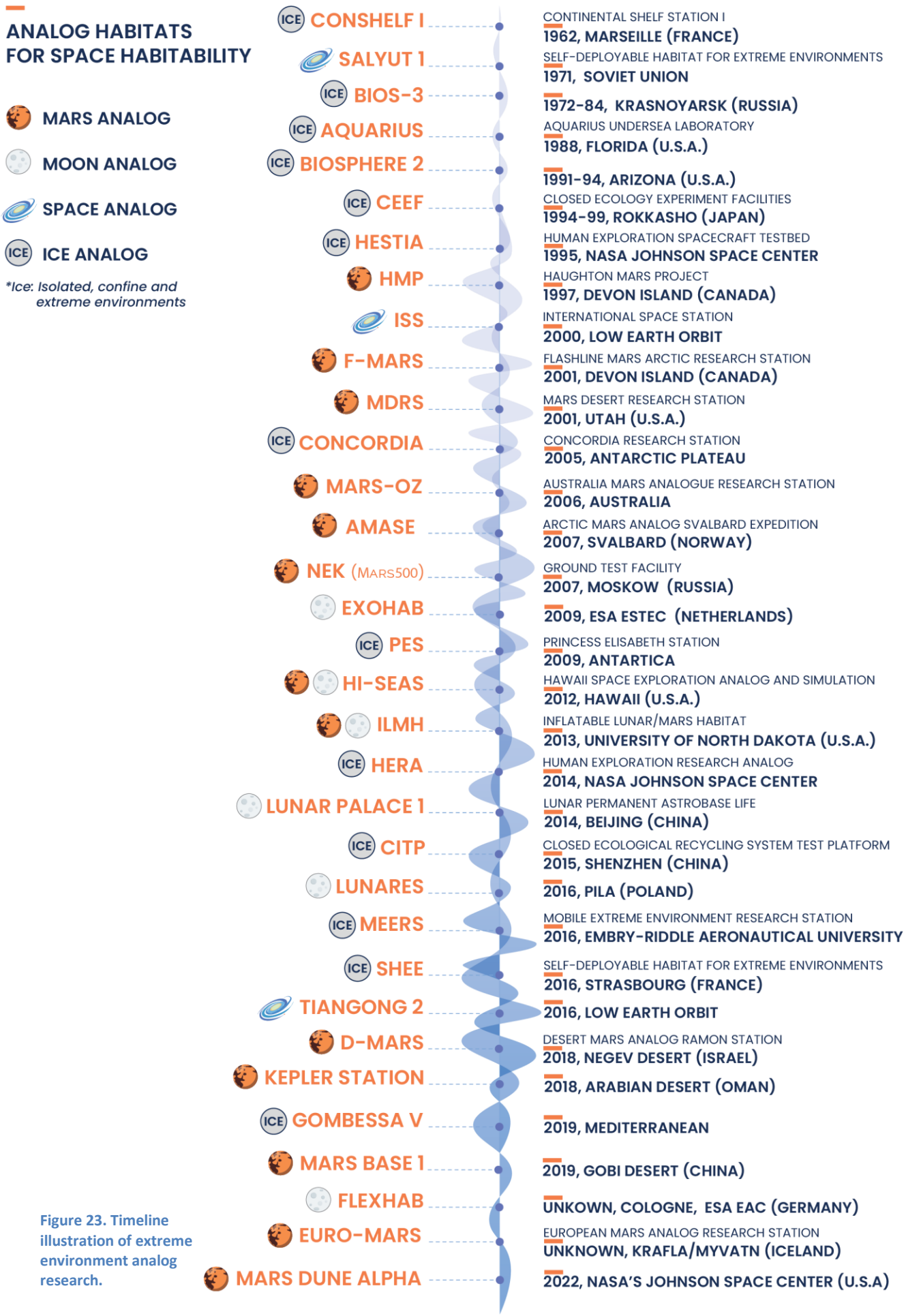

Figure 23. Timeline illustration of extreme environment analog research.

This chapter reviews the thirteen Mars analog missions between 33 published habitats for extreme environments to focus on identifying different elements of human-crewed Mars missions and needed habitation characteristics to preserve habitability. Furthermore, historical and current Mars simulation habitats can teach us how to build future Mars habitats. Even though all simulation habitats have been developed for terrestrial operation, they all seek to present a scientifically accurate environment; with this assessment, we want to identify design principles found functional and those that should be avoided in the future Mars expedition.

Figure 23 shows established research stations where scientists aimed to analyze human factors in space, Moon, Mars, and ICE (isolated, confined, and extreme environments). Between identified research stations, Mars analog research listed in Table 14 will be explained in detail to conduct comparative research to identify standard design and functional requirements.

Table 14. Mars analog research list.

	Name	Location	Agency	Objectives
1	HMP	Devon Island	Mars Society	Test new space technologies
2	FMARS	Devon Island	Mars Society	Martian surface simulation
3	MDRS	Southern Utah	Mars Society	Hardware testing and conceptual designs
4	Mars-Oz	Australia	Mars Society	Test habitats and space tools
5	AMASE	Norway	NASA	Testing of hardware and instruments, biological experiment.
6	Mars 500	Moscow	RAS/IBP	Psychological Implications of long spaceflight
7	HI-SEAS	Hawaii	NASA	Research in food, crew and dynamics, behavior, roles, and performance
8	ILMH	University of North Dakota	The U.S.A.	Only inflatable habitat intended for (terrestrial) habitation
9	D-MARS	Negev Desert	Israel/Austria	Robotic experiments
10	Kepler Station	Arabian desert, Oman	Austrian Space Forum	Mission scenario based around EVAs
11	Mars Base 1	Gobi Desert (China)	C-Space	Simulations of living on the Martian planet will be like a series of domed structures.
12	Euro-Mars	Iceland	Mars Society	Test habitats and space tools
13	Mars Dune Alpha	Johnson Space Center	NASA	Crew Health and Performance Exploration Analog

4.2.1. Houghton Mars Project

The Haughton-Mars Project (HMP) is an international multidisciplinary field research project dedicated to advancing planetary science and exploration. The HMP is supported by NASA and the project's research partners among academia, non-profit institutions, and industry (Mars Institute, 2020). The HMP was also supported by the Canadian Space Agency (CSA) as part of its Canadian Analogue Research Network (CARN) for the duration of that program (2006-2011) (Mars Institute, 2020).

The Haughton-Mars Project Research Station (HMPRS), the HMP's Base Camp on Devon Island, is located at 75° 26' N, 89° 52' W, in the northwestern rim area of Haughton Crater (Mars Institute, 2020). The HMPRS was established at its present location in 2000 (Mars Institute, 2020). Figure 24 shows the base camp and its site plan. The HMPRS is currently the largest privately operated polar research station globally and the only one dedicated to planetary analog science and exploration studies.

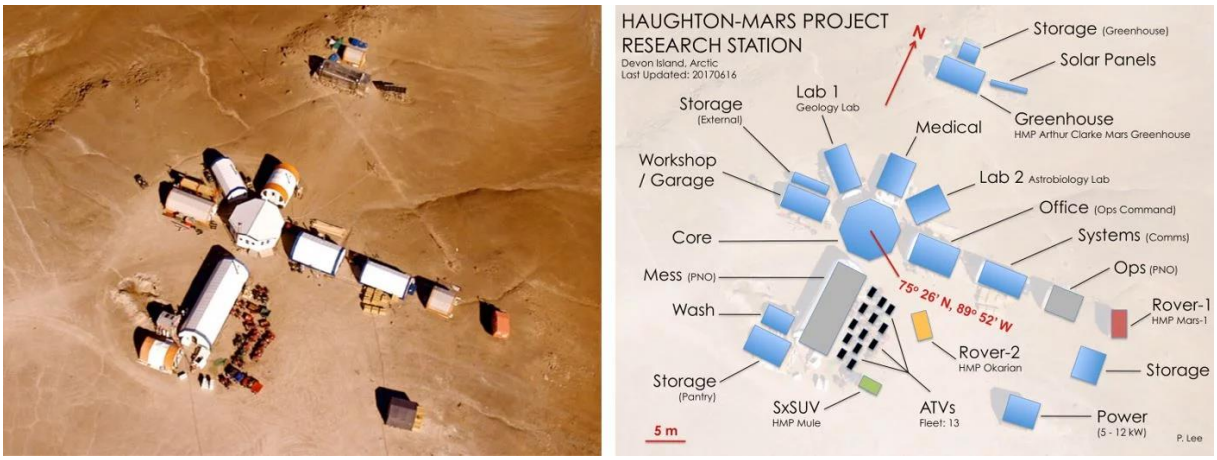

Figure 24. HMPRS's base camp and site plan diagram (Mars Institute, 2020).

The NASA HMP is a leading international Mars analog field research project centered on the Haughton meteorite impact crater site and surrounding terrain on Devon Island, High Arctic. As one of the most Mars-like places on Earth, the site is often referred to as Mars on Earth. Mars' surface is covered in craters of all sizes; therefore, the ground is made of loose rock, much like a construction site. Haughton Crater's landscape is similarly covered in loose rock, making it an excellent model for studying extravehicular activities (EVAs) and mining technology (Olson et al., 2011). Haughton Crater is also a good analog for scientific investigation since it has an extraordinary diversity of geological characteristics similar to those seen on Mars.

Furthermore, Haughton Crater is located on an uninhabited, isolated island with no infrastructure, making it a suitable model for planetary exploratory study (Olson et al., 2011). In addition to hosting around 100 participants each summer, this facility acts as a test bed for how a future Moon or Mars settlement may be planned and maintained. Like the Moon and Mars, Devon

Island poses several obstacles to human exploration, such as severe temperatures, remoteness, isolation, and a lack of infrastructure or vegetation. HMP researchers use this hostile habitat to discover safer and more efficient ways to investigate the Moon, Mars, and other planetary bodies (Olson et al., 2011).

Research at HMP is divided into two programs: Science and Exploration(Mars Institute, 2020). Over its twenty-four years, the NASA HMP has made many contributions to advancing Mars science and exploration through field studies at the site, including studies of UAVs (uncrewed aerial vehicles) (Pascal Lee, 2017). One option to make exploration safer is to delegate jobs to robots that do not need human skills or abilities (Olson et al., 2011). The HMP has a long history of putting cutting-edge robotics to the test. Another option to make exploration simpler and safer is to limit the crew's exposure to space-based contaminants as much as possible (Olson et al., 2011). To meet this difficulty, Hamilton Sundstrand created a spacesuit port that allows crew members to securely, quickly, and efficiently transfer from a pressurized spacecraft to a spacesuit, as seen in Figure 25, avoiding dust from the space environment entering the vehicle (Olson et al., 2011).

Some of the HMP's achievements, such as the automated drill project, result from successful technological demonstrations. The Drilling Automation for Mars Exploration (DAME) project at the HMP has been supervised by Dr. Brian Glass of NASA ARC since 2004 (Olson et al., 2011). The enhanced Construction and Resource Utilization Explorer (CRUX) Drill, as seen in Figure 25, was developed due to the DAME project, and it had several notable accomplishments in 2010 (Olson et al., 2011). The CRUX Drill team successfully evaluated the capabilities of the rotary-percussive drill to identify potential problems and take corrective action (Olson et al., 2011). The drill can work independently of human intervention, which is critical for planetary exploration since autonomous drilling may help prepare a place for human arrival by mining vital materials or starting outpost construction (Olson et al., 2011).

Figure 25. The construction and resource utilization explorer and spacesuit implementation (Olson et al., 2011)**.**

4.2.2. Flashline Mars Arctic Research Station

The Flashline Mars Arctic Research Station (FMARS) was established in 2000 and is the first of the Mars Society's two replicated Mars habitats (The Mars Society, 2017). Devon Island, a Mars analog habitat and arctic desert located around 165 kilometers northeast of the community of Resolute in Nunavut, Canada, is a site of the station (The Mars Society, 2017). The station overlooks the Haughton impact crater, which is 23 kilometers and was produced roughly 39 million years ago.

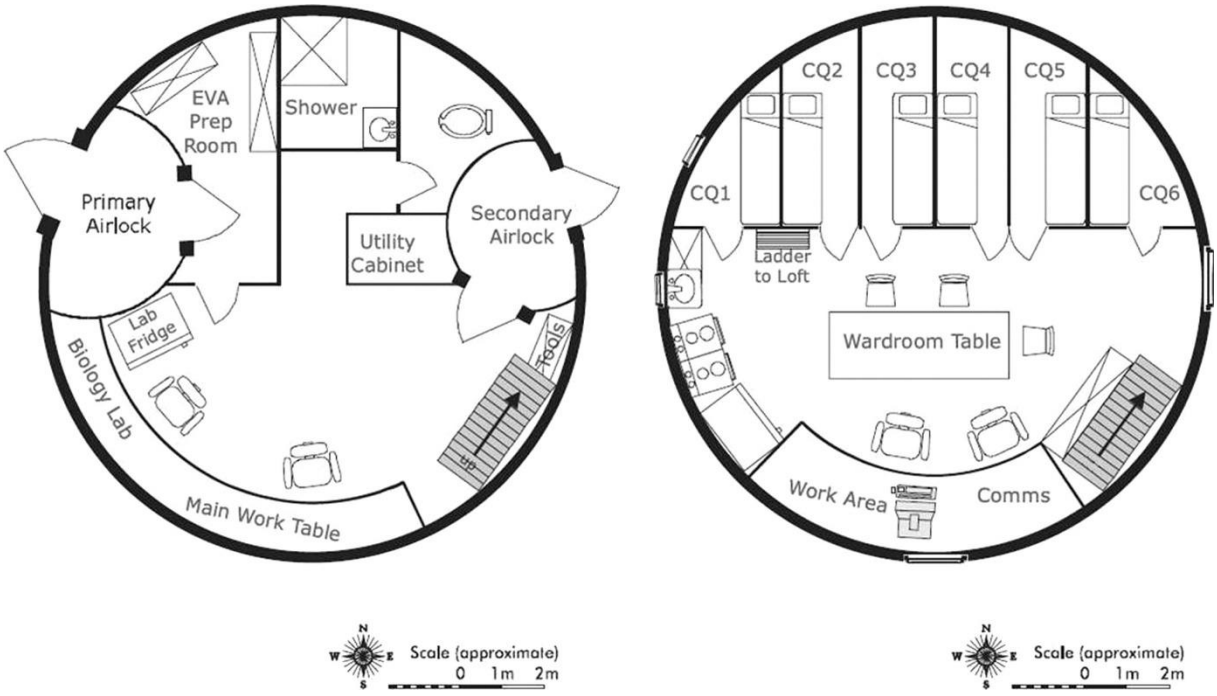

Figure 26. The lower (left) and upper (right) deck plans of FMARS (The Mars Society, 2017).

As shown in Figure 26, The FMARS is a two-deck structure with an 8-meter diameter and a 7.8-meter height. From the beginning of field operations in April 2001 to August 2017, twelve separate crews (consisting of 6–7 personnel) have inhabited the station. The station was a significant element in parallel investigations of the technologies, strategies, architectural design, and human factors involved in human missions to Mars as an operational testbed. Before scientists leave the field location and return to their home institutions, the facility provides the field with small laboratories where in-depth data analysis can proceed.

The habitat was designed to accommodate six crew members working cooperatively. On the lower deck of the FMARS station, the geo/biological laboratory, EVA preparation space, a common area, and a bathroom were located. Personal quarters, a communal area serving as a galley, wardroom, and storage were located on the upper deck to separate functional relaxation demands from the working environment.

As seen in Figure 27, research conducted on the July 2009 FMARS crew investigated the psychological issues crew members face (particularly the effects of isolation from family, disagreements among crew members, and nutrition) and the positive effects of problem-solving and exploration (Cusack et al., 2009). The laboratory equipment was organized on the workbench conducive to sample processing. The rock cutter, the rock polisher, the preparation and cleaning area, the slide preparation area, the microscope, the centrifuge, and the pigment/biomolecule extraction area can be seen from left to right.

Figure 27. "Earth-based" remote science team (Sklar & Rupert, 2004).

A study of subsurface water detection techniques (Figure 28) was undertaken by crew members living in the habitat. While wearing prototype space suits, crew members installed seismic sensors along the Haughton crater and then evaluated how the sensors responded to mini-earthquakes (caused by a sledgehammer) to create a three-dimensional subsurface map (Pletser et al., 2009). Additional tests were performed to see how well the FMARS crew members might collaborate with an "Earth-based" remote science team. In one case, remote science used aerial pictures to identify ten areas of scientific interest for the FMARS crew to investigate and study (Sklar & Rupert, 2004). This experiment assisted researchers in developing more efficient techniques for scouting and studying sites of interest while operating under the communications constraints of a crewed mission to Mars.

Figure 28. A study of subsurface water detection (Pletser et al., 2009).

4.2.3. Mars Desert Research Station

The Mars Desert Research Station (MDRS) is the second Mars analog habitat established by the Mars Society. MDRS is a space analog facility on the San Rafael Swell in Utah that supports Earth-based research in the quest for human space exploration technology, operations, and science. Professional scientists, engineers, and students stay for an eight-month field season in training for human operations on Mars (The Mars Society, 2022).

As seen in Figure 29, the facility's relative remoteness allows for intensive field studies and human factors research. Most personnel carry out their missions inside the parameters of a simulated Mars mission. Most expeditions last 2-3 weeks, though the operator of the research station has allowed more extended missions (The Mars Society, 2022). By 2022, thirteen field seasons by 218 crews (The Mars Society, 2022).

Figure 29. A view from Mars Desert Research Station (The Mars Society, 2022)**.**

The Mars Desert Research Station (MDRS) is a research station on Mars used to study how to live and work on another planet. It is also a habitat model that will land humans on Mars and serve as their primary base of operations for months of exploration in the inhospitable Martian environment (The Mars Society, 2022). A habitat like this is essential to current human Mars mission planning. MDRS is inhabited by teams of six to seven crew members, including geologists, astrobiologists, engineers, mechanics, physicians, human factors researchers, artists, and others, who live in complete isolation in a Mars-like environment for weeks to months at a time (The Mars Society, 2022).

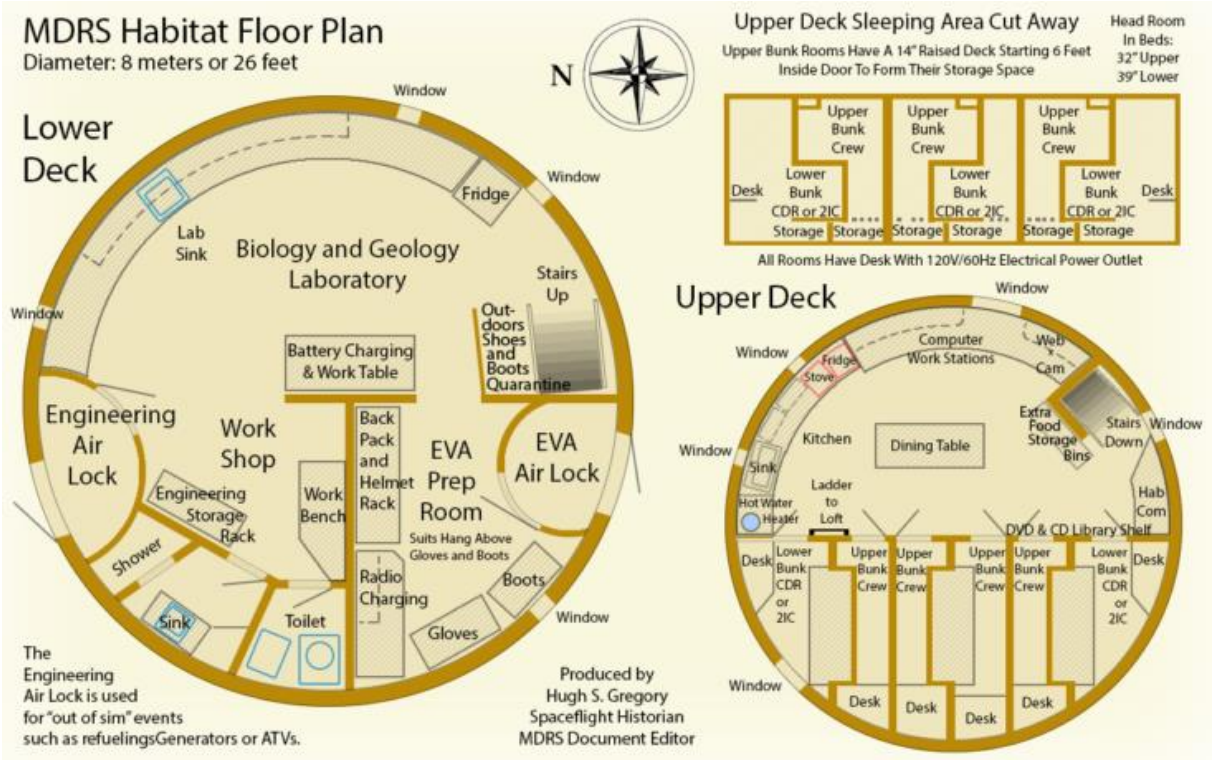

Figure 30. The lower (left) and upper (right) decks plans of the MDRS habitat unit (The Mars Society, 2022).

The MDRS campus consists of six structures. The habitat (Hab), as seen in Figure 30, is a two-story, eight-meter-diameter cylindrical building built in 2001 (The Mars Society, 2022). It can host up to seven crew members at once. The bottom deck houses the EVA prep room with spacesuit simulators, an outdoor airlock, a shower room, a toilet room, and a rear airlock leading to tunnels that reach additional structures. The upper deck holds the living accommodations, which comprise a shared work/living area, a fully functional kitchen, and seven bunk staterooms. Six staterooms are on the main floor, with a seventh in the loft.

The MDRS consists of an Observatory and the MDRS Robotic Observatory (The Mars Society, 2022). The Musk Observatory is a solar facility with a 100 mm refracting telescope and a double stack of hydrogen-alpha filters. The MDRS Robotic Observatory is automated. All observations are completed online. The Crew Astronomer selects the images to photograph over the Internet at any time of day or night, and the telescope captures the images on the next clear evening.

A greenhouse, science unit, and maintenance module are all included in the research station (The Mars Society, 2022). The GreenHab is a 3.65 m by 7.30 m structure containing traditional aquaponic growing systems and space for crop research. The Science Dome is a 7-meter-diameter geodesic dome that holds the control center for our solar system and a working microbiological and geological laboratory. The RAMM (Repair and Maintenance Module) is the most current structure on the property. Except for the Robotic Observatory, all structures are connected to the Hab through above-ground tunnels, allowing users to use these structures while remaining in simulation (The Mars Society, 2022).

4.2.4. Australia Mars Analogue Research Station

The centerpiece of MSA's (Mars Society Australia) technical program is the proposed Australia Mars Analogue Research Station (Mars-Oz) simulated Mars base. The simulated base aims to explore the issues of living and working on another planet, including facilitating research into social-psychological factors and related engineering design of crewed missions to Mars or the Moon (Willson et al., 2005).

The preferred site for the Mars-Oz simulated base is on the Arkaroola lease, Australia's first and largest private nature preserve (Willson et al., 2005). The facility consists of two 20-tonne road transportable modules designed around a concept mission using a 'Mars Semi Direct' architecture and horizontally landed iconic bent spacecraft (Willson et al., 2005). The facility is designed to house up to 8 people simultaneously and undergo progressive expansion with additional modules(Willson et al., 2005).

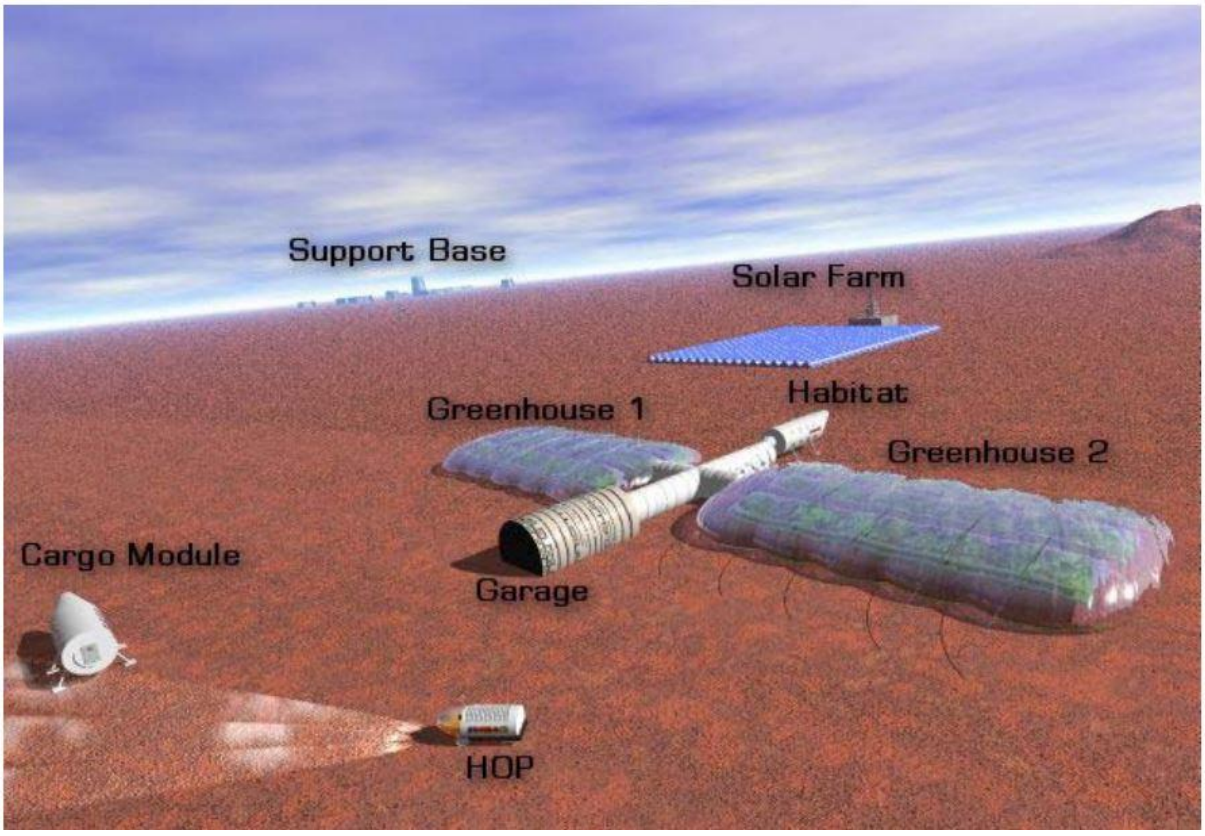

Figure 31. Three-dimensional model of Mars-Oz (Clarke, 2002).

As seen in Figure 31, habitat, inflatables (greenhouses & garages), solar farms, support bases, and cargo modules are the five components of the planned Mars-OZ (Clarke, 2002). Willson and Clarke have published extensively on a group of Mars landers. Three vehicles are used in the mission concept: a Habitat vehicle (or Hab), a Cargo vehicle (both of which land), and a Mars Transfer Vehicle (MTV) (which remains in orbit). A Mars Ascent Vehicle with an in-situ fuel processing plant is housed in a separate front segment of the Cargo vehicle. A pressurized rover, multi-port adaptors, flexible airlocks,

and other goods are housed in the garage in the back part (Willson et al., 2005). Habitat (Hab) - Travels to the Martian surface, direct from the earth, and becomes the Mars base's core. It consists of a cabin, propulsion module, heat shield, landing engines, and parachutes. Concept designs of the interior of the unit, including the floor plan and fittings, have been prepared by Kerstin Thompson Architects. Cargo Vehicle - Transports equipment to the Martian surface direct from earth two years before the crew's arrival. The equipment consists of a Mars Ascent Vehicle (MAV) for the crew to reach low mars orbit, hydrogen stock fuel, an in-situ resource utilization processing plant, a pressurized rover, and surface supplies. It also has a propulsion module, heat shield, landing engines, and parachutes. Mars Transfer Vehicle (MTV) - Travels to low Mars orbit from Earth. It transports the crew back to Earth from low mars orbit. It consists of a cabin, a landing capsule with a heat shield, and a propulsion module for return.

A cylinder cone is preferable to a strict biconic for simplicity of fabrication and transport. As shown in Figure 32, the planned habitat for Mars-OZ is a 12-meter-long, 4.5-meter-diameter cylinder with a 6-meter-long upswept nose cone (Clarke, 2002). The habitat sits 0.5 m above the ground on four movable legs (with skids for limited shifting) but will require an extra tie-down as a precaution against heavy winds (Clarke, 2002). The habitat's principal access and exit will be through an airlock on the habitat's flat back bulkhead. MARS-interior OZ's volume with these specifications is 238 m^3 (Clarke, 2002). The two-deck habitat module has ~122 m^2 of usable floor area, around the size of a small three-bedroom house. The upper deck is used for living and working, while the lower deck is used for sleeping, washing, and toileting.

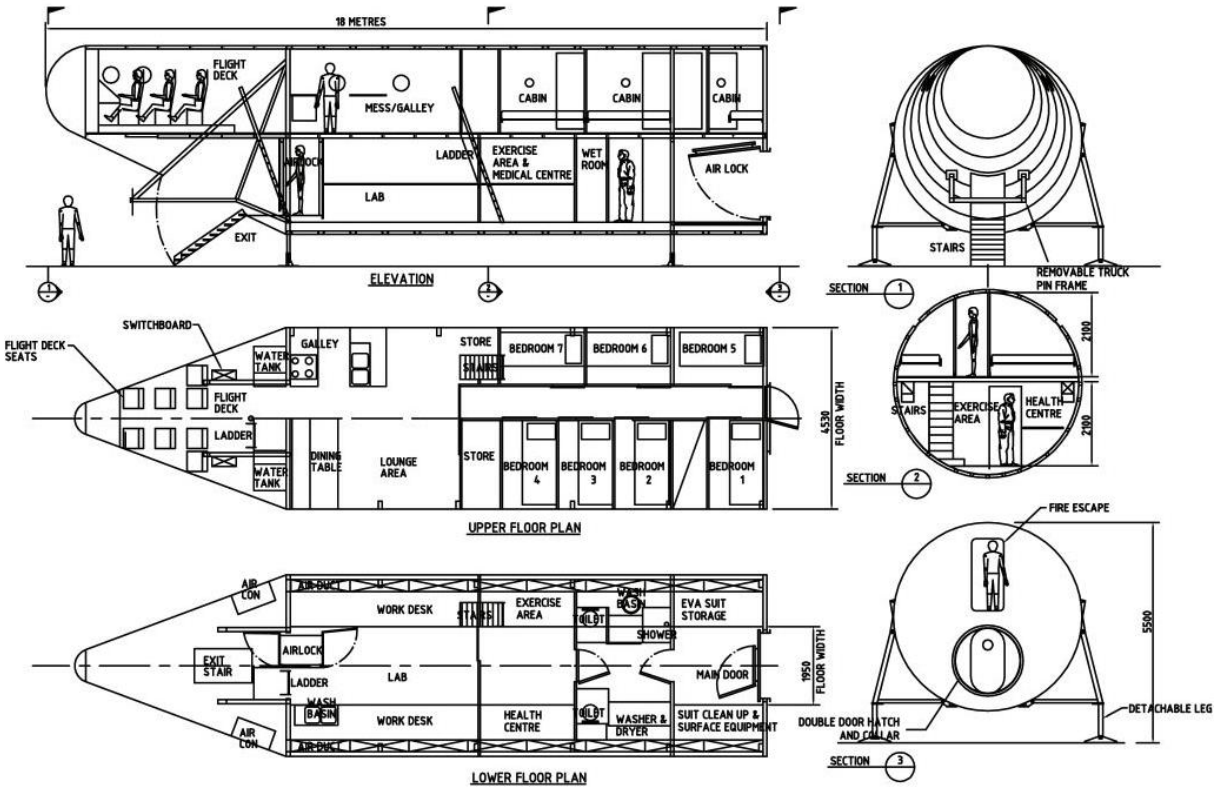

Figure 32. Technical drawings of Mars-OZ habitation (Clarke, 2002).

4.2.5. Arctic Mars Analog Svalbard Expedition

Arctic Mars Analog Svalbard Expedition (AMASE) uses Mars analog field sites on Svalbard for fundamental research within astrobiology and testing of payload instruments onboard future "Search for Life" missions to Mars (Mars Science Laboratory, Exomars and Mars Sample Return) (Research in Svalbard Database, 2011). AMASE activities on Svalbard were conducted between 2003 and 2014 and were funded through NASA, ESA, and the University of Leeds (Research in Svalbard Database, 2011).

The Arctic Mars Analogue Svalbard Expeditions (AMASE) 2010 were a series of expeditions supported by NASA ASTEP and ESA PRODEX, with the primary goals of 1) testing portable instruments for robustness as field instruments for life detection, 2) assessing Mars analog environments for biosignatures and biosignatures, 3) refining protocols for contamination reduction, 4) defining a minimal instrument suite for Astrobiology science on Mars, and 5) sample acquisition, collection, and caching of suitable samples by rover platforms containing sample acquisition hardware: Cliffbot (as seen in Figure 33) and Athena. AMASE served as a test bed for both in-situ robotic missions and Mars Sample Return mission architectures as NASA and ESA started a new era of collaboration.

The Bockfjord Volcanic Complex (BVC) is one of the main AMASE field sites with a unique combination of volcanoes, hot springs, and permafrost and is the only place on Earth with carbonate deposits identical to those in the Martian meteorite ALH84001 (Research in Svalbard Database, 2011; Steele et al., 2011). BVC provides a unique opportunity to study the interaction between water, rocks, and primitive life forms in a Mars-like environment and is an ideal testing ground for payload instruments onboard Mars missions (Research in Svalbard Database, 2011). Other field sites studied by AMASE include mixed evaporite- and clastic sediments in Billefjorden, Devonian redbeds, and Miocene flood basalts in the Bockfjord-Woodfjord area, Neo-Proterozoic stromatolites in Murchison Fjord, and the Pallander icecap (Research in Svalbard Database, 2011).

AMASE field experiments could address sample collecting, caching, and contamination issues that will be important in future sample return missions. Two experiments used during the AMASE 2009 campaign, X-ray diffraction (XRD) and evolved gas analysis (EGA), closely resembled similar experiments planned for the Mars Science Laboratory in 2011 (MSL) (Mahaffy et al., 2010).

Figure 33. Testing how Cliffbot can be used to support astronaut activities on Mars

4.2.6. MARS-500

The NEK (Nazemnyy Eksperimental'nyy Kompleks), as seen in Figure 34, located in Moscow, Russia, is the oldest and possibly most well-known of Mars analog bases. The complex was formerly known as "the Mars 500 facility", but it is currently known as "the Ground Test Facility" (NEK, corresponding to the Russian original) (Heinicke & Arnhof, 2021). During the 520-day simulation "Mars500," which remains the most extended spaceflight simulation, the EVA module and a small lander module were used for (only) a 10-day simulated surface stay, with the crew living in the three habitation modules for the rest of the mission.

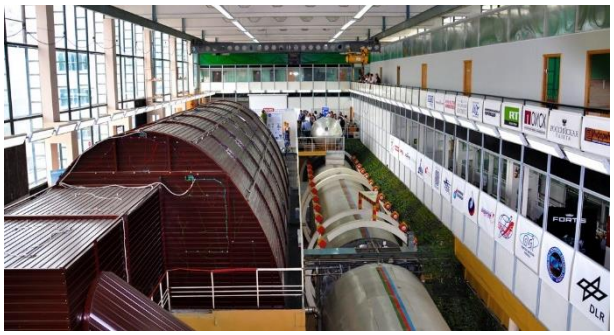

Figure 34. IBMP facility in Moscow (The European Space Agency, n.d.-c).

The Mars-500 mission was a series of experiments conducted between 2007 and 2011 and sponsored by Russia, the European Space Agency, and China. The primary focus of these experiments was to study the effects of long-term isolation on a small crew so that the psychological difficulties of a voyage to Mars and an extended stay on its surface may be better understood. Three separate missions were performed: 14-day isolation in November 2007, 105-day isolation completed on 14th July 2009, and 520-day isolation from 3rd June 2010 to 4th November 2011 (The European Space Agency, n.d.-b). Unlike other Mars Analog missions, Mars-500 did not occur in a Mars-like environment but at a Moscow research institute.

The final stage of the experiment, designed to replicate a 520-day crewed trip, was carried out by an all-male crew comprised of three Russians (Alexey Sitev, Sukhrob Kamolov, and Alexander Smoleevskij), a Frenchman (Romain Charles), an Italian (Diego Urbina), and a Chinese citizen (Yue Wang). The mock-up facility simulated a shuttle spacecraft from Earth to Mars, an ascent-descent craft, and the Martian surface (The European Space Agency, n.d.-a). Professionals with backgrounds in engineering, medicine, biology, and human spaceflight were among the volunteers in the three stages (The European Space Agency, n.d.-a). The experiment taught us a lot about the physical, social, and mental effects of living in close quarters for a long time.

Figure 35. 'Marswalk' at the simulated martian terrain of the Mars500 (The European Space Agency, n.d.-c).

As seen in Figure 36, the isolation facility, mission operations room, technical facilities, and offices were all part of the complex (The European Space Agency, n.d.-c). The isolation facility consisted of five modules (The European Space Agency, n.d.-c). The primary spacecraft was represented by three components: habitat, utility, and medical modules. The fourth module served as a model of the Martian lander and was linked to the main spacecraft. The fifth module was a Martian surface simulator (as seen in Figure 35). The modules had a total volume of 550 m^3, and the facility provided all the equipment required to experiment. Communications and control systems, ventilation systems, air and water supplies, electrical installations, sewage systems, air and water quality monitoring and partial recycling systems, medical equipment, fire and other safety monitoring systems, and emergency equipment were among them. The modules were kept at normal atmospheric pressure on Earth.

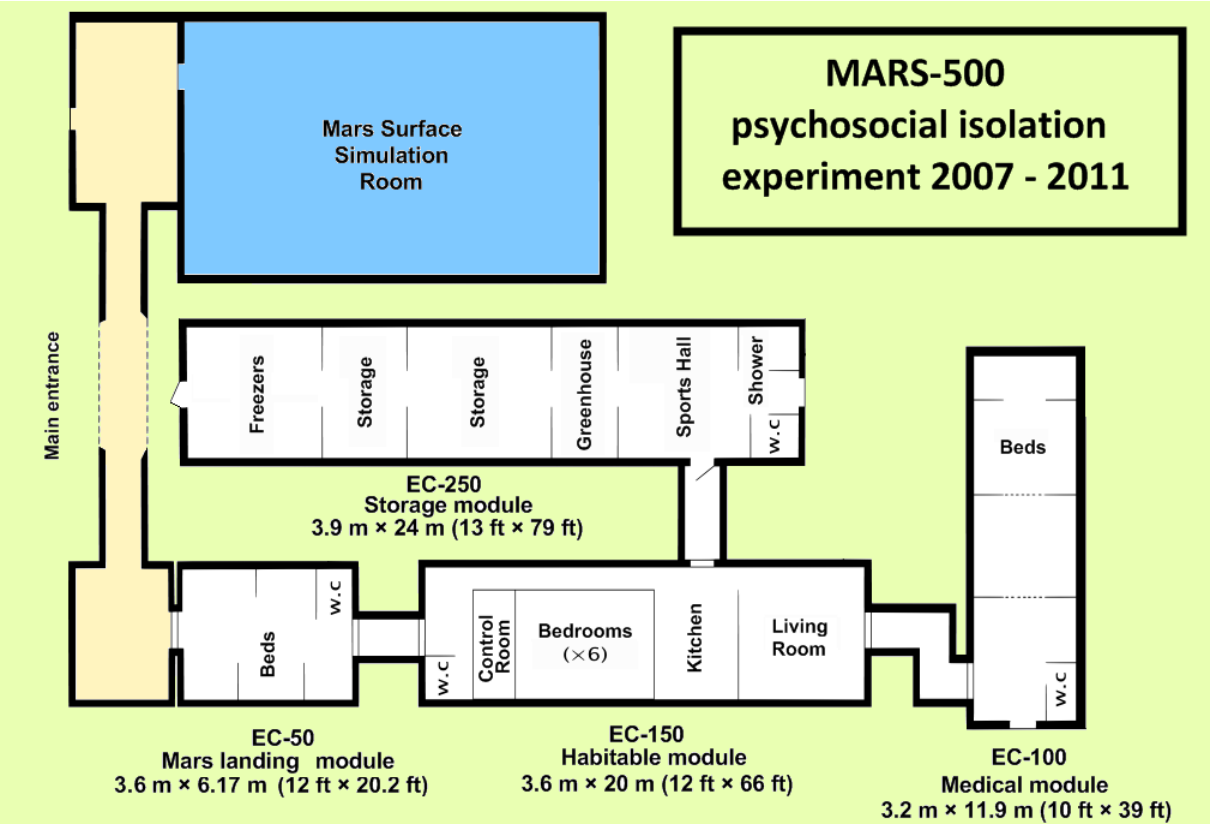

Figure 36. The isolation facility consisted of five different modules (The European Space Agency, n.d.-c).

The main living accommodations for the crew were in the habitable module (The European Space Agency, n.d.-c). Six independent crew compartments, a kitchen/dining room, a living room, the main control room, and a toilet were all included in the cylindrical 3.6 m x 20 m module(The European Space Agency, n.d.-c). A bed, a desk, a chair, and shelves for personal things were included in each 2.8-3.2 m^2 bedroom compartment.

Two medical berths, a toilet, and equipment for routine medical checks were placed in the cylindrical medical module, which measured 3.2 m x 11.9 m. It also had telemedicine, laboratory, and diagnostic testing equipment (The European Space Agency, n.d.-c). If any crew members became ill, they would have been quarantined and treated in the module.

As seen in Figure 37, the Mars landing module simulators were only used for the experiment's 30-day "Mars-orbiting" phase (The European Space Agency, n.d.-c). The 6.3 m x 6.17 m cylindrical module included three bunk beds, two workstations, and a toilet to accommodate three crew members. Among the ancillary systems are a control and data-collection system, a video control and communications system, a gas analysis system, an air-conditioning, and ventilation system, a sewage and water supply system, and a fire-suppression system.

The circular 3.9 m x 24 m storage module was divided into four compartments: a refrigerated food storage section, a nonperishable food storage compartment, an experimental greenhouse, and a bathroom, sauna, and gym compartment (The European Space Agency, n.d.-c).

An essential focus of the Mars-500 research has been the early diagnosis of “adverse personal dynamics” that would affect cooperation among the crew and the development of methods to overcome such issues (Institute of Biomedical Problems (IMBP), n.d.). Researchers decided that any psychological support on future missions must be tailored to each crew member, not just the group or subgroups belonging to different space agencies. Mars-500 also found that most psychological issues were exacerbated by isolation and a lack of stimulus, emphasizing the need to prevent sensory deprivation and boredom.

Figure 37. Interiors of Mars 500 modules (The European Space Agency, n.d.-c).

4.2.7. The Hawai'i Space Exploration Analog and Simulation

The Hawaii Space Exploration Analog and Simulation (HI-SEAS) program is organized by Cornell University and the University of Hawai'i at Mānoa (K. A. Binsted & Hunter, 2013), currently operated by the International MoonBase Alliance.

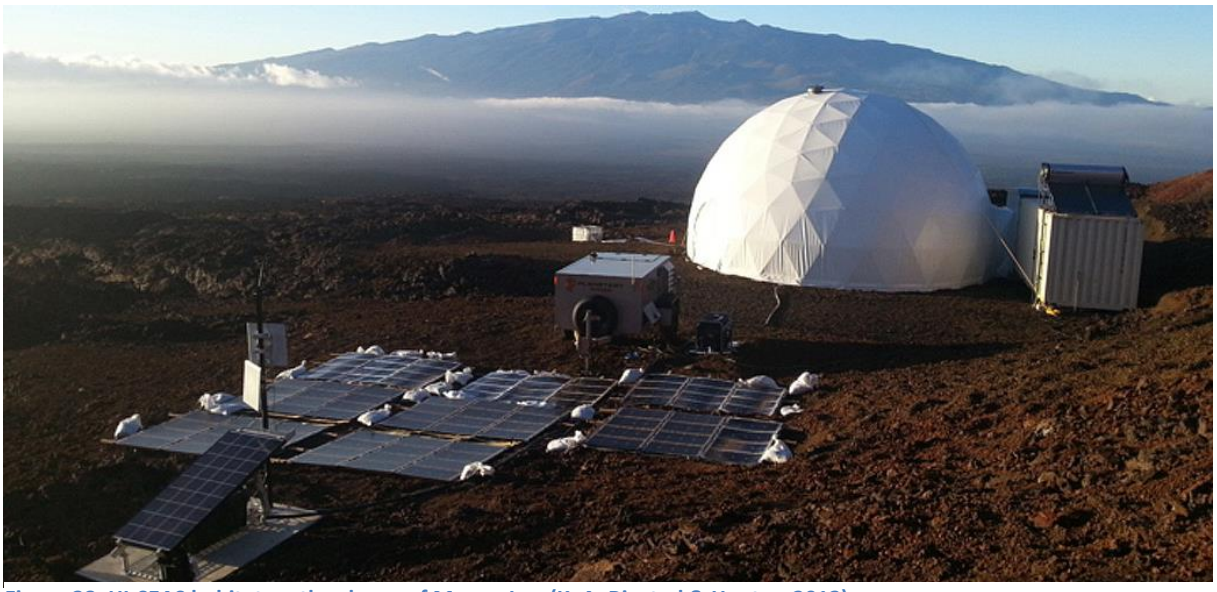

Figure 38. HI-SEAS habitat on the slopes of Mauna Loa (K. A. Binsted & Hunter, 2013)

As seen in Figure 38, The habitat is located 2,500 m above sea level on Mauna Loa on the Big Island of Hawaii (K. A. Binsted & Hunter, 2013). The habitat is built on a Mars and Moon-like site on the Mauna Loa volcano on the Big Island of Hawaii, also completely isolated from civilization and with built-in communication delay. The analog habitat resembles a realistic Mars habitat and has been used for multiple experiments lasting 4-12 months. The analog allows high fidelity geological field since the weathered basaltic materials in this part of Hawaii are similar to the Martian regolith.

The HI-SEAS Habitat is semi-portable, low-impact, and has desirable analog qualities for habitation on Mars and the Moon (HI-SEAS, n.d.). It features a habitable volume of ~368 m^3 and a functional floor space of ~111.5 m^2(HI-SEAS, n.d.). As shown in Figure 39, the ground floor has an area of 30.3 m² (usable 26,8 m²), with the second floor spanning an area of 39,4m² comprising six individual rooms and a small bathroom with toilet only (Häuplik-Meusburger et al., 2017). Attached to the habitat's exterior is a single shipping container, providing storage for food and other supplies and hosting the water and electrical systems. The upper floor (12,9 m²) accommodates six separate bedrooms and a bathroom with a toilet and washing basin. An additional 48,8m² converted shipping container is attached to the dome (Häuplik-Meusburger et al., 2017).

The HI-SEAS facility is visually isolated yet accessible through a rural road, and a hospital and other emergency services are only a one-hour drive away (HI-SEAS, n.d.). It features a mild, dry environment that varies slightly throughout the year, allowing for long-duration missions. HI-SEAS

provides more than just physical isolation and geological similarities (HI-SEAS, n.d.). The Station includes a sophisticated system of high-latency communication between the Crew and the Mission Support crew, which imposes a 20-minute delay on message reception each way, similar to Mars (and a few-second delay for analog lunar missions) (HI-SEAS, n.d.). Email is used for all asynchronous communication (no real-time interactions). HI-SEAS provides a setting in which communication latency and other mission characteristics can be adjusted to meet the needs of the investigation.

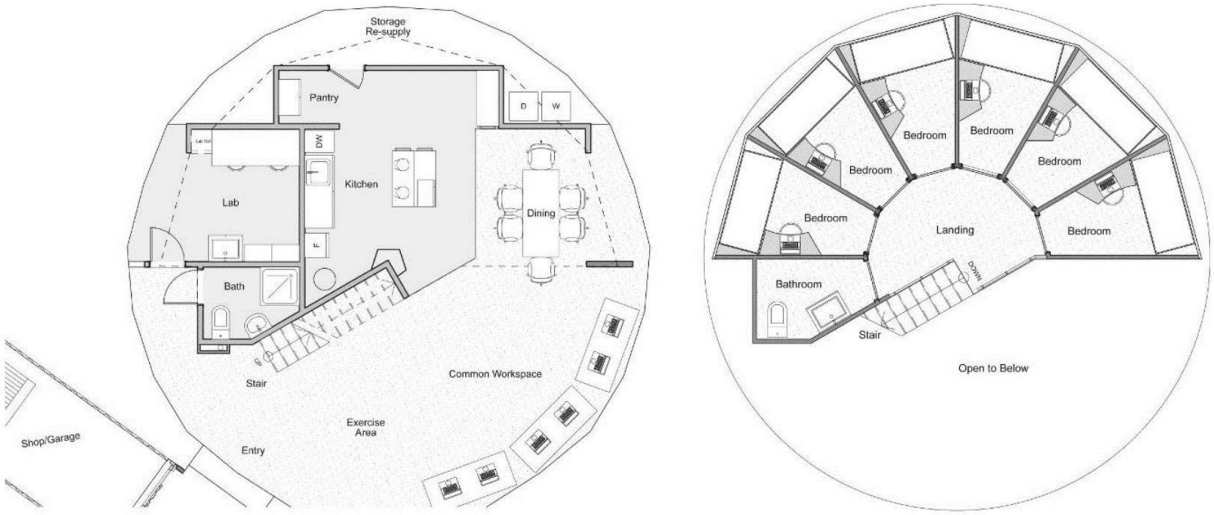

Figure 39. Ground and first-floor plans of HI-SEAS. (Layout montage by Angelo Vermeulen) (HI-SEAS, n.d.).

In 2012, NASA provided funding to the University of Hawai'i at Manoa for three campaigns with mission durations ranging from four to twelve months. Campaign 1 aimed to compare the resource costs and nutritional and psychosocial benefits of two food systems proposed for long-term space missions: pre-packaged "instant" foods and cuisines produced by the crew using shelf-stable, bulk-packaged materials. Campaign 2 aimed to collect data on team cohesion and performance through continuous monitoring of face-to-face interactions with sociometric badges, mitigation of the effects of isolation through immersive 3D virtual reality interactions with the crew's family and friends, and measurement of emotional and practical states through automated analysis of multiple forms of textual communications provided by crew members to identify relevant and effective team members. Campaign 3 focused on discovering psychological and psychosocial characteristics, measures, and combinations of these factors that can be used to create highly effective crews for autonomous, long-duration, and/or distant exploration missions. In addition to campaigns, HI-SEAS has run five missions without NASA funding; they are listed in Table 15 (Häuplik-Meusburger et al., 2017).

Table 15. HI-SEAS Mission Overview (Häuplik-Meusburger et al., 2017).

Mission	Crew Member	Start of Mission / Duration	Habitability related research
HI-SEAS I	6	April 2013; Four months	Culinary and psychological aspects (temperatures in artificial habitats, variation of astronaut diets).
HI-SEAS II	6	March 2014; Four months	Research on team cohesion and performance, 3D VR interactions with family and friends, and emotional and practical states using automated analysis of textual communication to identify effective teamwork behaviors.
HI-SEAS III	6	October 2014; Eight months	The extended version of the HI-SEAS II research tasks has the same focus for twice the duration.
HI-SEAS VI	6	August 2015; 12 months	Social and psychological effects of long-duration isolation on crew cohesion and task completion, the most extended mission so far, extended version of HI-SEAS II and III.
HI-SEAS V	6	January 2017; Eight months	Team composition and dynamics, and their effects on performance.

Like other missions, HI-SEAS evaluates the social and psychological status of the crewmembers while they live in isolation and conduct fieldwork in Mars-like environments and conditions. Early missions focused on the diet and nutrition of its crewmembers. More recent missions have focused on crew composition and communication, specifically in-mission crew interaction and mission debrief technique (Häuplik-Meusburger et al., 2017).

4.2.8. Inflatable Lunar-Mars Habitat

The University of North Dakota's (UND) Inflatable Lunar-Martian Analog Habitat (ILMAH, also known as ILMH or LMAH) is part of an exceptionally complete mission setup (as seen in Figure 40) that includes not only the habitat itself but also a Pressurized Electric Rover (PER) and the North Dakota Experimental (NDX)-2 space suit. The habitat is a unique hybrid inflatable structure with a rigid internal frame and an exterior inflatable bladder. The only pressurized facility using lightweight structures and inflatables is ILMH. Dimensions of habitation are 12 meters by 10 meters by 2.5 meters. A place for sleeping, cooking, toilet facilities, and a laboratory are all contained within this structure. ILMAH features its ventilation system, which is responsible for pressurizing the habitat, providing breathing air for the crew, and removing undesired particles from the airflow. The ILMAH uses a blower to draw ambient air for pressurization and breathing air supply.

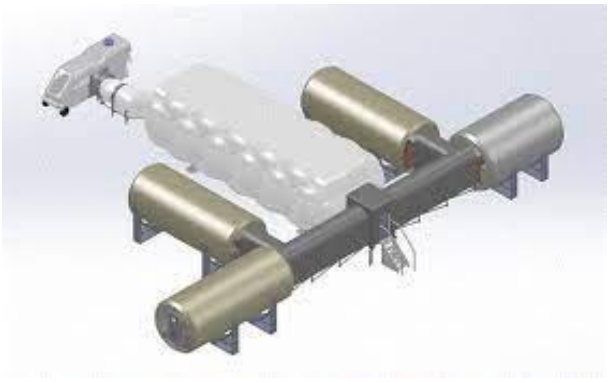

Figure 40. 3D Model of Inflatable Lunar Martian Analog Habitat (Swarmer et al., 2014).

The ILMH's research focuses on technological testing, medical aspects, and psychological consequences of ICE settings(Pedraza, 2013, 2018). The main module includes a workstation where most lab tests (such as reaction time and polygraph) are performed. A soldering and electronics station and a tool station are included in the EVA module (Swarmer et al., 2014).

As seen in Figure 41, the habitat has an emergency/EVA airlock and a docking tunnel airlock connecting the habitat and the electric rover (Swarmer et al., 2014). The electric rover is outfitted with a sample box airlock and two suit ports (Swarmer et al., 2014). According to Ortiz et al., the structure of the main habitation module may withstand a 1 m thick layer of regolith in Martian gravity (Ortiz et al., 2015). They propose making panels for the habitat's interior out of hydrogen-rich materials like polyethylene to improve the structure's radiation shielding capabilities.

Figure 41. Inflatable Lunar Martian Analog Habitat on Site (Swarmer et al., 2014).

The habitat's exterior is insulated with a 25.4 cm layer of fiberglass. During the 10-day simulation, this measure kept the internal temperatures in the habitat generally steady (between 16˚C and 21˚C) (Swarmer et al., 2014).

4.2.9. Desert Mars Analog Ramon Station

Desert Mars Analog Ramon Station (D-MARS) is a Mars analog station committed to advancing space exploration technologies, methodologies, processes, and knowledge (Rubinstein, Sorek-Abramovich, et al., 2019). D-MARS also aspires to encourage space-related education and technical innovation through analog mission operations and infrastructure.

D-MARS was established in 2017 and has directed Mars analog missions since 2018. D-MARS is located in Israel's Ramon Crater, a location, as seen in Figure 42, that geographically resembles the Martian surface. The Ramon crater is 11 km wide and 40 km long and is the biggest of three erosional craters in Israel's Negev desert in the south. The erosional crater ("makhtesh") is a geological phenomenon characterized by the formation of a valley at the crest of an anticline surrounded by cliffs (Benaroya, 2018). The climate within the makhtesh is hyper-arid on the rim and semi-arid within the makhtesh, with an average annual precipitation of 40-80 mm. The temperature difference between day and night is severe, with extreme temperatures ranging from 55 °C in the summer to 0 °C in the winter (Rubinstein, Abramovich, et al., 2019).

Figure 42. D-MARS Habitat analog environment. (Benaroya, 2018).

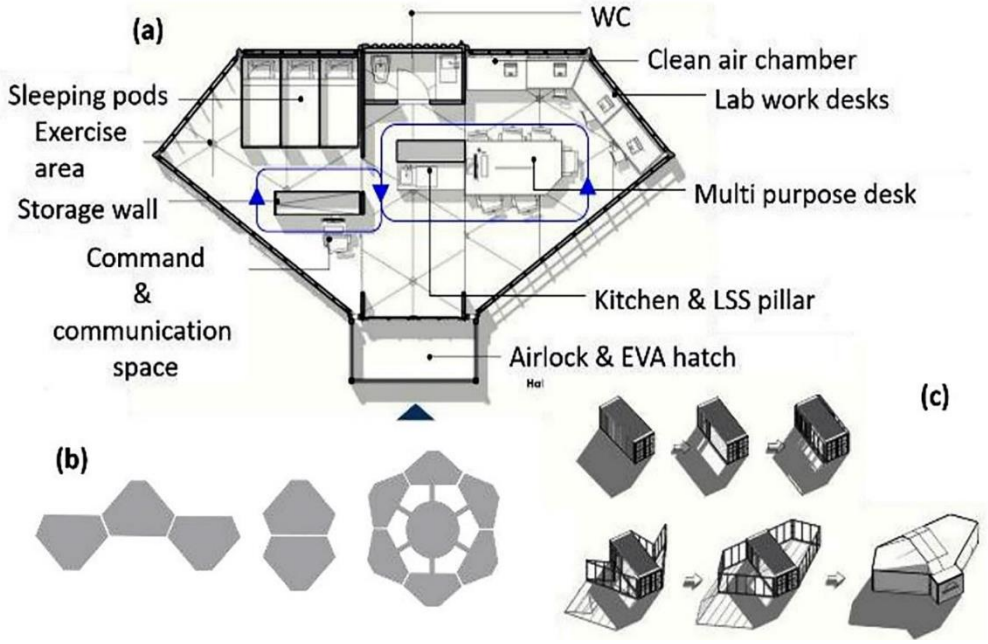

Figure 43. Plan and conceptual representation of D-MARS habitation (Benaroya, 2018).

As seen in Figure 43, the habitat structure is an unfolding structure built on the frame of a container structure that contains rigid infrastructure such as water pipelines, electricity, and communication equipment (Rubinstein, Abramovich, et al., 2019). D-design MARS's concept is built on three primary components: a deployed portable structure, a scalable habitat unit, and indoor spatial augmentation. It is a 15-square-meter moveable structure that can be expanded to 50 square meters, allowing us to mimic the mission story from launch to deployment and future expansion. Two movable wings are joined to this structure, transforming it from a 15-square-meter structure to a 60-square-meter one (Benaroya, 2018). This method enables us to mimic the expedition to Mars, from the launch stage and folding packing of the Habitat through landing, deployment, and day-to-day operations.

As shown in Figure 44, the habitat was developed to expand and evolve by adding new structures that link to form a more extensive and comprehensive system. This approach is achievable by establishing a network of interconnected Habitats to form a complete Mars outpost facility by developing a modular shell that can be joined to other structures (Rubinstein, Abramovich, et al., 2019).

Figure 44. The modularity of D-MARS habitation (Rubinstein, Abramovich, et al., 2019).

During 2018-2019, D-MARS members carried out Mars analog missions, as seen in Figure 45 (Rubinstein, Abramovich, et al., 2019). Several analog Mars missions were carried out during the 2019 field campaign (February – March 2019): An 11-day primary analog mission; a three-day "Landing on Mars" simulation mission to prepare and test infrastructure and technological equipment, simulating a crew in the landing phase on Mars; a two-day medical analog mission that included several medical emergency simulated events; and a dedicated high school student group performed three-day analog missions as part of the Young Astronaut Academy (YAA). During the primary 11-day mission, further scientific studies included soil analysis, environmental microorganisms metagenomics, isolation and characterization, rover usage for external mapping and situational investigation, various psychological assessments of crew health, and more (Rubinstein, Abramovich, et al., 2019).

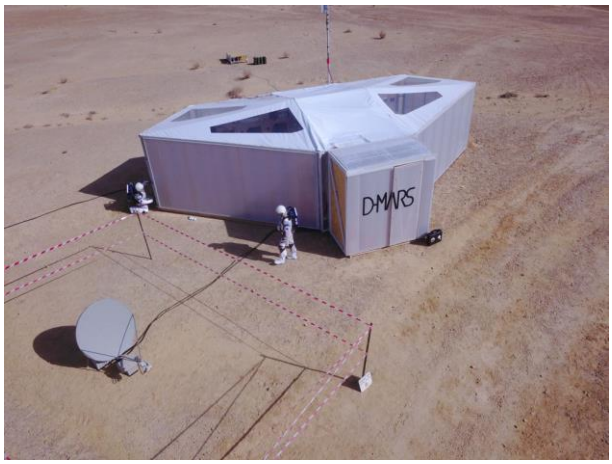

Figure 45. The habitat and two ramonouts from missions (Rubinstein, Abramovich, et al., 2019).

4.2.10. Kepler Station

From February 1 to 28, 2018, in collaboration with the Oman Astronomical Society and research teams from 25 countries, the Austrian Space Forum carried out the AMADEE-18 mission, a human-robotic Mars expedition simulation in the Sultanate of Oman's Dhofar area, which is shown in Figure 46. A carefully selected field team, assisted by a Mission Support Center in Innsbruck, Austria, carried out 19 experiments related to astrobiology, engineering disciplines, geology, operations research, and human aspects (Sejkora et al., 2018).

Figure 46. Kepler-Station for the AMADEE-18 Mars simulation in Oman (Sejkora et al., 2018).

AMADEE-18 included a carefully selected crew of 16 researchers and engineers and about 200 team members from 25 countries (Groemer et al., 2020). The AMADEE-18 mission's goals were to examine the operational procedures of a human/robotic Mars mission and conduct experiments that may be useful for future missions (Groemer et al., 2020). It was used to evaluate human factors observations, geoscientific approaches, and engineering tests and investigate the test site's analog potential (Groemer et al., 2020). The Analog Mission Performance (AMP) measure evaluates quantifiable milestones and measurable success criteria after the mission (Groemer et al., 2020).

As represented in Figure 47, the AMADEE-18 mission comprised two main components: (1) a base station (the "Kepler" station) in the Dhofar desert, which represented the Mars surface section, and (2) a Mission Support Center in Innsbruck, Austria, which represented the project's ground segment (Groemer et al., 2020). The Flight Control Team (FCT) was among those who observed the

(10-min time-delayed) telemetry data from the field. This unit was led by a Flight Director, whose team communicated with the field crew through a single point of contact ("EARTHCOM").

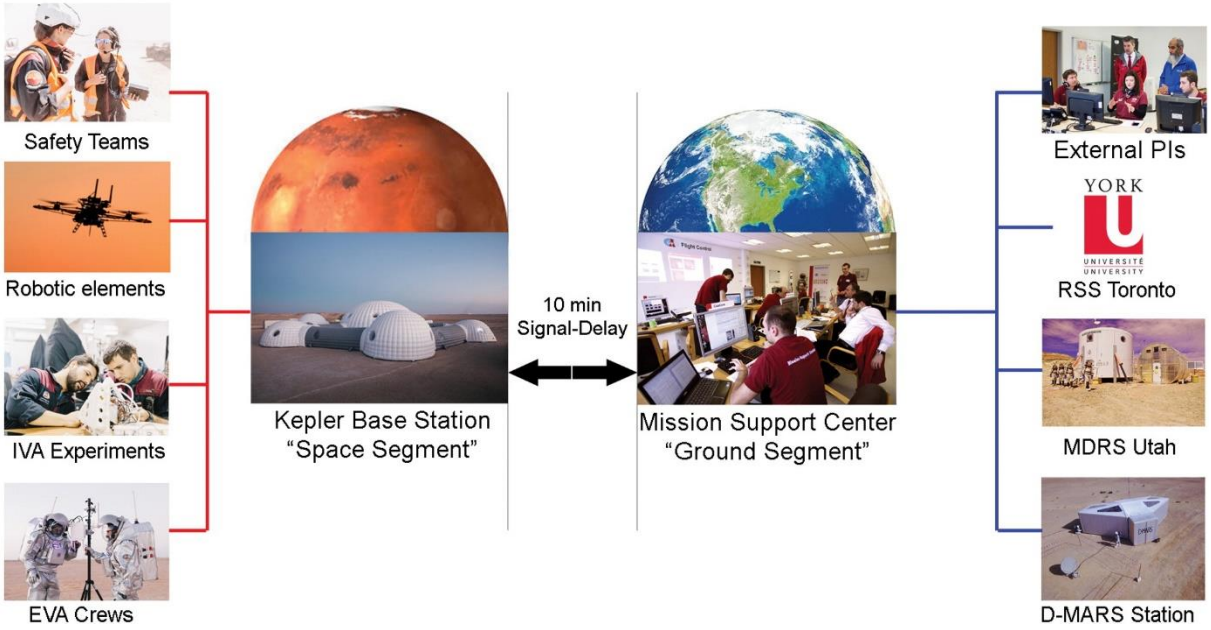

Figure 47. The AMADEE-18 mission architecture (Groemer et al., 2020).

The AMADEE-18 field station "Kepler," shown in Figure 48, was created with a custom-made inflated dome structure and rigid container elements for crew accommodation, hygiene, and the operations module (Groemer et al., 2020). The infrastructure includes a power grid with a 450-kW redundant generator, a 20 Mbit/s symmetric data connection, a greenhouse, science containers, storage containers, workshops with additive manufacturing capability, and a medical facility available at the Kepler station. There was also a mess, and the kitchen module was accessible.

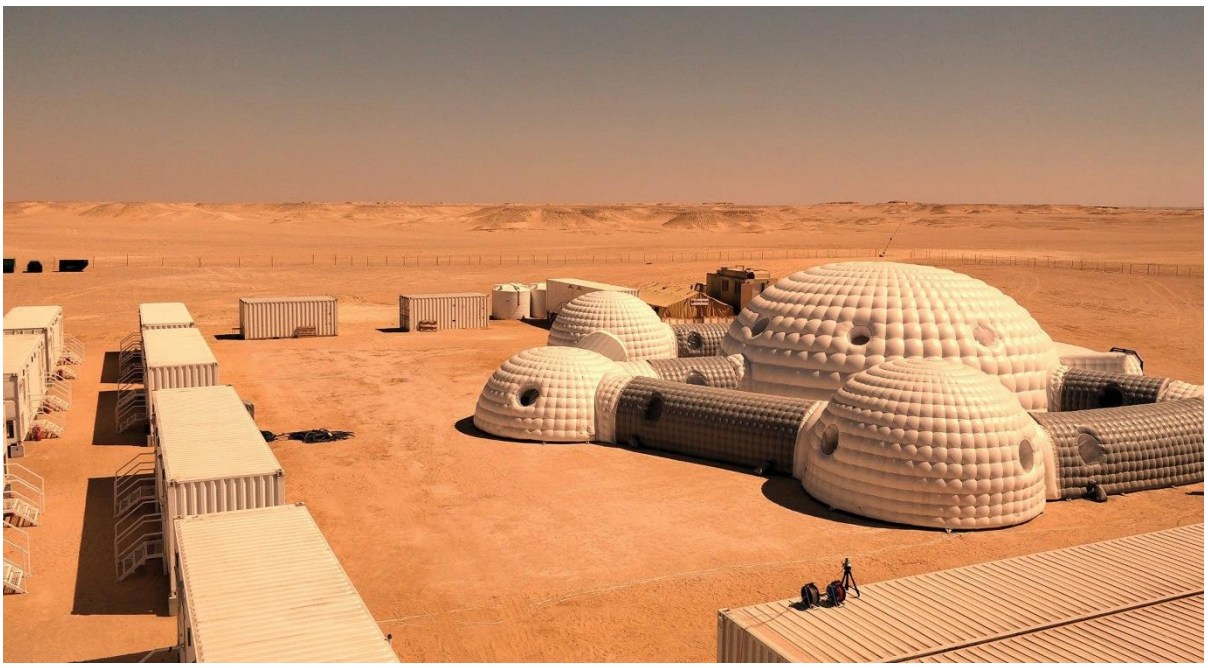

Figure 48. The Kepler base station (Groemer et al., 2020).

4.2.11. Mars Base 1

The C-Space Project “Mars Base 1,” as shown in Figure 49, a Mars simulation station, is constructed in the Gobi Desert in Jinchang, Gansu Province, China (GLOBAL TIMES, 2019). The C-Space Project Mars Base was formally launched on April 17, 2019, intending to educate youngsters and visitors about life on Mars and provide a safe environment for them to do so (GLOBAL TIMES, 2019). The facility, which covers 1115 m², is located in the Gobi Desert, about 40 kilometers from the town of Jinchang (GLOBAL TIMES, 2019). The region was selected to mimic life's terrain and severe circumstances on Mars.

Figure 49. Aerial image of the C-Space Project “Mars Base 1”

The facility is designed to mimic the experience of living on Mars. As seen in Figure 50, it was built by the education initiative C-Space with the help of the Astronaut Center of China and the China Intercontinental Communication Center and consists of nine capsules, including a control room, bio-module (a greenhouse/lab), airlock room, medical facilities, recycling unit, living quarters, and a fitness and entertainment room. A black monolith from the 1968 epic science fiction film 2001: A Space Odyssey is also nearby.

Teenagers dress up in spacesuits and embark on desert adventures, discovering caves in the Mars-like environment. The location has the sensation of a remote red planet thousands of kilometers distant in space. The goal is to inspire future space explorers and help China catch up to the US and Russia in the interplanetary exploration race.

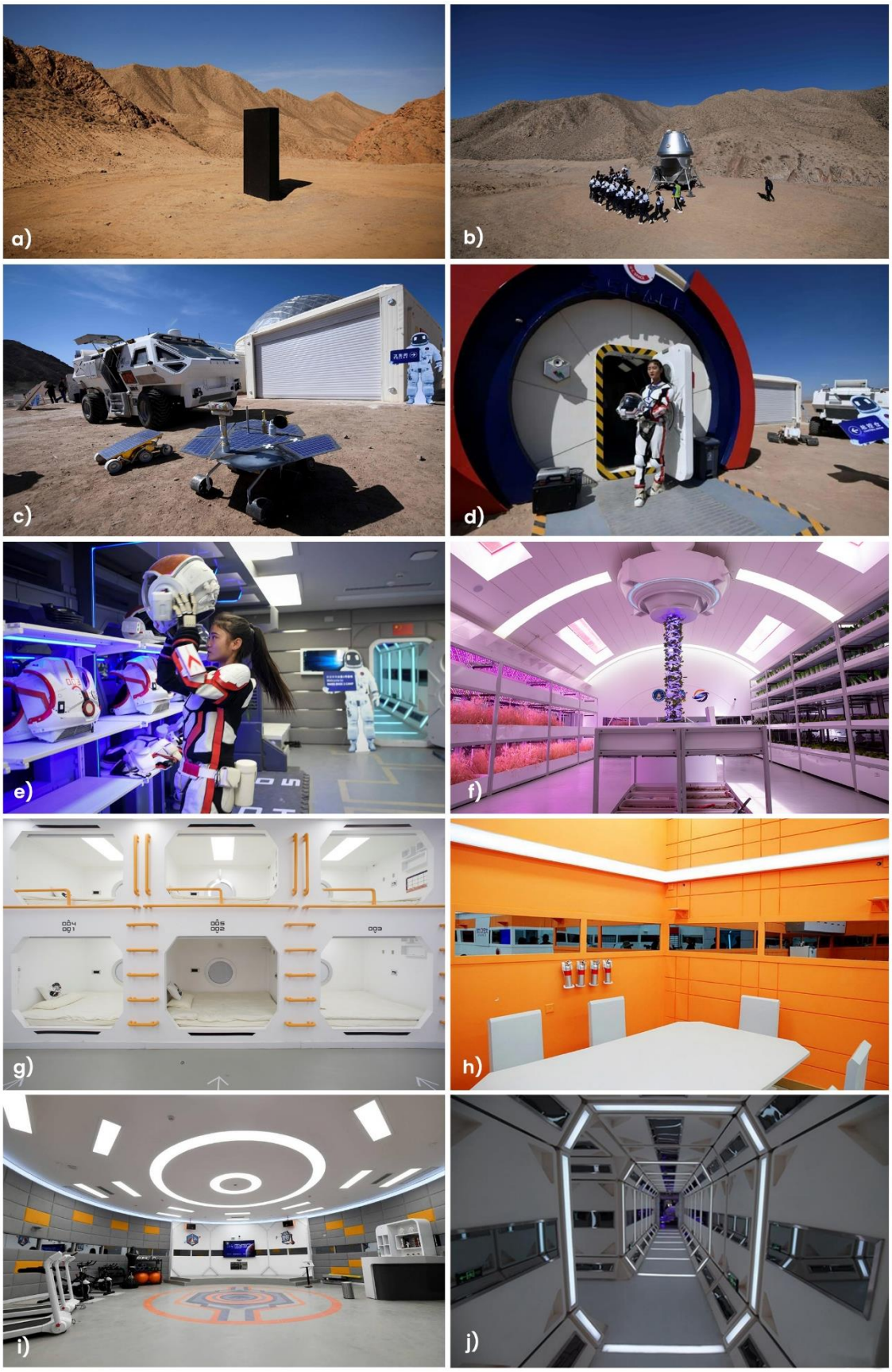

Figure 50. a) The black monolith from the science fiction film 2001: A Space Odyssey; b) A mock Mars lander; c) Mars rovers' models; d) The base entrance; e) Mock space suits; f) Greenhouse; g) Sleeping quarters; h) A restaurant; i) A recreation room; j) Connection corridor

4.2.12. European Mars Analog Research Station

The European Mars Analogue Research Station (Euro-MARS) is the third unit in the Mars Analogue Research Station (MARS) program of the Mars Society (Mars Society, 2022). The station was built in the United States with donations from the United States and the United Kingdom, but the structure was damaged beyond repair during storage and transport; therefore, the European chapters of the Mars Society sought funds to make a replacement habitat (Mars Society, 2022). Even though Euro-MARS was supposed to start field research in 2020, the station is still inactive owing to delays (Mars Society, 2022).

The Krafla/Myvatn volcanic region in North-Eastern Iceland is the primary location of Euro-MARS. Reykjavik is the nearest village with a 5-kilometer distance (Mars Society, 2022), and the nearest airport (Laxamyri/Myvatn) is 60 kilometers distant. The region has a highly Mars-like landscape and geological characteristics comparable to those already observed on Mars. The region is also home to various extremophile species, which may be met while exploring Mars. The Euro-MARS will conduct a wide range of Mars Society-sponsored research in technological development, human aspects, systems engineering, geology, and astrobiology, with a possible operational time of roughly seven months out of every 12 (Mars Society, 2022).

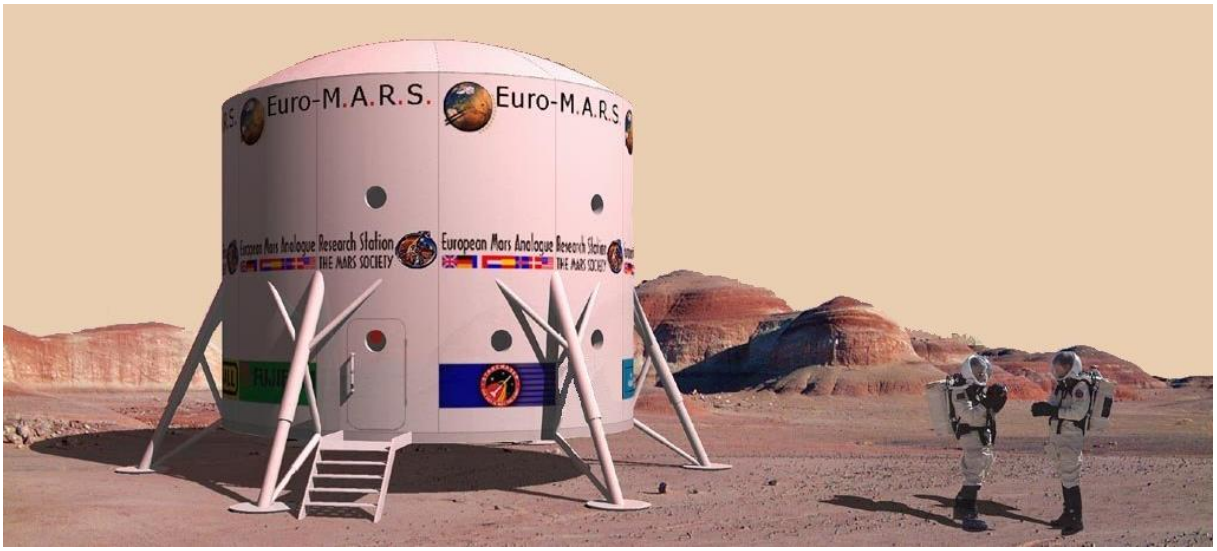

Figure 51. A view of the 3d Model of the Euro-Mars Station (Mars Society, 2022).

The habitat unit, shown in Figure 51, is the central component of each MARS base. It provides enough habitable volume for up to six people at a time, with its 8.6 meters in diameter and 8.4 meters in height. It is a multipurpose structure that includes living and sleeping rooms, work areas, labs, an exercise area, a galley, and a sick bay. The habitat unit will be built with three decks (Mars Society, 2022). The lower deck will include a large split laboratory/workspace for field science and the primary EVA preparation/decontamination facility connected to the two airlocks. The primary living and working areas will be located on the mid-deck. A vast living/communal room will be immediately

connected to a hygiene center, galley, and a "storm shelter/communications center." Two big diameters (35-50cm) windows, supported by two smaller diameter windows, will offer natural light into the living space. The "storm shelter" will hold the crew's principal communications equipment, habitat computer systems, and seating during simulated solar flares. The Upper Deck will hold the crew's sleeping quarters, divided into three pairs of cabins. Each grouping will have a unique interior arrangement (bed, personal workplace, etc.), allowing us to study more human aspects of living/sleeping facilities. The top deck will also have a second toilet (for safety and convenience) and an emergency egress hatch to the roof with a steel roll-up escape ladder for escape purposes. This hatch will also access any satellite communications antennas installed on the hab's top.

4.2.13. The Crew Health and Performance Exploration Analog

NASA will launch a Crew Health and Performance Exploration Analog (CHAPEA) program in 2022, and it will be three one-year simulations of human life on Mars's surface in 2022, 2024, and 2025 (Mars, 2021). The habitat shown in Figure 52 will mimic the difficulties of a Mars mission, such as resource constraints, equipment failure, communication delays, and other environmental stresses (Mars, 2021). Simulated spacewalks, scientific study, virtual reality, robotic controls, and exchanging communications will be possible crew responsibilities (Mars, 2021). The findings will give crucial scientific information for validating systems and developing solutions

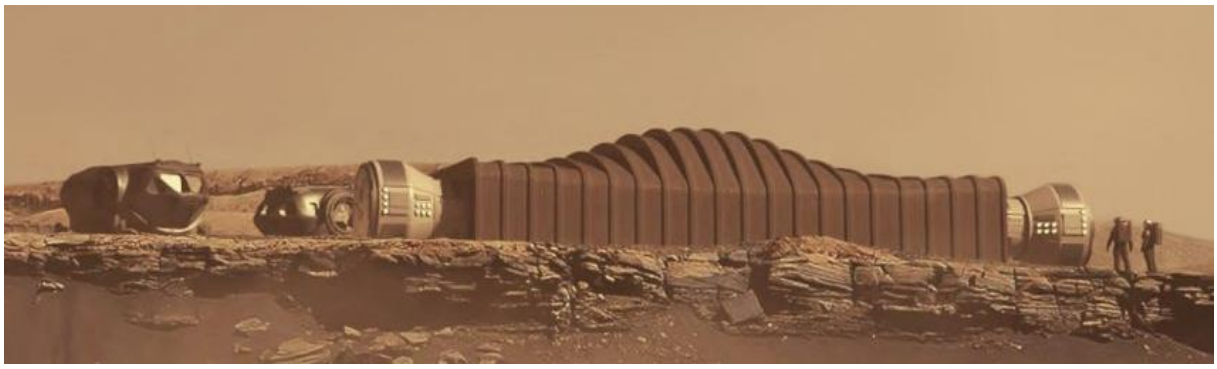

Figure 52. Illustration of a crewed Mars mission with Mars Dune Alpha habitation.

Bjarke Ingels' studio BIG collaborates with ICON and NASA to produce Mars Dune Alpha, a 3D-printed structure that simulates life on Mars. The 158-square-meter "home," now under development at the Johnson Space Center in Texas, USA, was developed by BIG and ICON to assist humans in preparing for life on Mars. Mars Dune Alpha is being constructed to support NASA's Space Technology Mission Directorate (STMD) and is included in The Crew Health and Performance Exploration Analog (CHAPEA).

The Mars Dune Alpha will house four people for lengthy periods, and by recreating the predicted experience of living on Mars, NASA will better understand the physical and mental problems that crew members may face during a long-duration space mission.

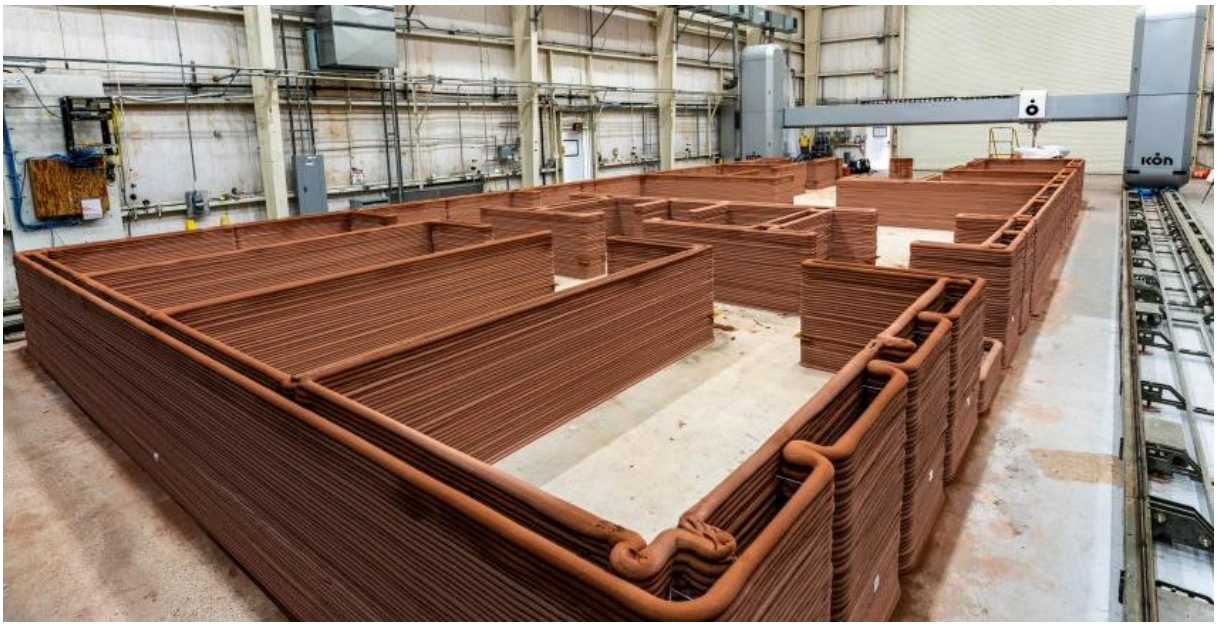

Figure 53. Portland Cement-based mix known as Lavacrete.

As seen in Figure 53, Mars Dune Alpha is being built utilizing 3D printers, as this is the preferred method of constructing extraterrestrial habitats due to the scarcity of essential building materials. The same technology being employed is Vulcan, ICON's 3D printing system that utilizes the company's proprietary Portland Cement-based mix known as Lavacrete, shown in Figure 54.

Figure 54. Additive construction of Mars Dune Alpha.

The structure, designed by BIG-Bjarke Ingels Group, is planned in a gradient of privacy, as seen in Figure 55. On one end of the habitat, four private crew quarters will be located; on the opposite end, dedicated workstations, medical stations, and food-growing stations will be located, with shared living spaces. Varying ceiling heights - vertically separated by an arching shell structure - emphasize each area's distinct experience, avoiding spatial monotony and crew member discomfort. A combination of fixed and movable furniture and configurable lighting, temperature, and sound

management will enable crew members to rearrange the habitat according to their daily demands, thereby regulating the crew's daily routine, circadian rhythm, and general well-being.

Figure 55. Architectural plan of Mars Dune Alpha.

As shown in Figure 56, the ceiling will be adjusted throughout to prevent monotony and crew member fatigue (ICON Technology, 2022). Each area has programmable lighting, temperature, sound controls, and fixed and mobile furniture, allowing users to reorganize and personalize (ICON Technology, 2022).

Figure 56. Interior of The Mars Dune Alpha (ICON Technology, 2022).

4.3.Assessment Of Mars Analog Habitat Plans Using Network Analysis

In the third chapter, the environmental facts of Mars' environments are examined to evaluate environmental factors that prevent the development of a space-resilient settlement. As solutions to the extreme conditions of Mars, an assessment for each condition has been conducted to define strategies and methods to overcome the environmental obstacles to habitability on Mars. Chapter 4 explains the hazards that NASA has defined for a crewed space mission and their impacts on human factors. Additionally, a review study of the analog missions that different institutions have conducted demonstrates what diverse methodologies have been utilized in the past to explore potential solutions to these five types of hazards. This section assesses analog missions and will serve as a guide to demonstrate the psychological aspects of habitability design for a crewed mission.

Table 16 shows the selected research stations where scientists aimed to analyze human factors on Mars, and which include habitat proposals with published plans which will be analyzed to learn how their designers plan to address the human factor problem of living in an isolated, confined and closed environment at a distance from Earth.

Table 16. Selected Mars analog research stations.

	Analog Mission	Location	Agency
1	FMARS	Devon Island	Mars Society
2	MDRS	Southern Utah	Mars Society
3	Mars-Oz	Australia	Mars Society
4	Mars 500	Moscow	RAS/IBP
5	HI-SEAS	Hawaii	NASA
6	D-MARS	Negev Desert	Israel/Austria
7	Mars Dune Alpha	Johnson Space Center	NASA

The functional requirements of habitats of selected analog stations will be analyzed to conduct comparative research to identify standard design and functional requirements and develop a required specification that considers the area and spatial configurations for human factor consideration. This paper provides an assessment of Mars analog missions, and the findings will serve as a guide to demonstrate the psychological aspects of habitability design for a crewed mission.

4.3.1. The context of the assessment strategy

A network is composed of "nodes and ties," or the connections between nodes (Scott & Davis, 2015). Networks, which can be viewed as structural and organizational models, are present in every aspect of modern life, from genes to electrical grids to social groups to transportation corridors (Kozikoğlu & ÇEBİ, 2015). Networks are functional because they focus on the structure of links between things, allowing us to learn about the fundamental principles and behaviors that govern several natural and artificial systems (Burke & Tierney, 2012; Lima, 2011).

Network graphs are essential data structures in computer science because they allow us to manipulate objects' values and relationships. They are often used for knowledge representation, symbolic reasoning, multi-agent simulations, and dynamical systems modelingAkhtar, 2014; Akhtar et al., 2013; J. Li et al., 2010; Monclar et al., 2011; Zelenkauskaite et al., 2012).

The systematic examination of graphs is known as social network analysis (Bryman & Hardy, 2004). Social network analysis (SNA) portrays networks as collections of nodes and connections, with nodes representing persons and connections indicating the many forms of interaction between them (e.g., friendship, kinship, organizational position, sexual relationships, etc.) (Zhang, 2010). As we live in a more interconnected world, social networks (SN) play a more significant part in our daily lives (Denis et al., 2017). Due to their importance in understanding human behavior and relationships, they are also extensively studied in the social sciences. Social networks rely heavily on graph theory, which provides a solid mathematical foundation. Social networks graph the connections between people and how they interact. Researchers are equipped with the mathematical knowledge (graph theory) and SNA-specific tools and methods required to identify and define an individual's impact on the system (Denis et al., 2017).

Depending on the context, the connections between nodes in a social network can be either directed or undirected (Zhang, 2010). A directed network is a graph in which it is not assumed that the edges connecting nodes are symmetric or mutually advantageous. Typically, directed edges are shown as arrows with the tail at the origin vertex and the head at the target vertex. Undirected networks are more constrained than directed graphs because hierarchical interactions cannot be modeled. Nevertheless, many real-world relationships are best described by undirected graphs, leading to their widespread application in reality. In architectural spatial design, connections between spaces are characterized by a reciprocal interaction that enables a changeable transition between spaces. For this reason, we suggested using undirected network analysis for this investigation.

The adjacency matrix is an additional network analysis component used to define relationships. Each row and column of the adjacency matrix corresponds to a set of vertices in a graph (Singh & Sharma, 2012). One approach to describe the presence or absence of an edge between two nodes in an adjacency matrix is with a 1 or 0 in the appropriate cell (Singh & Sharma, 2012). All rows in an adjacency matrix represent the "tail" or "beginning" of a potential edge, while all columns represent the "head" or "destination" of that edge.

Given that every constructed environment consists of a network of interconnected pieces, we may say that architects' primary responsibility is to design the unique configuration of the network. The architect's perceptions are presented using network relationships (Nourian et al., 2013). Once believed to be permanent, these exchanges serve as the foundation for user encounters via linkages and borders, which may include uncharted territories. They form the basis for the user and social

interactions by defining functional and latent connections, physical closeness, and neighbors. As Dovey and Dickson explain, architectural layouts can be viewed as social systems (Dovey & Dickson, 2002). While the functional configuration of a building may be represented as an adjacency matrix, the relations between functions may be represented as a social network.

4.3.2. Significant statistical measures for network analysis

It is necessary to look at a node and network-level measures to analyze network data. Degree, betweenness, closeness, and eigenvector are presented below as essential concepts used in network analysis measurements.

Each node's "connectedness" is measured by the number of edges leading to and from it, which is why the degree of centrality is the essential parameter of the centrality. The degree indicates the number of additional nodes connected to a node via edges.

Using the average shortest path from each node to each other node provides a measurement of betweenness centrality (Freeman, 1977). If a node is along the shortest path, its weight increases by 1 (between the starting and ending nodes). Therefore, it is essential to prioritize nodes with a high total weight when creating connections between them.

Calculating closeness centrality involves evaluating the shortest routes connecting each node and multiplying the weight of the beginning node by the number of nodes along each shortest path. Each node's "distance" may be determined using this metric, and their "proximity" can be determined by calculating the reciprocal of this number. High-closeness nodes serve as critical hubs, facilitating access to neighboring nodes (Bonacich, 1972, 2007).

As an extension of degree centrality, eigenvector centrality assigns a node greater significance if it is connected to other nodes with a comparable degree of importance (Bonacich, 2007). Specifically, each node is assigned a score of 1; these scores are recomputed as a weighted sum of the centralities of all nodes in its neighborhood, the score is normalized by dividing it by the maximum score for the entire network, and this process is repeated until the score no longer changes.

Network analysis considers not just the graph itself but also the roles played by each actor in the broader network. A community is a subgraph of a graph with more densely connected nodes than the remainder of the graph (Raghavan et al., 2007). A graph has a community structure if the number of links into any subgraph exceeds the number of links between subgraphs. Community detection is the process of identifying clusters of nodes in a network diagram. In recent years, numerous techniques for recognizing communities inside social networks have been developed (Bagrow & Bollt, 2005; Blondel et al., 2008; Clauset et al., 2004; Derényi et al., 2005; Raghavan et al., 2007). A common approach to community detection is the use of a hierarchical clustering method, which in this case would regard the social network to represent the composition of the multi-layer community. In 2007,

Raghavan et al. originally proposed a rapid community detection method employing label propagation (Raghavan et al., 2007). A network-based approach to label propagation that does not depend on the optimization of a fixed objective function or any prior knowledge of the relevant communities. Each node in the algorithm is assigned a unique label; over time, it acquires the label shared by most of its neighbors. When clusters of highly linked nodes converge on a single label, communities are generated using this iterative method.

4.3.3. Tool for analyzing social networks

Several tools and programs exist for finding, analyzing, visualizing, and simulating nodes (organizations or knowledge) and edges (relationships or interactions) from various forms of input data, including mathematical models of social networks. The five analytic tools (NetworkX, Gephi, Pajek, IGraph, and MuxViz) were selected to obtain more information. Each of these tools is open-source and can process enormous graphs without cost.

NetworkX is a Python-based package for modeling and analyzing complex networks, including their structure, behavior, and underlying components (Hagberg et al., 2009). This package does much more than create and study networks; it also allows you to import and store networks in standard data formats, generate a wide variety of random and classic networks, do structural analyses of networks, and create models of networks, among other things (Hagberg et al., 2009).

Gephi is a tool that may be used to explore and display any network, dynamic graph, or hierarchical graph. Compatible with all of the primary desktop operating systems, Gephi enables those who need to explore and grasp graphs to accomplish so. Like Photoshop, the user can alter the representation to reveal latent traits (Bastian et al., 2009).

Pajek is not just a popular tool for generating networks, but it also includes robust analytical capabilities that enable calculating multiple centrality measures, discovering gaps in network structure, generating lock models, and much more (Majeed et al., 2020).

The open-source IGraph program enables the creation and modification of graphs. It covers techniques like community structure search and implementations for traditional problems in graph theory, like minimal spanning trees and network flow (Akhtar & Ahamad, 2021). As a result of its efficient implementation, IGraph can process graphs with millions of nodes and edges. IGraph libraries are available for C, R, Python, and Ruby (Akhtar & Ahamad, 2021).

MuxViz (Visualization for Multilayer Social Network Analysis) is an open and free tool that serves as a platform for visualizing and investigating multilayer social networks or graphs in which individual nodes represent numerous interactions across many social media platforms (Majeed et al.,

2020). The MuxViz tool is used for a wide variety of multilayer network-like systems in engineering, biology, society, computing, and physics (Majeed et al., 2020).

For this research study, NetworkX is employed to execute SNA and LPA algorithms in the Python environment, while Gephi is utilized to visualize and export data as Excel files.

4.3.4. The methodology applied to the study of analog habitations

To quantify or characterize the impact of connections between spaces and individuals, we propose employing social network analysis (SNA) to examine the spatial networks of defined analog habitats. This section is meant to provide designers of habitats for extended space missions with a sense of the psychological factors that need to be considered.

In the analysis, we formed networks in which every habitation function was represented by a node and every connection between them by an edge. To quantify the degree to which specific locations in analog habitations serve as social interaction hubs, we aimed to employ social network analysis to study their centrality factors. In addition, we looked for communities in the network to better understand how various nodes might be connected based on their similar characteristics. The community analysis results may show which habitation functions can be integrated to build socially networked homes that reduce the psychological stress of long-term crewed space missions.

4.3.4.1. Data collection from habitation plans

Adjacency matrixes are used in mathematics and computer science to depict the relationships between a graph's vertices. As the initial stage in constructing the adjacency matrix that stands for a social network graph, we list each node as a row and column. Each pair of nodes, one from a row and one from a column, is then sequentially evaluated as a pair to discover the nature of their connections. 0 and 1 indicate the statement of the relationship between two nodes. If there is a connection between them, the number 1 is given; otherwise, the value 0 shows that no relationship exists. As the graph must be undirected and the final matrix will be symmetric, it has been predetermined that such a link between network nodes will be reciprocal.

To evaluate the design of analog habitations using social network metrics, we translate their architectural layouts into adjacency matrices, representing their floor plans as undirected graphs. As a node, each functional area is listed as a column and row. Then, their connections are analyzed and assigned values of 0 or 1. The exact process for matrix generation is implemented for each analog habitation with a documented plan. The table in Figure 57 shows the generated adjacency matrix for FMARS analog habitation. As a result, the matrices of seven analog habitations, FMARS, MDRS, Mars-

OZ, Mars500, HI-SEAS, D-MARS, and Mars Dune Alpha, are generated for subsequent assessment phases.

Habitation Layout Matrix	Primary airlock	EVA prep room	Lab/ Working area	Stairs	Utility cabinet	Toilet	Shower	Secondary airlock	Wardroom area	Command/ Working area	Storage	Personal quarter 1	Personal quarter 2	Personal quarter 3	Personal quarter 4	Personal quarter 5	Personal quarter 6
Primary airlock	0	1	0	0	0	0	0	0	0	0	0	0	0	0	0	0	0
EVA prep room	1	0	1	0	0	0	0	0	0	0	0	0	0	0	0	0	0
Lab/Working area	0	1	0	1	1	1	0	1	0	0	0	0	0	0	0	0	0
Stairs	0	0	1	0	0	0	0	0	1	0	0	0	0	0	0	0	0
Utility cabinet	0	0	1	0	0	0	0	0	0	0	0	0	0	0	0	0	0
Toilet	0	0	1	0	0	0	1	0	0	0	0	0	0	0	0	0	0
Shower	0	0	0	0	0	1	0	0	0	0	0	0	0	0	0	0	0
Secondary airlock	0	0	1	0	0	0	0	0	0	0	0	0	0	0	0	0	0
Wardroom area	0	0	0	1	0	0	0	0	0	1	1	1	1	1	1	1	1
Command/ Working area	0	0	0	0	0	0	0	0	1	0	1	0	0	0	0	0	0
Storage	0	0	0	0	0	0	0	0	1	1	0	0	0	0	0	0	0
Personal quarter 1	0	0	0	0	0	0	0	0	1	0	0	0	0	0	0	0	0
Personal quarter 2	0	0	0	0	0	0	0	0	1	0	0	0	0	0	0	0	0
Personal quarter 3	0	0	0	0	0	0	0	0	1	0	0	0	0	0	0	0	0
Personal quarter 4	0	0	0	0	0	0	0	0	1	0	0	0	0	0	0	0	0
Personal quarter 5	0	0	0	0	0	0	0	0	1	0	0	0	0	0	0	0	0
Personal quarter 6	0	0	0	0	0	0	0	0	1	0	0	0	0	0	0	0	0

Figure 57. FMARS analog habitation matrix.

4.3.4.2. Python programming for data exploration and analysis of networks

After data collection through matrices, obtained data is needed to be explored via social network analysis tools. NetworkX python package was chosen because it provides a standardized method for data scientists and other users of graph mathematics to work together in creating, designing, analyzing, and disseminating graph network models. Python users have flocked to the open-source tool NetworkX due to its scalability and portability. Moreover, it is the most widely used graph framework among data scientists, who have created a thriving community of Python packages that add functionality to NetworkX in areas such as numerical linear algebra and graphics. To better examine the information exported from NetworkX, Gephi is utilized to visualize the findings of the coding process for data exploration and analysis. This phase assists in answering questions including:

- What is the network's general architecture?
- Which functional areas are the network's virtual nodes or hubs?
- What subgroups and communities does the network contain?

Adjacency matrices of habitations are initially built in Excel before being imported as excel files into the Python environment. Installing the required built-in libraries in Python is the first step toward reading and manipulating data, building and analyzing networks, identifying communities within networks, and plotting data. The following lines are written to import libraries:

```
[1] import pandas as pd
[2] from operator import itemgetter
[3] import networkx as nx
[4] from networkx.algorithms.community.label_propagation import label_propagation_communities
[5] import matplotlib.pyplot as plt
[6] from matplotlib.pyplot import figure, text
```

Use the following command line lines to read the matrix associated with the specified analog habitation.

```
[7] data=pd.read_excel("Mars Dune Alpha Analog Matrix.xlsx")
```

To apply the same algorithm to other matrices, we need to import an excel file with data about other analog habitations and execute the remaining code as a function. In the function, we utilize the pandas' package to convert the data into a data frame and the .iloc method to choose values from the matrix, allowing us to reuse the same lines of code regardless of the matrix we are working with. Then, we apply the NetworkX library's functions to the matrix data to generate a social network. Additionally, nodes and edges can be colored and scaled differently based on the degree of nodes in the network. The syntax for applying the defined process is displayed in the following lines.

```
[8] def Analog_Analysis():
[9]      analog_df=data.iloc[: , 1:]
[10]    analog_matrix=analog_df.values
[11]    analog_graph=nx.from_numpy_matrix(analog_matrix)
[12]    pos = nx.spring_layout(analog_graph)
[13]    d = dict(analog_graph.degree)
[14]    nx.draw(analog_graph, pos=pos,node_color='lightgray', edge_color='darkgray',
[15]            with_labels=True,
[16]            node_size=[d[k]*260 for k in d])
```

The data must be labeled based on the Excel data to display the findings with the relevant functional area labels after the workflow. In the first row of the data frame, we provide the area names that correspond to each index number in the matrix. Then, we replace the network's label dictionary's values with the first row's names. The following command lines are utilized for the process outlined.

```
[17]    label_keys=list(analog_df.index.values)
[18]    label_values=list(analog_df.head())
[19]    label = {}
[20]    for key in label_keys:
[21]        for value in label_values:
[22]            label[key] = value
[23]            label_values.remove(value)
```

```
[24]                    break
[25]    analog_graph = nx.relabel_nodes(analog_graph, label)
```

Measures of centrality are widely used to assess a node's importance inside a network. Degree centrality, betweenness centrality, closeness centrality, and eigenvector centrality will be employed as these are the most widely recognized measurements of centrality.

One quickest and most common way to identify virtual nodes is by inspecting their degree. A node's degree equals the number of edges connecting it to other network nodes. Nodes with the highest degrees in a social network analysis represent the most active hubs of relationships. The easiest way to identify hubs, the center nodes in a network, is to compute their degree. Many nodes with high degrees also have high centrality by other measures, so this can be an effective measure. One criticism against degree centrality measurements is that they fail to account for an actor's indirect relationships with others by considering just their direct and neighboring connections. One actor might be linked to many others, but those others might be pretty isolated from the network. The actor may play an essential role in this scenario, but only regionally.

All shortest paths leading to and from that node are counted to determine a node's betweenness centrality. As a measure of a node's importance in a network, betweenness centrality counts how often it mediates connections between other nodes. In contrast to a hub, such a form of a node is commonly referred to as a broker. Betweenness centrality is just a quick indicator of which nodes are crucial because of their position as connectors and brokers between groups.

A node's closeness centrality in a connected graph is a measure of centrality in a network and is defined as the reciprocal of the sum of the shortest paths from that node to every other node in the graph. Accordingly, the closer a node is to the center of the graph, the closer it is to every other node. Informally, it is the "average distance" to every other node in the network.

Eigenvector centrality is a form of extension of degree—it looks at a combination of a node’s edges and the edges of that node’s neighbors. Even if the node is not a hub, Eigenvector Centrality considers how many hubs the node is connected to with their critical position in the network; that means if a node has many connections to other nodes that are also highly linked, it has a high eigenvector centrality.

A network's centrality measures can be calculated for each node using a few simple command lines via NetworkX's built-in functions. The generated values are normalized to a range from 0 to 1 to ensure that the processes calculating betweenness, closeness, and eigenvector centralities are comparable across nodes. The following Python script analyzes SNA centrality metrics in a network and assigns them to the analyzed nodes.

```
[26]  degree_dict = dict(analog_graph.degree(analog_graph.nodes()))
[27]  nx.set_node_attributes(analog_graph, degree_dict, 'Degree')
[28]  betweenness_dict = nx.betweenness_centrality(analog_graph)
[29]  nx.set_node_attributes(analog_graph, betweenness_dict, 'Betweenness Centrality')
[30]  closeness_dict = nx.closeness_centrality(analog_graph)
[31]  nx.set_node_attributes(analog_graph, closeness_dict, 'Closeness Centrality')
[32]  eigenvector_dict = nx.eigenvector_centrality(analog_graph)
[33]  nx.set_node_attributes(analog_graph, eigenvector_dict, 'Eigenvector Centrality')
```

The following analysis step is community detection, which aims to reveal a complex network's structure, behavior, dynamics, and organization by identifying different clusters of nodes (entities) that are similar to one another but distinct from others. The Label Propagation Algorithm (LPA) is a graph-based semi-supervised machine learning algorithm that labels datasets that have not yet been labeled. LPA is commonly used in large-scale networks due to its rapid ability to detect communities. Despite the benefits of LPA, the algorithm may not be remarkably stable. Label propagation algorithms can be executed in parallel on all nodes (synchronous model) or sequentially (asynchronous model); both models have disadvantages, e.g., algorithm termination is not guaranteed in the first case, and performance can be at its lowest in the second. The technique developed by Gennaro Cordasco and Luisa Gargano is accessible in a stable semi-synchronous version using the NetworkX Python library. Their proposal applies to undirected graphs and incorporates the most advantageous characteristics of synchronous and asynchronous models. This approach can detect communities using only the network's topology. The algorithm does not require prior knowledge of the communities or an established objective function. For it to perform as intended:

- Each node is assigned a unique label (identifier) at startup.
- Each node is assigned a unique label (identifier) at startup.
- These labels spread throughout the network.
- At each iteration of propagation, each node updates its label to that of the group to which the greatest number of its neighbors belong. Ties are severed uniformly and arbitrarily.
- LPA converges when each node has the majority of its neighbors' labels.

It is possible to identify each community using the following syntax, which includes labeling and adding nodes in a dictionary format to assign relevant data about the community label of each node as an attribute.

```
[34]  communities = label_propagation_communities(analog_graph)
[35]  community_label = {}
[36]  for i, a in enumerate(communities):
[37]          for name in a:
[38]                  community_label[name] = i
```

```
[39]  nx.set_node_attributes(analog_graph, community_label, 'Community Label')
```

The following command line for exporting analysis results in the Gephi-compatible gexf format is included to finalize the function.

```
[40]  nx.write_gexf(analog_graph, 'Analog_Quaker_network.gexf')
```

In the following block, the function name is a command that executes the defined function, and the matplotlib library is used to display and save the resulting network graph.

```
[41] Analog_Analysis()
[42] plt.show()
[43] plt.savefig("Analog_ANALYSIS.png", dpi=600, bbox_inches='tight')
```

In the analysis, we formed networks in which every habitation function was represented by a node and every connection between them by an edge. In order to quantify the degree to which specific locations in analog habitations serve as social interaction hubs, we aimed to employ social network analysis to study their centrality factors. In addition, we looked for communities in the network to better understand how various nodes might be connected based on their similar characteristics. The community analysis results may show which habitation functions can be integrated to build socially networked homes that reduce the psychological stress of long-term crewed space missions.

4.3.5. SNA results for analog habitations

Adjacency Matrix

FMARS Analog Habitation Matrix

Functinal Areas		0	1	2	3	4	5	6	7	8	9	10	11	12	13	14	12	16
Primary airlock	0	0	1	0	0	0	0	0	0	0	0	0	0	0	0	0	0	0
EVA prep room	1	1	0	1	0	0	0	0	0	0	0	0	0	0	0	0	0	0
Lab/Working area	2	0	1	0	1	1	1	0	1	0	0	0	0	0	0	0	0	0
Stair	3	0	0	1	0	0	0	0	0	1	0	0	0	0	0	0	0	0
Utility cabinet	4	0	0	1	0	0	0	0	0	0	0	0	0	0	0	0	0	0
Toilet	5	0	0	1	0	0	0	1	0	0	0	0	0	0	0	0	0	0
Shower	6	0	0	0	0	0	1	0	0	0	0	0	0	0	0	0	0	0
Secondary airlock	7	0	0	1	0	0	0	0	0	0	0	0	0	0	0	0	0	0
Wardroom area	8	0	0	0	1	0	0	0	0	0	1	1	1	1	1	1	1	1
Command/Working area	9	0	0	0	0	0	0	0	0	1	0	1	0	0	0	0	0	0
Storage	10	0	0	0	0	0	0	0	0	1	1	0	0	0	0	0	0	0
Personal quarter 1	11	0	0	0	0	0	0	0	0	1	0	0	0	0	0	0	0	0
Personal quarter 2	12	0	0	0	0	0	0	0	0	1	0	0	0	0	0	0	0	0
Personal quarter 3	13	0	0	0	0	0	0	0	0	1	0	0	0	0	0	0	0	0
Personal quarter 4	14	0	0	0	0	0	0	0	0	1	0	0	0	0	0	0	0	0
Personal quarter 5	15	0	0	0	0	0	0	0	0	1	0	0	0	0	0	0	0	0
Personal quarter 6	16	0	0	0	0	0	0	0	0	1	0	0	0	0	0	0	0	0

Social Network Diagram

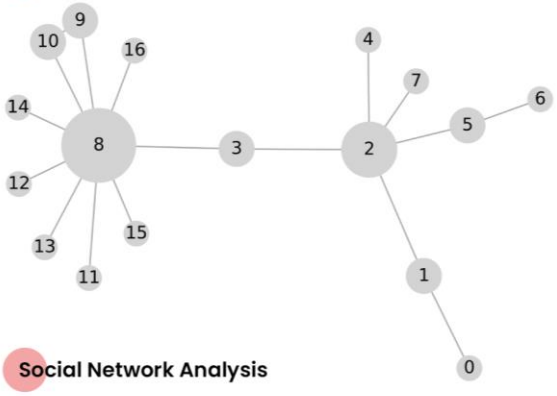

Social Network Analysis

Id	Label	Degree	Betweenness Centrality	Closeness Centrality	Eigenvector Centrality	Community Label
8	Wardroom area	9	0.758333	0.516129	0.671552	2
2	Lab/Working area	5	0.608333	0.457143	0.137018	1
1	EVA prep room	2	0.125	0.333333	0.047793	0
3	Stair	2	0.525	0.5	0.254162	2
5	Toilet	2	0.125	0.333333	0.047793	3
9	Command/ Working area	2	0	0.355556	0.307862	2
10	Storage	2	0	0.355556	0.307862	2
0	Primary airlock	1	0	0.253968	0.015024	0
4	Utility cabinet	1	0	0.32	0.043071	1
6	Shower	1	0	0.253968	0.015024	3
7	Secondary airlock	1	0	0.32	0.043071	1
11	Personal quarter 1	1	0	0.347826	0.211091	2
12	Personal quarter 2	1	0	0.347826	0.211091	2
13	Personal quarter 3	1	0	0.347826	0.211091	2
14	Personal quarter 4	1	0	0.347826	0.211091	2
15	Personal quarter 5	1	0	0.347826	0.211091	2
16	Personal quarter 6	1	0	0.347826	0.211091	2

Machine Learning Community Diagram

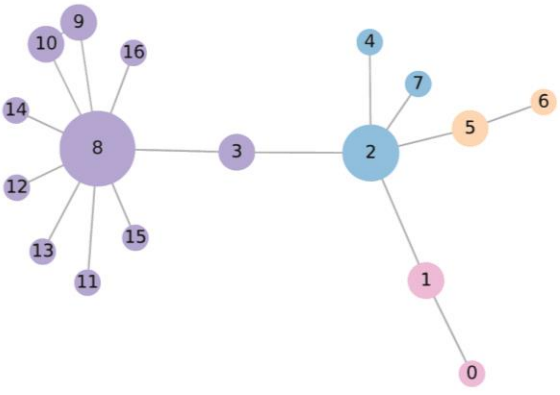

Figure 58. SNA findings for FMARS habitation module.

FMARS, a two-story cylindrical habitat module, was the first station operated by the Mars Society. As displayed in Figure 58, the adjacency matrix of habitation is formed, a social network graph is generated, SNA is conducted in Python, and the ML algorithm detects communities in the network to analyze FMARS's layouts.

The degree centrality results indicate that the wardroom has the most potential to function as a hub, with a degree of 9, followed by the lab/work area, with a degree of 5. The analysis of betweenness centrality reveals that the wardroom area, the lab/working area, and the stairs are the most significant nodes due to their roles as connectors and brokers between functional groups. The closeness centrality values reveal that functional spaces with the most significant average distance from other nodes are those with the same function. The eigenvector centrality analysis demonstrates that the wardroom area has the highest network connectivity due to its and its neighbors' high number of connections. Command/working area and storage share the same eigenvector centrality as the second-highest value. The other node with a high eigenvector is the stairs. Lastly, four communities in the network are identified by the ML algorithm. The first group consists of the primary airlock and the EVA prep room; the second group consists of the lab/working area and the utility cabinet; the third group consists of the stairs, the wardroom area, the command/working area, storage, and personal quarters; and the fourth group consists of the toilet and the shower.

Adjacency Matrix

MDRS Analog Habitation Matrix

Functinal Areas		0	1	2	3	4	5	6	7	8	9	10	11	12	13	14	15	16	17
Engineering Air Lock	0	0	1	0	0	0	1	0	0	0	0	0	0	0	0	0	0	0	0
Workshop Area	1	1	0	1	1	0	1	0	0	0	0	0	0	0	0	0	0	0	0
Toilet	2	0	1	0	1	0	0	0	0	0	0	0	0	0	0	0	0	0	0
Sink	3	0	1	1	0	1	0	0	0	0	0	0	0	0	0	0	0	0	0
Shower	4	0	0	0	1	0	0	0	0	0	0	0	0	0	0	0	0	0	0
Biology and Geology Laboratory	5	1	1	0	0	0	0	1	1	1	0	0	0	0	0	0	0	0	0
Shoe cabinet	6	0	0	0	0	0	1	0	0	0	0	0	0	0	0	0	0	0	0
Stairs	7	0	0	0	0	0	1	0	0	0	0	0	1	0	0	0	0	0	0
Eva Prep Room	8	0	0	0	0	0	1	0	0	0	1	0	0	0	0	0	0	0	0
Eva Air Lock	9	0	0	0	0	0	0	0	0	1	0	0	0	0	0	0	0	0	0
Working Area	10	0	0	0	0	0	0	0	0	0	0	0	1	0	0	0	0	0	0
Kitchen and Dining Area	11	0	0	0	0	0	0	0	1	0	0	1	0	1	1	1	1	1	1
Sleeping quarter 1	12	0	0	0	0	0	0	0	0	0	0	0	1	0	0	0	0	0	0
Sleeping quarter 2	13	0	0	0	0	0	0	0	0	0	0	0	1	0	0	0	0	0	0
Sleeping quarter 3	14	0	0	0	0	0	0	0	0	0	0	0	1	0	0	0	0	0	0
Sleeping quarter 4	15	0	0	0	0	0	0	0	0	0	0	0	1	0	0	0	0	0	0
Sleeping quarter 5	16	0	0	0	0	0	0	0	0	0	0	0	1	0	0	0	0	0	0
Sleeping quarter 6	17	0	0	0	0	0	0	0	0	0	0	0	1	0	0	0	0	0	0

Social Network Diagram

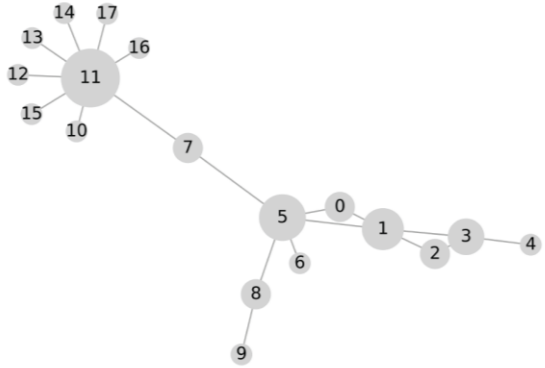

Social Network Analysis

Id	Label	Degree	Betweenness Centrality	Closeness Centrality	Eigenvector Centrality	Community Label
11	Kitchen and Dining Area	8	0.669118	0.435897	0.488232	1
5	Biology and Geology Laboratory	5	0.654412	0.459459	0.403951	0
1	Workshop Area	4	0.308824	0.369565	0.355098	0
3	Sink	3	0.117647	0.288136	0.206545	0
0	Engineering Air Lock	2	0	0.346939	0.255481	0
2	Toilet	2	0	0.283333	0.189039	0
7	Stairs	2	0.529412	0.459459	0.300289	1
8	Eva Prep Room	2	0.117647	0.333333	0.153333	0
4	Shower	1	0	0.226667	0.069519	0
6	Shoe cabinet	1	0	0.320755	0.135962	0
9	Eva Air Lock	1	0	0.253731	0.051609	0
10	Working Area	1	0	0.309091	0.164327	1
12	Sleeping quarter 1	1	0	0.309091	0.164327	1
13	Sleeping quarter 2	1	0	0.309091	0.164327	1
14	Sleeping quarter 3	1	0	0.309091	0.164327	1
15	Sleeping quarter 4	1	0	0.309091	0.164327	1
16	Sleeping quarter 5	1	0	0.309091	0.164327	1
17	Sleeping quarter 6	1	0	0.309092	0.164328	1

Machine Learning Community Diagram

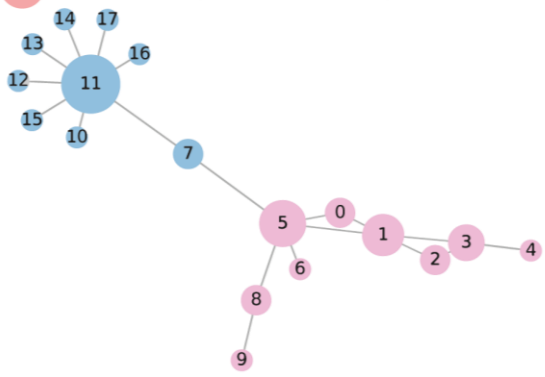

Figure 59. SNA findings for MDRS habitation module.

The next habitation examined is the MDRS, which consists of a cylinder with a diameter of around 8 meters and two stories. Figure 59 depicts the steps taken to study MDRS'S layouts.

The degree centrality analysis shows that the kitchen and dining area may serve as a hub the best, with a score of 8, followed by the biology and geology lab, with a score of 5, and the workshop area, with a score of 4. Based on their roles as connectors and brokers between functional groups, the kitchen/dining area, biology/geology lab, and the stairs rank highest in betweenness centrality analyses. Values of closeness centrality show that nodes with the most significant average distance from other nodes are those with the same function. The eigenvector centrality study shows that the kitchen and dining area are highly connected to the rest of the building's networks because of the many connections between them and their neighbors. Also, with the second-highest eigenvector centrality, the biology/geology lab is an excellently connected node in the network. The workshop is the other node that has a high eigenvector.

Subsequently, the ML algorithm recognizes two distinct communities within the network. There are two groups of functions: the first has the kitchen, dining area, working area, sleeping quarters, and stairs; the second contains the biology and geology lab, workshop area, engineering airlock, Eva prep room, Eva airlock, sink, toilet, shower, and shoe cabinet. Ultimately, finding communities shares the same practical distinction as current architectural configurations.

Adjacency Matrix

Mars-OZ Analog Habitation Matrix

Functinal Areas	0	1	2	3	4	5	6	7	8	9	10	11	12	13	14	15	16	17	18	19	20	21	22	23	24
Main Entrance	0	0	1	1	0	0	0	0	0	0	0	0	0	0	0	0	0	0	0	0	0	0	0	0	0
Eva Suit Storage	1	1	0	0	0	0	0	0	0	0	0	0	0	0	0	0	0	0	0	0	0	0	0	0	0
Suit Clean up and Surface Equipment	2	1	0	0	0	0	0	0	0	0	0	0	0	0	0	0	0	0	0	0	0	0	0	0	0
Passage Area1	3	1	0	0	0	1	1	1	0	0	0	0	0	0	0	0	0	0	0	0	0	0	0	0	0
Bathroom	4	0	0	0	1	0	0	0	0	0	0	0	0	0	0	0	0	0	0	0	0	0	0	0	0
Washer and Dryer	5	0	0	0	1	0	0	0	0	0	0	0	0	0	0	0	0	0	0	0	0	0	0	0	0
Passage Area 2	6	0	0	0	1	0	0	0	1	1	0	1	0	0	0	0	0	0	0	0	0	0	0	0	0
Exercise Area	7	0	0	0	0	0	0	1	0	0	1	0	0	1	0	0	0	0	0	0	0	0	0	0	0
Health Centre	8	0	0	0	0	0	0	1	0	0	0	0	0	0	0	0	0	0	0	0	0	0	0	0	0
Stairs	9	0	0	0	0	0	0	0	1	0	0	0	0	0	1	1	0	0	0	0	0	0	0	0	0
Lab	10	0	0	0	0	0	0	1	0	0	0	0	1	0	0	0	0	0	0	0	0	0	0	0	0
Air Lock	11	0	0	0	0	0	0	0	0	0	0	1	0	1	0	0	0	0	0	0	0	0	0	0	0
Exit Stair	12	0	0	0	0	0	0	0	1	0	0	0	1	0	0	0	0	0	0	0	0	0	0	0	0
Store	13	0	0	0	0	0	0	0	0	1	0	0	0	1	0	0	0	0	0	0	0	0	0	0	0
Galley	14	0	0	0	0	0	0	0	0	1	0	0	0	1	0	1	1	1	0	0	0	0	0	0	0
Lounge Area	15	0	0	0	0	0	0	0	0	0	0	0	0	0	1	0	0	0	0	0	0	0	0	0	0
Command Area	16	0	0	0	0	0	0	0	0	0	0	0	0	0	1	0	0	0	0	0	0	0	0	0	0
Passage Area 3	17	0	0	0	0	0	0	0	0	0	0	0	0	0	1	0	0	0	1	1	1	1	1	1	1
Personal quarter 1	18	0	0	0	0	0	0	0	0	0	0	0	0	0	0	0	0	1	0	0	0	0	0	0	0
Personal quarter 2	19	0	0	0	0	0	0	0	0	0	0	0	0	0	0	0	0	1	0	0	0	0	0	0	0
Personal quarter 3	20	0	0	0	0	0	0	0	0	0	0	0	0	0	0	0	0	1	0	0	0	0	0	0	0
Personal quarter 4	21	0	0	0	0	0	0	0	0	0	0	0	0	0	0	0	0	1	0	0	0	0	0	0	0
Personal quarter 5	22	0	0	0	0	0	0	0	0	0	0	0	0	0	0	0	0	1	0	0	0	0	0	0	0
Personal quarter 6	23	0	0	0	0	0	0	0	0	0	0	0	0	0	0	0	0	1	0	0	0	0	0	0	0
Personal quarter 7	24	0	0	0	0	0	0	0	0	0	0	0	0	0	0	0	0	1	0	0	0	0	0	0	0

Social Network Diagram

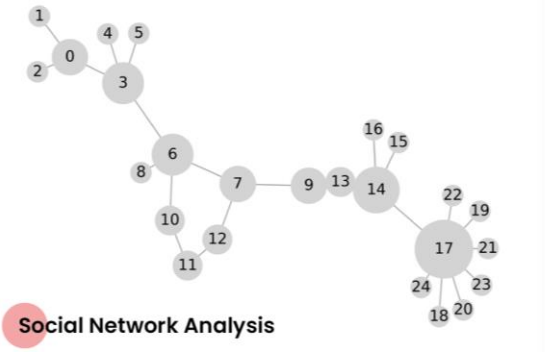

Social Network Analysis

Id	Label	Degree	Betweenness Centrality	Closeness Centrality	Eigenvector Centrality	Community Label
17	Passage Area 3	8	0.507246	0.303797	0.58572	5
14	Galley	5	0.568841	0.342857	0.451345	3
3	Passage Area1	4	0.369565	0.272727	0.03573	1
6	Passage Area 2	4	0.503623	0.32	0.071065	1
0	Main Entrance	3	0.163043	0.224299	0.014858	0
7	Exercise Area	3	0.547101	0.347826	0.1264	2
9	Stairs	3	0.521739	0.352941	0.26548	3
10	Lab	2	0.028986	0.252632	0.032009	4
11	Air Lock	2	0.003623	0.235294	0.026843	4
12	Exit Stair	2	0.050725	0.269663	0.050098	2
13	Store	2	0	0.3	0.234338	3
1	Eva Suit Storage	1	0	0.184615	0.004858	0
2	Suit Clean up and Surface Equipment	1	0	0.184615	0.004858	0
4	Bathroom	1	0	0.216216	0.011682	1
5	Washer and Dryer	1	0	0.216216	0.011682	1
8	Health Centre	1	0	0.244898	0.023233	1
15	Lounge Area	1	0	0.258065	0.14755	3
16	Command Area	1	0	0.258065	0.14755	3
18	Personal quarter 1	1	0	0.235294	0.191477	5
19	Personal quarter 2	1	0	0.235294	0.191477	5
20	Personal quarter 3	1	0	0.235294	0.191477	5
21	Personal quarter 4	1	0	0.235294	0.191477	5
22	Personal quarter 5	1	0	0.235294	0.191477	5
23	Personal quarter 6	1	0	0.235294	0.191477	5
24	Personal quarter 7	1	0	0.235294	0.191477	5

Machine Learning Community Diagram

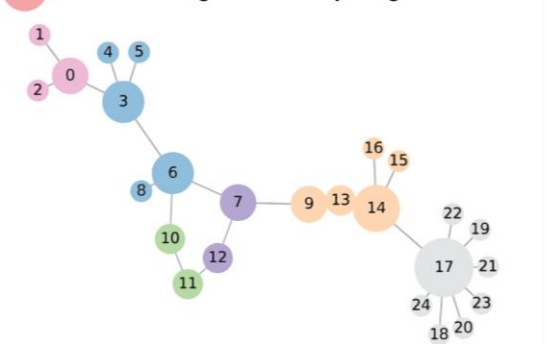

Figure 60. SNA findings for Mars-OZ habitation module.

Mars-Oz, the third examined habitation, consisted of two landing vehicles: the Hab and the Cargo. The habitation unit is a horizontally landed, 18-meter-long, 4.7-meter-diameter, bent iconic vehicle with a 6-meter-long upswept nose cone. Figure 60 illustrates the processes taken to investigate Mars-OZ layouts.

The passage on the upper deck (passage area 3) has the most connected nodes with a number of 8, followed by the galley with a score of 5 and the passage areas on the lower deck with a score of 4. In betweenness centrality analyses, the galley, the exercise area, the stairs, and passage 2 have the highest scores. The closeness centrality values indicate that most nodes have equal closeness centrality, with the stairs, the exercise area, and the galley having the greatest values, respectively. Comparing other nodes, the eigenvector centrality analysis reveals that the passage on the upper deck (passage area 3) and the galley are exceptionally well-connected to the rest of the habitation networks.

Following that, the ML algorithm identifies six different subcommunities within the network. The first group includes the main entrance, Eva suit storage, a suit cleaning area, and the surface equipment area; the second group includes the passage areas on the lower deck, bathroom, washer and dryer area, and health center; the third group includes the exercise area and the exit stairs; the fourth group includes the galley, the lounge, the command area, the store, and the stairs; the fifth group includes the lab and the air lock; and the sixth group includes the passage areas on the upper deck and the personal quarters.

Adjacency Matrix

Mars500 Analog Habitation Matrix

Functinal Areas		0	1	2	3	4	5	6	7	8	9	10	11	12	13	14	15
Main Entrance	0	0	1	0	0	0	0	0	1	0	0	0	0	0	0	0	1
Freezers	1	1	0	1	0	0	0	0	0	0	0	0	0	0	0	0	0
Storage 1	2	0	1	0	1	0	0	0	0	0	0	0	0	0	0	0	0
Storage 2	3	0	0	1	0	1	0	0	0	0	0	0	0	0	0	0	0
Greenhouse	4	0	0	0	1	0	1	0	0	0	0	0	0	0	0	0	0
Sports Hall	5	0	0	0	0	1	0	1	0	0	0	0	0	0	1	0	0
Bathroom	6	0	0	0	0	0	1	0	0	0	0	0	0	0	0	0	0
Sleeping Area	7	1	0	0	0	0	0	0	0	1	0	1	0	0	0	0	0
Toilet 1	8	0	0	0	0	0	0	0	1	0	0	0	0	0	0	0	0
Toilet 2	9	0	0	0	0	0	0	0	0	0	0	1	0	0	0	0	0
Control Room	10	0	0	0	0	0	0	0	1	0	1	0	1	0	0	0	0
Bedrooms	11	0	0	0	0	0	0	0	0	0	0	1	0	1	0	0	0
Kitchen	12	0	0	0	0	0	1	0	0	0	0	0	1	0	1	0	0
Living Room	13	0	0	0	0	0	0	0	0	0	0	0	0	1	0	1	0
Medical Area	14	0	0	0	0	0	0	0	0	0	0	0	0	0	1	0	0
Mars Surface Simulation Room	15	1	0	0	0	0	0	0	0	0	0	0	0	0	0	0	0

Social Network Diagram

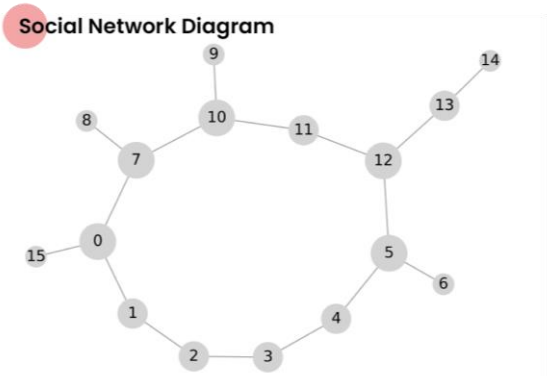

Social Network Analysis

Id	Label	Degree	Betweenness Centrality	Closeness Centrality	Eigenvector Centrality	Community Label
0	Main Entrance	3	0.27619	0.3125	0.319235	0
5	Sports Hall	3	0.295238	0.326087	0.306957	2
7	Sleeping Area	3	0.342857	0.340909	0.379112	3
10	Control Room	3	0.380952	0.357143	0.381316	4
12	Kitchen	3	0.42381	0.357143	0.362605	2
1	Freezers	2	0.157143	0.288462	0.210796	0
2	Storage 1	2	0.147619	0.288462	0.162523	1
3	Storage 2	2	0.152381	0.288462	0.160639	1
4	Greenhouse	2	0.171429	0.3	0.204601	2
11	Bedrooms	2	0.319048	0.357143	0.325508	4
13	Living Room	2	0.133333	0.277778	0.196232	5
6	Bathroom	1	0	0.25	0.134312	2
8	Toilet 1	1	0	0.258621	0.165882	3
9	Toilet 2	1	0	0.267857	0.166847	4
14	Medical Area	1	0	0.220588	0.085863	5
15	Mars Surface Simulation Room	1	0	0.241935	0.139683	0

Machine Learning Community Diagram

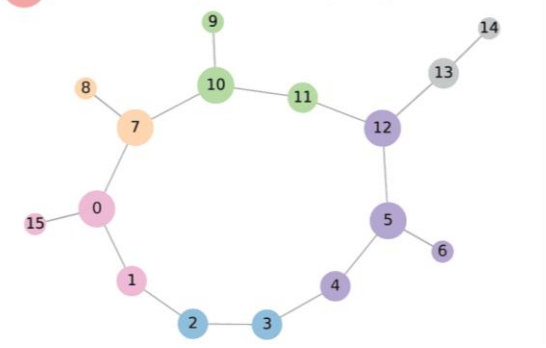

Figure 61. SNA findings for Mars500 habitation module.

The NEK/Mars500 facility is the fourth examined habitation; it consists of four horizontal cylinders, one of which is not connected to the actual living space (landing module) and links to a simulated Martian surface in a different module. Major modules for living quarters, healthcare, and utilities can all be found within the horizontal cylinders. A simulated Mars lander and the surface module were employed to test these components. Processes for examining Mars500 designs are shown in Figure 61.

Based on the degree centrality data, the most promising hub nodes are the sports hall, sleeping area, control room, and kitchen (other than the main entrance). The kitchen, control room, and sleeping area emerge as the most prominent nodes in a betweenness centrality study. The closeness centrality numbers show that all the rooms are somehow close to each other on average, but the control room, the kitchen, and the bedrooms are the greatest of all, with a value of 0.357143. The control room and its neighbors have a high number of connections, as shown by the eigenvector centrality analysis. After the control area, the most central eigenvectors are found in the kitchen and the sleeping area.

Lastly, the ML algorithm discovers six different functional groups inside the network. The main entrance, Mars surface simulation room, and freezers make up the first group, while the storages make up the second, the sports hall, kitchen, greenhouse, and bathroom make up up the third, the sleeping quarters and toilet 1 make up the fourth, the control room, bedrooms, and toilet 2 make up the fifth, and the living room and medical area make up the sixth.

Adjacency Matrix

HI-SEAS Analog Habitation Matrix

Functional Areas		0	1	2	3	4	5	6	7	8	9	10	11	12	13	14	15	16
Entrance Area	0	0	1	0	1	0	0	0	1	1	0	0	0	0	0	0	0	0
Exercise Area	1	1	0	1	0	0	0	0	0	0	0	0	0	0	0	0	0	0
Common Workspace	2	0	1	0	0	1	1	0	0	0	0	0	0	0	0	0	0	0
Stairs	3	1	0	0	0	0	0	0	0	0	1	0	0	0	0	0	0	0
Dining Area	4	0	0	1	0	0	1	0	0	0	0	0	0	0	0	0	0	0
Kitchen	5	0	0	1	0	1	0	1	0	0	0	0	0	0	0	0	0	0
Storage	6	0	0	0	0	0	1	0	0	0	0	0	0	0	0	0	0	0
Bathroom 1	7	1	0	0	0	0	0	0	0	1	0	0	0	0	0	0	0	0
Lab	8	1	0	0	0	0	0	0	1	0	0	0	0	0	0	0	0	0
Landing Area	9	0	0	0	1	0	0	0	0	0	0	1	1	1	1	1	1	1
Bathroom 2	10	0	0	0	0	0	0	0	0	0	1	0	0	0	0	0	0	0
Bedroom 1	11	0	0	0	0	0	0	0	0	0	1	0	0	0	0	0	0	0
Bedroom 2	12	0	0	0	0	0	0	0	0	0	1	0	0	0	0	0	0	0
Bedroom 3	13	0	0	0	0	0	0	0	0	0	1	0	0	0	0	0	0	0
Bedroom 4	14	0	0	0	0	0	0	0	0	0	1	0	0	0	0	0	0	0
Bedroom 5	15	0	0	0	0	0	0	0	0	0	1	0	0	0	0	0	0	0
Bedroom 6	16	0	0	0	0	0	0	0	0	0	1	0	0	0	0	0	0	0

Social Network Diagram

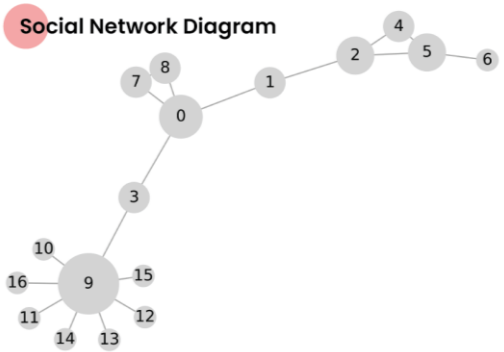

Social Network Analysis

Id	Label	Degree	Betweenness Centrality	Closeness Centrality	Eigenvector Centrality	Community Label
9	Landing Area	8	0.7	0.410256	0.665562	2
0	Entrance Area	4	0.608333	0.410256	0.220569	0
2	Common Workspace	3	0.325	0.290909	0.055912	1
5	Kitchen	3	0.125	0.238806	0.034325	1
1	Exercise Area	2	0.4	0.347826	0.095789	0
3	Stairs	2	0.533333	0.421053	0.307001	2
4	Dining Area	2	0	0.235294	0.031265	1
7	Bathroom 1	2	0	0.301887	0.116928	0
8	Lab	2	0	0.301887	0.116928	0
6	Storage	1	0	0.195122	0.011893	1
10	Bathroom 2	1	0	0.296296	0.230584	2
11	Bedroom 1	1	0	0.296296	0.230584	2
12	Bedroom 2	1	0	0.296296	0.230584	2
13	Bedroom 3	1	0	0.296296	0.230584	2
14	Bedroom 4	1	0	0.296296	0.230584	2
15	Bedroom 5	1	0	0.296296	0.230584	2
16	Bedroom 6	1	0	0.296296	0.230584	2

Machine Learning Community Diagram

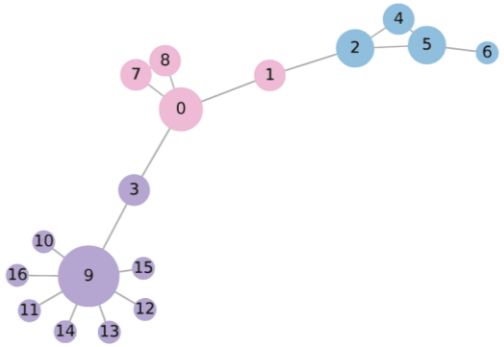

Figure 62. SNA findings for HI-SEAS habitation module

HI-SEAS, the fifth habitat examined, is a two-story geodesic dome with a diameter of roughly 11 m and encloses approximately 385 m^3 of usable living and working area. Figure 62 illustrates the methods used to examine HI-SEAS's layouts

With a degree of 8, the landing area on the upper floor has the most potential to serve as a hub, followed by the entrance area, which has a degree of 4. The betweenness centrality analysis demonstrates that the same landing area is the most central node due to its functions as connectors or brokers between floors. Other nodes with strong betweenness centrality scores are the entrance area and the stairs. The stairs also have the highest closeness centrality and the most significant average distance from other nodes, followed by the entrance and landing areas, which have equal closeness centrality values. According to the eigenvector centrality analysis, the landing area has the highest network connectivity. The value of the staircase is the second-highest.

Additionally, the ML algorithm identifies three communities in the network. The first group includes the entrance, exercise area, lab, and bathroom 1; the second group includes the workspace, kitchen, dining area, and storage; and the third group includes the landing, bathroom 2, and bedrooms. Finally, finding communities identified the same practical function segmentation as existing architectural configurations.

Adjacency Matrix

D-MARS Analog Habitation Matrix

Functional Areas		0	1	2	3	4	5	6	7	8	9	10	11	12
Airlock and Eva Hatch	0	0	1	0	0	0	0	0	0	0	0	0	0	0
Entrance Area	1	1	0	1	1	1	1	0	0	0	0	0	0	0
Command and Communication Space	2	0	1	0	0	0	0	0	0	0	1	0	0	0
Kitchen and LSS pillar	3	0	1	0	0	1	1	0	0	0	0	0	0	0
Multi-purpose Area	4	0	1	0	1	0	1	1	1	0	0	0	0	0
Corridor	5	0	1	0	1	1	0	0	1	1	1	1	1	1
Lab Area	6	0	0	0	0	1	0	0	1	0	0	0	0	0
Clean air chamber	7	0	0	0	0	1	1	1	0	0	0	0	0	0
Toilet	8	0	0	0	0	0	1	0	0	0	0	0	0	0
Exercise Area	9	0	0	1	0	0	1	0	0	0	0	0	0	0
Sleeping Pod 1	10	0	0	0	0	0	1	0	0	0	0	0	0	0
Sleeping Pod 2	11	0	0	0	0	0	1	0	0	0	0	0	0	0
Sleeping Pod 3	12	0	0	0	0	0	1	0	0	0	0	0	0	0

Social Network Diagram

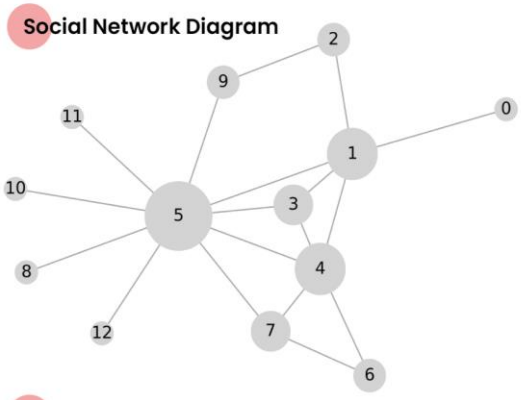

Social Network Analysis

Id	Label	Degree	Betweenness Centrality	Closeness Centrality	Eigenvector Centrality	Community Label
5	Corridor	9	0.684343	0.8	0.541983	0
1	Entrance Area	5	0.260101	0.631579	0.389029	0
4	Multi-purpose Area	5	0.133838	0.631579	0.435817	0
3	Kitchen and LSS pillar	3	0	0.571429	0.341625	0
7	Clean air chamber	3	0.045455	0.521739	0.289715	0
2	Command and Communication Space	2	0.015152	0.428571	0.139827	1
6	Lab Area	2	0	0.413793	0.181339	0
9	Exercise Area	2	0.042929	0.5	0.170412	1
0	Airlock and Eva Hatch	1	0	0.4	0.097234	0
8	Toilet	1	0	0.461538	0.135464	0
10	Sleeping Pod 1	1	0	0.461538	0.135464	0
11	Sleeping Pod 2	1	0	0.461538	0.135464	0
12	Sleeping Pod 3	1	0	0.461538	0.135464	0

Machine Learning Community Diagram

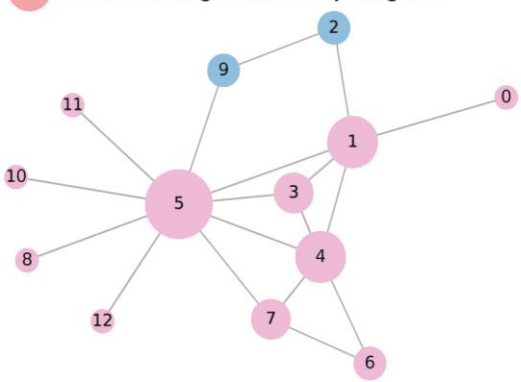

Figure 63. SNA findings for D-MARS habitation module.

D-MARS, the sixth habitat we have examined, is a modular shell that can be joined to other structures to construct a network of interconnected habitats that collectively comprise a complete Mars colony complex. It allows for various adaptations by combining the various functional modules required. Figure 63 illustrates the method of studying D-MARS's layouts.

Results from the degree centrality measure show that, except for the corridor and the entrance area, the multi-purpose space with a score of 5 may operate as a hub in the network, followed by the kitchen and the lss pillar, which earned a score of 3. The corridor has the highest betweenness centrality because it is the only place in the habitation that functions as a connector or mediator between several functional groups (with a value of 0.684343). With the most significant average distance to every other node, the corridor has the greatest closeness centrality value, followed by the entrance area and the multi-purpose area, which share the same score as the second highest value. The modular structure ensures that their closeness values are appropriately high, making it simple to examine related functions. Eigenvector centrality analysis illustrates the significance of the corridor and multi-purpose area for the interconnectivity of the other nodes.

As a result, the ML system could only identify two communities in the network. The algorithm separated the whole habitation to define functionally relevant groups, leaving only the communication and exercise areas together.

Adjacency Matrix

Mars Dune Alpha Analog Habitation Matrix

Functional Areas		0	1	2	3	4	5	6	7	8	9	10	11	12	13	14	15	16
Main Entrance	0	0	1	0	0	0	0	0	0	0	0	0	0	0	0	0	0	0
Work room	1	1	0	1	1	1	1	1	1	0	0	0	0	0	0	0	0	0
Bathroom 1	2	0	1	0	0	0	0	0	0	0	0	0	0	0	0	0	0	0
Fitness area	3	0	1	0	0	0	0	0	0	0	0	0	0	0	0	0	0	0
Robot Station	4	0	1	0	0	0	0	0	0	0	0	0	0	0	0	0	0	0
Treatment room	5	0	1	0	0	0	0	0	0	0	0	0	0	0	0	0	0	0
Kitchen	6	0	1	0	0	0	0	0	1	1	0	0	0	0	0	0	0	0
Recreation area	7	0	1	0	0	0	0	1	0	0	1	0	0	0	0	0	0	0
Crop Area 1	8	0	0	0	0	0	0	1	0	0	0	1	0	0	0	0	0	0
Crop Area 2	9	0	0	0	0	0	0	0	1	0	0	1	0	0	0	0	0	0
Corridor	10	0	0	0	0	0	0	0	0	1	1	0	1	1	1	1	1	1
Secondary Entrance	11	0	0	0	0	0	0	0	0	0	0	1	0	0	0	0	0	0
Bathroom 2	12	0	0	0	0	0	0	0	0	0	0	1	0	0	0	0	0	0
Personal quarter 1	13	0	0	0	0	0	0	0	0	0	0	1	0	0	0	0	0	0
Personal quarter 2	14	0	0	0	0	0	0	0	0	0	0	1	0	0	0	0	0	0
Personal quarter 3	15	0	0	0	0	0	0	0	0	0	0	1	0	0	0	0	0	0
Personal quarter 4	16	0	0	0	0	0	0	0	0	0	0	1	0	0	0	0	0	0

Social Network Diagram

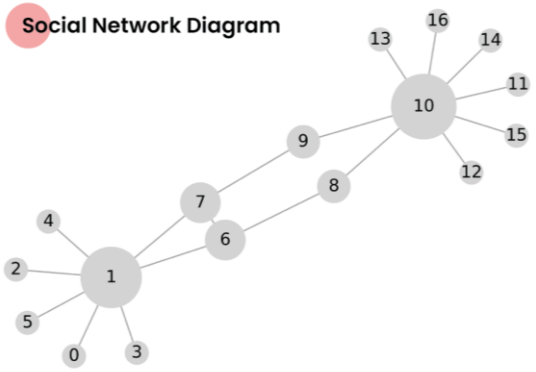

Social Network Analysis

Id	Label	Degree	Betweenness Centrality	Closeness Centrality	Eigenvector Centrality	Community Label
10	Corridor	8	0.633333	0.457143	0.437618	1
1	Work room	7	0.541667	0.421053	0.463566	0
6	Kitchen	3	0.233333	0.457143	0.342028	0
7	Recreation area	3	0.233333	0.457143	0.342028	0
8	Crop Area 1	2	0.233333	0.457143	0.252113	1
9	Crop Area 2	2	0.233333	0.457143	0.252113	1
0	Main Entrance	1	0	0.301887	0.149902	0
2	Bathroom 1	1	0	0.301887	0.149902	0
3	Fitness area	1	0	0.301887	0.149902	0
4	Robot Station	1	0	0.301887	0.149902	0
5	Treatment room	1	0	0.301887	0.149902	0
11	Secondary Entrance	1	0	0.32	0.141513	1
12	Bathroom 2	1	0	0.32	0.141513	1
13	Personal quarter 1	1	0	0.32	0.141513	1
14	Personal quarter 2	1	0	0.32	0.141513	1
15	Personal quarter 3	1	0	0.32	0.141513	1
16	Personal quarter 4	1	0	0.32	0.141513	1

Machine Learning Community Diagram

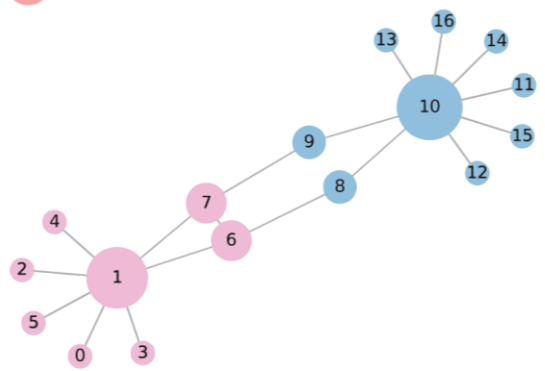

Figure 64. SNA findings for Mars Dune Alpha habitation module.

Mars Dune Alpha's livable framework is created to high standards thanks to the comprehensive CHAPEA research effort. Crew quarters, crop fields, recreation areas, full kitchens, fitness rooms, shared workspaces, medical facilities, robot control stations, and a fitness center are all part of the habitat. Figure 64 depicts the method used to assess the habitat.

The degree centrality data shows that both the corridor and the office have the potential to serve as hubs, with a score of 8 and 7, respectively. Due to its role as a connector, the corridor has the highest betweenness centrality of any location (0.63333), followed by the office (0.541667). As the proximity centrality values illustrate, there is a relatively small average distance between many distinct nodes, such as the hallway, the kitchen, the recreation area, and the crop regions. Eigenvector centrality analysis shows that the office is connected to its neighbors and the rest of the network. The corridor is the second most central node in the network in terms of eigenvector centrality.

As a result, the ML algorithm identifies two separate subcommunities within the network. The first community has the main entrance, work room, exercise area, recreation area, kitchen, robot station, treatment room, and bathroom 1. The second neighborhood has a corridor, crop areas, a secondary entrance, bathroom 2, and private quarters. Public and private activities seem to be used to define communities.

4.3.6. Conclusion of social network analysis

This study aimed to apply graph metrics from Social Network Analysis (SNA) to investigate the relationships between adjacent functional spaces of Mars analog habitations and to enhance our understanding of how their functional spaces interact. The mission of the analyzed habitats is to conduct investigations on the hazards of long-term Mars missions and to develop countermeasures. We hypothesized that understanding the roles of functions in analog habitations will allow designers to construct more space-resilient habitations against the social and psychological factors of long-term space missions—the more examination of layout networks, the greater the habitability of future long-term space missions for explorers.

Figure 65 depicts the outputs of centrality analyses, highlighting the most critical spaces in the habitations, particularly the hub or "key" areas, i.e., those areas that play a significant role in enabling the operation of many other network activities. Figure 65 illustrates the top three centrality measure results for each habitation design, allowing a comparison of core functions across design alternatives. The functional spaces have been classified as service, circulation, working, and relaxation areas to see the type of spaces with the highest scores.

Figure 65. Top results of centrality analysis of social network graphs of analog habitations

SNA analysis	Analysis rank	FMARS	MDRS	Mars-OZ	Mars500	HI-SEAS	D-MARS	Mars Dune Alpha
Degree analysis	1st	Wardroom area	Kitchen and Dining Area	Passage Area 3	Main Entrance	Landing Area	Corridor	Corridor
	2nd	Lab/Working area	Biology and Geology Laboratory	Galley	Sports Hall	Entrance Area	Entrance Area	Work room
	3rd	Stairs	Workshop Area	Passage Area1	Sleeping Area	Common Workspace	Multi-purpose Area	Kitchen
Betweenness Analysis	1st	Wardroom area	Kitchen and Dining Area	Galley	Kitchen	Landing Area	Corridor	Corridor
	2nd	Lab/Working area	Biology and Geology Laboratory	Exercise Area	Control Room	Entrance Area	Entrance Area	Work room
	3rd	Stairs	Stairs	Stairs	Sleeping Area	Stairs	Multi-purpose Area	Kitchen
Closeness Analysis	1st	Wardroom area	Biology and Geology Laboratory	Stairs	Kitchen	Stairs	Corridor	Corridor
	2nd	Stairs	Stairs	Exercise Area	Control Room	Landing Area	Entrance Area	Kitchen
	3rd	Lab/Working area	Kitchen and Dining Area	Galley	Bedrooms	Entrance Area	Multi-purpose Area	Recreation area
Eigenvector Analysis	1st	Wardroom area	Kitchen and Dining Area	Passage Area 3	Control Room	Landing Area	Corridor	Work room
	2nd	Command/ Working area	Biology and Geology Laboratory	Galley	Sleeping Area	Stairs	Multi-purpose Area	Corridor
	3rd	Storage	Workshop Area	Stairs	Kitchen	Bathroom 2	Entrance Area	Kitchen

Legend
Service Area
Circulation Area
Working Area
Relaxation Area

The degree of a node indicates the number of other nodes with which it is directly connected. For FMARS and MDRS habitations with comparable floor designs, relaxation areas have the highest number of connections with other network nodes. As a result of being a connection node, however, different types of circulation areas in the networks of other habitations have the most connections.

For the second-highest degree of network analysis, kinds of working spaces represent FMARS, MDRS, and Mars Dune Alpha habitation modules, while types of relaxation areas represent Mars-OZ and Mars500. The HI-SEAS and D-MARS entrance areas have the second-highest degree within their respective networks. In the networks of Mars 500, D-MARS, HI-SEAS, and Mars Dune Alpha, the third highest degree values correspond to types of relaxation areas, whereas it is a kind of circulation area for FMARS and Mars-OZ and a type of working area for MDRS.

If a node is positioned along several connections to other nodes, its betweenness centrality will be high. If they control the flow of activities between other nodes, nodes in a network with a high degree of betweenness can have a significant influence. Due to their central location on multiple routes, they are also the nodes whose removal would cause the most damage to the whole network. The highest betweenness centrality values in the networks of FMARS, MDRS, Mars-OZ, and Mars500 belong to a relaxation area, indicating that relaxing activities are essential for these habitations. In contrast, the same values correspond to a type of circulation area for other habitations. Different working areas in FMARS, MDRS, Mars500, and Mars Dune Alpha networks have the second-highest betweenness centrality values, indicating that nodes for working activities have numerous crossings with other nodes. A relaxation area in the Mars-OZ network and the HI-SEAS and D-MARS systems entrances have the same ranking. The third highest betweenness centrality corresponds to the stairs of habitations in the networks of FMARS, MDRS, Mars-OZ, and HI-SEAS, whereas it corresponds to a form of relaxation area for Mars500, D-MARS, and Mars Dune Alpha.

The closeness centrality metric of a node is the average shortest distance between it and other nodes. The highest closeness degree belongs to a type of circulation area in the networks of Mars-OZ, HI-SEAS, D-MARS, and Mars Dune Alpha, whereas it is a type of relaxation area for FMARS and Mars500 and a type of working area for Mars-OZ, indicating that circulation areas are positioned so that they are as close as possible to other functional locations. The second values of closeness centrality correspond to kinds of circulation areas for FMARS, MDRS, HI-SEAS, and D-MARS, a relaxation area for Mars-OZ and Mars Dune Alpha, and a type of working area for Mars500. The third-highest closeness values correspond to a type of relaxation area within the social network of five habitations. The closeness analysis demonstrates that circulation areas in habitations should be located on connections of the shortest paths to make them easily accessible from other locations. The analysis also reveals that relaxation areas are extremely crucial spaces to be accessible for better habitability.

The significance of a node is measured by its eigenvector centrality, which additionally considers the significance of its neighbors. As a more complex measure of centrality, eigenvector centrality permits a node with very few connections to obtain a high value if all its linkages route to highly connected nodes. This measure requires an indicator of activity categories to establish which

activities are crucial in the social networks of the analyzed dwellings. The types of circulation areas have the highest eigenvector centrality values in the social networks of Mars-OZ, HI-SEAS, and D-MARS, whereas the highest values correspond to the wardroom area, the kitchen and dining area for FMARS and MDRS, and the control room and work room for Mars500 and Mars Dune Alpha, respectively. The areas with the second-highest eigenvector centrality values are the command/working area, the biology, geology laboratory, the galley, the sleeping area, and the multi-purpose area, except for circulation areas for HI-SEAS and Mars Dune Alpha. The kitchen and workshop have the third-highest eigenvector centrality scores among the common areas for socializing or working. This metric demonstrates that common relaxation areas, such as the wardroom, galley, and eating areas, have a significant impact on the social network of habitations, and also common working areas, such as the control room, work room, and labs, also perform a considerable role in the social network of habitations.

In this study, the Label Propagation Approach (LPA) is proposed as a fast algorithm for identifying communities in a graph. The LPA algorithm of the NetworkX package uses a semi-synchronous label propagation strategy to discover network communities, combining the most advantageous aspects of synchronous and asynchronous models. Neither an objective function nor any other prior information is required to identify the communities; an investigation of the network's topology is involved.

Using the machine learning technique of the NetworkX package, the Python programming environment was utilized to detect communities in habitation layouts. The algorithm labels nodes within the same communities with identical labels. The resultant community data for each analog habitation is exported as an Excel file using the Gephi tool, and the collected data is restructured to create a comparative representation of the communities of the habitation layouts. The final documentation in Figure 66 can be utilized as a design guideline to generate layout configurations for a habitation project. The guideline reveals that detected communities generally contain spaces with exact functional needs. It provides sufficient information to make decisions on the positioning, grouping, and interconnection of functional activities of habitation in order to develop a more space-resilient design.

Consequently, comprehensive evaluations demonstrate that social network analysis methodologies can be employed to analyze habitation designs and enhance functional advancement when their floor plans are represented as undirected networks. In addition, the study reveals positive results for the initial implementation of SNA in the design of habitations.

Figure 66. The representation of community detection results as a guideline for habitation layout design.

05 th Chapter
ADVANCED DESIGN PROJECTS FOR A MARS HABITATION

Chapter 5 provides implemented habitations technologies and describes the prerequisites for an advanced habitation built without Earth-dependent resources and human assistance. Afterwards, the chapter provides advanced habitation proposals from various institutions that collaborate with space agencies. Lastly, the habitation design requirement is finalized by integrating the findings of the previous chapter's assessment rapor with the findings of the comprehensive assessment report of habitation proposals.

In terrestrial analog simulation scenarios, extreme circumstances and uncontrollable external factors have been associated, as stated in the previous chapter. Numerous studies undertaken with analog missions have contributed to technological advancements in habitability systems, from human-in-the-loop investigations to evaluations of human reactions to the habitat.

The habitation structure contains the habitation systems like life support, environmental monitoring, crew health, and protection against fire and radiation and serves as the house for future explorers in deep space. NASA is now conducting a series of trade studies to determine the optimal module construction method and is collaborating with the US industry to improve concepts further and produce prototypes for testing. The construction of the habitat modules will need to protect humans from drastic temperature variations, micrometeoroids, and space radiation.

The first phase in developing a habitat is determining the required fidelity to be delivered to the site. The Technology Readiness Levels (TRLs) assess the fidelity, which ranges from 1 to 9, with 9 being the most advanced technology. The first four stages are design phases, levels five and six are simulation processes, and levels seven through nine are when the design is evaluated in a real-world setting in an analog environment. The TRL table criteria in Figure 67 change between organizations. However, NASA and ESA have the same criteria employed in this research (Mankins, 1995).

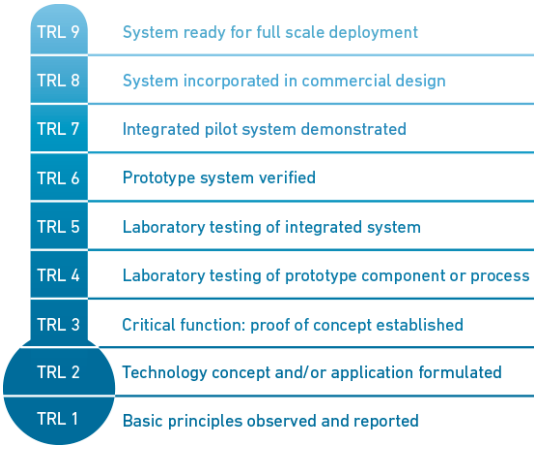

Figure 67. TRLs criteria for habitat technologies (Lim & Herrmann, n.d.)

The second phase in developing a habitat is to specify aimed habitation class which defines the minimum required technology level. Materiality, structure type, and engineering complexity are still used to classify habitats rather than trip durations or purposes. NASA has recognized three types of habitats based solely on technical considerations (Häuplik-Meusburger & Bannova, 2016):

In the Class I category, components are pre-integrated, which means they are built and tested on the ground before being shipped to space. The benefit is that it can be used immediately, but the disadvantage is that the structure's volume and weight are constrained due to payload limits. In the Class II category, components are made on Earth and assembled in space. Some subsystems can be integrated and tested, but the final outfitting occurs at the destination. More significant amounts can be deployed, and launch vehicle size or mass capability is less restricted, but the disadvantage is that any malfunctioning components cannot be repaired once it has left Earth. In Class III, a habitation is made and assembled in the exact location where it will be used. On-site construction, installation, integration, and testing are part of the process. However, because there are no constraints on volume, mass, or launch vehicle dimensions, this method has the disadvantage of requiring on-site manufacturing facilities to be set up before the launch can begin.

In 2016 Wilkinson suggested that the classes could be increased to V, with Class IV being a module constructed entirely of local materials and Class V being a module and process that use ISRU and are thus complete (Wilkinson et al., 2016). Table 17 shows the habitation classification according to its sustainability properties.

Table 17. Indications for habitation design (Häuplik-Meusburger & Bannova, 2016; Wilkinson et al., 2016).

TRL	Class	Required technology
8-9	CLASS I	pre-integrated hard-shell module.
5-8	CLASS II	the prefabricated module type that is assembled at the destination.
3-5	CLASS III	ISRU-derived structure with integrated Earth components.
2	CLASS IV	module build only with local materials.
1	CLASS V	both the module and process are using ISRU and are ultimately Earth-independent.

Earth's independence is the main requirement of a sustainable habitat design in an extreme environment where resource delivery is not feasible. Habitat classes can also quantify this requirement, with the higher class indicating the habitat's independence. According to the defined classes and their requirements, a Class-V habitat will be the sustainable target for an advanced habitat. However, this technology is not yet ready, and only progressively, by testing different classes within the Martian environment, will this extremely sustainable standard be accomplished. The primary objective of this thesis is to define a design methodology that will be used to design a Class-V habitation to survive in extreme environments like Mars.

5.1. An Overview of Space Habitation Strategies

In the late 1990s, NASA's emphasis began to turn away from the International Space Station's architecture, for which the Russian Space Agency launched the first module in 1998 (Cohen, 2015). Given the immense demands placed on personnel and resources by the International Space Station (ISS), NASA responded by becoming more systematic and process-oriented in its approach to nearly every program and its systems and technologies to make them more predictable (Cohen, 2015). This approach developed program and technology "roadmaps" on a semi-standardized template to make programs and projects more predictable, reasonable, and sustainable over time (Cohen, 2015). Space habitats were included in this technical "road mapping" effort. Cohen and Kennedy presented a "Habitats and Surface Construction Roadmap for the Moon and Mars" to arrange a classification system for habitat types (Cohen, 2015). This roadmap was founded on an architectural taxonomy of habitat variants and evolved in sophistication through several iterations of planning and construction. It classified habitats into three categories:

Class 1: Pre-Integrated (e.g., ISS module or tuna can),

Class 2: Deployable (which includes constructible, deployable, and inflatable),

Class 3: Constructed or produced from In-Situ Resources.

Initially, these classifications served to identify separate phases of the exploratory program. Class 1 was considered the possible candidate for the First Lunar or Mars Habitat (Cohen, 2015). Class 2 habitats served as the "growing" area for pre-integrated habitats, establishing a link to in-situ construction (Cohen, 2015). Haym Benaroya wrote extensively about Class 3 habitats for permanent bases and settlements, particularly the Moon (Cohen, 2015).

Beyond Class 1, habitat ideas' evolution demonstrates a more significant typological hybridization. Three examples of hybridization may be found in NASA's Mars Design Reference Mission 5.0 (Drake et al., 2010), the International Space University (ISU) (al Husseini et al., 2009), and Cohen, Fox, and Thangavelu (Cohen, 2015). The MDRM 5.0 proposes a lunar lander with a combined surface habitat with a pre-integrated descent module and an airlock with an inflatable habitat, effectively combining Class 1 and 2 habitats. The ISU combines Class 1, 2, and 3 on Mars by inserting inflatable and pre-integrated habitats inside lava tubes. Cohen, Fox, and Thangavelu's program for the Technical University of Vienna's "Destination Moon" architectural design studio calls for modules that can be pre-integrated or inflatable to be put under a 3 m cover of lunar regolith, thereby combining Class 1 and Type 2 habitats. Some refinements and variations have occurred within these initial types, implying that the triadic category may no longer adequately describe the taxonomy; enhancements and additional detail in the typology may be required to keep pace with technological advancements and design concepts.

5.1.1. Pre-Integrated modules

The pre-integrated module is the most prominent extra-terrestrial modular habitat module today. Titanium, steel, and aluminum are the most common materials used. Modules are typically sized to fit a launch vehicle and comprise a single principal function, such as a greenhouse, workshop, or mission-specific science modules. The International Space Station comprises pre-integrated modules focusing on crew quarters, materials science, or the ability to view Earth (Valle et al., 2019).

The Cupola module in Figure 68 was designed to allow astronauts to view Earth from space, making the station seem more spacious and allowing astronauts to spend more on hobbies like photography (Valle et al., 2019). Despite the prevalence of pre-integrated modules, several limitations are inherent in using a rigid body to create a module. A launch vehicle may only carry so much into space, both in weight and volume, which often limits the delivery of just one module into orbit. Multiple launches would assemble the modules if a station or base required a specific volume.

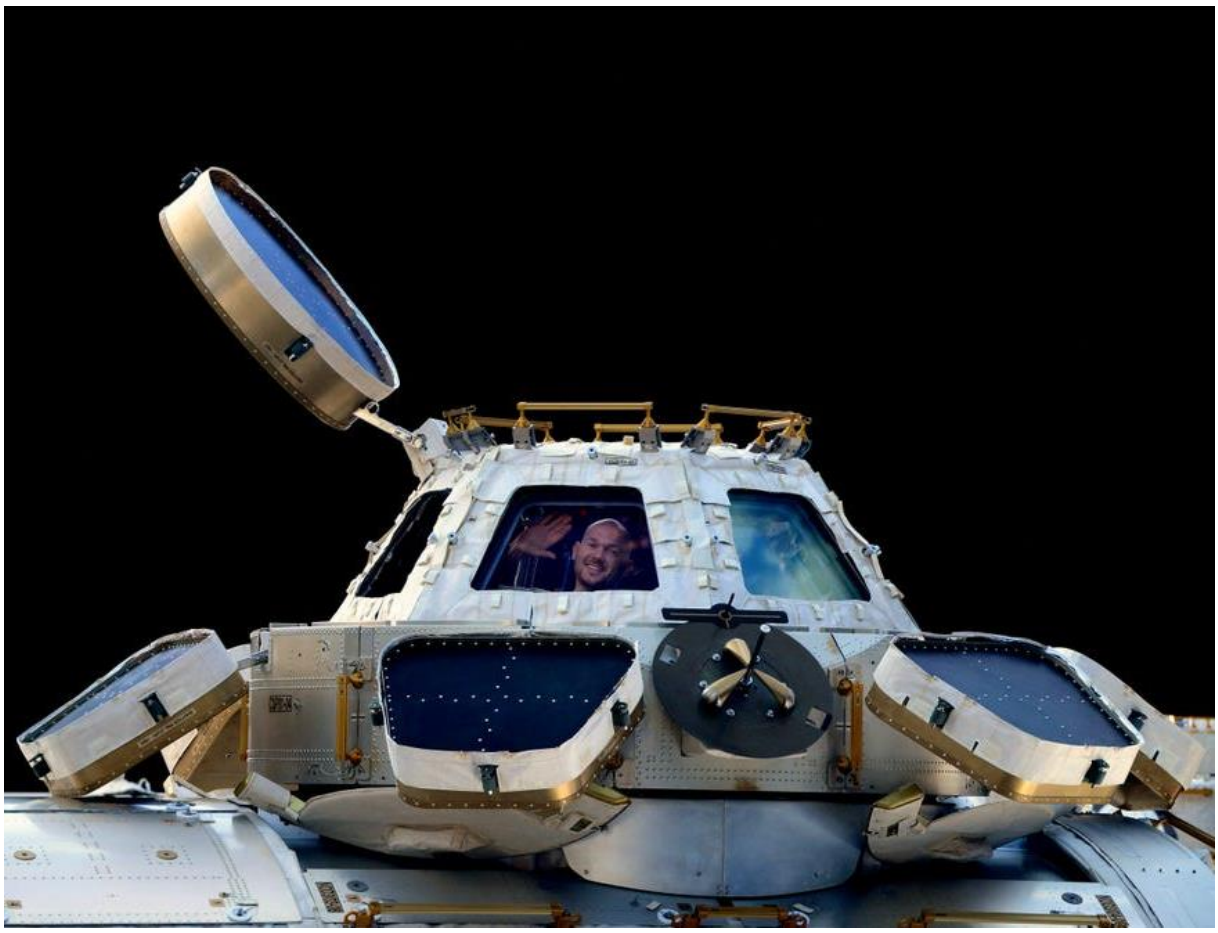

Figure 68. The Cupola module (Valle et al., 2019).

5.1.2. Deployable modules

Inflatable modules were developed due to research into robust materials that can fold and hold pressure against a vacuum. The modules comprise composite layers of textiles and impermeable materials that are densely folded into the rocket's payload bay, and while not inflatable, they can survive the outer space environment. Once in orbit, the atmosphere causes these modules to open and extend to dimensions more considerable than those possible with hard-bodied modules.

The Bigelow Expandable Activity Module (BEAM) in Figure 69 is the only module on the ISS that is not hard-bodied, and it serves as a test-bed for novel approaches to inflatable modular construction, which is now linked to the International Space Station and gives 16m^3 of habitable space (Valle et al., 2019). While several more launches would be required to outfit the modules and carry people aboard, using inflatable modules for harsh habitats in space, on the Moon, or Mars has the potential to cut habitat construction costs while boosting usable volume substantially.

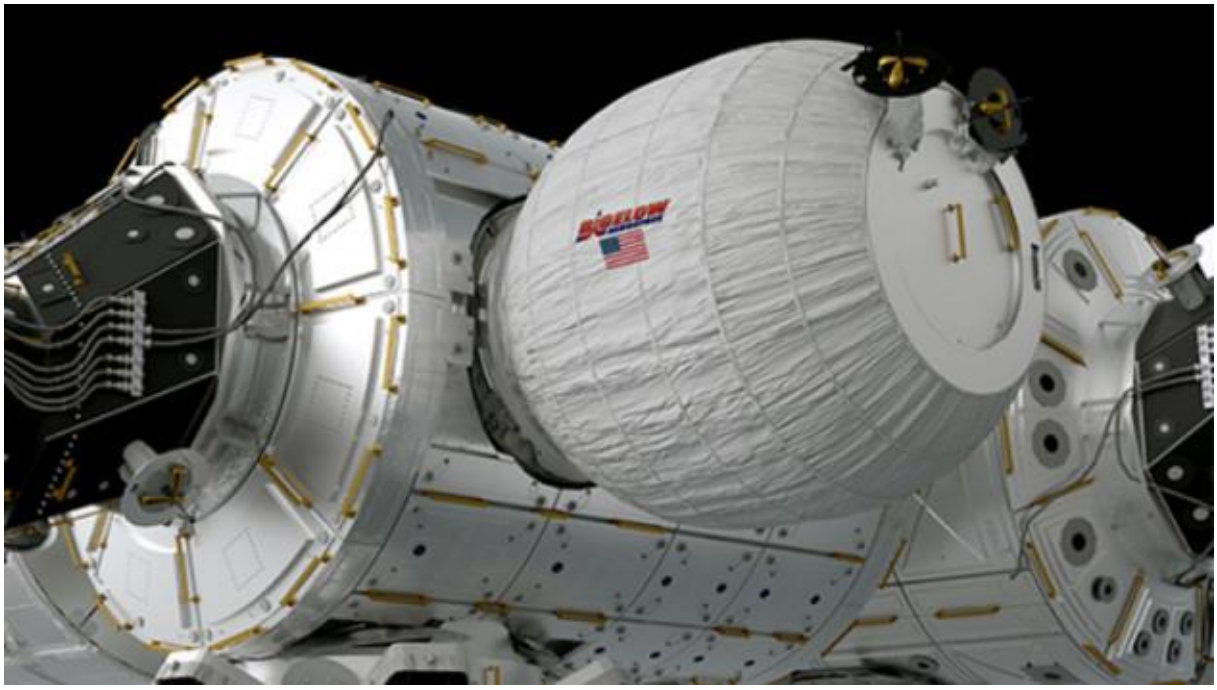

Figure 69. The Bigelow Expandable Activity Module (Valle et al., 2019).

Table 18 demonstrates that the physical properties of inflatable modules are superior to those of hard-bodied modules. To save weight, the thickness of walls in traditional hard-bodied modules may be as thin as 10 cm (Valle et al., 2019). While made of titanium, aluminum, and other metals, modules are rigid and take the full impact of a hit from space debris, though shielding exists to minimize impacts. A Bigelow expandable module averages 46 cm thick and will flex under the impact (Valle et al., 2019). The physical properties of an inflatable module and the Kevlar and materials that provide additional durability allow impacts to be absorbed. Tests on the ground have shown inflatable modules to be twice as resistant to impacts as hard-bodied modules. The walls feel as strong as concrete to the inhabitants of an inflated module.

Table 18. Comparison of inflatable and pre-integrated modules (Valle et al., 2019).

	Module	Launch Mass (Kg)	Pressurized Volume (m^3)	M/V (Kg/m^3)
Inflatable	TransHab (not flown)	13200	340	39
	BA330 (not flown)	18500	330	56
	BEAM	1415	16	88
Pre-integrated	PMM (ASI Leonardo MPLM)	4428	77	58
	Cygnus PCM (enhanced)	2000	27	74
	Cygnus PCM (standard)	1700	19	90
	Columbus (ESA Lab)	10275	75	137
	Harmony (Node 2)	14288	76	189
	Tranquility (Node 3)	15500	76	205
	Skylab Orbital Workshop	28300	302	94

5.1.3. 3D-printed Habitation Strategies

The advancement of 3D printing technology is a current trend in habitat development that is especially relevant in space architecture. Three-dimensional printing is the additive manufacturing of an object or structure by depositing a substrate in layers to create a more complicated form. This type of manufacturing may produce a wide range of objects, from a fork to the essential structural components of habitat and a wide range of objects. Additive manufacturing can create objects on various scales and materials, including plastic, metal, and even locally available raw materials like basalt. Additive manufacturing is distinct from other types of construction, such as form-casting or reductive manufacturing, in which an object is made by removing material from a more significant mass. These manufacturing methods generate excessive waste in the form of destroyed formwork or resources wasted during the shaping of an object, both undesirable attributes in the resource-constrained situations of extreme habitat. Additive manufacturing produces significantly less waste and is far faster than these construction methods. Because of these characteristics, 3D printing can guide expedition planning by modifying resource consumption and creating habitat.

The International Space Station (ISS) has been used as a testbed for 3D-printing objects in a microgravity environment, with NASA attempting to transition away from relying on spare parts or machined tools shipped from Earth and toward a system based entirely on low-weight ABS plastic and an on-board 3D-printer (Werkheiser et al., 2014). Removing the need for spare parts on the station frees up space that would otherwise be utilized for storage, which is advantageous in limited environments like the ISS. The printer is being used as an additive manufacturing trial to see the technology's limits and use it in future design projects. The Zero-G 3D printer in Figure 70, developed by Made in Space, has completed parabolic flight tests and operates on the International Space Station (Werkheiser et al., 2014). As 3D printing scales up to construct larger objects and the spectrum of additive materials available expands, the technique may become critical for long-term living in other worlds.

Figure 70. The Zero-G 3D-printer (Werkheiser et al., 2014).

The benefits of 3D printing when designing and constructing within extreme environments range from the economical, due to the immensely reduced costs of certain kinds of construction, to the practical, such as the ability to print objects as needed. In creating a single-use part for a specific function within a habitat, the cost of that part would be the electricity required to operate the printer and the substrate used in printing. Creating a part as needed is cheaper than that required for a company on Earth to create a machined part through molding or subtractive manufacturing. Printing a part also negates the transportation cost of shipping that part to the habitat. For example, on the ISS, the cost of spare parts currently in reserve on the station, including their manufacture and shipping costs, is roughly 1.2 billion dollars (Bassingthwaighte, 2017). These funds may be put to better use in the space program, mainly because most of these components have never been used and are only there as a backup.

Another advantage of 3D printing technologies is that once the essential habitat is built, the 3D printers remain on-site, enabling habitat growth and manufacturing other essential structures without requiring them to be delivered from Earth (Mueller et al., 2014). 3D printers only require solar power or another energy source and printing material. Renewable energy and locally produced resources give a habitat or colony more resource independence from Earth than achievable [38]. This construction would be less expensive than transporting habitat modules and would be completed considerably faster once printers were installed on location, thanks to the simplicity of printed designs. It is also possible to construct structures beyond the transport capability of launch vehicles. Printed

designs would include a complex of modules that could be expanded upon as needed instead of a single, pressurized habitat that would need to be brought up from Earth at a high cost.

Several kinds of research have looked into using Lunar or Martian regolith as a 3D-printing material and discovered beneath the surface of distant worlds like Mars (Mueller et al., 2014) (M. Morris et al., 2016a). Compared to the costs of bringing modules to the site, a 3D printer capable of employing these resources would enable in-situ and comparatively economical habitat construction. New habitats or habitat additions, like in Figure 71, may be printed as needed, significantly lowering the cost of moving materials to the location. Because the procedure is quick and does not rely on chemical reactions, it can be employed in places without an atmosphere or very little gravity. The developed system is also a technology that can be applied to almost any rocky planet. Both the Moon and Mars are covered in massive volumes of powdered regolith, which can be used for construction projects, making them uniquely suited for 3D printing.

1. Regolith

Regolith is the principal construction material 3D printers will employ to create extreme habitats on the Moon or Mars (Mueller et al., 2014). The material, which makes up most of both planetary bodies' surfaces, is called Lunar Regolith or Martian Regolith, depending on which astronomical body is discussed. Regolith comprises sands, powdered basalt, small rocks, and other loose surface particles. Both worlds' regolith is similar to Earth's soil but devoid of nearly all water and known biological components.

Regolith differs from terrestrial soil because it has finer particles than terrestrial soil. The lack of a hydrological cycle and an active climate has kept the Moon's and Mars's surfaces unchanged for millions, if not billions, of years. Covering habitats with regolith is a cheap and straightforward approach to ensure that habitats put in harsh settings on the Moon or Mars are secure from radiation (Mueller et al., 2014). In 2019, a design and engineering competition was organized by NASA to research using in-situ materials for on-site habitation construction as an example of radiation shielding implementation. The winner's implementation is shown in Figure 71 (M. C. Roman et al., 2016).

Figure 71. 2019 NASA 3D-printed habitation competition winner (M. C. Roman et al., 2016).

2. Water

Extreme habitats on the Moon or Mars are some of the most challenging places for humans to live, but such environments allow for otherwise inconceivable architectural solutions due to their extreme characteristics. These habitats are nearly entirely defined by below-freezing temperatures, a feature that permits water to be exploited as a construction material (Bassingthwaighte, 2017). While summer at the equator on Mars or direct sunshine on the Moon would be too hot for this construction method, there are many places on both worlds where the temperature is consistently below freezing.

Ice can be used as a principal construction element in the external walls of habitats if the environment is suitably cold. Using water or ice as a building material is not new; indigenous peoples in the Arctic have been doing it for thousands of years. A NASA-sponsored 3D-printing competition in 2016 showcased modern instances of specific usage of water in construction (M. Morris et al., 2016a). Ice House in Figure 72 won first prize for its design, which involved extruding water/ice into the shape of a dome and coating the ice with an Ethylene Tetrafluoroethylene membrane to prevent the ice structure from sublimating in Mar's thin atmosphere.

Water enables the construction of ice formations that can screen radiation while allowing natural light into the habitat. The ambient radiation on Mars can be reduced to levels safe for humans with as little as 25.4 cm of ice, yet the Icehouse design used a coating thicker than 25.4 cm throughout the project (M. Morris et al., 2016a). Building with ice may also have psychological benefits. The materials used in its creation are translucent, allowing natural light to enter and providing vistas in all directions.

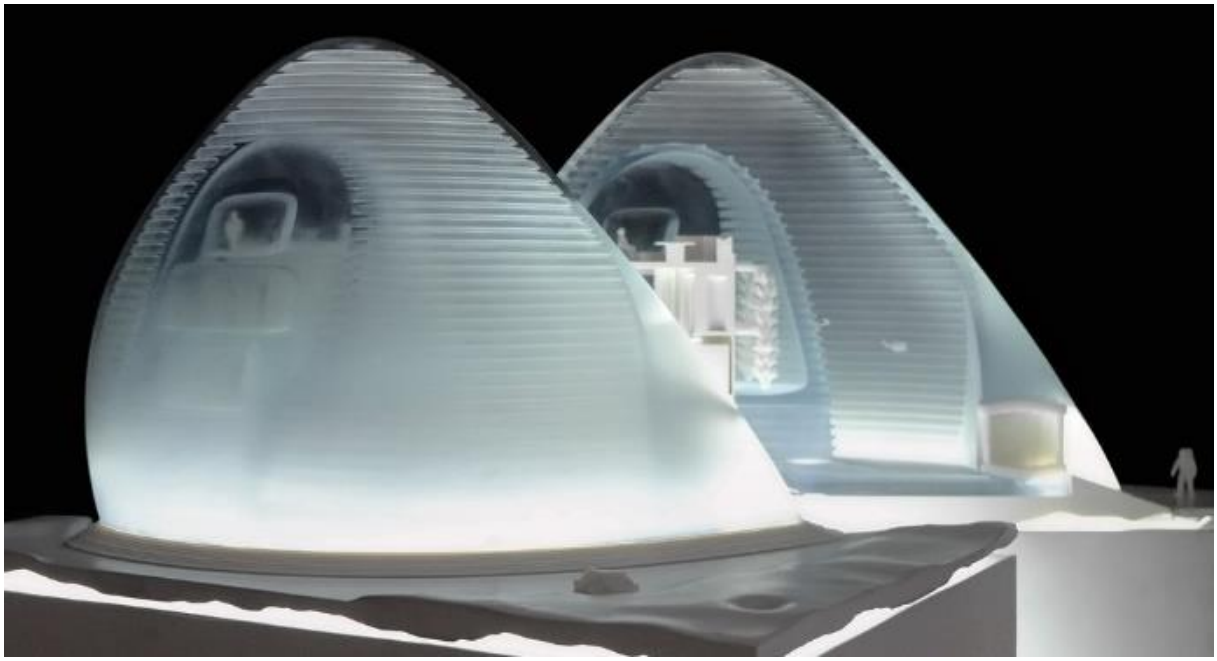

Figure 72. The Model of Ice House Mars Habitation (M. Morris et al., 2016a).

5.1.4. Natural Habitation Strategies: Lava Tubes, Skylights, Craters

Habitat design necessitates much thought, whether hard-bodied, inflatable, or printed, but it is also essential to consider where habitats will be constructed (Daga et al., 2009). Natural aspects of extreme environments can be included in habitat design; in some circumstances, a natural feature may even become the dominant component of the habitat.

Natural features are rarely used in habitat design on Earth due to their generally friendly environmental conditions, but they are pretty likely to be used in habitat designs for outer space or other worlds, mainly owing to the radiation protection provided by natural rock. In high-radiation areas like the Moon or Mars, a habitat built into a tunnel or lava tube provides occupants with an essentially physically safe environment (Daga et al., 2009). The geology of distant planets, craters, skylights, and lava tubes are all possible habitat places illustrated in Figure 73. The Moon and Mars have various impact craters on their surfaces due to billions of years of asteroid bombardment.

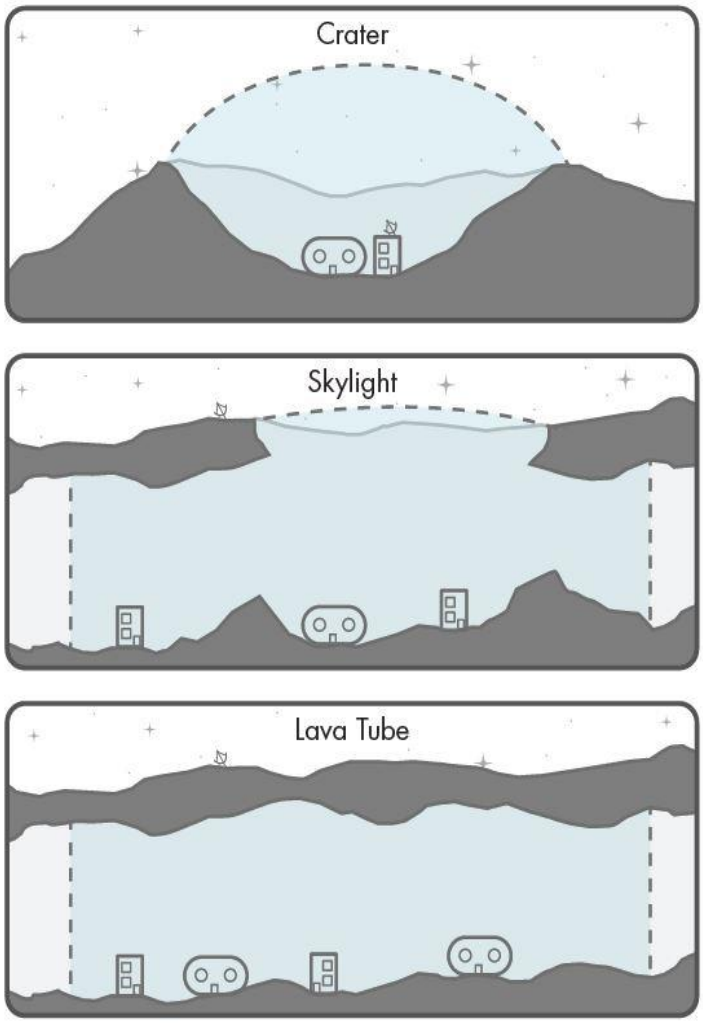

Figure 73. Natural habitation strategies (Daga et al., 2009).

5.2. Design Projects for a 3D-printed Mars Habitation

Developing a safe, space-resilient, and protective habitat is essential for future expeditions to Mars. Preceding the arrival of a crew, autonomous habitats will be built on Mars. Local and indigenous resources will be critical and pre-integrated systems and technology from Earth that can facilitate robotic construction and development in these settlements. One of the most fundamental principles of autonomous construction for future surface habitats is in-situ resource utilization (ISRU). Because of the high cost of transportation, constructing an autonomous surface habitat by depending solely on a habitation system imported from Earth is not an option. ISRU's production of materials, technology, and resources for surface habitat development is motivated primarily by payload mass optimization. High-value scientific and engineering research will necessitate the development of a permanent settlement on the surface of Mars in the future.

Combining in-space manufacturing techniques with sophisticated additive manufacturing and autonomous robotic assembly technologies is the next logical step for ISRU habitat development. However, research on large-scale additive manufacturing in micro- and reduced-gravity environments employing cementitious 3D printing is still in its infancy.

Since 2005, as a program of the Space Technology Mission Directorate (STMD), NASA has organized Centennial Challenges “to generate revolutionary solutions” to the problems related to space innovations through “diverse and non-traditional sources (YEĞEN, 2019). In 2014, NASA announced the 3D-Printed Habitat Challenge, a research competition in which teams from industry and academics were challenged to develop a design and complete system for autonomous extra-terrestrial building, specifically for Mars (M. Morris et al., 2016a). Because of the time lag between Earth and Mars, the habitat had to be designed to accommodate four people for an entire year, and its construction had to be self-sufficient.

The competition is broken up into three stages, each with three sessions. In the first stage, which concluded in 2015, competitors had to focus on the design aspect and produce architectural designs based on the possibilities of 3D-printing technologies. The second phase, finished in 2017, centered on utilizing local, sustainable materials and cutting-edge material technology. There were two different competitions under Phase 3: virtual and physical construction. Participants employed building information modeling (BIM) tools to create architectural models of habitation at full scale and offer comprehensive data on material, design, and construction for a virtual construction competition, which concluded in 2019 with the announcement of the winners. The winners of Phase 1 as a design project and the winners of Phase 3 will be described and evaluated to comprehend their problem-solving strategies.

5.2.1. Mars Ice House

Phase I of the 3D-Printed Habitat Challenge, held by NASA, was an architectural concept competition. The objective of this phase was to develop state-of-the-art architectural concepts that take advantage of the unique capabilities offered by 3D printing. The design proposal in Figure 74, the Mars Ice House, is the winner of the Phase I competition from SEArch+ (Space Exploration Architecture) and Clouds Architecture Office. The project includes all construction parts, from collecting water to figuring out how things work to semi-autonomous robotic 3D printing.

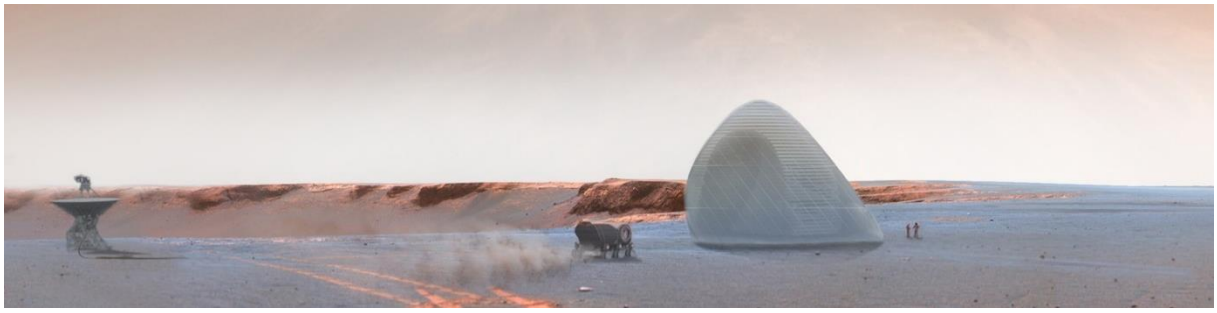

Figure 74. Mars Ice House proposal (M. Morris et al., 2016b).

Site Selection

Because construction techniques and transit vehicles are critical to the habitat's overall success, Mars Ice House has suggested a deployment and construction sequence that includes a proposed mars descent vehicle, a deployable membrane, and semi-autonomous robotic printers to collect and collect deposit subsurface water (M. Morris et al., 2016b).

Water is abundant on Mars, both at high and low latitudes. The site selection criteria included balancing access to a shallow ice table from the surface (within 20 cm - 1 m) with temperatures below freezing throughout the Martian year. As seen in Figure 75, they chose a region on the northern flanks of Alba Mons between 45 N-50N latitudes and 230 E–270 E longitude, considering construction requirements such as reasonably easy slopes and soft ground and the goal for maximum feasible sun exposure (M. Morris et al., 2016b).

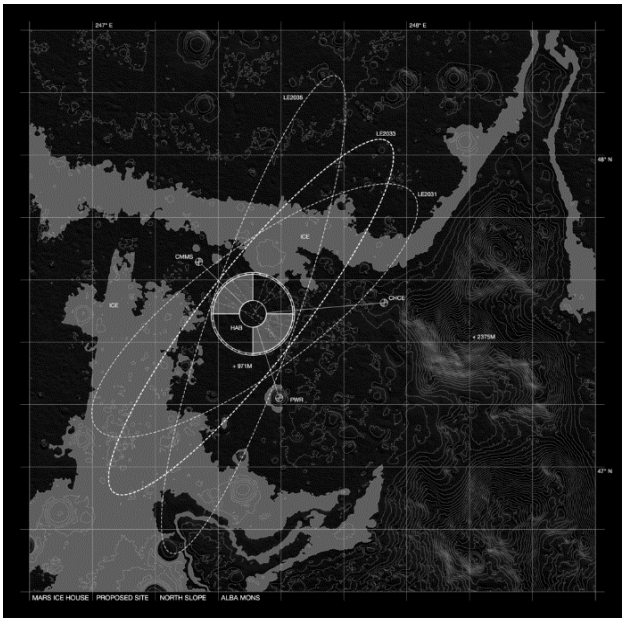

Figure 75. The chosen location for Mars Ice House (M. Morris et al., 2016b).

Material Selection and Radiation Shielding

The Mars Ice House uses subsurface ice instead of Martian regolith to build a solid H_2O 3D-printed habitat instead of most typical design approaches (M. Morris et al., 2016b). According to NASA's "follow the water" exploration strategy and a human-centered design approach that seeks to connect primarily interior habitats to light and vistas of the surrounding landscape for psychological well-being, H_2O acts as a radiation barrier, absorbing shorter wavelength radiation light in the visible ranges but allowing longer wavelength light to pass through (M. Morris et al., 2016b). The result is a 92-square-meter transparent vertical habitat with maximum surface visibility, allowing visible light to enter the interior (M. Morris et al., 2016b).

Conceptual Design Decisions

The Mars Ice House's habitat is an interaction between the complicated mechanical services stored in the equipment deployed from Earth and the "space" provided by the 3D-printed construction. The lander acts as the primary backbone upon which all services, including water, electricity, and ECLSS, operate, leaving the habitat area to function as functional human spatial volumes (M. Morris et al., 2016b). The vertically oriented lander adopts the orientation of the crew's (MTV) Transit Habitat, easing the crew's transition to life on Mars. The stacked floors of the habitat organize core programs according to activity within the lander, introducing a range of private to shared interior spaces. Interior efficiency results in substantial storage pockets at the lander's base for the bots and four Environmental Control and Life Support Systems (ECLSS) (M. Morris et al., 2016b). Once the inflated ETFE membrane is deployed, prefabricated bridges from within the lander unfurl (M. Morris et al., 2016b). A spiral staircase in the lander's core provides access to the upper floors.

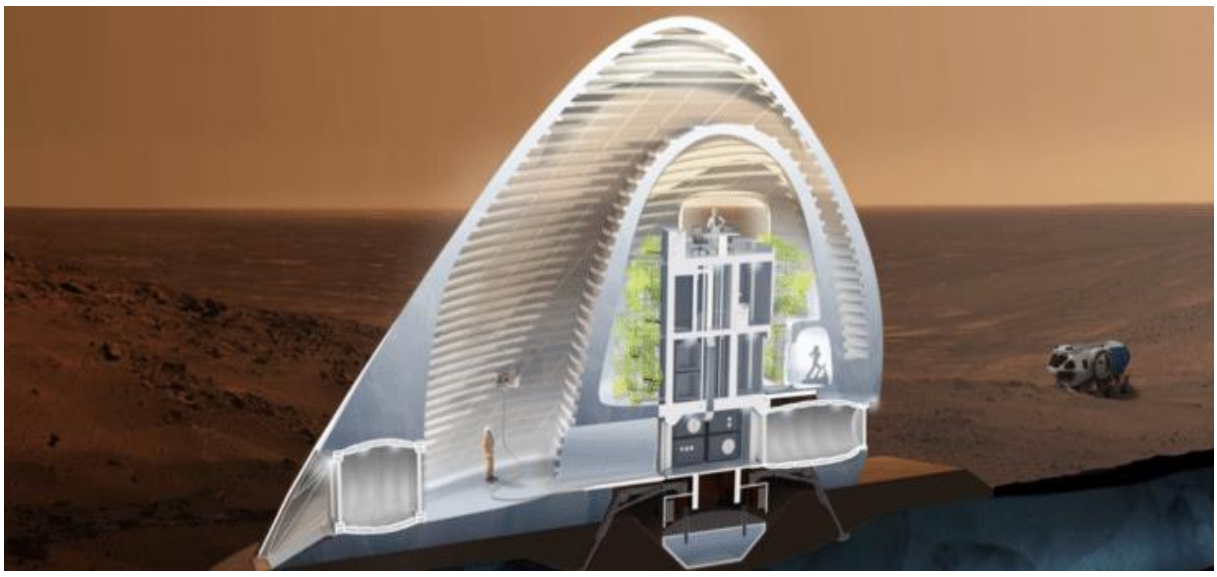

Figure 76. Sectional view through the interior revealing double wall condition (M. Morris et al., 2016b).

As seen in Figure 76, green plant life surrounds the inhabitants between the lander core and the ice interior. Vertical hydroponic gardens break up the monotony of Mars' surface while also supplying the crew's food and oxygen requirements. The gardens permit the cultivation of experimental consumable products, and their placement between programmatic zones provides the crew with exposure to natural plant life and colors during their daily scheduled duties. The ensuing varied "dappled" light effects assist the crew's psychological and mental well-being, while the 'yard' gives room to exhale any surplus oxygen created.

Programming and Functional Organization

The interstitial space between the domes provides a cold but pressurized environment that allows for movement without needing the EVA suit (M. Morris et al., 2016b). The architectural objective was to create a redundant layer of external protection, internal venting, and overflow while extending the living volume with an abstract inspirational area.

The functional distribution of habitation requirements across various floor designs is illustrated in Figure 77 (M. Morris et al., 2016b). The habitat's first level contains laboratory space, a medical and exercise facility, and a small contemplation/meditation area facing north with a window to the exterior. Despite this fact, the second level of the habitat is devoted to southern northwest-oriented sleeping quarters and the first (of two) hygiene units. Although their design provides each crew member with individual sleeping compartments complete with visual and acoustical privacy, the units' layout counters potential crew isolation by spatially

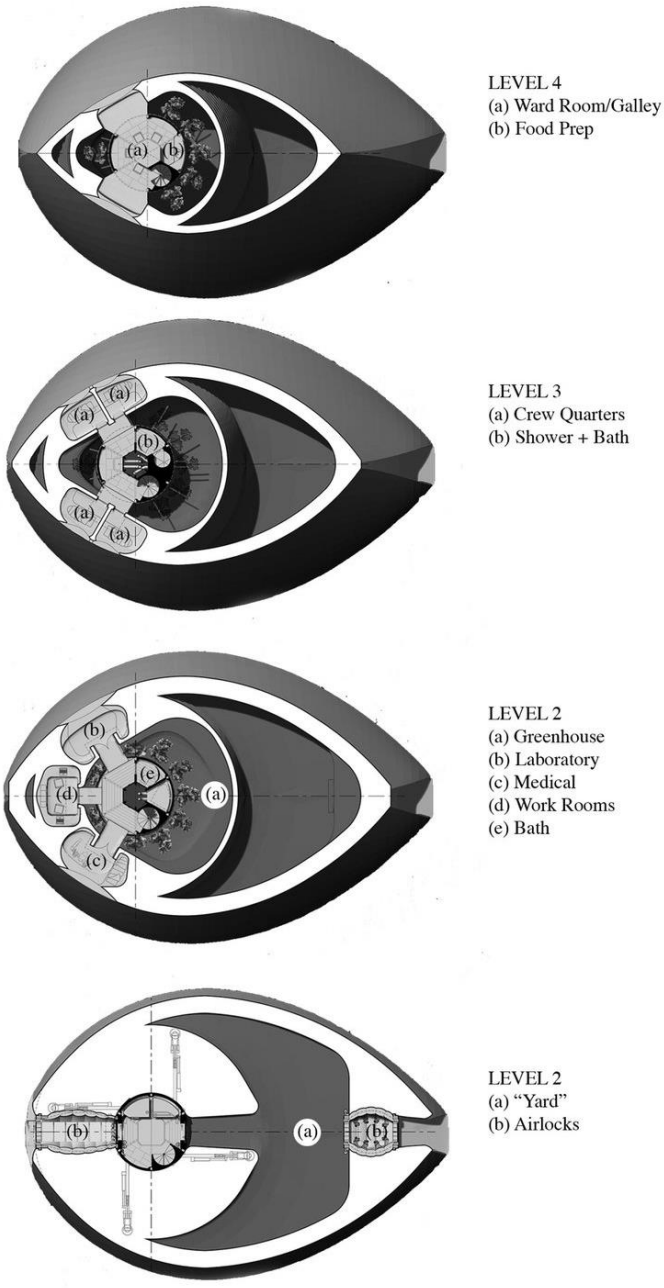

Figure 77. Architectural plans of Mars Ice House (M. Morris et al., 2016b).

encouraging socialization between crew members. The third (and final) uppermost level offers an open domed loft wardroom with a communal table at its center. A counter-height galley contains a pantry, sink, food preparation station, and secondary hygiene unit, affording the astronauts a light-filled 360-panoramic domed space.

Construction System

A lander scaled for the currently available payload of a SpaceX Falcon Heavy or NASA's Space Launch System (SLS) initiated the mission, both under development and testing. Before printing any ice, a pressurized interior must be created in which H_2O will remain solid. As a result, it is proposed that the lander inflate a translucent membrane that functions as a pressure vessel. Ethylene tetrafluoroethylene (ETFE) is a material considered because of its high tensile strength and ability to work across a wide temperature range (M. Morris et al., 2016b). This inflatable translucent exterior, reinforced along biased stress lines with Dyneema, a high-molecular-weight polyethylene, must be deployed before interior construction. Once deployed, ice-printing robots are freed from the lander base and begin the deposition of ice layer by layer inside and along the pressurized membrane. Following the ice deposition, an inside layer of insulating material would be produced. The concept of operations and deployment for habitat construction is depicted in Figure 78. Following a vertical landing on Mars's surface, a robotic water extraction operation must be carried out before deploying the pressure ETFE membrane. After establishing a closed environment with the ETFE membrane, the interior three-dimensional printing process begins using climbing robotics (M. Morris et al., 2016b).

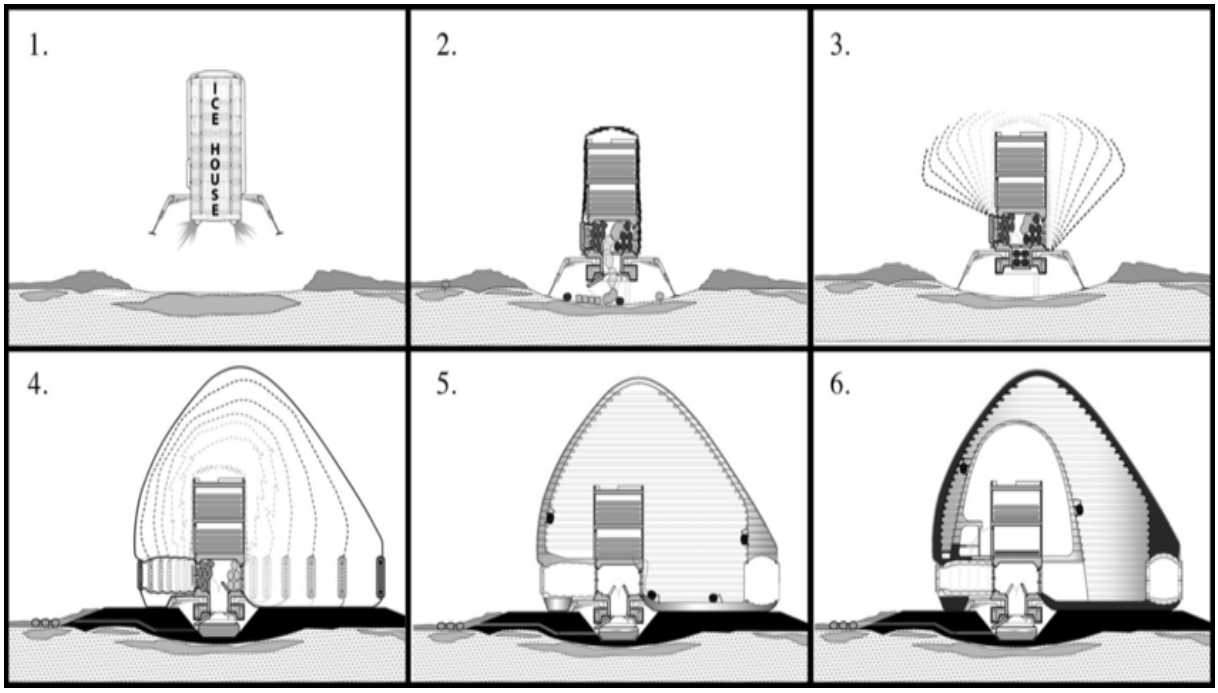

Figure 78. Mars Ice House construction process illustration (M. Morris et al., 2016b).

Structural Design and Loading Conditions

The Mars Ice House concept asks for air confinement via an Earth-supplied strengthened pressure membrane on the habitat's exterior (rather than the interior). Additionally, unlike conventional inflatable techniques that include an interior bladder and a structural restraining layer, simulations analyzing stress indicate that the membrane can bear the whole load, leaving the ice to carry only its gravity load. Internal pressure was calculated using data from the space shuttle's 70 kPa environment (M. Morris et al., 2016b). Figure 79 depicts a stress model created using finite element analysis by a structural engineering firm, Leslie E. Robertson Associates, for a pressure membrane (M. Morris et al., 2016b).

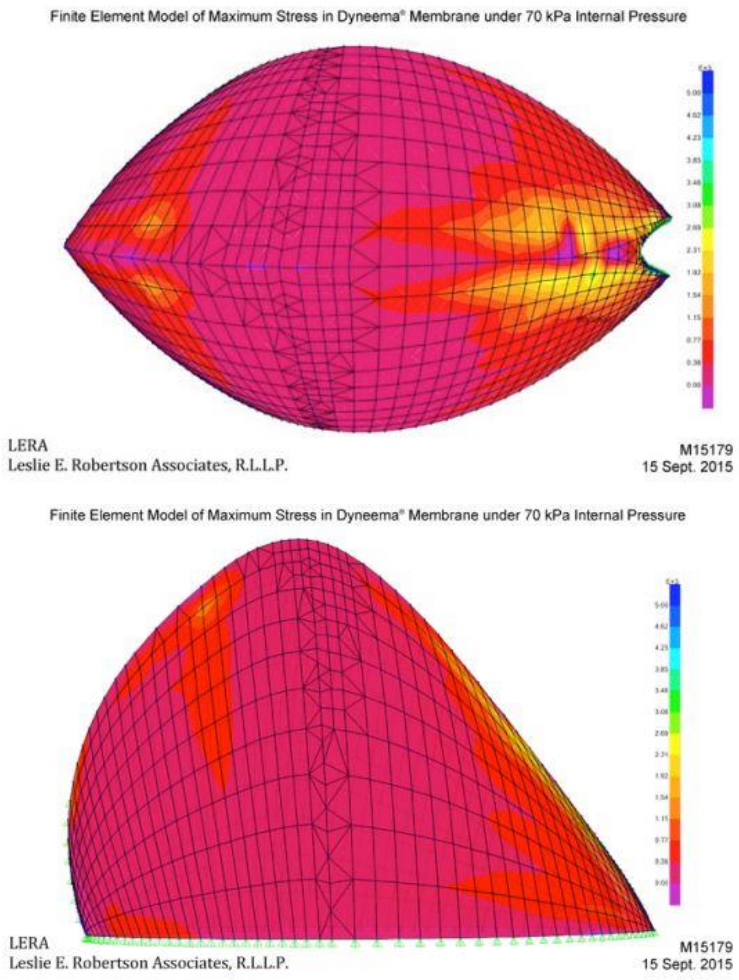

Figure 79. Finite element analysis model of Mars Ice House (M. Morris et al., 2016b).

Formally a catenary dome, the ice house's architecture can bear its weight and stand gravitationally during the deposition process. The ice is self-supporting, beginning with 0.6 m thick walls and diminishing to 6 cm.

Thermal Comfort Considerations

Thermal regulation of the inner habitat and the ice itself is critical in the concept design of an ice structure. The nested concept is illustrated in Figure 80 (M. Morris et al., 2016b). It refers to a wall section where the exterior layers of ice remain at Mars temperatures or a maximum of 0°C, while the interior is around room temperature at about 20°C. The interior is expected to be heated primarily by mechanical systems but will also gain heat through the sensible and latent heat of the occupants and some sunlight gain via the fine structure. There will be a requirement to vent or radiate heat to the exterior without compromising the ice wall's integrity.

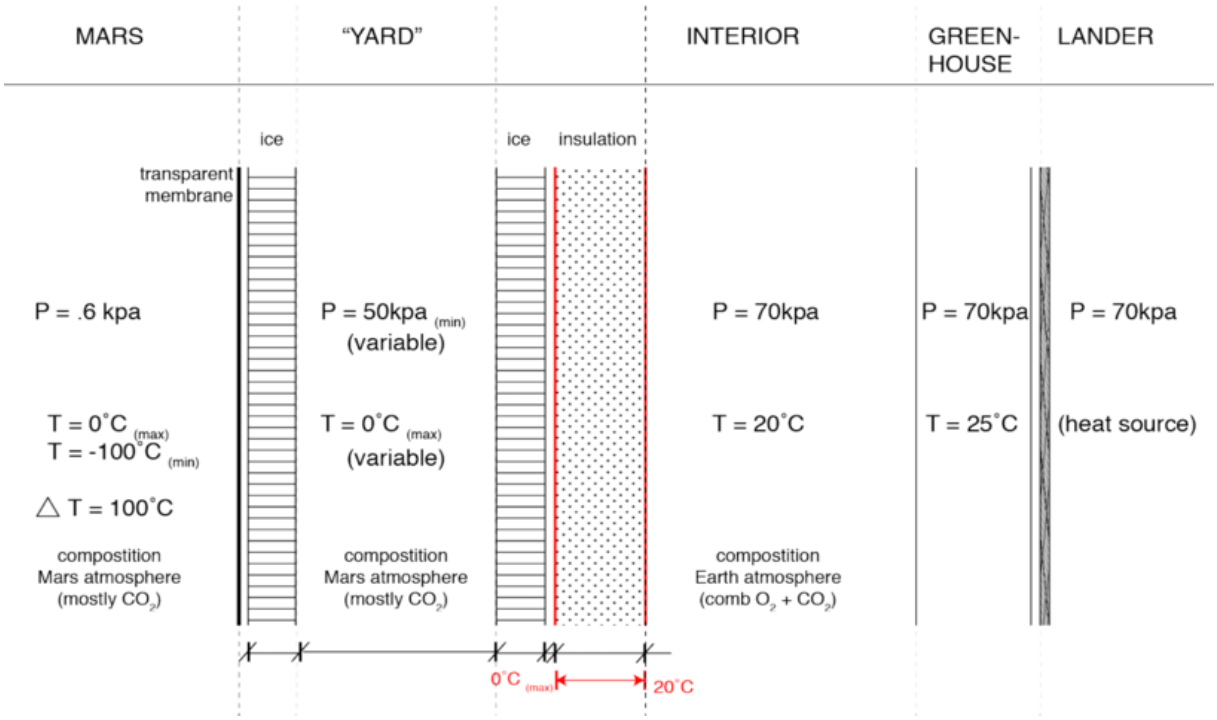

Figure 80. Conceptual wall section of Mars Ice House. (M. Morris et al., 2016b).

To temper the heat between the lander and habitable areas, a vertical "greenhouse" is supposed to surround the interior core, absorbing and redistributing some heat to the habitation spaces (M. Morris et al., 2016b). The translucent hydrophobic aerogel layer with a U value of 1 $W.m^2K$ and a light transmittance of 66% is printed between the inner ice shell and the inhabited programmatic spaces to ensure thermal comfort. A porous substance that is 99.8 percent space by volume, this additional lightweight material supplied from Earth could act as an efficient air gap, establishing the essential thermal break and possibly preserving the habitat's translucent nature. This insulation layer is likewise assumed to be 3D printed due to the nature of the 3D-produced voids (M. Morris et al., 2016b). Aerogels have been investigated for their capacity to be manufactured additively, and many studies with graphene aerogels have been successful at Kansas State University and the University of Buffalo. This insulating layer allows the inner volume to reach livable temperatures without causing the ice structure to melt.

5.2.2. Mars X-House V2

In 2018, SEArch+ and Apis Cor won Phase 3 of NASA's 3D-Printed Habitat Centennial Challenge's Virtual Construction Competition, which intended to design and construct habitable structures for the Moon, Mars, and other planets. The MARS X-House V2, as seen in Figure 81, is a 3D-printed, long-lasting habitation that utilizes autonomous robots and local resources. The planned vertical habitation has a double-layered shell and is formed like an arch facing inward (a hyperboloid) (Yashar, 2022). The system is kept cold and protected by an inner layer of high-density polyethylene (a polymeric material with good radiation shielding properties) and an exterior layer of regolith (Yashar, 2022).

Figure 81. Mars exploration illustration with X House V2 (Yashar, 2022).

Site Selection

The Erebus Montes is a series of mountains on Mars located in the Diacria quadrangle (Yashar, 2022). One of the rare sites with big ice at low elevations. The low elevation makes an entry, descent, and landing easier. Large atmospheric masses provide excellent radiation protection. Large regions of flat terrain facilitate ground transportation. HiRISE (The High-Resolution Imaging Experiment) photos reveal the presence of loose regolith suitable for construction.

Material Selection

Regolith is the most common and easily accessible material on planet surfaces, making it an ideal substrate for manufacturing (Yashar et al., 2019). On the Moon and Mars, basalt is another critical component in 3D printing because it is easily accessible within the regolith (Yashar et al., 2019). To create basalt fibers, heat the rock in an extruder at high pressure and temperature. Basalt fibers have twice the strength of steel yet weigh only a third as much. Plastics will be a crucial supplementary material for space building (Yashar et al., 2019). It would serve as a protective barrier against the possibly poisonous regolith and as a non-porous outer layer for airtight constructions and provide the raw material for windows, doors, and floors. HDPE and other plastics can be made on Mars thanks to the availability of the chemical ethylene.

Conceptual Design Decisions

As shown in Figure 82, enclosing a pressure environment in the near-vacuum of Mars is a primary design driver. The most significant force, especially in 1/3 gravity, pushes outwards from the interior. Pressure vessels typically favor tension structures, such as balloons or inflatables, or materials that can withstand tension, such as aluminum. The construction was designed and tested assuming normal (Earth-based) atmospheric pressure within the habitat; therefore, the internal pressure will be close to 100.7 kPa (Yashar, 2022).

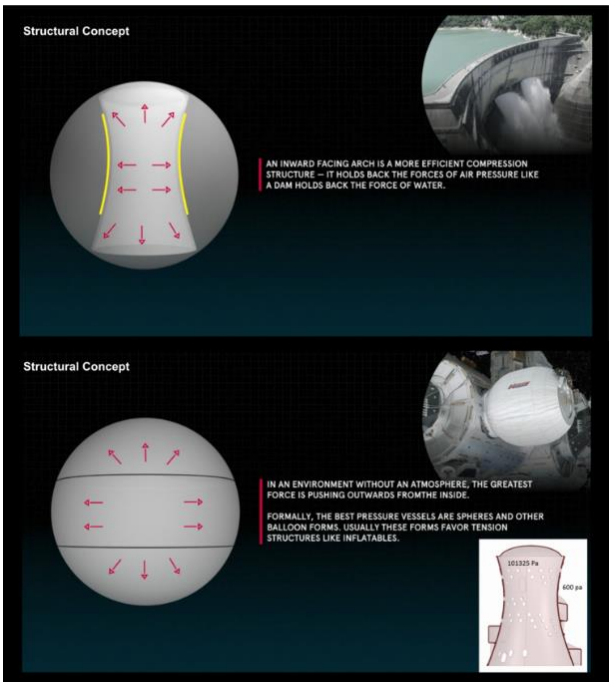

Figure 82. Mars X House's structural concept illustration (Yashar, 2022).

Programming and Functional Organization

The mechanical core of MEP and ECLSS habitat systems is pre-integrated and serves as the habitat's wet core (Yashar, 2022). In the case of an emergency, three autonomous service zones protect the two lab portions on the lower floor and the living areas. Airlocks isolate each lab from the rest of the habitat to maintain a clean working environment. In a fire emergency, a stairway on the building's outside gives access to levels 1, 2, and 5 (Yashar, 2022). Using the stair system as a safe place, the crew can plan and strategize before engaging in an extra-vehicular activity or completely evacuating the building because it is segregated from the main structure.

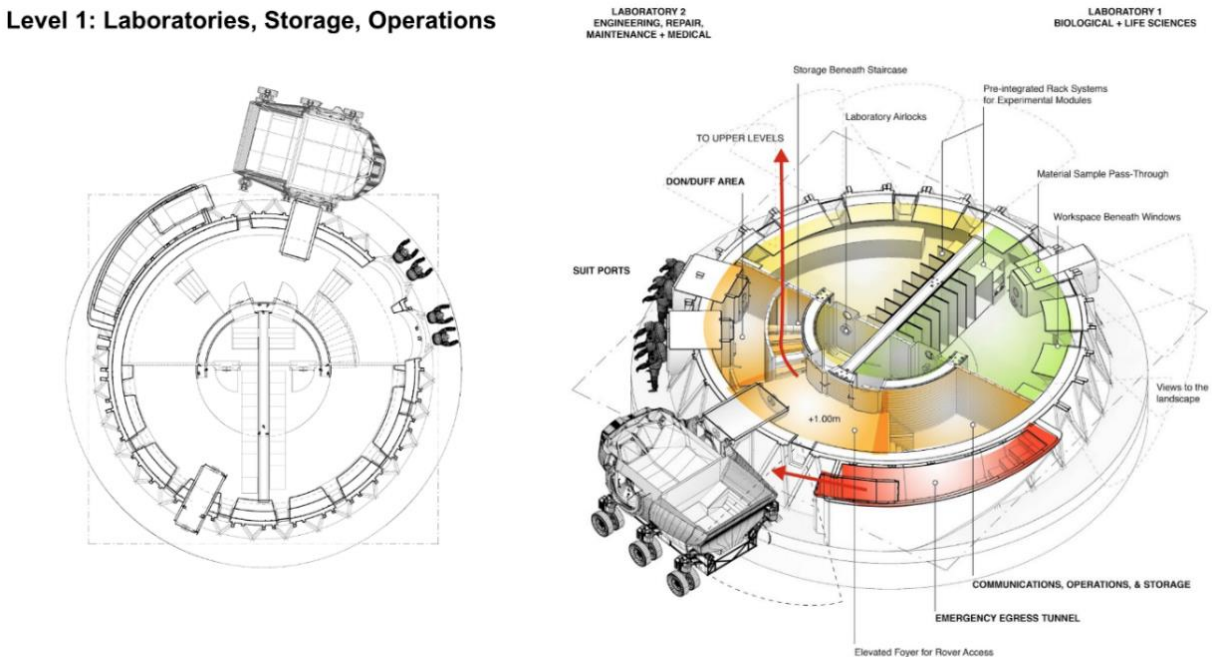

Figure 83. First-level plan and three-dimensional illustration (Yashar, 2022).

As shown in Figure 83, the first-level floor includes a communications and operations room next to the habitat's main power cables (inside the sub-floor), giving elevated access to the rover port (Yashar, 2022). Mission-critical materials such as food are stored beneath the habitat's main staircase and within the subfloor. Astronauts will be actively studying sample rocks and soils on the planetary surface for life detection, metrology, characterization, and other purposes on a future Mars mission. Examining foreign extraplanetary material is extremely perilous, and every precaution must be taken to protect the crew from potentially lethal infections. As a result, both laboratories needed to be environmentally separated from the private and public living areas via airlocks and have distinct and independent ventilation systems. Laboratory 2 will serve as the habitat's engineering, repair, and medical care center. The lab includes experimental medical diagnostics, medicines, and manufacturing modules. The lab also has a big, open work area for 3D-printing parts, and tools, fixing hardware, and maintaining other habitat engineering elements.

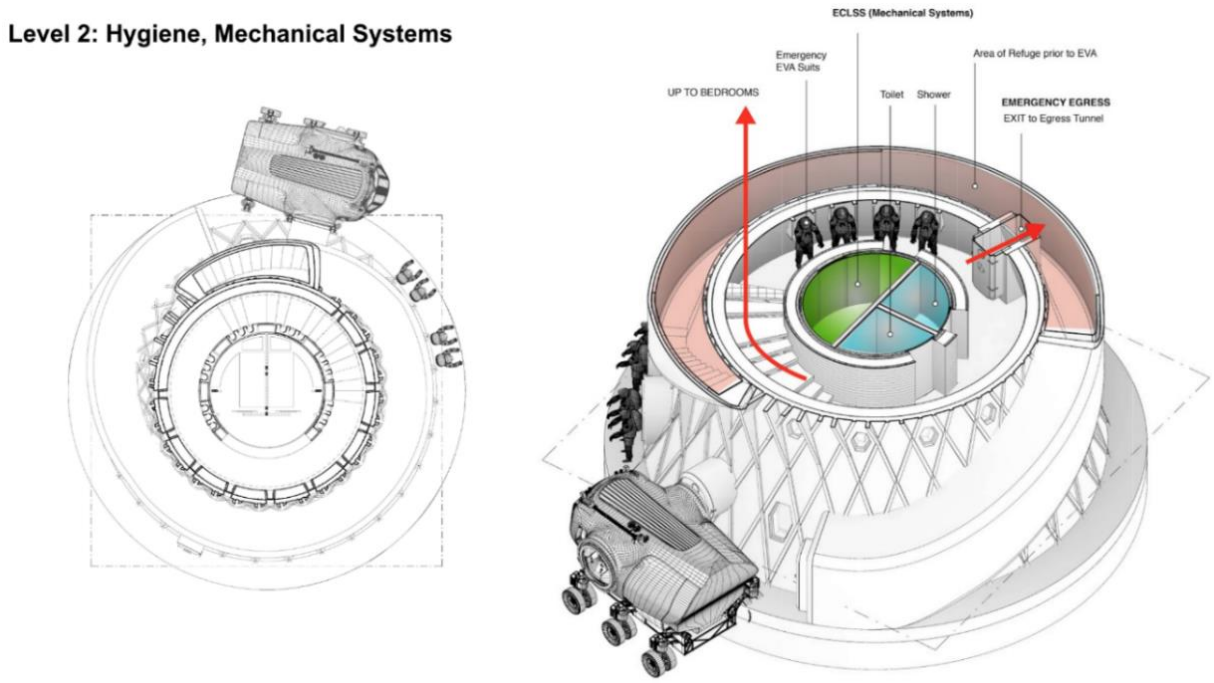

Figure 84. Second-level plan and three-dimensional illustration (Yashar, 2022).

The pre-integrated mechanical core, shown in Figure 84, contains the ECLSS hardware and the hygiene program, which can be accessed at level 2 (Yashar, 2022). Additionally, the larger landing of the emergency escape tunnel is accessible from Level 2, which can be used as a shelter and a place of preparation in the event of an emergency. Additional EVA suits are provided if the rear-entry suit-ports docked on the exterior of the hab at ground level are compromised.

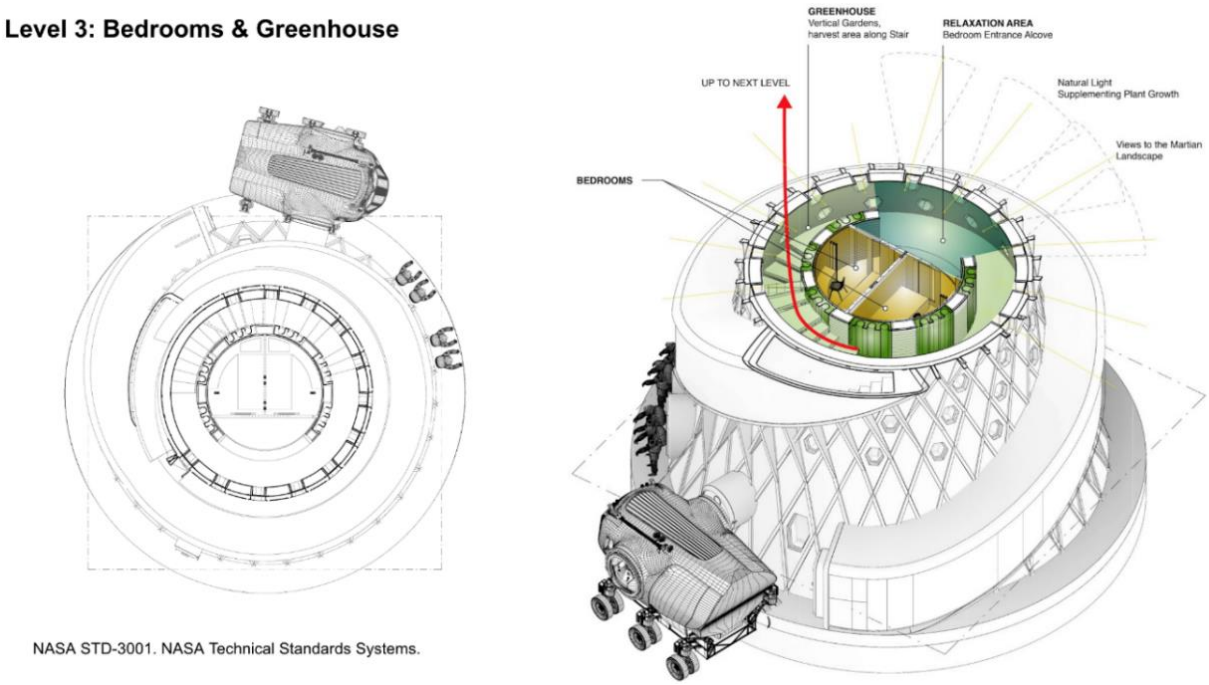

Figure 85. Third-level plan and three-dimensional illustration (Yashar, 2022).

The third and fourth levels contain two crew quarters bedrooms, as shown in Figures 85 and 86. The bedrooms are sized following NASA's minimum living space guidelines. A bedroom entrance alcove on each level gives space for pre and post-sleep activities, enjoyment of the garden, and views of the martian landscape. Because the crew spends most of their time in the sleeping sections, they are positioned within a second interior wall and are thus more heavily shielded from radiation. These walls also function as MEP walls, hosting air supply and return within 3D printed chase walls.

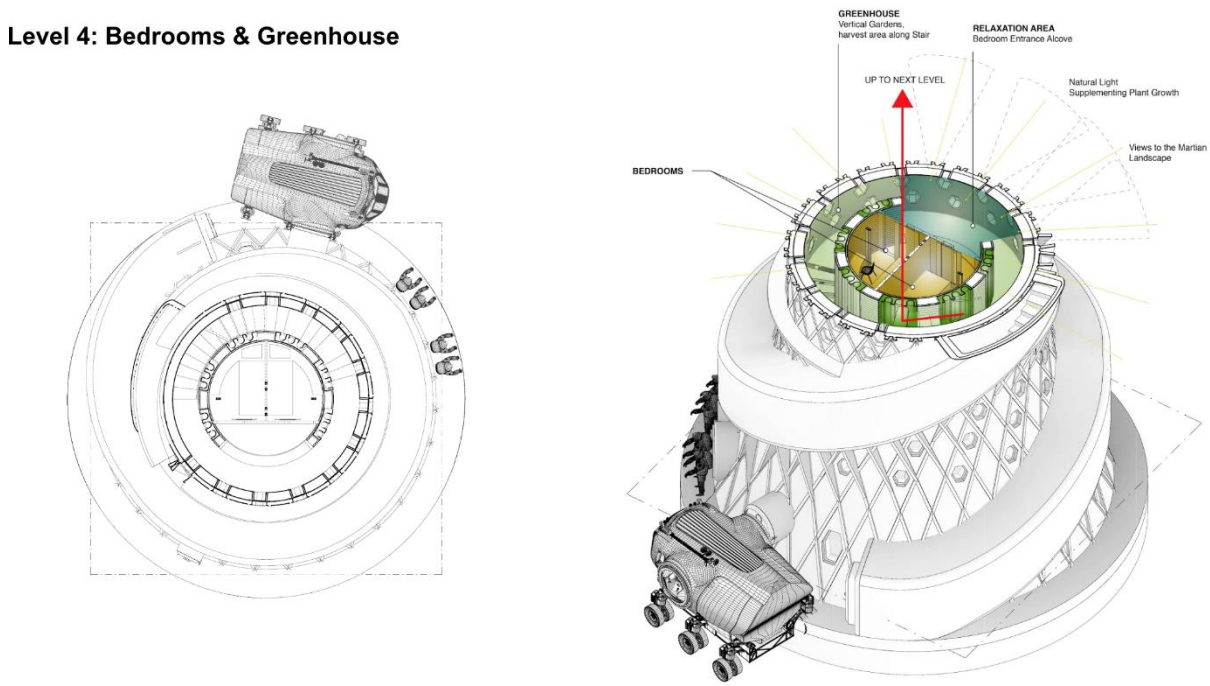

Figure 86. Fourth-level plan and three-dimensional illustration (Yashar, 2022).

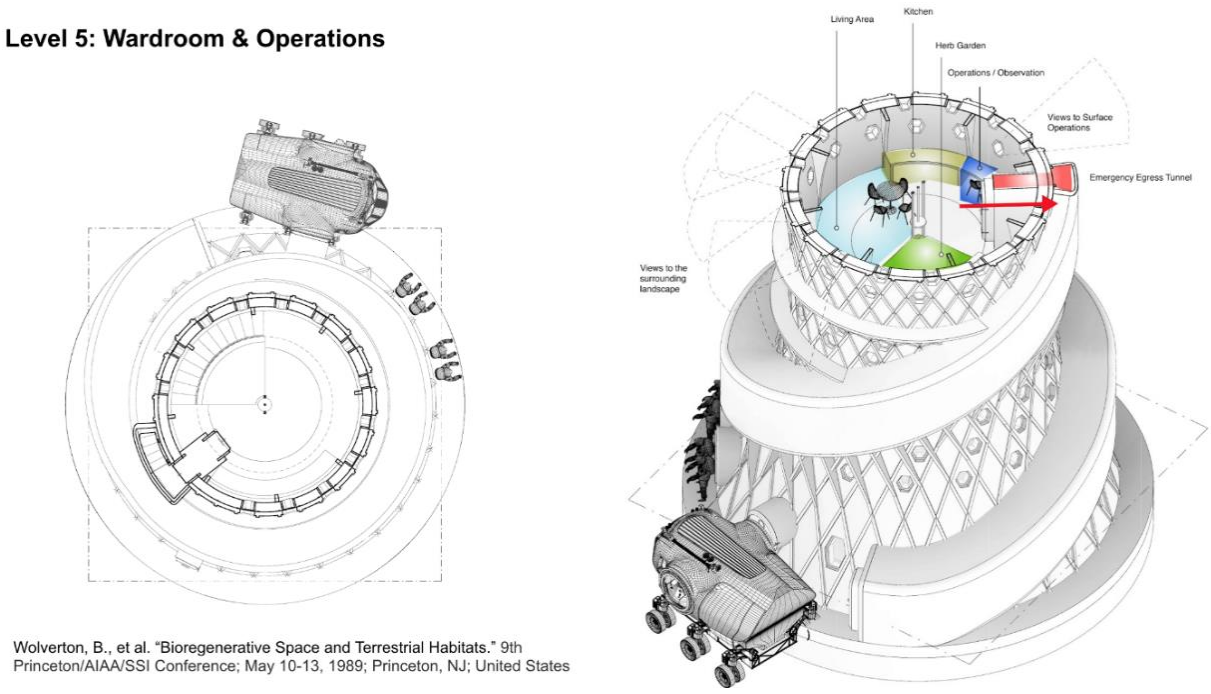

Figure 87. Fifth-level plan and three-dimensional illustration (Yashar, 2022).

Level 5, as shown in Figure 87, includes a living and communal room, a kitchen and food prep area, and a workstation for mission operations that would benefit from elevated views of the tremendous Martian environment (Yashar, 2022). A little garden area supplies herbs for the kitchen and natural plantings to purify the air pumped through the plantings below. The air supply plenum travels via the roots of the plantings, providing natural bioremediation opportunities.

Construction System

Using Apis Cor's current construction technologies and the size limits of the Hercules lander, a mobile 3D printer and mobile platform have been developed for Mars X-House (Yashar et al., 2019). An innovative telescoping mechanism at the printer's base allows on-site deployment (Yashar et al., 2019). The print head is supplied with material by a six-axis robotic arm connected to a boom-arm system (Yashar et al., 2019). During the printing process, the mobile telescopic platform has been designed to accommodate two mobile printers (Yashar et al., 2019). This platform eliminates the danger and expense of developing an overly tall printing technology crane system(Yashar et al., 2019). The mobile printer was designed to fit within the Hercules lander's 6-meter diameter circular cargo port and 20-ton weight restriction (Yashar et al., 2019).

Structural Design and Loading Conditions

Figure 88 shows the design proposal's integration of materiality and structural concepts (Yashar, 2022). Diagonal and circumferential hoop (horizontal) basalt reinforcement acts as a perimeter truss structure around the hyperboloid to resist tensile forces. Circumferential hoop reinforcement has been installed above and below window penetrations at regular elevation intervals. A single layer of expandable polyethylene foam is put between the HDPE and the regolith-concrete shell to anticipate polymer expansion and contraction. An expandable polyurethane foam layer is an expansion gap between materials with different moduli of expansion and contraction. The laboratory experimental modules' mechanical core and rack system are then integrated into the habitat. Before the diagonal basalt reinforcement or circumferential hoop reinforcement is printed, a single layer of concrete regolith is printed. The emergency exit tunnel is printed after the top hyperboloid shape and reinforcement to preserve the building's stability and avoid overturning.

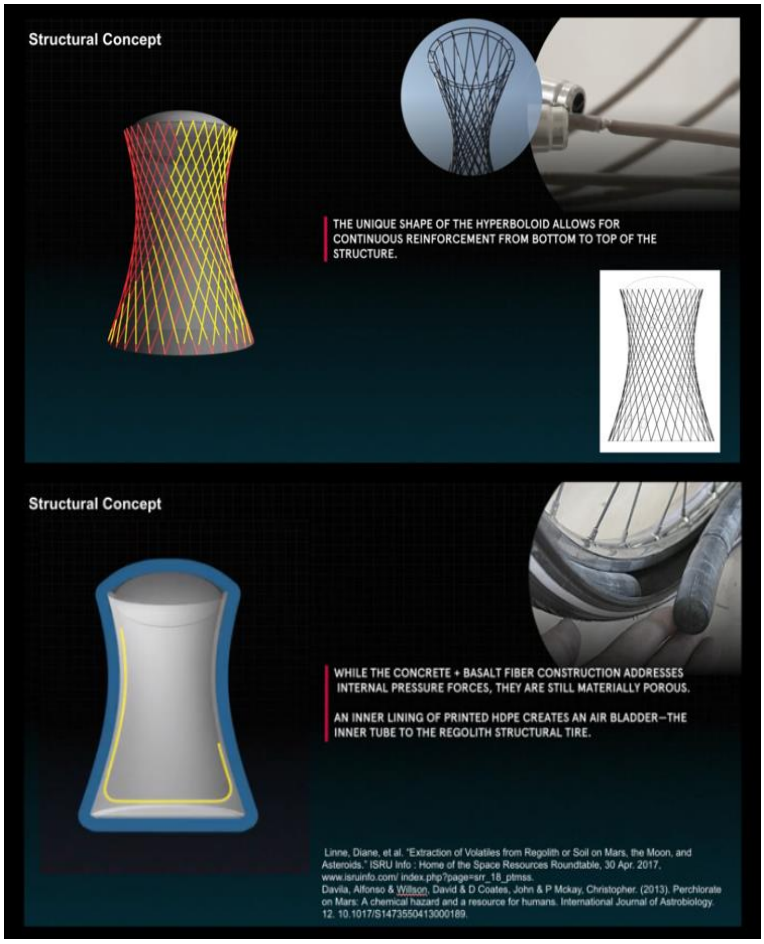

Figure 88. The structural concept with materiality (Yashar, 2022).

The structural analysis of the habitat was conducted under two load conditions: pressurization of the regolith-concrete shell and operation of the mechanical core/water bladder (Yashar, 2022). Analyzing the regolith-concrete shell influenced a critical design decision to include additional reinforcement running perpendicular to the continuous diagonal reinforcement endpoints within the dome structure.

Radiation Shielding and Thermal Comfort Considerations

A simple overhang or colonnade is one standard method of shielding high-angle radiation. High-angle solar radiation must be prevented in hot climates to maintain a comfortable indoor temperature. Figure 89 shows wall thickness design considerations of the X-House, which is designed to take advantage of the thickness of the wall construction to produce passive radiation "overhangs" at each window, effectively shading each opening against rays that are angled more than 30° (Yashar, 2022). Additionally, X-House employs thicker shielding in areas of the habitat where the crew is expected to spend the most time based on their daily schedule. By considering the astronauts' routines while designing the habitat layout, X-House protects the astronauts in the areas of the habitat where they spend the most time.

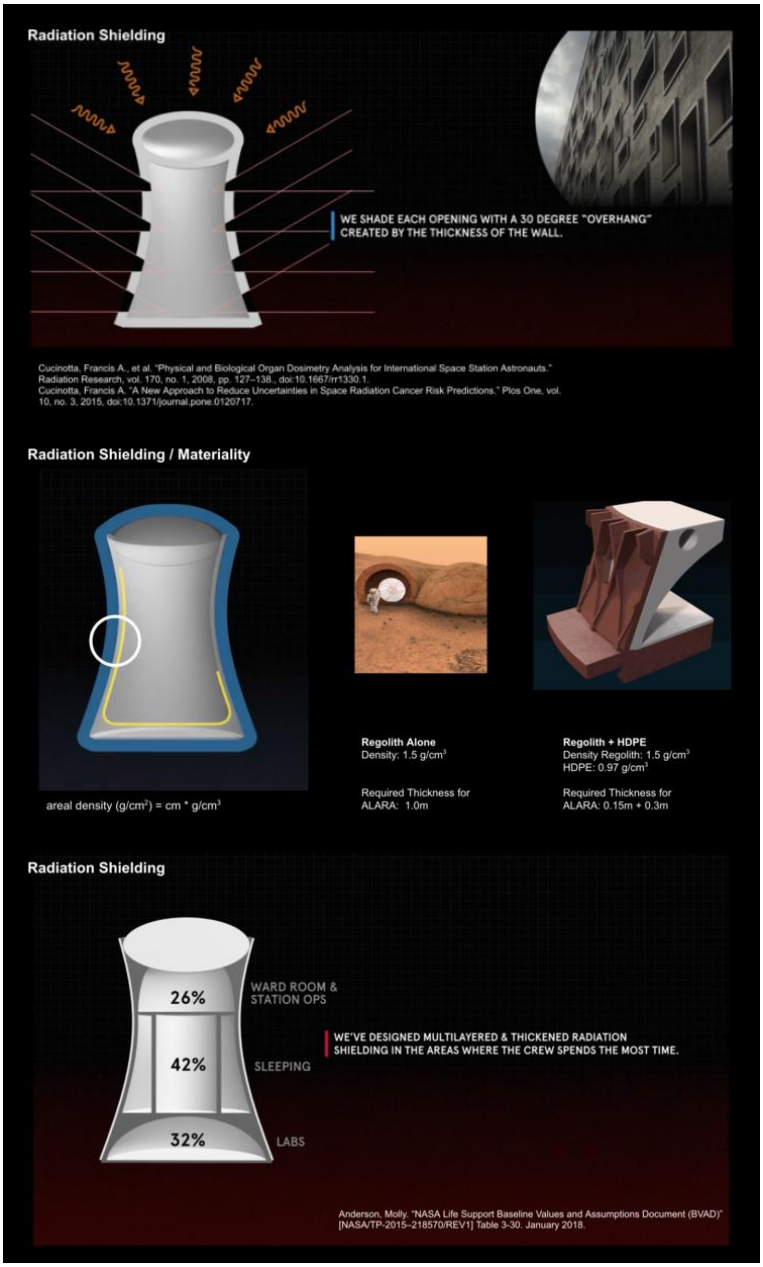

Figure 89. Wall thickness considerations of the X-House (Yashar, 2022).

5.2.3. Marsha

Marsha, as depicted in Figure 90, is a 3D-printed Mars habitat designed by AI SpaceFactory for NASA's 3D Printed Habitat Centennial Challenge. It won first place in the On-site Construction Competition and was selected as one of the top ten projects in the Virtual Construction Competition during Phase 3. AI SpaceFactory utilizes the most advanced robotic systems, computational techniques, materials, and design to provide a comprehensive 3D printing building solution.

Figure 90. Mars exploration illustration with Marsha Habitat (AISpaceFactory, 2018).

Conceptual Design Decisions

MARSHA is a ground-up reimagining of what a Martian habitat may be — not another low-lying dome or limited, half-buried structure, but a bright, multi-level, corridor-free structure that stands upright on Mars's surface (AISpaceFactory, 2018). Martian circumstances necessitate an optimized construction capable of withstanding internal air pressure and thermal stresses. Marsha's unusual vertically oriented, egg-like structure, as shown in Figure 91, minimizes mechanical loads at the base and top, which increase in diameter (AI Space Factory, 2022). The tall, narrow structure eliminates the need for a construction machine to rove on the surface continuously, decreasing risk and enhancing speed and accuracy.

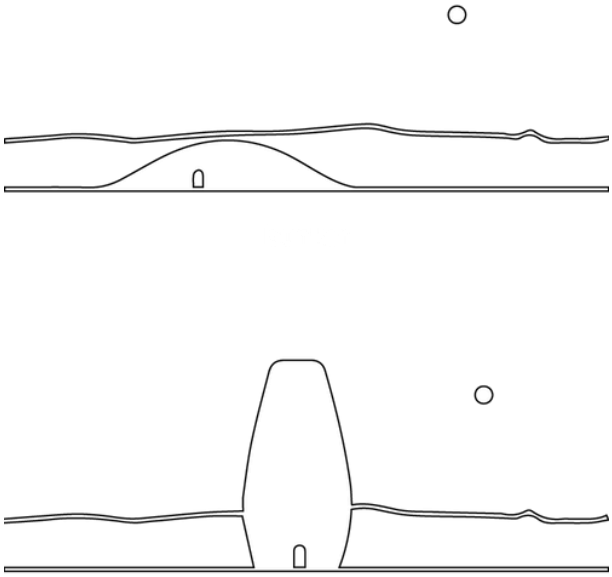

Figure 91. Sketch of the conceptual design decision for Marsha.

Programming and Functional Organization

MARSHA's functional spaces are distributed across four levels, as shown in Figure 92, each with its distinct interior ambiance that promotes mobility and avoids monotony (AISpaceFactory, 2018). Marsha's ground level has a garage and a wet lab with space for residents to work. Even on the bottom floor, light filters down from the skylight above, allowing the staff to operate in the same manner as they would at home. Additionally, the ground floor contains an EVA preparation area where astronauts can practice for "extravehicular activities" to transport them outdoors into the Martian environment. The second story has additional common space, including a kitchen and a dry lab. On the second story, the office space is adjacent to the kitchen. The third story has a garden, a sanitation pod, and personal spaces for the residents. A community recreation and fitness space on the fourth floor of Marsha takes advantage of the light from the skylight above. There is a gap between the dual shell works as a light well, supplying diffuse natural light to all levels via the enormous skylight above and intermittent windows. This one-of-a-kind location enables a stair to curve softly from floor to floor, bringing dimension to everyday life.

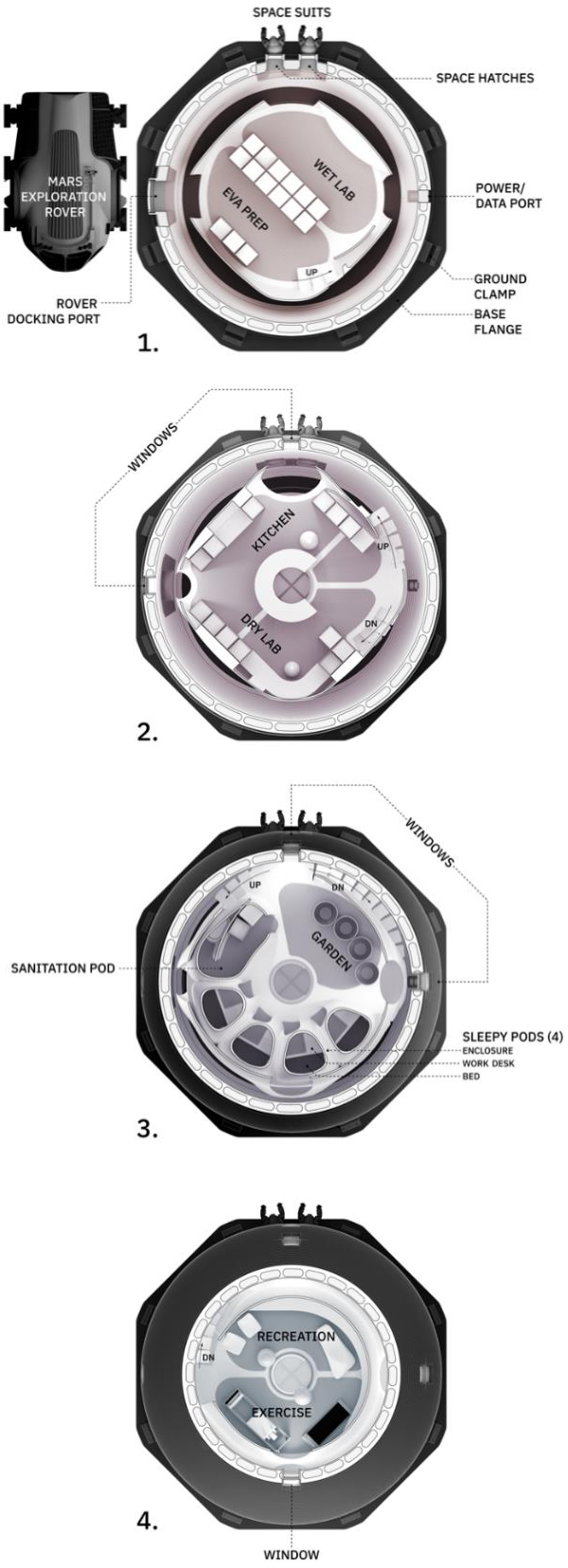

Figure 92. Marsha's floor plan illustrations (AISpaceFactory, 2018).

Each level contains at least one window that encompasses the entire 360-degree panorama. The enormous water-filled skylight and intermittent windows flood the inside with indirect natural light while protecting the crew from hazardous solar and cosmic radiation. Circadian lighting is used to optimize crew health (AISpaceFactory, 2018). It is designed to replicate Earthly light.

Development of a Novel Material and Additive Construction of Habitat

A substance created by the AI SpaceFactory known as "Mars polymer," made of compounds contained on the planet, is used to build a simplified model of MARSHA, as seen in Figure 93. (Reilly, 2020). Designers developed a novel blend of basalt fiber from Martian rock, and renewable bioplastic (polylactic acid, or PLA) manufactured from Mars-grown plants.

Basalt fibers are renowned for their exceptional tensile strength. It is equivalent to carbon fiber and kevlar but is significantly easier to manufacture. Plastics are efficient barriers against ionizing cosmic radiation due to their low atomic weight. Because PLA is a bioplastic, its emissions are benign, unlike petrochemical plastics, which emit high levels of harmful microparticles such as styrene. PLA is highly sought after due to its low conductivity, and basalt is one of the most effective insulators. They work in tandem to protect against the harsh outside environment.

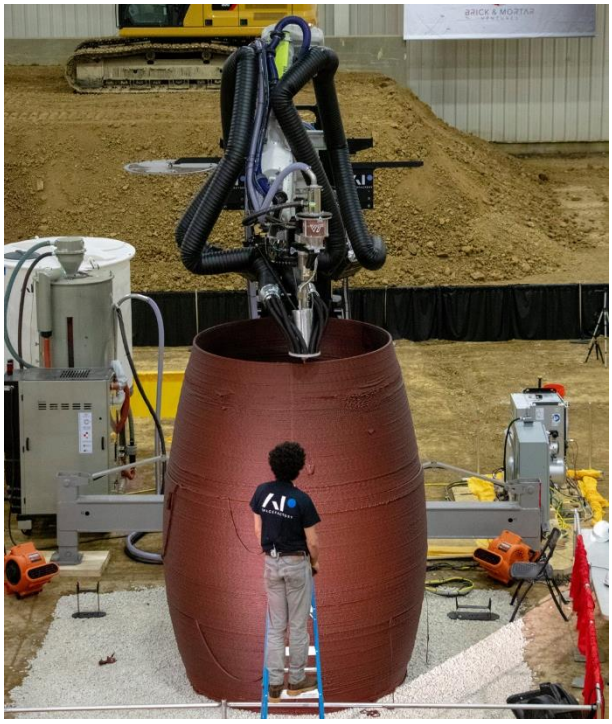

Figure 93. 3d-printing process of 1:3 scaled Marsha prototype (Reilly, 2020).

After material tests at NASA were completed, a 1:3 scale habitation prototype was conducted with an additive manufacturing process. According to ASTM testing, this space-grade material is two to three times stronger than concrete in compression and five times more durable in freeze-thaw temperatures. Figure 94 shows a 3d-printed façade opening mock-up to implement developed novel material (Reilly, 2020). NASA's strength, durability, and crush tests revealed that this recyclable polymer composite surpassed concrete.

Figure 94. Material and façade opening mock-up (Reilly, 2020).

Thermal Comfort Considerations

MARSHA uses a novel dual-shell design, as shown in Figure 95, to protect the habitable zones from the structural strains caused by Mars' high-temperature changes (AI Space Factory, 2022). The dual shell liberates the interior environment from the constraints imposed on the outside shell, which keeps its simple and functional design. The zone between the two shells serves as a light well and a stair location that ascend in a gentle spiral.

Figure 95. Marsha's dual shell three-dimensional model (AISpaceFactory, 2018)

Marsha to Tera

With inspiration from MARSHA, AI SpaceFactory built TERA in Upstate New York with views of the Hudson River as seen in Figure 96, a futuristic Earth-based residence that provides insight into our future living on Mars terrestrial counterpart to this building style. It is constructed entirely of recycled, biodegradable materials that can be composted into the soil at the end of their useful life. Marsha is designed to be printed using sustainably sourced materials: a basalt and biopolymer mix derived from crops such as corn or sugarcane.

Figure 96. TERA on-site in New York.

AI SpaceFactory states that the developed substance is 50% stronger than concrete yet compostable. Tera's objective is to demonstrate how sustainable building principles may be applied to make construction more environmentally friendly on Earth without relying on non-recyclable materials.

5.2.4. Penn State Mars Habitation

In NASA's 3D Printed Habitat Centennial Challenge, Phase 3's On-site Construction Competition, a team led by researchers from The Pennsylvania State University (PSU) placed second place with a 1:3 scale prototype of a habitation they had developed and built. Keunhyoung Park, a member of the PSU team, published his Master's thesis in 2020 and several research articles, detailing the proposed habitation with its Finite Element Analysis (FEA) simulations (Park, 2020).

Design Decisions

The design of the 3D-printed Mars habitation is impacted by the requirements of the three essential criteria (Park et al., 2020). The habitat's structural strength must first and foremost be sufficient to withstand the extreme Mars environment. The second criterion for a space habitat is sufficient space and spatial programming for four astronauts to conduct a one-year research project. The habitat must also provide adequate shielding from the space radiation that reaches the surface of Mars.

Programming and Functional Organization

The final design of modular architecture of the habitat, as shown in Figure 97, is intended to maximize the crew's chances of survival and the success of the space exploration mission (Park, 2020). As needed, the habitat can be enlarged by connecting more modules with its own space. The radius of all three modules is 7.3 meters, making the total living space 93.61 square meters (Park, 2020). The walls inside the habitat are 2.13 meters high, and the overall construction, from the ground to the rooftop, is 11.2 meters high (Park, 2020).

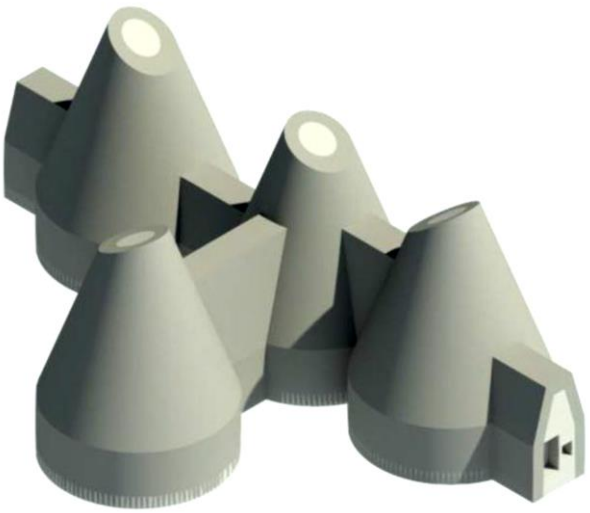

Figure 97. The PSU team's final habitat design Park et al., 2020.

The PSU team developed alternative spatial plans, as shown in Figure 98, for the required minimum size, which incorporates areas for private living, laboratory work, and leisure activities (Park, 2020). The proposal on the left for the habitat's base adopts a spatial program to minimize its footprint to the greatest extent (Park, 2020). The spatial program layout on the right maximizes scalability and spatial functionality by grid-connecting modules (Park, 2020). The roof's conical shape offers additional space for the ECLSS (Environmental Control and Life Support System) to be installed (Park, 2020).

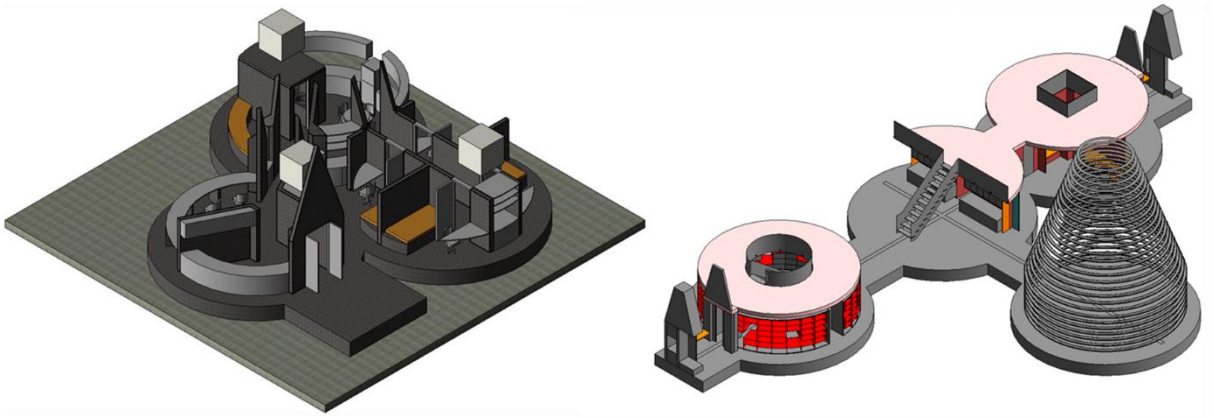

Figure 98. The alternate spatial designs proposed by the PSU team (Park, 2020).

However, the closeness of the units reduces their interdependence. In addition, by joining the units in a grid pattern, it is simple to increase habitat sizes. As a result, the habitat may accommodate expansion by easily integrating new modules. The team selected the Mars habitation proposal on the right side of Figure 98 as the optimum final design for the Virtual Construction (BIM) Level 2 of NASA's 3D-printed Habitat Centennial Challenge.

Structural Design Conditions

Compared to Earth, the environmental condition on Mars' surface are considerably more severe. The FEA analysis of the habitation proposal under Mars conditions requires considering the main loading factors that directly affect the habitat area's structural framework, as shown in Table 19 and Table 20, which are the gravity load, atmospheric pressure, internal air pressure, and temperature variation. The thermal load analyses will be implemented for three conditions: maximum, lowest, and average outside of the habitat because of the sunlight variations. Data given in the tables are extracted from the research study by Park et al. about the structural analysis of the designed Martian habitat (Park et al., 2020).

Table 19. Environmental loads at the Mars surface and the interior of the habitation (Park et al., 2020).

Loading Case	Mars Surface	Interior of the habitat
Gravity Acceleration	3.721 m/s^2 (146.496 in/s^2)	
Air Pressure	0.6 kPa (6.0 mbar; 0.087 psi)	52.67 kPa (526 mbar; 7.639 psi)

The habitat must create a balanced atmosphere for astronauts to explore without wearing extra life maintenance equipment. The gravitational effect on the Mars surface is less than expected since the acceleration of gravity on the Mars surface is much less than it is on the Earth (38% of Earth's gravity).

On the other hand, after the habitat's interior is pressurized to Earth's atmospheric level to ensure a comfortable atmosphere for astronauts within the habitat, the external air pressure on Mars'

surface (0.6 percent of Earth's atmospheric pressure) becomes a vital consideration to analyze. Simultaneously, thermal expansion is estimated to trigger a significant stress concentration due to changing Mars surface temperatures. According to NASA's standard for human-crewed missions, it is possible to safely decrease internal pressure to values lower than those experienced on Earth, with minimum pressures of 1150 psf (55.06 kPa) and 1100 psf (52.67 kPa) proposed for regular activities on the Moon and Mars, respectively.

In addition to gravity and internal air pressure, one of the critical load factors for the habitat architecture on Mars is the significant difference in air temperature on the Martian surface, as seen in Table 20. The thickness of the habitat's wall, which is needed to provide sufficient protection against space radiation, may result in sizeable thermal expansion stresses. Temperature loads will be simulated in three scenarios: average, lowest, and highest temperature differences from interior temperature.

Table 20. Environmental loads at the Mars surface and the interior of the habitation (Park et al., 2020).

Loading Case	Mars Surface	Interior of the habitat	Temperature Difference (Δ)
High Temperature (Viking 1 lander site)	-31°C (242K; -24°F)		56°C (56K; 101°F)
Low Temperature (Viking 1 lander site)	-89°C (184K; -128°F)		114°C (114K; 205°F)
Highest Temperature (Equator)	20°C (293K; 68°F)	25°C (298K; 77°F)	5°C (5K; 9°F)
Lowest Temperature (South pole)	-153°C (120K; -243°F)		178°C (178K; 320°F)
Average Temperature	-63°C (210K; -82°F)		88°C (88K; 158°F)

Material and Construction System

The team's research into the material properties and the capabilities of the printing process guided the design of the habitation. The designers were able to rapidly explore several design options thanks to the parametric design model that encoded predefined constraints.

Motivated to practice eco-friendliness, the research team experimented with numerous concrete formulas consisting of components from Mars (M. Roman et al., 2020). They considered building sulfur concrete with basalt aggregates, which would not require water, and magnesium oxide mixtures, which harden very quickly, but ultimately decided to create MarsCreteTM, a dry geopolymer binder formed of minerals already found on Mars and Earth (M. Roman et al., 2020). Marscrete consists of indigenous minerals including basalt, which is crushed and used as aggregate; kaolinite, which is used to obtain metakaolin, which is used as a binder; and sodium and silicon compounds, which are used as agents to activate metakaolin with water obtained from ice on Mars.

The team envisioned a team of robots capable of harvesting, sorting, blending, and storing the necessary elements and the final dry mix to create dwellings with 100 percent automation under the harsh circumstances of Mars. Since only a small amount of water was required to be added to the created mixture to print, that water could have been derived from Martian ice.

The team's technique for transitioning between concrete and borate glass provides natural light and views of the exterior while ensuring a very secure interior. The team's engineered geopolymer concerete and borate glass are two examples of graded composite materials designed to prevent a seamless, impermeable transition between opaque and transparent surfaces. The composite material is lightweight, thermally insulating, resistant to chemicals, freezing, and fire, impermeable, and shielding against cosmic radiation.

Radiation Shielding

For the radiation shielding purpose, The Penn State research team intended to use functionally graded materials created by gradually replacing sand with lightweight aggregates such as cork grains, which are utilized in the heat shielding of spacecraft. Utilizing functionally graded materials selectively allows designers to improve the structural, optical, and thermal performance of the habitat. The percentage of cork gradient increases toward the exterior wall surface, providing a protective barrier that will shield the habitat from cosmic radiation and cold temperatures. (M. Roman et al., 2020).

The team determined that the outer wall of the full-scale habitat must be at least 600 mm thick to provide an appropriate safety factor in radiation protection, given the maximum radiation exposure permitted by the nuclear power generation facility's safety regulations (Park, 2020).

The Structural Analysis of Full-scale Habitation

Park (2020) conducted finite element analysis for each structural force case separately using Autodesk Nastran integrated into Inventor 2019. According to the results of the FEA analysis for the full-scale Mars habitat design, the anticipated loading conditions significantly impact the Mars habitat's structural capabilities. The following load scenarios have been considered: 1) the gravity of Mars, 2) the air pressure resulting from Mars' low atmosphere density, and 3) the temperature load resulting from the difference in temperature between the interior of the habitat and the surface of Mars. The Air pressure load case suggests that the connection components between modules require additional restraining devices to reduce the printed envelope's weight. The temperature load case necessitates the installation of insulation inside the habitat. Although the gravity and air pressure load independently produced strains that could be tolerated, the low temperature on the surface of Mars would be crucial to the structural integrity of the habitat. The low and average temperatures resulted

in severe stress concentrations on the habitat's surface foundation. For specific information on the impacts of each case, we suggest researchers look into the thesis study of Park (2020).

Additive Construction of Habitat

The Penn State team was qualified for Phase 3's on-site construction level of the competition after the successful completion of the virtual design and construction phases of NASA's 3D Printed Habitat Centennial Challenge. The aim of this level was to construct a 1:3 sub-scale habitation with additive manufacturing techniques. The team proposed an alternative design solution for Earth's inhabitants, which was successfully printed, as shown in Figure 99 (Mueller et al., 2019). For autonomous deployment, Penn State University utilized two robots in conjunction (Mueller et al., 2019). In this operational proposal, one robot was used to build the structure with cementitious materials, while another was employed to position the components (Mueller et al., 2019). The construction process is required a high level of proficiency and cooperation between the two robots. In future NASA space missions, teams of robots ("cobots") may work alongside humans to construct infrastructure and habitats (Mueller et al., 2019).

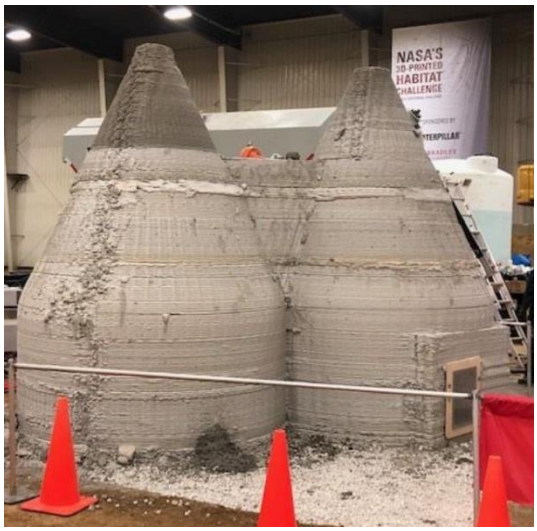

Figure 99. The printed alternative habitat proposal of PSU for Earth's inhabitants (Mueller et al., 2019).

5.3.Technical Assessment of 3D-Printed Mars Habitat Proposals

To assess their technical particulars, we have outlined the winners of the design competition (Mars Ice House), the virtual construction competition (Mars X-House V2), and the winners and runners-up of the on-site construction competition (Marsha and Penn State Mars Habitation, respectively). The evaluation is based on four technical factors that could hinder the viability of the habitations.

• The system for construction and/or printing. Which technological objects or methods are used to build or print habitats?

• The type of building materials. Which resources are utilized in the construction of the habitats, and are they imported from Earth or discovered in situ? Does a connection exist between material and site selection?

• The implemented design decisions against Mars' extreme environment. How is the conceptual design of the habitat handled? What decisions have been made for radiation, extreme temperature fluctuations, gravity, and low air pressure?

• The plan layouts and circulation systems. How is the space within the habitat employed, and what activities does the design permit?

The assessment parameters are derived from previous study sections and will serve as the basis for a comparative analysis of the four design options.

5.3.1. Construction systems assessment

The Mars Ice House has been meticulously designed and constructed to function independently. It would be easy for an automaton system like a robot to assemble a habitat if it could climb up to different levels. Mars Ice House has presented a process of deployment and construction that includes a fictional Mars descent vehicle, a deployable membrane, and semi-autonomous robotic printers for harvesting and depositing subsurface water. Even though the proposed system would be completely independent of Earth, the technology required to implement the construction plan is extremely advanced, and the question of how to repair or maintain the system in the case of a failure remains unanswered.

The Mars X-House V2 required a mobile 3D printer and movable platform due to the limitations of the Hercules lander and the current level of construction technology at Apis Cor. The printer's clever telescoping base makes it easy to set up in any location. Feeding the print head is accomplished with the help of a six-axis robotic arm mounted on a boom-arm system. When fully extended, the mobile telescopic platform can accommodate not one but two mobile printers, which can then be used concurrently in various stages of the printing procedure. The suggested system meets the requirements of the Hercules lander's circular cargo port, which has a maximum diameter of 6 meters and a load capacity of 20 tons. In the design system of Mars X-House V2, integrating a regolith shell with a hyperboloid continuous basalt-fiber reinforcing system is proposed as a solution to the structural integrity problem. As a result of the system's tremendous complexity, the autonomous construction process for a Martian habitation in its harsh environment is becoming increasingly complex.

The Marsha project of AI SpaceFactory proposed several creative solutions for Mars exploration. The Marsha habitation is more cost-effective, environmentally friendly, and secure than other suggested construction systems. Constructing it on Mars with readily available resources and recent technologies is feasible. A tall, cylindrical, four-story habitat was proposed to reduce the need for extensive foundation work and uplift loads by permitting the layering of mission activities. In addition, keeping the 3D-printer stationery and constructing vertically rather than moving about to complete horizontal operations is easier on the equipment. After the construction of Marsha habitation in a 1:3 scaled version, AI SpaceFactory realized it had created technology that could be immediately applied to the building sector on Earth by addressing off-grid power, autonomous

construction, and in situ resource exploitation for Mars. Their 2020 TERA project, which featured recycled components from the final MARSHA print, shows how these ideas might improve our world. AI SpaceFactory's 3D-printed habitat for Earth is likewise autonomously constructed; it is called Tera, designed to reduce environmental damage. A basic construction system is suggested by the designers of Marsha, thanks to their design decisions.

Penn State assembled a multidisciplinary team of professionals from architecture, mechanical, agricultural, civil, and environmental engineering, among others. They conceived a framework for automated, autonomous additive construction; they devised and engineered their materials and printing equipment and planned the deployment logistics. The study strategy at Penn State involved modeling and coordinating the intricate interplay between several interconnected factors, such as material qualities, printing method, and design. This model was encoded using building information modeling (BIM) technology and artificial intelligence (AI) techniques, which were also employed in the simultaneous design of the habitat's operation logistics, printing system and setup, toolpath and printing process, and design. Simple cylinder structures were chosen as the basic unit to withstand the pressure of air being forced outward and spread against the inside walls of the Mars habitation. The habitat is enclosed by a series of cylindrical buildings that decrease to a conical dome at the top. In the third and final phase, the team could print an entire structure without using structural supports or prefabricated elements, including the roof. This success proved that the technology could function reliably in extreme environments on Earth and beyond.

5.3.2. In-situ material assessment

Depending on the characteristics of the project, the proportion of a project's utilization of indigenous resources may vary considerably. While concepts such as the Mars Ice House and Marsha make substantial use of Mars' fundamental materials in the architecture of the habitat, others, such as the Penn State proposal and Mars X-House V2, rely on more complex material compositions. If a habitat depends on imported components that are not produced locally, its expansion may be limited. The same holds for robots, rovers, and construction materials. If the habitat construction attempt is unsuccessful, there is a potential that the mission will be canceled.

Nevertheless, if the autonomous robots are only permitted to use locally sourced materials, they could construct a new habitat if the previous one were destroyed, as long as the resources were easily accessible and the robots had a sufficient power source. To reduce costs, as little of the habitat and infrastructure as possible must be transported from Earth. In addition, the design should maximize the utilization of existing local resources and reduce the number of materials transported from Earth.

The Mars Ice House uses subsurface ice to build a permanent H_2O 3D-printed habitation instead of Martian regolith due to the water availability on Mars at both high and low latitudes. Sites

had to meet specific requirements, including being below freezing for at least part of the Martian year and having easy access from the surface to a shallow ice table. If astronauts are to use the habitat to study the ecology of Mars, their studies will either be restricted to this region or need extensive travel. The habitat design is inapplicable to parts of Mars with greater temperatures because the site must remain below freezing throughout the year; exploring other regions would necessitate using a different building material. If there is more water scarcity than anticipated, the technological solution of using water to construct the habitat could lead to psychological and cultural problems. When establishing a habitat, it is crucial to remember that if surrounding water is drained, the expansion of the habitat may be slowed if additional habitats are constructed far away from the original one because they require water. If the transition between habitats is inconvenient, ecosystems could become isolated. As the habitat is a single structure, psychological difficulties such as overpopulation may make it difficult for astronauts to find privacy.

In order to maintain the system's stability, the site selection of Mars X-House V2 is based on habitability and operational circumstances, and the chosen region is favorable to further settlement. Regolith is chosen as the primary in-situ construction material for the habitat, and basalt, one of the most abundant rocks on the Martian surface, is chosen as a reinforcement material. These substances resist fire, low and high temperatures, and radiation. In addition to shell materials, it is recommended that HDPE be used to divide the internal and outside surfaces of habitation to reduce the harmful effects of regolith and basalt. In addition, it is hypothesized that HDPE will be made using indigenous resources on the surface of Mars. Although material selection tackles many of the risks and challenges of constructing a Martian settlement, reliance on several materials while living in extreme environments may become crucial for the system's expansion and maintenance.

The in-situ resource utilization (ISRU) method of harvesting and 3D printing with materials derived directly from the surface of Mars is key to the AI SpaceFactory's proposed construction strategy for Marsha. As a solution to the problem of making do with local materials, the team came up with a biopolymer (PLA material cultivable on Mars) and basalt (mined from Mars rock) fiber matrix instead of concrete (since water is a limited resource for oxygen and fuel, and would sublimate in the thin, freezing environment during curing). The completion of the building phase verified this choice. Precision, cleanliness, novel use of Martian resources, and a high degree of independence were all hallmarks of the team's printing efforts using biopolymer. The material displayed exceptional compressive and tensile strengths, which bodes well for its potential use in earth-based projects. This one-of-a-kind fiber shields from radiation and has remarkable tensile strength, while recyclable PLA provides structural stability and low conductivity.

The PSU research team was motivated to test sustainable procedures by testing with numerous concrete formulas made from Mars-based materials. They projected a group of robots to

be in charge of harvesting, sorting, blending, and storing the essential components and the final dry combination in order to construct fully automated habitations in the harsh circumstances of Mars. Water for the manufacturing process might have been derived from Martian ice if only a limited quantity had been added to the mixture. They also anticipated using recycled lightweight aggregates with insulating properties to generate functionally-graded concrete, which might screen the interior from cosmic radiation and low temperatures while enhancing the structural performance of the design. The team's mixing concrete with borate glass boosts the building's protection and transparency to the outside environment. The material design approach of the PSU team suggested the use and investigation of any in-situ material types for the desired solution.

5.3.3. Environmental design assessment

Thermally and atmospherically stable conditions must be maintained on Mars to ensure the life of its inhabitants. The structure must be capable of withstanding the significant seasonal and sol-related temperature changes on Mars without exhibiting any symptoms of stress. The habitat must be able to shield humans from specific forms of radiation, as neither moving the habitat further away from the radiation source nor decreasing the duration of exposure is possible without stopping the mission.

Even though radiation is not a problem for the Mars Ice House due to the use of ice as an in-situ material, the environmental integration still heavily depends on Earth-provided technologies. The outer air isolation system of the Mars Ice House requires an Earth-supplied strengthened pressure membrane. In reality, stress models reveal that the membrane can absorb the entire force, allowing the ice to bear only the force of gravity. The architecture of the Mars Ice House may endure gravity forces during the deposition process and its weight, according to a finite element analysis. However, the system is not tested for extreme temperature fluctuations.

The form of Mars X-House V2 is revealed by comparing its conceptual form to the morphologies of pressure vessels. Nevertheless, the lower and upper habitation levels may decrease internal pressure and weaken the structure. The structural analysis systems were not conducted under the high-temperature changes of Mars' surface, which would have resulted in enormous loads on the habitat shell. Utilizing an overhang or colonnade to shield against high-angle radiation is a typical practice. The designers of the Mars X-House V2 used the wall thickness to construct passive radiation "overhangs" at each window to protect the windows from solar radiation with an angle of at least 30 degrees. In addition, Mars X-House employs additional shielding in the rooms where the crew spends the most time daily, based on their routine. Integrating the Mars X-House V2's material and structural systems is crucial for environmental integration.

The vertical egg-shaped Marsha project is designed to withstand internal air pressure and structural forces. AI SpaceFactory has also developed novel approaches to ensuring the vertical structure can withstand Mars temperatures. The dual-shell design in Marsha keeps the inside from expanding and shrinking due to the wide range of temperatures on Mars, and the inside feels open and airy, just like a house on Earth.

The Penn State research team proposed using FEA analysis of habitat structure under Mars's environmental circumstances, which directly affect the habitation's structural framework. The FEA was performed with the forces of gravity, external air pressure, internal air pressure, and temperature fluctuations. The Penn State study group also found that the maximum radiation exposure allowed by the safety rules of the nuclear power generation facility necessitated an exterior wall of the full-scale habitat to be at least 600 mm thick to offer a sufficient safety factor in radiation protection. The adopted design technique enabled high environmental integration with Mars' harsh conditions.

5.3.4. Human factor assessment

The primary purpose of a Martian habitat is to offer shelter that protects and sustains a high quality of life for its residents while also facilitating the astronauts' work, relaxation, and general activities.

Water has a dual purpose in the creation of the Mars Ice House. First, it acts as a radiation shield by blocking the transmission of shorter-wavelength radiation light in the visible ranges while allowing longer-wavelength light to enter; second, it improves the mental health of humans by establishing a connection between indoor spaces and natural light and outdoor views. It lets natural light enter the habitat's interior, creating a clear vertical habitat with maximum visibility on the surface. The interior design of Mars Ice House separates the space into distinct areas for various functions. However, these areas are relatively modest compared to the habitat as a whole. The central area, intended to imitate a garden, is largely deserted, particularly at the building's top, where none of these activities occur. There is a pressurized region between the domes where the temperature is suitable for human movement without an EVA suit.

In comparison to other Mars habitation proposals, the detailed level of life support and operation systems for Mars X-House V2 is remarkable. Each floor's horizontal and vertical function separations are well-studied for various circumstances, including emergencies. The most notable architectural decision is using two stairways to separate the inside and external circulation paths. The other human-centric design decision is the vertically oriented hydroponic greenhouse incorporated inside the MEP walls along the central stairway. Although two distinct circulation routes give access and exit flexibility for operational and emergency scenarios, they often restrict the facade surfaces of rooms, which may increase the psychological impact of a confined space.

Moreover, with thickness variation in the shell and overhangs on the facade, the impact of radiation is diminished. Thicker shielding is utilized in parts of the habitat where the crew is projected to spend the most time based on their daily schedule. The overhangs on the facade are positioned at each window, effectively shielding each opening from rays with an angle greater than 30 degrees. Radiation mitigation techniques are advantageous for the crew's physical and mental well-being.

Each of the four floors of Marsha's working spaces has its distinctive internal atmosphere that encourages movement and minimizes monotony. Under a vast skylight, the top floor of the Marsha structure is a recreation and fitness center for the community. Thanks to the skylight that illuminates the entire building, including the basement, the crew can operate as efficiently as they would at home. The area between the two shells serves as a light hole, allowing all floors to be softly illuminated by natural light from the massive skylight on the roof and the occasional windows. At least one window per level captures the whole 360-degree panorama.

Compared to previous projects, the PSU research team's planned habitat demonstrates a significant lack of human factor design and planning. They argue that to maximize the crew's chances of survival and the overall success of the space exploration mission, the team decided on a habitat with a simple modular shape. To expand the size of the established habitat, more modules, each with its function, can be attached. The PSU group developed floor plans that meet the minimum size requirements and provide adequate living, working, and recreational spaces.

5.3.5. Conclusion of assessment for a space-resilient habitation

In the sixth chapter, the critical argumentation and contents of this thesis study to explain a novel design methodology are based on the following design requirements, which have been identified and examined based on case studies and their assessments:

The first design requirement for a space-resilient Mars habitation is to choose a construction site with maximum sunlight duration, optimum average temperatures, and minimal temperature fluctuations. Several criteria, such as the proximity of subsurface ice and the availability of various construction materials, must be considered while making this selection.

The second design requirement is to select an in-situ material with low reliance on Earth. All of the Martian habitats presented suggest the utilization of local resources. As a result, using in-situ materials such as regolith or ice to build a habitation for a crewed mission on Mars is the most advantageous option. However, relying too heavily on ice can lead to mission failure. The selected substance could be collected from Martian soil independently of the landing site and resist harsh conditions. Martian regolith has been studied as a building material using binder-based and direct-sintering methods. Regolith is the primary ingredient capable of achieving mechanical strengths comparable to conventional concrete.

The utilization of additive printing technology to allow construction automation without human intervention is the third design requirement for a space-resilient Mars habitation. Marsha's design exemplifies a straightforward and practical method of combining design with additive manufacturing. The vertical orientation of the habitation functions limits the area where the 3D printer can travel throughout the construction process and reduces weak connection points between inhabited areas by bringing them all into the same habitable volume. Furthermore, to make the living system more durable and dependable, the 3D printing process should use as few materials from the area as possible.

The fourth design requirement is to develop a radiation shielding method to safeguard the internal environment of habitation. While Mars Ice House recommends an ice shell as a barrier and Mars X-House V2 recommends a regolith shell with wall thickness variations as a design strategy, Marsha recommends a dual shell with a basalt shell for the exterior and a PLA shell for the interior to create a separation between the interior and exterior interactions of habitation. On the other hand, the PSU team calculates a safety factor in radiation protection based on material characteristics and defines wall thickness based on the determined result. The PSU team's methodology is adaptable to any material with varying wall thicknesses.

The fifth design requirement is to use pressure-vessel geometry and concepts to create a volume responsive to low air pressure. All suggested design solutions adhere to the same conceptual approach to consider the pressure difference between the inside and exterior. Except for the Penn State Mars Habitation, the functional activities of the other three habitations are divided into multiple floors and oriented vertically to form a single volume, suggesting pressurization of the various floors within the same volume. Even if technological advances allow the critical problem to be solved in an atmosphere-free environment, developing a pressure vessel or inflatable-like shape for Mars habitation is scientifically required. The vertical design of circulation space within the same volume is crucial for resolving the problem with the least amount of resources.

Establishing functional activity configurations based on human factor considerations is the sixth requirement for a space-resilient habitation design. Each habitation plan suggests a comparable strategy for resolving functional interactions in layout considerations, except for the Penn State Mars Habitation. They aimed to reduce the total footprint while meeting many functional needs on the same floor. With limited space, multi-functional spaces must be constructed with sufficient quality to accommodate most common functional areas, such as dining, recreational, and exercise areas; work areas; a library; multi-potential lab; and sample storage areas; as well as a central communication area. In addition to resolving space limitations, the design solutions also addressed communication and privacy concerns to ensure the crew's well-being. In multi-story homes, functional needs are often

separated into zones emphasizing the separation of work, living, and recreation areas to make the habitation floor area as efficient as possible.

The seventh design requirement is to develop a habitable volume by considering environmental influences. Compared to Mars X-House V2 and Marsha, the Mars Ice House's design approach considers gravity forces and material self-weight. On the other hand, Mars X-House V2 and Marsha consider the air pressure of the Mars environment, as well as gravity and material qualities. Through material selection and design approaches, these three habitation designs solve the radiation issue. In contrast, the PSU Mars Habitation designer team created novel construction materials based on local resources on Mars and defined gravity, air pressure, and temperature variations as structural forces based on data from the literature and NASA missions to simulate their proposal under these conditions. The PSU team's FEA simulation variables could be used in the design phase to construct an adaptive habitation for Mars' severe circumstances.

The eighth design requirement is to allow natural light and visual connection with the habitation surrounds through windows or skylights to reduce the consequences of isolation and confinement.

06th Chapter
A NOVEL HABITATION DESIGN METHODOLOGY

Chapter 6 establishes a novel habitation design methodology based on the integrated knowledge presented in the third, fourth, and fifth chapters, with the intention of addressing all of the specified assessment findings and design principles. The chapter concludes with a description of the suggested iterative habitation design approach and literature-derived design tools.

Designing safe and space-resilient structures appears to be a novel challenge that requires extensive study and effort due to Mars' severe and hostile environmental conditions. Without developing or proposing a novel material, this research's main objective is establishing a space-resilient habitation design methodology.

In the third chapter, the environmental variables of Mars have been investigated, and a report on their impacts has been formulated in order to provide feasible methodological solutions for sustaining the crew's physical health despite the planet's severe conditions. The fourth chapter presents a review and assessment of habitability research via analog habitat missions to examine their habitability approaches using data science methods. The chapter gives a design guideline for functional configurations of a Mars habitat to maintain the psychological health of the crew's habitability. In the fifth chapter, the winners of NASA's 3D-Printed Habitat Centennial Challenge are reviewed and analyzed to assess their design approaches and identify standard design requirements for space-resilient habitation.

The synthesis of the preceding chapters' findings demonstrates that a habitation system that considers environmental and human factors and meets the previously described design requirements is necessary to protect the crews of future Mars missions. In addition, the automation of the design and construction process in harsh and changing conditions with a communication latency of up to 24 minutes remains a concern. In order to accomplish design automation and provide solutions to the issues outlined above, this chapter proposes incorporating machine learning into the generative design process. After the foundation of background knowledge, a novel machine learning-aided design methodology for Mars habitation will be explained step by step to frame a systematic solution for each phase of the design problem.

Pre-integrated Earth systems and technology can facilitate robotic development and construction in these extraterrestrial settlements. Due to transportation costs, In-situ resource utilization (ISRU) is crucial to constructing habitats, as it is impractical to construct a surface habitat with a system based on Earth. ISRU develops habitat-related materials, technology, and resources to reduce payload. In-space manufacturing, additive manufacturing, and robotic assembly may be utilized in developing ISRU habitats. More than a decade has been devoted to studying large-scale additive manufacturing using cementitious 3D printing under micro- and reduced-gravity environments.

In addition to research for the technical advancement of construction systems, the Space Technology Mission Directorate (STMD) of NASA has performed multiple initiatives since 2005 "to generate innovative solutions" for space innovation issues. NASA initiated the 3D-Printed Habitat Challenge in 2014, tasked with designing an autonomous Mars habitation system by academic and industrial teams. The competition consisted of three separate sessions. In the first session, participants concentrated on the design of 3D-printed habitations. The second phase focuses on developing local, sustainable materials and cutting-edge technology for their application. The third phase comprised both virtual and physical construction contests. Participants utilized BIM tools for a virtual construction competition to generate full-scale architectural models and submit material, design, and construction data. After studying the winning designs for NASA's 3D-Printed Habitat Challenge in the fifth chapter, it is clear that integrating automation into Mars habitation's design and construction processes is crucial.

This dissertation is not concerned with the simulation of an additive manufacturing process; however, it is anticipated that the implementation of an additive construction technique will involve generative design methodologies and design automation tools, which will contribute to the autonomy of the construction process. This chapter examines the background of generative design techniques and the design strategies implemented using generative design tools to illustrate their applications in the architectural design process. Following that, a brief description of previously implemented SNA and LPA techniques is provided, along with the Python syntax that enables the user to implement these methodologies throughout the early phases of a habitation's design.

The chapter concludes with a comprehensive explanation of the unique approach suggested, which is formed by integrating generative design methodologies with the described SNA and LPA methods. In conclusion, the following chapter will present a methodology for autonomous habitation design for further implementation.

6.1. An Overview Of Generative Design Methodologies

Design is a complex problem-solving process that systematizes design restrictions and requirements as a set of constraints and analyzes potential solutions to meet those constraints. However, design solutions created by conventional modeling methods rarely meet such constraints, especially when examining the spectrum of viable design solutions to boost the quality of components and meet the challenges provided by continually altering design parameters. In this context, the Generative Design Approach (GDA) is considered an efficient method for exploring a wide variety of potential design outputs by recasting the design problem as a configuration problem. GDA's foundation consists of a design framework and a library of design elements used to discover and store all pertinent data. Therefore, iterative design methodologies make it easy to explore the design space by configuring variable design elements in different ways.

Moreover, the finalized model is a design solution and concept that designers may modify to test alternative, unanticipated solutions. In addition, GDA paves the way for additive manufacturing by providing more sophisticated design possibilities. Traditional computer-aided design (CAD) restricts us from working with known geometry and encourages reusing previously created models, resulting in reliable but suboptimal outcomes. By introducing generative systems and optimization tools for specific targets, generative design methodologies offer to bridge the gap between additive manufacturing and the design process. This section presents an overview of primary generative design methodologies to explain the foundation upon which generative design methodologies are used in the habitation design process.

Stiny and Gips defined an algorithm as an explicit statement of a sequence of operations needed to perform some task (Stiny & Gips, 1978). Generative design is a process through which algorithms can determine various potential design solutions. Generative Systems are briefly characterized: Algorithmic systems, the basic system in all Generative Systems; Parametric systems, a particular case of algorithmic systems; and then more specialized versions, such as Shape Grammars; L-systems; Cellular Automata; Genetic Algorithms; and Swarm Intelligence

6.1.1. Algorithmic systems

All Generative Systems begin with algorithmic systems. Algorithms are sequences of instructions for solving a problem or attaining a goal that must be stated step by step or in discrete steps and written in a fixed vocabulary (Berlinski, 2001). Algorithms are sometimes called procedures, processes, and techniques, which refer to a collection of instructions for solving a problem. Algorithms may take on various forms, including code, graphics, and verbal descriptions. Algorithms are limited to discrete units in computers, such as numbers, alphabets, or geometric elements. Algorithms are critical

to how computers process information, as a computer program is essentially an algorithm that instructs the machine on how to do specified actions.

By simplifying the implementation and calculation of algorithmic processes, computers popularized and broadened the concept of coding in architecture. Algorithmic design systems necessitate the expression of unambiguous design intents in defined phases and units. They involve data generation and interpretation components, and the data can take on various forms, including locations, shapes, and shape attributes. Associations, constraints, and rules all facilitate communication between components. Associations are relationships that enable a series of changes to be triggered simply by altering the value of variables. Constraints are required conditions. While the term "constraint" may imply something limiting, it can refer to anything the architects desire the model, or building, to do (Mark et al., 2008). Constraints help ensure that the model behaves in each way, but if it is over-constrained, it may remove possible solutions or impede the generation process. A rule is a set of conditions that, when met, cause an action to occur. Developing design rules requires designers to evaluate and unpack the relationships and dependencies inside a design problem to represent it using a set of clearly defined rules.

An algorithmic design method necessitates a rationalization process that compels designers to organize their thoughts around linkages and task sequences. Algorithmic systems are the most configurable and adaptable type of generative system. They make no demands on the form or nature of connections. These systems allow the architect to apply his or her algorithm (El-Khaldi, 2007).

6.1.2. Parametric systems

Parametric systems are a subset of algorithmic systems. Parametric design or parametric modeling is a broad term that describes design challenges using variables (Woodbury, 2010). In 1957, Patrick J. Hanratty produced PRONTO, the first commercial software including parametric algorithms for converting data from computers to industrial machines, and Ivan Sutherland created Sketchpad in 1963, demonstrating the first graphical depiction of parametric (Shukla & Deshmukh, 2016). In the 1980s, the parametric design was promoted, and now, many CAD software allows for establishing parametric connections and using variables. Instead of redrawing or editing their designs, parametric systems let them regenerate them. The parameters of a given design are defined in parametric systems, not the exact shape.

Parametric modeling is built on the relationships between the variables and the objects they regulate. Establishing relationships between design elements enables them to alter individually, defining an associative geometry. Alternative models can readily be developed by assigning different values to the variables. The "parametric systems" refers to hierarchical algorithmic systems governed by one-way interactions. Dependencies only operate in one direction, establishing linkages between

dependent and independent components to ensure changes are propagated from independent to dependent components. Commercially accessible parametric software defines a parametric model in two distinct ways. One possibility is to program the model in a textual programming language. As demonstrated by tools like Generative Components and Grasshopper, the other approach uses visual programming languages to create diagrams or graphs representing the algorithm to build the parametric model. These apps generally automate the procedure to a limited extent but sufficiently to enable efficient exploration of parametric variations of forms (Celani et al., 2011). One well-known implementation of a parametric system is the International Terminal at Waterloo Station in London, designed and built in 1993 by Nicholas Grimshaw and Partners. The structure is a long, curving train shed with a changeable span that increases progressively. Constraints on the location dictated its curve and varying span. Its roof structure comprises a sequence of arches with varying dimensions but identical configurations that follow the site's-imposed curve. To address these issues, they developed a parametric model that connected the span and curvature of individual arches and encoded the rules for the entire family of arches rather than modeling each arch individually (Szalapaj, 2001). The parametric model was expanded beyond the structural description of the arches to include the cladding elements that connect them, i.e., the entire structure (Kolarevik, 2003). The change was propagated throughout the model when a parameter's dimension was changed.

6.1.3. Shape grammars

Stiny and Gips invented Shape Grammars (SG) in 1972, laying the groundwork for research into algorithmic design methodologies for design analysis and synthesis (Alfaris, 2009). A shape grammar is a collection of shape rules applied sequentially to generate a collection, or language, of designs. Shape grammars are spatial algorithms rather than textual or symbolic (Knight, 2000). Each rule defines a shape and substitutes a different shape for it. Shape operations such as addition and subtraction and transformations such as mirroring, rotating, and scaling are used to build designs. A distinguishing feature of these grammars is that they are predicated on the promise of simulating the thought process of a designer via the concept of recognition (Alfaris, 2009).

Shape grammars are based on the concept of recognition, as they treat shapes as non-atomic entities that can be freely disassembled and recomposed (Knight, 2000). Any shape is termed a maximal element since it encompasses all potential more minor elements with the same topology. For instance, a rule that applies to a line segment, surface, or solid may apply to all embedded smaller line segments, surfaces, and solids inside the entire element. This capability enables the creation of new shapes or the capacity to identify shapes that are not expressly described in a language but emerge from any created shapes' components (Duarte, 2001).

The primary impediment is that SGs are based on visual computations, but computers can only perform symbolic computations. SGs, on the other hand, are a rigorous method for understanding and teaching architectural styles, as well as for assisting architects in formally expressing design intentions by compelling the designer to clarify ideas and hierarchically approach the design, with stages and design priorities expressed and formalized (Alfaris, 2009).

6.1.4. Lindenmayer Systems

Aristid Lindenmayer, a biologist, offered a mathematical theory of plant development in 1968 based on the core concept of string rewriting. The method can quickly simulate the growth of simpler plants (Prusinkiewicz et al., 1996). Lindenmayer Systems, or L-systems for short, are these types of systems. L-systems can be broken down into two processes: generating and interpretive. String rewriting is the primary concept underlying the generating process. Each character in an initial string is replaced with another character or sequence of characters according to the concurrent application of established rules. When replacing rules are applied, a new string is created and subjected to the same rules. Generally, this procedure is repeated for multiple generations. The interpretation procedure involves reading the symbols of one or more generations of strings and interpreting them as growth patterns or shapes. Strings can be seen in various ways, including a mapping or turtle interpretations. The mapping interpretation renders many generations of strings simultaneously using various mapping approaches. Symbols can be mapped to the vertices of a surface or the properties of an item, such as scaling, rotation, or position, resulting in various outcomes, including surfaces or individual objects (Hansmeyer, 2003).

Symbols can be enhanced with parameters whose values are used by the rules to determine their applicability and compute the new values for the parameters in the replacement symbols. These systems are referred to as Parametric L-systems, and they differ from basic L-systems in that the parameters can encode data during the interpretation phase. L-systems are vital for designers (Fasoulaki, 2008) because they can generate incredibly complex designs from extremely modest inputs (Hansmeyer, 2003).

6.1.5. Cellular Automata

Cellular Automata (CA) are generative systems that Von Neumann, one of the first scientists to investigate such a model in the late 1940s, summarized as self-reproducing systems. A cellular automaton is a collection of cells structured in orthogonal grids, each having a finite number of states expressed by colors or numbers. These cells update their states in discrete time units according to update rules applied to all cells in the grid. Each cell's update depends on its present state and the current state of its nearby cells. CA are sequential systems in which each cell's behavior is determined by the conduct of its neighbors (Alfaris, 2009). There are numerous possibilities regarding the grid on

which a cellular automaton is computed; for example, it could be a line, a square, or a triangle. Elementary CA is the simplest type of CA, as the "grid" is a line. This sort of cellular automata has a minimum of three cells required for the existence of a neighborhood, and each cell has two possible states, black or white, or 0 or 1, in numerical representation. As a result, the application of rules is entirely dependent on the state of the cell, the cell to its left, and the cell to its right.

Cellular automata can exhibit four distinct types of behavior, defined by the frequency of specific behaviors during a specified period: fixed point, periodic, chaotic, or random. After a brief time, a CA with fixed-point behavior reaches a fixed state. Periodic behavior exhibits a recurring pattern over a specific period. A Chaotic or Aperiodic system appears to repeat its activity over time, steps of varying durations. Random conduct does not appear to be repeatable (El-Khaldi, 2007). Its utility has been demonstrated in various fields, including mathematics, engineering, and behavioral sciences. In architecture, applying CA with chaotic and random behaviors is limited, as predicting the outcome is extremely difficult (Alfaris, 2009). However, most CA behavior is periodic, so they are utilized for pattern development (El-Khaldi, 2007). The architect Dimitris Gourdoukis's experimental work exemplifies the use of CA in architecture (GOURDOUKIS, 2016). He viewed the several generations of CA as segments of a single thing. The active cells' centers, denoted by black, were utilized to produce a Voronoi diagram, a type of Generative System. The Voronoi cell edges were the structural structure, while a smooth surface defined the enclosed region. The Voronoi diagram was developed to decompose space into sections composed entirely of convex polygons. Each polygon has a unique generating point, and each point within a polygon is closer to its generating point than any other (Fasoulaki, 2008). The Voronoi diagram's boundaries are defined as equidistant points from two generating points, while the vertices are defined as equidistant from three or more generating points.

6.1.6. Evolutionary systems and genetic algorithms

The model of nature is proposed as the generative factor for architectural form in evolutionary architecture (Frazer, 1995). The design is encoded in a collection of chromosomes subjected to reproduction, gene crossover, and mutation laws (Kolarevic, 2003a). The genetic algorithm (GA), a critical component of biological evolution, is the central notion of these evolutionary models. The numerous design parameters are recorded in a structure akin to a string, and their values are modified during the generative process, resulting in the generation of several similar forms, or "pseudo-organisms" (Kolarevic, 2003a). After applying evolutionary notions of selection and inheritance to the created forms, the best solutions from one generation are used to generate the next. The successful solutions' "genes" are crossed over to generate new solutions, and variations are introduced by mutating some of the new solutions' "genes." The selection procedure is established and is based on fitness functions. This principle is critical since it is through the selection that

advantageous characteristics are passed on to future generations. GAs can be utilized in architecture as both form-generating and optimization techniques. When optimization is utilized, the selection process prioritizes solutions that perform better according to specific criteria.

GAs are occasionally used in conjunction with other generative systems, such as L-systems and Cellular Automata, to use their capacity to represent growth. This type of implementation can be seen in a study by architect Marilena Skavara that investigates Cellular Automata and optimizes their output using genetic algorithms (Caldas & Rocha, 2001). Another application of GAs in architecture is the mass customization of prefabricated dwellings by Atelier Kolatan and Mac Donald (Caldas & Rocha, 2001). The models represent four hypotheses from a collection of digitally acquired models, all generated using the same genetic method. This project examines the serial and organic composite nature of architecture and the capacity of digital systems to generate heterogeneity over multiple iterations. GAs was utilized as optimization tools to optimize one of Alvaro Siza's School of Architecture in Oporto (Caldas & Rocha, 2001).

6.1.7. Agent-based modeling and swarm Intelligence

Agent-based models (ABMs) are frequently used to implement collective or social behaviors (Macy & Willer, 2002). Agents are autonomous software programs that act under their own beliefs. In a society, agents can act individually or engage and communicate with one another to compete or collaborate and achieve their goals collectively. A variation of ABM has been applied in design, for example, in the works of Kunz, Levitt, Jin and Maher, Smith, and Gero (Kunz et al., 1998; Maher et al., 2003).

Swarm Intelligence (SI) is a system's feature in which the aggregate behaviors of unsophisticated agents interact with their environment locally to induce the emergence of coherent functional global patterns (Bonabeau et al., 1999a). Typically, SI systems are composed of a population of simple agents interacting with one another and their environment locally. Nature, particularly biological systems, frequently serve as inspiration. SI establishes a foundation for investigating joint or distributed issue resolution in the absence of centralized control or the supply of a global model. Swarms are defined by Bonabeau, Dorigo, and Theraulaz in terms of self-organization and synergy (Bonabeau et al., 1999b). Structures emerge at the global level of a self-organizing system due to interactions between its lower-level components using local knowledge and without reference to the global pattern. The term "global pattern" refers to a system's emergent feature. Theraulaz and Bonabeau explain how a three-dimensional lattice swarm can be used to construct building forms (Theraulaz & Bonabeau, 1995). Feedback, randomness, and interactions all contribute to self-organization.

6.2. Design Strategies Via Intelligence Of Generative Design

Specific design goals necessitate the use of some Generative design methodologies over others. Because the quality of solutions tends to improve with each generation, Genetic Algorithms (GAs) have mainly been employed for optimization (Mitchell, 1997; Salge et al., 2008).

Shape grammars (SG) and L-systems (LS) are well adapted to generating emerging shapes and patterns from repeated operations on terminal shapes. Because it is challenging to visualize emergent shapes, developing SG and LS is an iterative process that frequently necessitates iterative experiments to discover the appropriate terminal shapes and production rules. The 'function-follows-form' philosophy is commonly followed by SG and LS, which means that once the form is formed, the emergent shape is evaluated for its functionality. SGs are commonly used to create 2D shapes and compositions, space layouts, and, in some circumstances, 3D compositions (Duarte, 2001; Halatsch et al., 2008; Koning & Eizenberg, 1981; Stiny & Gips, 1978). LS is commonly used to create fractals, repetitive patterns, and natural organic forms like plants and fractals (Alfonseca & Ortega, 2000; Lam & King, 2005; Lindenmayer & Rozenberg, 1972; Palubicki et al., 2009; A. R. Smith, 1984). LS has also been utilized in design to generate city roads and networks (Parish & Müller, 2001), terrains and textures (Dai & Ozawa, 1997), and building forms (Dai & Ozawa, 1997; Müller et al., 2006).

Since they are context-sensitive, cellular automata (CA) tend to follow the 'form-follows-function' philosophy. The required functionality produces the emergent form. CA helps solve urban planning difficulties, zoning, block design, and building massing chores by facilitating the examination of social consequences through simulations based on neighborhood characteristics (Krawczyk, 2002b, 2002a).

Agent-based Models (ABM) and swarm intelligence (SI) can be applied in various ways. Agents can evaluate the usability of a design environment, such as navigation and social behavior patterns. Agents that are intelligent and have much information can be employed as avatars and design agents that interact with each other, their environment, and the human designer.

As explained in the previous paragraphs, some generative design techniques are better suited to specific design needs and strategies than others, and the following parts of this section explain specific design strategies commonly implemented via generative design tools.

6.2.1. Spatial configuration via generative design

The architectural industry experimented with generative design applied to environments for a long time. If we regard spatial arrangement as a fundamental characteristic of architecture that influences the expected social performance of buildings, then spatial analysis should be a necessary component of the architectural design process.

Most cases of autonomous space formation rely heavily on random processes such as mutation or generate chaotic maps such as cellular automata. Simon's Evolving Floorplans is purely optimization-oriented(Simon, 2019). By combining a genetic algorithm, physics simulation, graph contraction, and ant colony pathing, we can generate a one-story Voronoi floor layout with rooms and halls that meet the criteria for daylight. He asserts that shape is the constraint, regardless of convention or constructability.

With his AI Architecture Generative Design Housing, Chaillou utilized a Generative Adversarial Nets approach (Chaillou, 2020). He generates one-story floor plan images with furniture using the pix2pix GAN model and Google deep learning tools. The drawback is that the generation is limited to 2D and does not allow for expanding the pool of room kinds without using machine learning.

Nisztuk and Myszkowski's ELISi is a program that uses metaheuristics to generate a one-story floor plan using a Hybrid Evolutionary Algorithm (NSGA-II algorithm + Greedy-based algorithm) (Nisztuk & Myszkowski, 2019). The constraint is that all room location preferences must be preset. Additionally, there is no interaction with the surrounding world.

Egor et al. research has created a grasshopper component, Magnetizing Floorplan Generator, which produces some compelling results (Egor et al., 2020). Each room in a building is connected by a corridor, which means that the entire communication structure is interconnected, with a single corridor connecting all rooms (Egor et al., 2020). They analyze the floor plan graph and determine the room placement order based on each room's degree. Because the highest room is likely the hardest to locate, it is placed first. They then optimize the location by iterating and reverting to prior iterations if something goes wrong.

Pirouz Nourian criticized the notion of architecture as an automated evolutionary process in 2016. More precisely, he views architecture as primarily concerned with spatial configuration or the arrangement of functional areas in a certain way to serve a higher goal (Nourian, 2016). He proposed an interactive syntactic design process fueled by real-time analytic input on spatial features in which designers retain complete intellectual control over spatial configuration and evaluation while using computation for systematic analysis and synthesis. As Pirouz Norian noted in his study, bubble diagrams have been extensively employed throughout architectural design (Nourian, 2016). Typically, architectural spaces are represented by bubbles and their connections by lines that connect each

bubble. Such geographical relations can be quantitatively described using nodes and links (or vertex and edges) in graph theory:

- Nodes represent virtual spaces.
- Links show circulations.
- The weights assigned to links indicate the significance of their adjacency or connectedness.

In the proposed design approach shown in Figure 100, a reflective cycle of "see-move-see" (Schon, 1987) was proposed rather than an automated problem-solution procedure (Nourian et al., 2013). The entire design workflow proposed by the methodology is about moving from an abstract graph description of spatial connections to a topological planar embedding of that graph, analyzing that graph in real time, and then finding feasible geometric cell configurations that can accommodate the proposed graph of connections (Nourian et al., 2013).

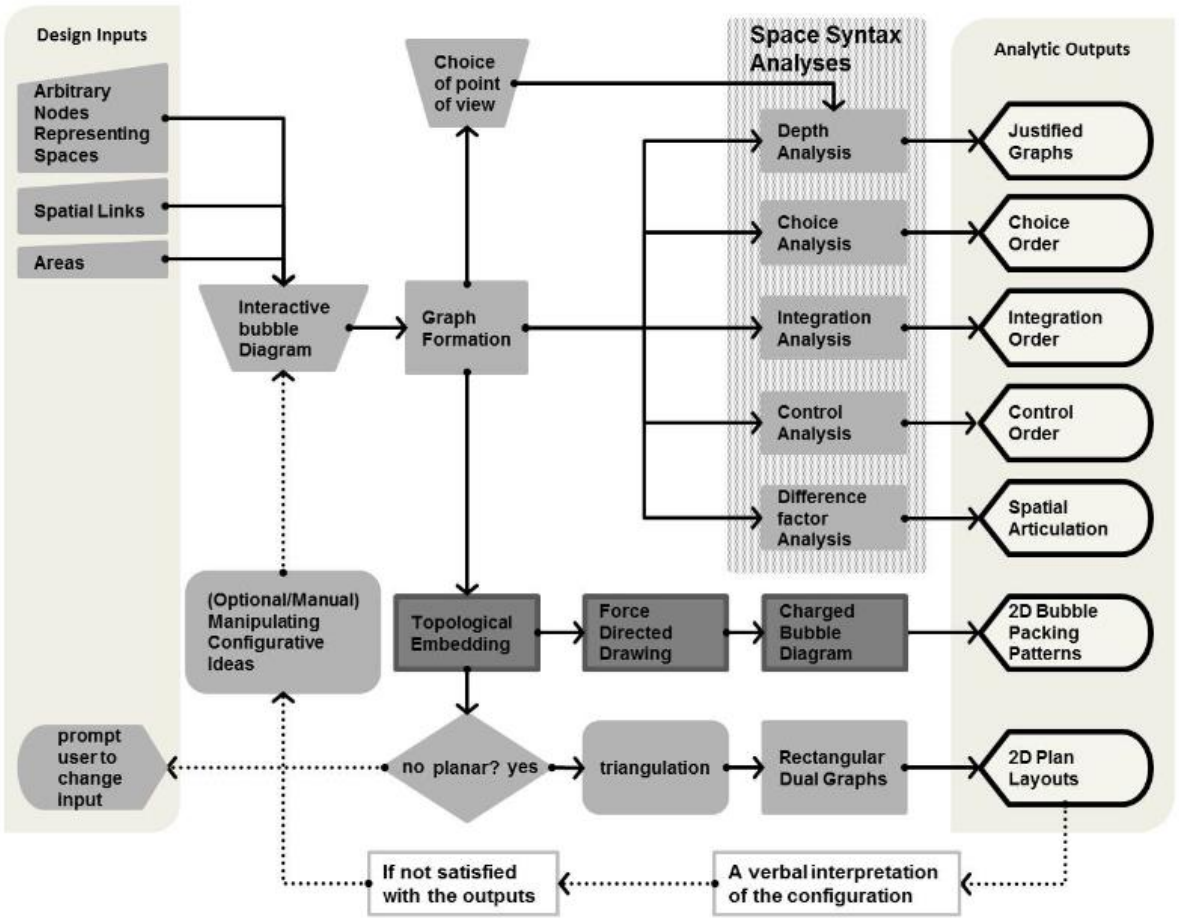

Figure 100. A flowchart describing space-syntax-based generative design methodology (Nourian et al., 2013).

Nourian et al. (2013) created a digital design approach and a toolbox known as Syntactic to bridge the gap between space syntax and architectural design practice using this representation. Analyzing plan layout patterns by sketching spatial configuration using an "interactive bubble diagram" that reflects a spatial connectivity graph is the goal of the developed Syntactic toolset.

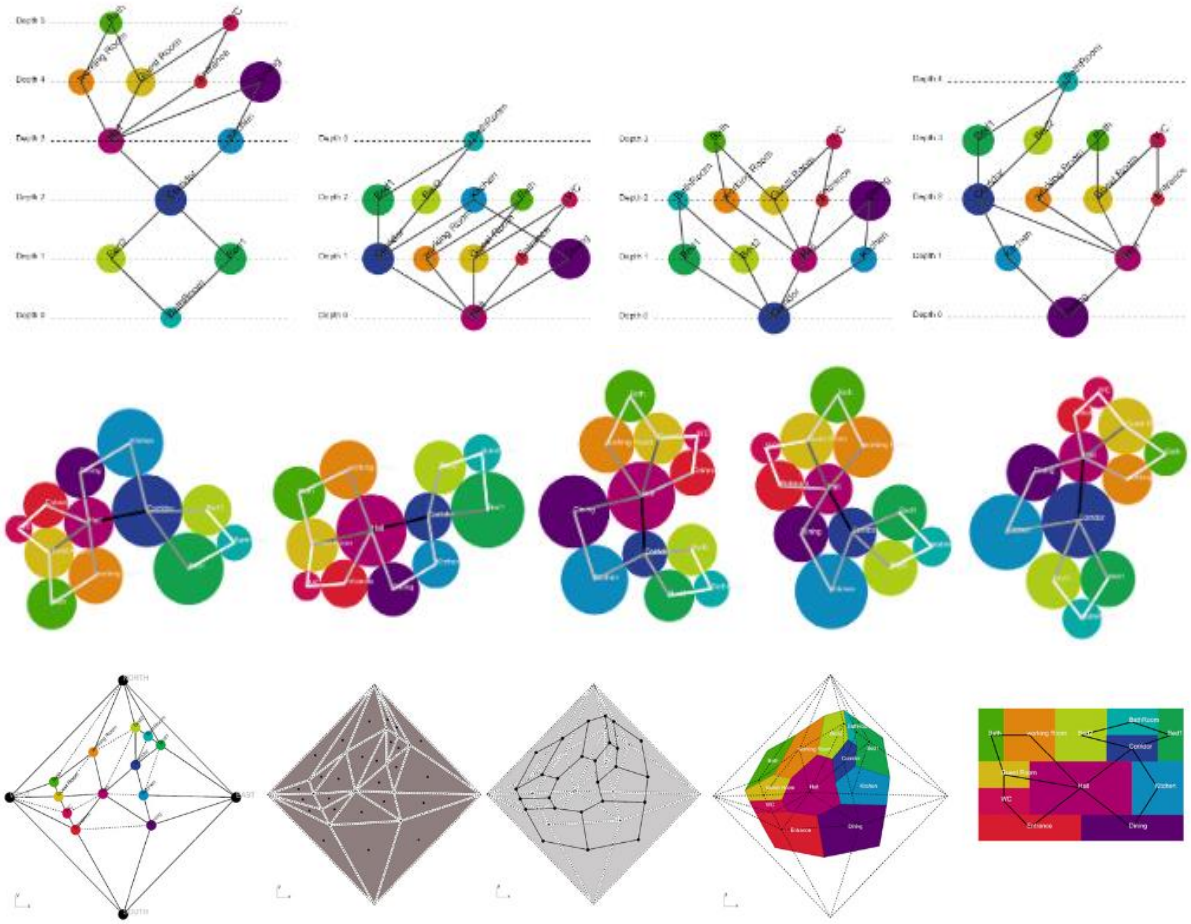

Figure 101. The phases of layout generation via Syntactic (Nourian et al., 2013).

The illustrated methodology shown in Figure 101 by Nourian et al., 2013 shows a feasible generative design process for the initial phases of architectural design to answer which configuration is the most integrated architectural layout. Using bubble diagrams and space-syntax theorem may also provide a feasible automated layout planning to design a habitation because circular forms are preferable to create a pressure-vessel or inflatable-like geometry in the case of space architecture.

6.2.2. Physic-based generative design methodologies

Real-world design scenarios frequently involve the interaction of several phenomena (structural, vibration, fluids, electromagnetics, etc.) within a single load state or across many load conditions. Generative Design must address the relevant physics for the design scenario under examination. To be widely deployable and applicable, Generative Design workflows must support a reasonable set of combinations of different physics with distinct design objectives and constraints, such as structural, thermal, and vibration, that correspond to the use cases currently being used without Generative Design.

Physics-based processes are fundamentally simulations of complex natural phenomena. Additionally, it is considered an active area of progressive formation and mutation, allowing for the dynamic evolution of highly plastic shapes via the interaction of simulation components (Suzuki, 2020). Numerous of these tools can be used in conjunction with one another as part of a broader generative process to generate new forms and intriguing designs, as shown in Figure 102.

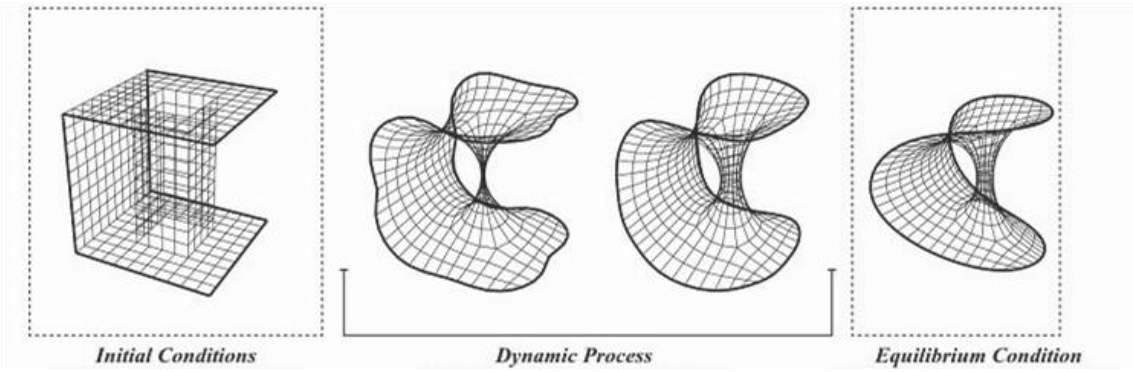

Figure 102. A modeling sample for the linear physics simulation process (Suzuki, 2020).

The typical way to identify the shape is via a physics-solvers to represent it as a network of nodes subject, as seen in Figure 103, to internal and external pressures and then compute the final shape as the system's equilibrium state (Deuss et al., 2015). For example, Kilian and Ochsendorf use particle-spring systems to discover structural forms composed entirely of axial forces (Kilian & Ochsendorf, 2005). Their method, which utilizes an implicit Runge-Kutta solver to determine the equilibrium state, enables the user to interact with the simulation while running. A live physics engine built on top of Grasshopper, Kangaroo uses a similar force-based approach (Piker, 2013). The Kangaroo is a popular tool among architects because it can perform form-finding, physics modeling, constraint solving, and optimization.

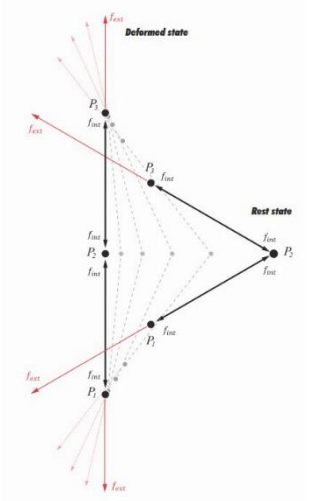

Figure 103. The equilibrium state of a network condition (Suzuki, 2020).

For a long time, computer graphics have been captivated by physics-based modeling and related optimization approaches for geometric interaction (Harada et al., 1995). Additionally, special effects technologies have been used to aid in the early stages of dynamic sketching for design projects (Mark, 2007). Physics simulators or algorithms are a cloud of points whose placements are updated in a cycle. These points are connected by springs, represented computationally as vectors with direction and magnitude. The singularity calculates new force vectors in each cycle and uses the vectors to update the positioning of points. This loop is typically repeated until the points no longer move or move less than a certain distance in each loop, a process known as converging. Physics modeling helps designers simulate real-time physical conditions like tensile or compression forces on an object or collision of several geometries to find their equilibrated state according to defined parameters.

Designing a habitation for space missions has always been an evolving process. The minimum or required volume parameter is permanently changed after every mission; functional requirements are always adapted into new human factor considerations; mission plans and technological background are still changing, and so on. A space habitation's design parameters might continue to alter over time, and the design must adapt to changing conditions. This study hypnotizes that functional parameters in a habitation design process should be considered a parameter that must be equilibrated to find a comprehensive design methodology.

6.2.3. Simulation-based generative design

Architects have increasingly turned to computer simulation in recent decades to create more functional, sustainable, and engaging buildings. It is critical to view buildings as static constructions and complex dynamic systems influenced by highly stochastic factors such as weather and human behavior. Numerous modeling methods have been developed to simulate various aspects of a structure, including thermodynamics, lighting, plug loads, crowd behavior, and structural integrity under internal and exterior loads.

Including simulations in the design workflow enables a more dynamic framework to be created during the early stages of design. Historically, architects have experimented with animation technologies as a generative process and a means of comparing forms (Burry et al., 2005). Architects can explore new design ideation techniques by addressing design as a set of factors responding to dynamic, material, and changing contextual pressures across time via animation as simulation(Kolarevic, 2003b). The appeal of such a dynamic approach stems from designers' increased interest in nature as a source of unique processes and their correspondingly novel consequences. Simulation as a performance-driven design tool has already enabled architects to investigate unique approaches to design problems, resulting in an increasing number of projects in which simulation is a necessary component of the form-seeking process (Oxman, 2008).

Previously, structures have been optimized iteratively, using a more trial-and-error technique. With the addition of visual programming capabilities via the embedded application Grasshopper, Rhinoceros has gained significant traction among architects and civil engineers seeking to increase their productivity while modeling BIM models. Additionally, FEA software developers have seen the opportunity and are now offering plug-ins that enable bidirectional interchange between their products and the modeling capabilities offered by Rhinoceros. With Grasshopper, the user can create programs that generate complex geometry that would be inconvenient to generate manually. Karamba3D is a Grasshopper-based FEA plug-in that enables structural analysis to be scripted like geometry is usually scripted in Rhinoceros. It is hugely "compact," delivering rapid answers to structural analysis problems described by geometry and data coded in a Grasshopper script. This capacity makes it ideal for generative design optimizers such as Galapagos and Octopus, explained under the following topic.

Another main simulation subject is environmental conditions. Based on Grasshopper's parametric framework, environmental simulation plug-ins such as Ladybug and Honeybee are used to investigate microclimates. Environmental considerations can be examined quickly and effectively by connecting the early design phase to environmental analyses. EPW (EnergyPlus Weather) data can be imported into Ladybug's data analysis and visualizations based on the designer's specifications. Honeybee's tools can assist Ladybug in doing energy analysis calculations. Ladybug and Honeybee generated energy analysis and visualization using well-known simulation engines such as DAYSIM in Radiance, THERM, EnergyPlus, and OpenStudio.

In the case of designing habitation for an extreme environment such as Mars, harsh environmental loads must be incorporated into design phases for a scientific solution of the design problem and process standardization, and structural and environmental loads must be simulated to define a sustainable solution.

6.2.4. Design optimization via genetic algorithms

GA (Genetic Algorithm) was inspired by Darwin's evolutionary theory, which simulated the survival of fitter species and their genes. A genetic algorithm (GA) is a population-based algorithm. Each solution is a chromosome, and each parameter is a gene. GA utilizes a fitness (objective) function to determine each member's fitness in the population.

The GA (Genetic Algorithm) algorithm begins with a randomly generated population. This population can be produced using a Gaussian random distribution to boost diversity. This population contains numerous solutions that correspond to an individual's chromosomes. Each chromosome has a set of variables that serve as a model for the genes. The initialization step's primary purpose is to

distribute solutions uniformly across the search space to promote population diversity and raise the likelihood of discovering attractive regions.

The following stage determines which chromosomes to enhance (Marano et al., 2021). Natural selection is the primary source of inspiration for this GA algorithm component. The fittest individuals have a better chance of obtaining food and mating in nature. This process results in their genetic information contributing more to the following generation of the same species. Inspired by this simple concept, the GA algorithm uses a roulette wheel to assign a probability to people and pick them proportional to their fitness (objective) values for the following generation. This technique mimics natural selection in nature, which favors the fittest individuals. Due to the random nature of a roulette wheel, poor individuals have a low possibility of contributing to the following generation's formation. It is worth noting that the roulette wheel is just one of the selection operators described in the literature. Several additional selection operators are Boltzmann selection, tournament selection, rank selection, stable state selection, truncation selection, local selection, fuzzy selection, and steady-state reproduction via linear rank selection (Marano et al., 2021).

Following their selection by a selection operator, the individuals must be utilized to generate a new generation (Marano et al., 2021). In nature, the male and female genes' chromosomes are merged to form a new chromosome. This process is emulated in the GA algorithm by merging two solutions (parent solutions) chosen by the roulette wheel to create two new solutions (child solutions). Two distinct crossover operator strategies are described in the literature: single-point and double-point. Before and after a single point, the chromosomes of two-parent solutions are switched. However, two points are crossed in a double-point crossing, and just the chromosomes between the points are switched. Other crossover strategies available in the literature are uniform, half-uniform, three-parent, partially matched, cycle, and position-based, heuristic crossover (Marano et al., 2021).

The final evolutionary operator is a mutation, in which one or more genes are modified following the generation of children's solutions (Marano et al., 2021). The mutation rate is kept low in GA because it converts the algorithm to a primitive random search when it exceeds a certain threshold. The mutation operator maintains the population's diversity by injecting an additional level of randomness. Indeed, this operator prevents solutions from becoming identical and increases the possibility of the GA algorithm avoiding local solutions. Several of the literature's most often used mutation approaches are power mutation, uniformity, non-uniformity, gaussian, shrinkage, supervised mutation, and uniqueness mutation (Marano et al., 2021).

Most EAs (Evolutionary Algorithms) employ the three evolutionary operators of selection, crossover, and mutation. Each generation is subjected to these operators to increase the quality of the genes in the following generation. Another typical evolutionary operator is elitism, in which the best solution or solutions are preserved and passed on unchanged to the following generation. When

crossover or mutation operators are applied, the primary goal is to avoid degrading such solutions (elites) (Marano et al., 2021).

The GA algorithm begins with a population of randomly chosen individuals. Using the three operators discussed previously, this algorithm enhances the population until the end condition is reached. The optimal solution found in the previous population is returned as the closest approximation to the global optimum for a particular problem. This approach, which implements artificial intelligence in the generative design process, is commonly used to optimize models by identifying the most suited parameters. The selection rate, crossover, and mutation can be modified or fixed during optimization to maintain constant values.

Evolutionary design methodologies can be used to optimize the design parameters of habitation proposals to reveal unknown design variations and choose the fittest as a habitation definition. Galapagos, the most widely used evolutionary solver, is a program invented by David Rutten that significantly popularized and made evolutionary solvers accessible in Grasshopper and the building sciences. Galapagos searches for combinations of input parameters in a Grasshopper description using single-objective optimization methods. Since the release of Galapagos, numerous more third-party developers have established evolutionary computation interfaces for multi-objective and interactive optimization. Another well-known solver is Octopus, as seen in Figure 104 enables simultaneous search for several goals, generating a range of optimum trade-off solutions between each goal's extremes. Many other solvers like Biomorpher enable single-objective optimization methods to help designers interact with the evolutionary process. Wallacei is an evolutionary engine that enables users to execute evolutionary simulations in Grasshopper 3D using exact analytical tools.

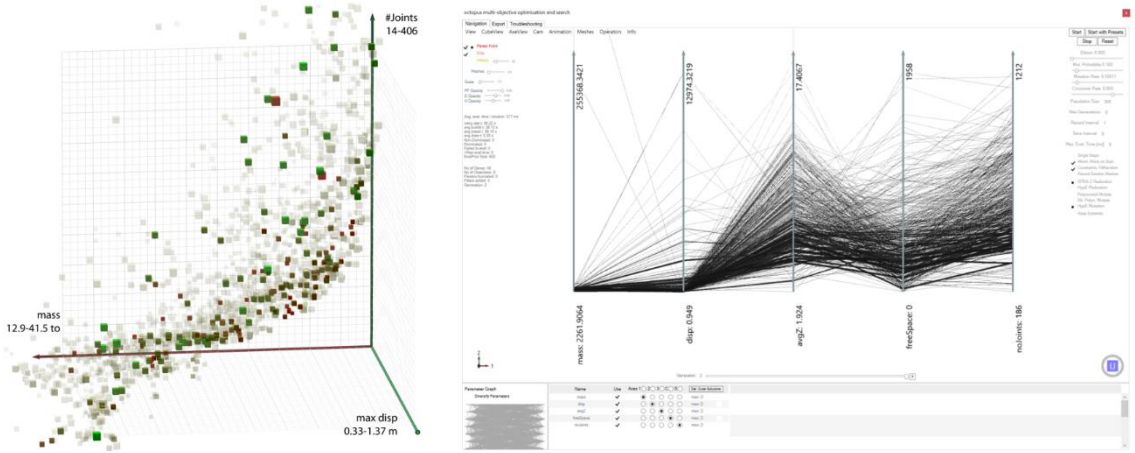

Figure 104. Octopus interface for multi-objective optimization (Source: Food4Rhino Octopus page).

6.3. Machine Learning-Aided Generative Design Methodology

Human needs a pre-defined strategy with sustainable solutions to survive on Mars condition. Up to the last decade, different habitation design proposals have been conducted to send humans for long-term space missions; however, these strategies depend on transportation solutions from Earth to the aimed space environment. After developing additive manufacturing technologies, NASA and other space agencies have collaborated with private companies to find a self-sufficient and sustainable habitation strategy. In recent years, researchers and scientists have been investigating ISRU technologies to use local materials as living and construction resources; furthermore, different design and engineering companies have been founded to design the most independent habitation module using local resources. This chapter aims to suggest a novel design methodology that could be implemented to find a design solution to live in the most extreme environments.

The model needs to be reviewed and optimized without human involvement to progress autonomously after completing the form generation. A decision-maker will be needed to integrate all design characteristics to identify the optimum fit for extreme conditions and building technologies executed by robotic technologies to end the conceptual design phase of habitation proposals.

As a decision-maker of typology definition, machine learning algorithms can be integrated into two phases of research study: the definition and analysis of functional spaces in a floor plan and the detection of functional communities in a related plan to separate each community as a layout plan to provide separation between communities according to their relevance. The habitation floor plan or plans will be protected under the same habitable shell to make the pressurization and 3D construction process more manageable and feasible under extreme Mars conditions.

While robotic and artificial intelligence technologies are required for daily life after landing, humanity needs these technologies to design and construct their habitations with other structural components before landing on Mars. Environmental extreme conditions and communication delays compel autonomous systems to make everything ready for humans before their landing. A novel design methodology is suggested for implementation in long-term space missions. Further chapters will explain the methodological and theoretical background of the suggested methodology, and a design implementation will be conducted to show its practical capabilities and evaluate for further research.

6.3.1. A Novel Typology Decision Methodology for Habitation Design

In the fourth chapter, we discussed using data science to study the floor plans of prior Mars analog missions to learn about human aspects from design and planning choices. In the study of analog habitations, network centrality measurements derived from Social Network Analysis (SNA) are used to investigate how nearby functional areas of Mars analog habitations interact. The outcomes of centrality analyses identify the most vital regions in habitations, particularly hub or "key" areas, which significantly facilitate other network activities.

- A node's betweenness centrality measure is high if it is related to numerous other nodes. If they manage activity flow, nodes with high betweenness in a network can have a significant impact. Due to their central location on multiple routes, their removal would be detrimental to the overall network.
- Closeness centrality is the average distance between nodes that is the shortest. Typically, a type of circulation region has the most significant closeness.
- Eigenvector centrality measures the significance of a node by considering its neighbors. As a more complex measure of centrality, eigenvector centrality permits a node with few connections to receive a high score if all its linkages route to highly connected nodes. This metric necessitates an activity category indicator to establish which activities are significant in the social networks.

The Label Propagation Approach (LPA) is also presented in Chapter 4 as a graph-based semi-supervised machine learning approach for detecting communities in a network. The LPA algorithm of the NetworkX python package utilizes semi-synchronous label propagation to identify network communities, integrating synchronous and asynchronous models. To identify the communities, neither an objective function nor prior information is required; the network's topology is required. The algorithm identifies nodes belonging to the same community. It provides sufficient information to position, combine, and link functional activities of a habitation for a more space-resilient design.

Comprehensive evaluations in Chapter 4 indicate that social network analysis can be utilized to study and enhance habitation designs when their floor plans are represented as undirected networks. In addition, the study also reveals insightful results for the application of SNA in the early design phase of a habitation.

After obtaining remarkable results in the previous study, we propose using SNA and LPA algorithms to integrate human factors into the habitation design process to develop a machine learning-aided design methodology for a more space-resilient habitation design.

Before the implementation of the previously defined methodology in Chapter 4 for a new design process, we need to define the functional requirements of an optimum habitation to establish

functional adjacency matrices to define alternative layout plans from the beginning of the design process. which will be sufficient to accommodate a crew of selected people for a long-term exploration mission.

In the literature, space habitats are referred to by a variety of terms: "inhabited space systems" (Osburg, 2002), "human-rated spacecraft" (C. S. Allen et al., 2003), or any pressurized element that implies crew presence, such as a lander, base, station module, or crew transfer/entry/ascent/descent vehicle. A space habitat's fundamental goal is to offer a pressurized environment where humans can live and work (Kennedy, 2017). The habitats must have enough volume to accommodate all the equipment and consumables required to support the crew and complete their daily and work-related activities (Larson & Pranke, 1999). The study conducted by Stromgren et al. is based on the volumetric definitions of functional requirements and its fundamental process established at the 2012 Net Habitable Volume (NHV) Workshop and confirmed by NASA's Chief Medical Officer (Stromgren et al., 2020).

Table 21. Functional space requirements for long-term space habitation (Stromgren et al., 2020).

Function Labels	Minimum Height	Volume (m^3) For 4-crew
Logistics-2 (Temporary Stowage)	2,76	6,00
Maintenance-1 (Computer) / EVA-2 (EVA Computer/Data)	2,00	3,40
Maintenance-2 / Logistics-1 (Work Surface) / EVA-1 (Suit Testing)	2,31	4,82
Mission Planning-2 (Computer/Command) / Spacecraft Monitoring	2,00	3,42
Group Social-1 (Open Area) / Mission Planning-3 (Training)	2,00	18,20
Medical-1 (Computer)	2,00	1,20
Medical-3 (Medical Care)	2,00	5,80
Human Waste-1 (Waste Collection)	1,52	2,36
Human Waste-2 (Cleansing) / Hygiene-1 (Cleansing)	2,00	4,35
Waste Management	2,00	3,76
Group Social-2 (Table) / Meal Consumption / Mission Planning-1 (Table)	2,00	10,09
Meal Preparation-1 (Food Prep)	2,00	4,35
Meal Preparation-2 (Work Surface)	2,00	3,30
Exercise-1 (Cycle Ergometer)	1,92	3,38
Exercise-2 (Treadmill)	2,10	6,12
Exercise-3 (Resistive Device)	2,03	3,92
Private Habitation-1 (Work Surface) / Medical-2 (Ambulatory Care)	1,91	17,40
Private Habitation-2 (Sleep & Relaxation) / Hygiene-2 (Non-Cleansing)	2,50	13,96

The operational data for the research projects, as seen in Table 21, is extracted from the research study of Stromgren et al. in 2020. Firstly, the team identified particular functional activities or duties that the crew must do throughout a lengthy exploratory mission. The team then defined the minimum operational volume required for each indicated function. After defining individual functions

and volume needs, the team looked for functional overlaps within categories, where individual functions may overlap with overlapping functions that could be accommodated in the same space. A final set of 'Functional Spaces' was established based on identified overlaps, which are the distinct collection of volumes' ability to manage all of the category's indicated functions. Each Functional Space is capable of supporting one or more needed functions. While the data in Table 21 contains required functional areas with their corresponding volumes for crews with four members, it also reveals the minimum height requirements of each function to provide habitable zones in a habitation.

Using the functional areas provided in Table 21, we will generate a variety of adjacency matrices that a designer or space architecture expert can establish. At the end of the fourth chapter, we provided a representation of the guideline to illustrate and compare the communal structures of analog habitations' layouts. We recommend that adjacency matrices be developed based on the data illustrated in the guideline. The established matrices must be evaluated using social network analysis (SNA) to show the centrality measurements of each functional area in order to determine whether or not an adjustment in relations is necessary. For SNA analysis, each functional area will be represented as a node, and their relationships, according to adjacency matrices, will be represented as lines to produce an analyzable network graph. After social network analysis (SNA) is completed, we will acquire centrality estimates of functional areas and an undirected network illustration of defined matrices for use in the Label Propagation Approach (LPA). The LPA algorithm in the NetworkX package is a graph-based semi-supervised machine learning technique that does not require any preliminary data for implementation; it only needs to recognize nodes and their relationships from a network graph. The algorithm starts to label each node with a unique label, and the labels of the nodes are iteratively updated according to the majority of the labels of the neighboring nodes. As a result, a functional separation of nodes is revealed as communities in the network, which is our case's functional network diagram of habitation. After detecting communities, we suggested using each community as a floor area to define the typology of habitation in the early design stages. If the community number is equal to one, the defined matrix can be utilized to create a horizontally oriented habitation layout. If the number of communities is more significant than one, it will be utilized to designate each community as a floor plan and orient them vertically to generate a multi-story habitation development. In two configurations, habitations will be constructed beneath a single protective shell to construct and pressurize it more easily, efficiently, and inexpensively. Additionally, this will enhance the durability of the habitation system because there would be no need for connection components between volumes.

6.3.2. Habitation layout and form generation methodology

After identifying communities in a pre-defined adjacency matrix and the design typology of the habitation project, the collected data must be turned into a generative design process to launch a design generation based on scientific knowledge. In addition, we aim to develop a generative algorithm for an autonomous design that will be initiated, continued, and constructed based on the output of each design phase and scientific evidence. In this project, we propose to combine space syntax methodologies and physic solver simulations to construct a self-designed conceptual form of habitation.

6.3.2.1. Utilization of space syntax in the planning of a Mars surface habitation

Space Syntax presents a collection of approaches for analyzing spatial configurations, mainly when they affect human affairs. The Space Syntax methodology enables designers to predict the anticipated implications of their designs on both the micro and macro scales. As a tool for analyzing space and its relationship to a space user, Space Syntax tries to measure space's quality. In this context, "space quality" refers to a space's characteristics. From a Space Syntax perspective, some features include the following: space can be convex or concave, have a greater or lesser viewable area, and be more or less integrated with the surrounding spaces. According to Space Syntax Theory, people respond differently to spaces with varying features, which explains why some spaces become more popular than others or why people experience varying emotions within various spaces. People's implicit awareness of various spatial qualities (characteristics) could explain this response to various spaces. It is not a deliberate reaction to space because people do not analyze the place as they walk down a street; instead, it is a human psychological response to particular traits in an area.

The methodology for developing Space Syntax attempts to explain human behavior in terms of spatial characteristics. It is possible that if Space Syntax is capable of defining the attributes of a space, it will enable the development of a technique for predicting how people would behave in that space. Space Syntax seeks to elicit an examination of what forms the character and attributes of space, thereby predicting how people would respond. As a result, this research article will use Space Syntax as an analytical technique for habitation planning.

Space Syntax Theory considers three significant issues: the perception of mobility through space, human interaction in space, and viewing ambient space from the point of view. Space Syntax employs mathematics to create a logically and mathematically defensible and reproducible approach. The Space Syntax technique aims to produce an output allowing designers to evaluate their designs before construction.

After adjacency matrix finalization, SNA analysis, and community detection using LPA have been completed, the network of functional areas must be defined as functional layout diagrams with

corresponding area information in the generative design environment. In this study, the space syntax methodology proposed by Pirouz Nourian (2013) is used to generate the most integrated plan configurations using Syntactic, a Grasshopper plugin developed by Pirouz Nourian and Samaneh Rezvani at TU Delft. This plugin brings Space Syntax theory into generative design workflows with diagrammed configurations of input data. Syntactic allows designers and researchers to triangulate the augmented connectivity graph to generate and analyze their studies. The following simple meanings are essential for understanding the analyzing procedure. Four syntactic steps can be computed: integration, connectivity, depth, and control value.

Integration, also called availability, is a parameter that indicates how a space in its context is linked to other spaces. This step is the primary parameter for the understanding user and environment connections. The more space integration, the more people will use it, and spaces will be more accessible. The main conclusion is that the axis system brings users into the best-interconnected areas in the system. Likewise, less integration means less population and unwanted reality

Depth/degree of depth is the minimum series of syntactic steps necessary to reach from one space to another (in a topological context).

Connectivity is the number of neighboring axes directly connected to space measured by connectivity analysis. It determines the number of an axis's immediate neighbors.

The control value is the sum of the opposite values of the connectivity parameter for all the selected axial line neighbors. It tests the degree to which the defined space blocks access to all of the axis line's close surroundings. It takes into account all the alternate interactions these neighbors have. It is a dynamic local indicator.

For space habitation, the interior layout's organization follows the crew's functional needs, such as working, hygiene, exercise, preparing, and eating food. The "Bubble Diagram" is a standard graphical tool used by architects to study the relationship between the sizes, adjacencies, and approximate shapes of the spaces required for various activities.

An optimal connectivity diagram's definition requires identifying each functional relationship using analytic techniques. In order to comprehend the functional logic underlying the mission-oriented spatial design of a space habitat, the adjacency matrix generated in the previous phase will be used as a guide to construct the corresponding connection diagram and undertake space-syntax analysis.

The functional requirements derived from literature for the corresponding crew number are defined as a random point, and connection lines are drawn between each space according to the adjacency matrix of SNA analysis. The outcome is a connectivity diagram, which is then used to generate a space-syntax bubble diagram and corresponding analysis.

The parametric tools shown in Figure 105 in the Syntactic plugin construct a "kissing disk" drawing of the bubble diagram using a force-directed graph-drawing method. This method is simple

to implement and generates real-time bubble diagrams perfectly arranged according to the defined areas and connectivity graph. The bubble diagram developed illustrates the initial appearance of the habitation plan in an architectural context. *Graph from Nodes and Links* component is used for configurative concepts to draw a line between each pair of points (the center of circles indicates functional spaces). The architectural configuration graph is precisely drawn with the *Force-Directed Graph Drawing Algorithm* tool. *Disk Graph Drawing* tool is the graph reader component to interpret the supplied links and points as a graph and gives the user vocal relationships between spaces. *The justified Graph Drawing* tool draws depth-level graphs of spaces according to identifying the first space input.

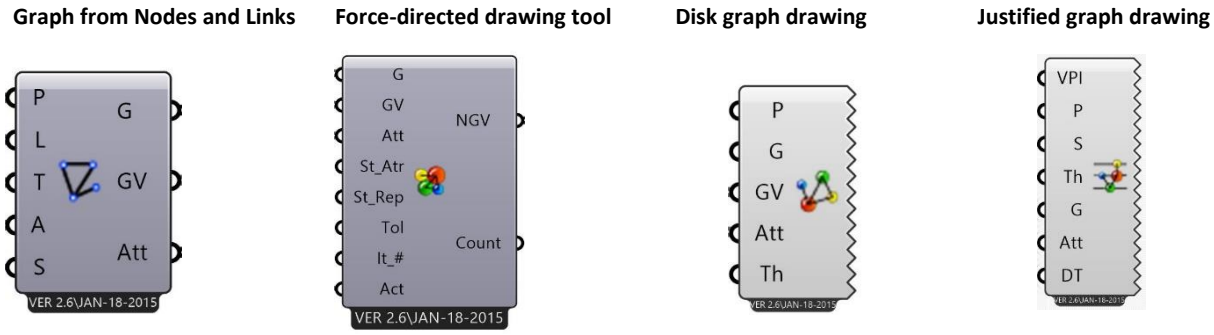

Figure 105. Diagram generation tools of Syntactic plug-in.

As a result of the generation of bubble diagrams, space syntax analysis can examine the relationships between functional areas and their interconnections by using illustrated tools in Figure 106. *Integration analysis* determines the degree to which space is common or private, as described in 'The Social Logic of Space.' According to this metric, a more significant number indicates more private space, while a lower value indicates more communal space. *Control analysis* determines the strength with which a vertex in a graph is connected to other points. The degree of *choice analysis* quantifies how frequently a space is on the shortest path between other spaces. *Entropy analysis* reveals how a system's space is connected. The larger the value, the more difficult it is to move across spaces and vice versa.

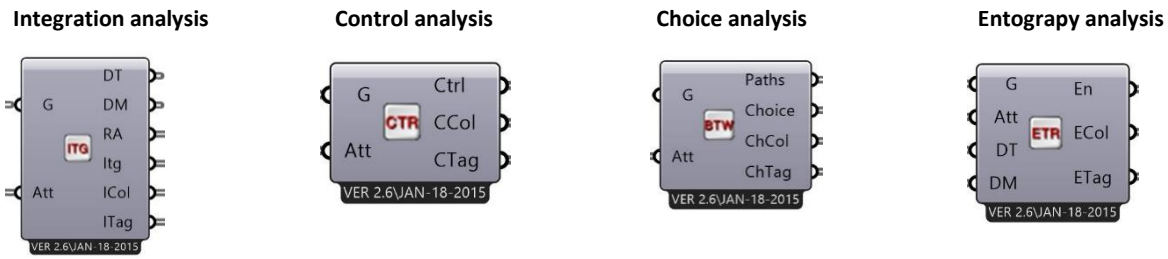

Figure 106. Space-syntax analysis tools of Syntactic plug-in.

6.3.2.2. The use of physic simulation for habitation layout generation from diagrams

The development of bubble diagrams must be followed by their transformation into functional layouts to create a layout design methodology. The environmental conditions of the space environment dictate the shape of a space habitat, as detailed in the fourth and fifth chapters. For pressurized space habitat shells, two distinct morphologies exist. The first group incorporates "inflatable-like" shapes, i.e., the morphology of pressure vessels and inflatables, for the artificial atmosphere envelope. The second group seeks to turn pneumatic bubbles into more recognized architectural forms, such as nearly flat walls and orthogonal or hexagonal nesting. As mentioned in previous chapters, the geometries of floor areas of habitats are often circular to create pressure vessel geometries. In this study, we suggest adopting generative physics simulations to convert bubble diagrams into circular floor plans.

Kangaroo, shown in Figure 107, is "a Live Physics engine" designed by Piker (2013) for interactive simulation, form-finding, optimization, and constraint solution. It is a Grasshopper/Rhino add-on that directly integrates physical behavior into the 3D modeling environment and enables users to interact with it 'live' while the simulation runs(Piker, 2013). Kangaroo operates by calculating the total force vector F for each particle by summing up all the many forces that act on it, calculating the acceleration using Newton's second law, and numerically integrating the resulting differential equation of motion over time to discover new positions for all of the particles. Additionally, a position in Kangaroo is said to be in equilibrium when the weighted average of the motion vectors from all goals acting on it equals zero. Additionally, the solver can be viewed as minimizing the (weighted) sum of the squares of the distances between each point's rest positions."

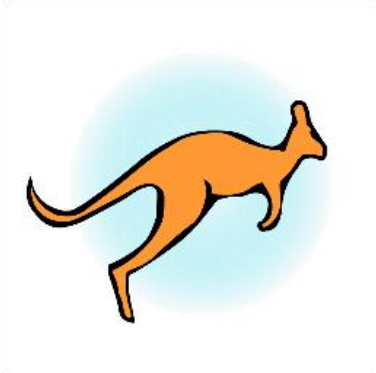

Figure 107. Kangaroo plug-in for Grasshopper.

Bubble diagrams are used to depict architectural layouts schematically. However, the generated space-syntax diagrams lack a border to restrict habitation sites and reduce total size for the most efficient integrated design. Physic simulation tools are proposed to provide constructible, realistic geometries for developing a pressure-vessel shape for a space habitat to convert the visual representations into functional layouts. This phase explains how physics simulation tools can be utilized to simulate a circular packing simulation to fit the disks of a bubble diagram into a circular area with the same value as the total equivalent area of the functional spaces used in the generation of the bubble diagram.

Creating a circle packing algorithm can be divided into two phases: first, develop a structure for the circle packing algorithm by using output elements of space syntax diagram, and then adjust

that structure while retaining the tangency feature. One method to use Kangaroo's physical simulation features is to configure collision simulation to solve problems such as circular packing. The objective of the optimization is to discover a more optimal solution that minimizes 'unused space' and overlapped space. The Kangaroo physics engine allows the user to simulate collision movements, and thanks to that, circle packing functions are implemented into the parametric interface of Grasshopper. In this project, circles from the bubble diagram will be defined as collision circles, and the circular boundary will be used to limit the area in which collision simulation will happen. In the end, circles and their adjacencies will be maintained, and the bubble diagram and circular area will be overlapped according to defined physics parameters.

Components of the Kangaroo tool shown in Figure 108 are the essential components of an explained collision simulation. The *Kangaroo solver* is the main component where physic goals are combined and applied to run a simulation. *The collider* component defines collisions between line segments and spheres. *The Onplane* component is utilized to keep specified points on a given plane. *The length* component attempts to maintain two points (line endpoints) at a specified distance apart, and with a greater Strength, the points will move less. *The anchor* component is used to maintain points in a particular position.

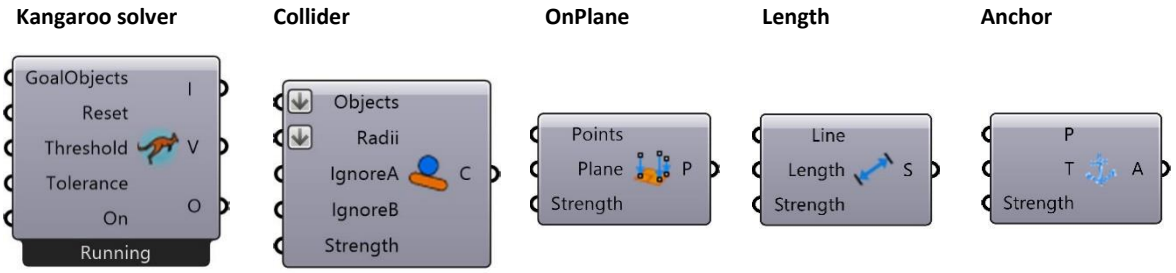

Figure 108. Collision simulation components of Kangaroo plug-in.

Once the simulations for circle packaging are complete, the disks from the bubble diagrams will be distributed and positioned within the defined circular area in accordance with the laws of physics, and an overlapping representation of the disks of each functional space and the total circular area's boundary curvature will be generated. A mathematical description of the functional layout is then formulated using the representation. Using circular geometries, we propose employing the Voronoi tool depicted in Figure 109 by applying the centers of the disks' circles to produce Voronoi-based segregation of circular area. The Voronoi diagram is the mathematical representation of the method through which a given set of points divides a region into smaller regions. Each point defines its region's bounds inside the larger region based on its neighbors' positions (Coates et al., 2005).

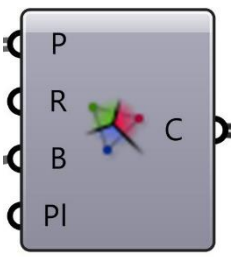

Figure 109. Voronoi tool in the grasshopper design environment.

6.3.2.3. The generation of a preliminary dual habitation envelope for structural analysis

The next step in the habitation design process, following the generation of circular layouts, is the specification of habitation volume. As previously indicated, the atmospheric pressure on Mars is exceedingly low compared to Earth, and the radiation intensity on the surface of Mars is substantially higher than the resistance threshold of the human body. In addition, the planet is inhospitable for even a single second due to its extremely low temperatures and temperature fluctuating during daytime and seasonal conditions. Moreover, seasonal dust storms occur on the surface of Mars. Due to the severe conditions, the design of the habitat must be centered on functional demands to protect the crew.

The fifth chapter describes the design principles of the 3D-printed Mars habitation projects for NASA's competition. The designs of Mars Ice House and Marsha imply a double-layered shell structure to divide the interior from the exterior environment. The layer between the interior and exterior of habitation is either a garden as a relaxation area or a circulation space to access the upper floors. This volume diffuses light to the lower habitation level and provides more protection from external hazards.

The number of levels and the circular area of each level, established by the SNA and LPA analyses, will determine the geometry of the habitation structure in this study. If the results of these phases indicate that the created network contains a single community, the habitation design will be generated as a circular plan, and its height will be determined by the functional space that requires the greatest height according to the data provided by Stromgren et al. (2020). In the remaining instances, circular floor plans will be aligned from their centers to produce a vertically oriented habitation. To take into account human factors revealed in the fourth chapter, the logistic and work areas will be located on the lower levels, while the common and personal areas will be situated on the upper levels, and the relaxation areas will be positioned on the top level of habitation to have a view of the sky. After the layout is oriented, their boundary curve will be employed to generate an autonomous form design based solely on the results of prior design decisions. The created layer will serve as the inner envelope of the habitation and can be constructed using standard 3D-printable materials without consideration for the harsh conditions of Mars. This shell will be offset by 150 centimeters to create a dual envelope simulating the second layer as a regolith shell structure. The intermediate void will be recommended for use as a circulation volume for the construction of stairs using additive manufacturing techniques, and it will also facilitate the diffusion of natural light from the top of the habitation to the lower floors.

The described process will be carried out using standard Grasshopper algorithmic tools, and the output will be used as input for structural simulations in which environmental forces will be simulated as structural loads to create a space-resilient habitation shell.

6.3.3. Integration of Environmental Forces into Design Decisions

In the third chapter, we identified the types of environmental factors on Mars and assessed environmental conditions to reveal how we could handle these problems to protect the crew. The effects of Mars' gravity, temperature, atmospheric pressure, wind, radiation, seismic activity, and meteorites on the viability of a human settlement were investigated. We also found the optimal locations on Mars for surface operations, water availability, plant growth, and the availability of local materials. If we want to develop a habitable structure that can withstand the harsh environment of Mars, we must consider all environmental concerns from the outset of the design process.

The first stage of the design process involves selecting the optimal exploration site, considering research goals, operational requirements, and the possibility for new information to be revealed about Mars. We analyzed three different methodological studies to understand their approach to deciding the landing site of a Mars mission, and the synthesis of their outcomes is revealed to make a final location decision to settle for a Mars exploration mission. The site selection evaluation presented in the third chapter finds that Mawrth Vallis is the optimal landing site for a long-term crewed surface mission due to its favorable latitude, altitude, landforms, distance from ice reserves, and plant-friendliness for cultivating local foods.

The second environmental design factor in the preliminary design phase is selecting an in-situ material with minimal dependence on the Earth. Using Mars soil to construct a structure on Mars is preferable to the highly costly alternative of transporting all building materials from Earth. The Martian concrete invented by Wan, Wendner, and Cusatis (2016) is a one-of-a-kind substance for on-site construction. It is composed of synthetic Martian soil material and molten sulfur, as Mars has always been a "sulfur-rich planet." Using the mechanical qualities of Martian concrete, a manufactured habitation might be designed and built on Mars.

Mars' gravity is the next major environmental factor, contributing to an acceleration of around 3.71 m/s^2 (van Ellen, 2018). This force will impact the design and development of human settlements. In order to ensure the security and stability of the system, it is necessary to model gravity as a structural force throughout the design phase.

Extreme surface temperatures and their substantial variations throughout the day and seasons pose the most significant design challenges regarding system durability. Mars is estimated to have an average temperature of -63 degrees Celsius, with minimums of -153 degrees Celsius and maximums of 20 degrees Celsius (Park et al., 2020). The temperature may range from +27 to -133.2

degrees Celsius throughout the day and night. Even while the Martian coldness has already put significant thermal pressures on a habitable system, the environmental conditions resulting from temperature variations provide a significantly greater risk of system failure. Extreme temperature events must therefore be modeled as early as possible during the design phase.

Mars' typical atmospheric pressure is 600 Pa, making it the next factor in environmental design. Since the habitat's internal pressure needs to be equal to or very close to that of Earth's atmosphere, a pressure difference will always exist. Because of the pressure difference, the structure will grow in size, so the material must be strong enough to withstand the loads imposed. NASA suggests a minimum internal pressure of 52.67 kPa for everyday operations on Mars (Park et al., 2020); although it is lower than the pressure on Earth, it is still within the safe range for human occupants. For this reason, the minimum pressure differential that might support human life on Mars is 48.655 kPa. Consequently, the system's architecture must be capable of withstanding 4961.429234244 kilograms per square meter.

The influence of Mars' wind on the planet is the sixth environmental factor considered during the initial design process. As indicated in the third chapter, Mars has reported wind speeds of up to 30 meters per second (Miscio, 2018), which is significantly slower than the highest wind speeds ever measured on Earth. The equation described in Chapter 3 is also used to estimate the dynamic pressure of maximum wind velocity on the surface of Mars. On the surface of Mars, the atmosphere has a density of around 0.02 kg/m^3 (NASA, 2021b). Therefore, the maximal wind pressure on the surface of Mars is 9 Pa (9 N/m^2), which must be simulated as a design force during the initial design stage.

The radiation level on Mars' surface is the seventh environmental factor, and it is exceedingly harmful to human health and must be shielded with a thick enough protection layer to prevent harm. It has been previously stated that Mars' typical annual natural radiation dose is 600 mSv (Hassler et al., 2014; McKenna-Lawlor et al., 2012). NASA guidelines state that an astronaut should only be exposed to 50 mSv of radiation each year; hence any structures or bases astronauts might inhabit must have a protection factor of at least 91.67 percent. We estimate that a shield composed of Martian regolith must be at least 60.99 centimeters thick to provide adequate radiation protection using the radiation shield formula stated in the third chapter and a protection factor of 91.67 percent. Estimating the requisite shell thickness with average annual radiation of 3.6 mSv over Mars' solar cycle yields a protection factor of 99.4 percent against 600 mSv for a Mars surface mission, which is required if we desire to provide an Earth-like lifestyle for Mars explorers. The findings of the calculations indicate that a regolith shell thickness of 125.59 centimeters provides sufficient protection against daily radiation levels comparable to those on Earth. To shield the crew from the high radiation levels on Mars' surface, we can design our structure with a regolith shell thickness between 60.99 and 125.59 centimeters thick.

Incorporating seismic activity on Mars as an environmental element into the design process is an additional factor to consider. As noted previously, earthquakes are caused by the shifting of tectonic plates. However, Mars lacks tectonic plates, and its entire crust is a single, continuous rock formation (Andrew et al., 2021). In the absence of plate tectonics on Mars, seismic activity should be low compared to Earth. NASA asserts that "marsquakes" are created by the same forces that cause rock fractures and crustal fissures on Earth, thereby explaining the phenomenon (Andrew et al., 2021). The signal would need to be amplified approximately 10 million times to hear a typical Martian earthquake. In addition, the response periods of the structures and the impacts they create are minimal because the surface accelerations induced by such forces are of a magnitude order (Banerdt et al., 2020). As previously stated, seismic events have a maximum ground velocity of 1.2×10^{-5} meters per second, a relatively low velocity for human ears. Seismic activity on the surface of Mars can be included in designs by expressing it as a proportion of the gravitational force. The earthquake shaking forces are a percentage of gravity (% g) (USGS, 2022). Compared to the acceleration of gravity (980 cm/sec/sec), the strongest Marsquake measured might generate an acceleration of up to 12×10^{-4} cm/sec^{-2}. Therefore, the shaking force is only 12.10^{-4}/980 g, or 0.0000012245 g, or 0.00012245% g, which is negligible and should not be considered during the design phase.

The influence of micrometeorites on Mars is the final environmental concern covered in Chapter 3. We contend that a micrometeoroid's destructive capability depends on its dimensions, velocity, density, and impact angle (M. Bell, 1999). Materials, thickness, temperature, stress, and the number and spacing of panels (including shielding) all affect the physics of an impacting structure (M. Bell, 1999). Most particles entering Mars have a velocity of fewer than 15 kilometers per second, with estimates ranging between 5.7 and 8 kilometers per second (Tomkins et al., 2019). We may assume the mass density of a meteoroid to be 2.5 g/cm^3 (M. Bell, 1999). It may be essential to conduct a simulated impact test on a single structure to determine how well regolith surface structures on Mars can withstand micrometeorite impacts. Micrometeoroid impact was ruled out as a design element for this thesis because it is not a constant force throughout Mars's environmental events and occurs infrequently. For scientists interested in this discipline, it will be offered as a topic for future research.

The generated habitation envelope must be analyzed as a shell structure since the system has to be formed with solid in-situ material, and the shape's behavior must exhibit rigidity like a shell structure under extreme environmental conditions. Generated habitation form is based on the explained form-finding methodology, but its shape has to be re-optimized directly for the flow of structural and environmental forces, which is why the shell structure has to be designed based on its weight against constant stresses.

Karamba3D is suggested for simulating the exterior shell of habitation design with explained environmental forces. The Karamba3D Grasshopper plugin (shown in Figure 110) was developed by Clemens Preisinger and Bollinger + Grohmann Engineers to assist in real-time interactive and parametric structure analysis during all phases of implementation (Preisinger, 2013). Since this plugin was developed with the interests of architects and engineers in consideration, it enables a continuous exchange of data between structural and geometric representations. It allows a precise evaluation of spatial trusses, frames, and shells throughout the earliest design stages. Using Karamba3D simplifies the combination of complicated geometric shapes with load calculations and finite element analysis on a single platform and makes the process considerably simpler to investigate a diverse range of complex parametric structure models. Moreover, Karamba3D easily incorporates optimization tools like Galapagos and Octopus into geometric models.

Figure 110. Structural simulation plug-in named Karamba 3D for Grasshopper

The Karamba3D numerical finite element modeling (FEM) tools will be utilized during a Martian habitat's analysis and development phase; the Karamba3D structural analysis tool will be integrated into the Grasshopper interface to synchronize the structural requirements of the habitation design.

6.4. Conclusion for a Space-resilient Design Methodology

This study aimed to develop a scientific methodology for designing a Mars habitat that can resist harsh conditions. As depicted in Figure 111, a machine learning-assisted generative design technique is developed to facilitate a practical and sustainable design cycle.

The developed design process contains ten steps for implementation. Initially, the designer generates an adjacency matrix by considering the design guide described in Chapter 4.

In the second stage, the matrix is defined as a graph network using Python's NetworkX package to represent spaces as nodes and interactions between spaces as lines. Then, the Social Network Analysis (SNA) algorithms are executed to analyze the network to reveal each space's degree and centrality measures to reconsider their positions in the network. If necessary, the adjacency matrix is justified to attend a space in a more or less crucial position in the network.

In the third phase, a semi-supervised community detection algorithm based on the Label Propagation Approach (LPA) is executed in Python to detect communities in the network representation of an adjacency matrix. The algorithm assigns a label to each of the network's nodes, and it concludes when all nodes are labeled based on their neighbors' labels; hence, several groups of nodes are identified by specifying different labels for each community.

In the fourth step, detected communities are suggested as floor plans for a habitation design solution. For example, if a detected community number equals 1, it means all spaces will be on the same floor, and a one-story horizontal habitation typology is a good design solution to keep all spaces on the same floor with the specified network relations. Otherwise, each community will be defined as a floor area by keeping the connections between spaces the same.

The discovered communities and their interconnections will be defined once in the generative design environment of Grasshopper during the fifth step. For community networks, it is suggested that space-syntax tools be used to display them as optimized bubble diagrams in a space-syntax context.

In the sixth phase, it is suggested to use a physics simulation to simulate disks of created bubble diagrams as colliding objects in order to develop more coherent representations. The relocated circles are then superimposed with a circle whose area is equal to the overall space represented by functional areas in the respective community.

In the seventh phase, the Voronoi pattern algorithm is carried out utilizing the superimposed circles and the areal circle to split the areal circle into spaces based on the orientation of the circle centers. The procedure will result in a circular region subdivision with a conclusion suitable for floor layouts.

The resulting floor plans are aligned in the Z direction to generate a lofted habitation form in the eighth step. The form will be automatically defined based on the outputs of the preceding processes.

In the ninth step, the produced form is offset by 1.5 m to create a dual shell-like Marsha habitat to define a circulation volume and void to disperse light to the lower floors.

In the final step of the design methodology, the outer layer of the dual shell is studied as a shell structure under the environmental loads of Mars, which were turned into design parameters in the preceding chapters. At this level, the primary objective of the design problem is to adapt architectural design processes to extreme parameters.

In the following chapter, several design implementations will be performed to describe the execution of the established design methodology in detail, thereby revealing the potential and limitations of the established process for future research.

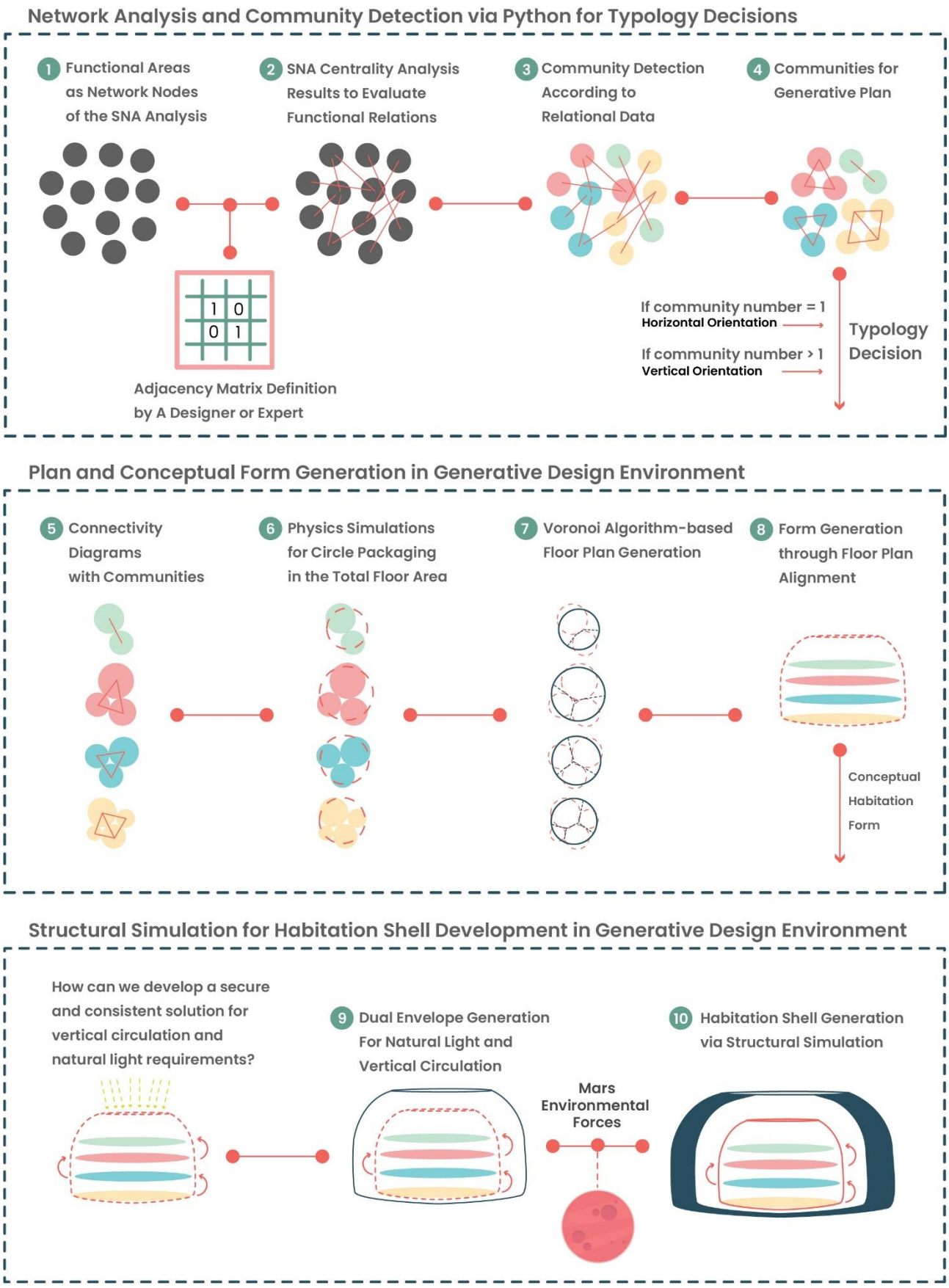

Figure 111. Machine learning-aided generative design methodology for a Mars habitation design process.

07th Chapter
DESIGN STUDIES : MACHINE LEARNING-AIDED HABITATION DESIGNS

In Chapter 7, the phases and results of an implemented design methodology are presented via three habitation design processes. This methodology tests and validates the output and workflow definitions of designers while they engage in real-time feedback prediction and interactive optimization in combination with performance-driven environments and fully automated optimization. Additionally, the section reveals the effects of each Mars' environmental force on designing three different habitation shells.

In the previous chapter, we introduced a novel methodology that automates the process of designing a habitation by utilizing generative design tools, Social Network Analysis (SNA), and Label Propagation Approach (LPA), a graph-based semi-supervised machine learning algorithm for detecting communities in a network.

In this chapter, three implementation studies are conducted to explain the continuous workflow involved in the developed methodology. The results are then compared to demonstrate the methodology's viability concerning the effects of extreme conditions on Mars' surface habitation that must be resistant to environmental challenges.

The methodology outlined in the preceding chapter will be implemented in three phases: habitation typology determination via community detection; plan and form generation via space syntax, physics simulations, and algorithmic design; and habitation shell generation via structural simulation employing Mars' environmental forces as design parameters. Initially, each design phase under three headings will be explained in detail, and the results of each environmental factor's impact on the habitation design process will be presented.

In conclusion, the generated habitations will be reviewed to highlight the design methodology's strengths and limitations and identify future research directions.

7.1. Habitation Typology Decision via Data Science Methodologies

In the first part of this section, we will introduce three different habitation adjacency matrices that may be used in conjunction with the python code block that will be introduced in the same section to perform SNA and LPA methodologies. The development approaches for adjacent matrices will also be briefly explained. Subsequently, the three adjacency matrices will be examined using the python syntax to reveal SNA and LPA findings. The second section assesses the results of an SNA performed on three habitation matrices to identify critical nodes in each network for planning habitation layouts. As a final step, the LPA-identified communities in the matrices will be analyzed to determine the habitation typologies before being fed into the generative design environment.

7.1.1. Methodology

The first step in implementing the habitation design methodology is the formulation of adjacency matrices of required functional relationships, which may be developed by a designer or an expert in space architecture. Each functional space as an id number is positioned in the row and column of a square matrix to create relations between spaces by the indicators of 0 and 1.

In the first matrix, as seen in Figure 112, functional spaces are related to a basic approach, which is considered a work or relaxation area. The working areas are strongly linked to establishing a compact working zone where all operational activities can be undertaken. Service areas like waste collection and management are likewise connected to these areas because their usage is typically required for working-related operations. The communal spaces with ID numbers 4 and 10 are considered connection points to other spaces. Moreover, relaxation spaces, including private areas, are interconnected from a private and a social aspect to aid crew members in maintaining their mental health.

Id	0	1	2	3	4	5	6	7	8	9	10	11	12	13	14	15	16	17
0	0	0	1	0	1	0	0	0	0	1	0	0	0	0	0	0	0	0
1	0	0	1	0	1	0	0	0	0	0	0	0	0	0	0	0	0	0
2	1	1	0	0	1	0	1	1	0	0	0	0	0	0	0	0	0	0
3	0	0	0	0	1	0	0	0	0	0	0	0	0	0	0	0	0	0
4	1	1	1	1	0	0	1	1	1	0	1	0	0	0	0	0	0	0
5	0	0	0	0	0	0	1	0	0	0	0	0	0	0	0	0	0	0
6	0	0	1	0	1	1	0	0	0	0	1	0	0	0	0	0	0	0
7	0	0	1	0	1	0	0	0	0	1	1	0	0	0	0	0	0	0
8	0	0	0	0	1	0	0	0	0	0	1	0	0	0	0	0	0	0
9	1	0	0	0	0	0	0	1	0	0	0	0	0	0	0	0	0	0
10	0	0	0	0	1	0	1	1	1	0	0	1	1	0	1	0	1	0
11	0	0	0	0	0	0	0	0	0	0	1	0	1	0	0	0	0	0
12	0	0	0	0	0	0	0	0	0	0	1	1	0	0	0	0	1	0
13	0	0	0	0	0	0	0	0	0	0	0	0	0	0	1	1	0	0
14	0	0	0	0	0	0	0	0	0	0	1	0	0	1	0	1	1	0
15	0	0	0	0	0	0	0	0	0	0	0	0	0	1	1	0	0	0
16	0	0	0	0	0	0	0	0	0	0	1	0	1	0	1	0	0	1
17	0	0	0	0	0	0	0	0	0	0	0	0	0	0	0	0	1	0

Id	Definition of Functional Areas	
0	Logistics-2 (Temporary Stowage)	Working Area
1	Maintenance-1 (Computer) / EVA-2 (EVA Computer/Data)	
2	Maintenance-2 (Work Surface) / Logistics-1 (Work Surface) / EVA-1 (Suit Testing)	
3	Mission Planning-2 (Computer/Command) / Spacecraft Monitoring	
4	Group Social-1 (Open Area) / Mission Planning-3 (Training)	
5	Medical-1 (Computer)	
6	Medical-3 (Medical Care)	
7	Human Waste-1 (Waste Collection)	
8	Human Waste-2 (Cleansing) / Hygiene-1 (Cleansing)	
9	Waste Management	
10	Group Social-2 (Table) / Meal Consumption / Mission Planning-1 (Table)	Relaxation Area
11	Meal Preparation-1 (Food Prep)	
12	Meal Preparation-2 (Work Surface)	
13	Exercise-1 (Cycle Ergometer)	
14	Exercise-2 (Treadmill)	
15	Exercise-3 (Resistive Device)	
16	Private Habitation-1 (Work Surface) / Medical-2 (Ambulatory Care)	
17	Private Habitation-2 (Sleep & Relaxation) / Hygiene-2 (Non-Cleansing)	

Figure 112. The adjacency matrix for the first design methodology implementation.

In the second matrix seen in Figure 113, management-related activities with IDs 0, 3, and 9 are isolated from other working and service-related spaces to distinguish communal mission activities from more personal and passive activities. The space with ID 10 is structured as a common area for relaxation activities, while the space with ID 4 is organized as a communal area for mission-related activities.

Id	0	1	2	3	4	5	6	7	8	9	10	11	12	13	14	15	16	17
0	0	0	1	1	1	0	0	0	0	1	0	0	0	0	0	0	0	0
1	0	0	1	0	1	0	0	0	0	0	0	0	0	0	0	0	0	0
2	1	1	0	0	1	0	1	1	1	0	1	0	0	0	0	0	0	0
3	1	0	0	0	1	0	0	0	0	0	0	0	0	0	0	0	0	0
4	1	1	1	1	0	0	1	1	1	0	1	0	0	0	0	0	0	0
5	0	0	0	0	0	0	1	0	0	0	0	0	0	0	0	0	0	0
6	0	0	1	0	1	1	0	0	0	0	1	0	0	0	0	0	0	0
7	0	0	1	0	1	0	0	0	0	1	1	0	0	0	0	0	0	0
8	0	0	1	0	1	0	0	0	0	0	1	0	0	0	0	0	0	0
9	1	0	0	0	0	0	0	1	0	0	0	0	0	0	0	0	0	0
10	0	0	1	0	1	0	1	1	1	0	0	1	1	1	1	1	1	0
11	0	0	0	0	0	0	0	0	0	0	1	0	1	0	0	0	0	0
12	0	0	0	0	0	0	0	0	0	0	1	1	0	0	0	0	0	0
13	0	0	0	0	0	0	0	0	0	0	1	0	0	0	1	1	1	0
14	0	0	0	0	0	0	0	0	0	0	1	0	0	1	0	1	1	0
15	0	0	0	0	0	0	0	0	0	0	1	0	0	1	1	0	1	0
16	0	0	0	0	0	0	0	0	0	0	1	0	0	1	1	1	0	1
17	0	0	0	0	0	0	0	0	0	0	0	0	0	0	0	0	1	0

Id	Definition of Functional Areas	
0	Logistics-2 (Temporary Stowage)	Working Area
1	Maintenance-1 (Computer) / EVA-2 (EVA Computer/Data)	
2	Maintenance-2 (Work Surface) / Logistics-1 (Work Surface) / EVA-1 (Suit Testing)	
3	Mission Planning-2 (Computer/Command) / Spacecraft Monitoring	
4	Group Social-1 (Open Area) / Mission Planning-3 (Training)	
5	Medical-1 (Computer)	Service Area
6	Medical-3 (Medical Care)	
7	Human Waste-1 (Waste Collection)	
8	Human Waste-2 (Cleansing) / Hygiene-1 (Cleansing)	
9	Waste Management	
10	Group Social-2 (Table) / Meal Consumption / Mission Planning-1 (Table)	Relaxation Area
11	Meal Preparation-1 (Food Prep)	
12	Meal Preparation-2 (Work Surface)	
13	Exercise-1 (Cycle Ergometer)	
14	Exercise-2 (Treadmill)	
15	Exercise-3 (Resistive Device)	
16	Private Habitation-1 (Work Surface) / Medical-2 (Ambulatory Care)	
17	Private Habitation-2 (Sleep & Relaxation) / Hygiene-2 (Non-Cleansing)	

Figure 113. The adjacency matrix for the second design methodology implementation.

In the third matrix, as depicted in Figure 114, the logistics, human waste collection, and waste management sections with corresponding IDs 0, 7, and 9 are grouped. Other work-related and service areas are organized around the ID 2 work area, which serves as a work surface and suits the testing area. In addition, spaces with IDs 2, 4, and 10 that serve as communal areas for work and relaxation purposes are vital for the continuation of functional configuration. The space with ID 4 is located between spaces with IDs 2 and 10 as a bridge between work and relaxation areas, while other spaces, including private zones, meal preparation areas, and exercise areas, are accessible via space with ID 10.

Id	0	1	2	3	4	5	6	7	8	9	10	11	12	13	14	15	16	17
0	0	0	1	0	0	0	0	0	0	1	0	0	0	0	0	0	0	0
1	0	0	1	1	0	0	0	0	0	0	0	0	0	0	0	0	0	0
2	1	1	0	1	1	0	1	0	0	0	0	0	0	0	0	0	0	0
3	0	1	1	0	0	0	0	0	0	0	0	0	0	0	0	0	0	0
4	0	0	1	0	0	0	1	0	0	0	1	0	0	0	0	0	0	0
5	0	0	0	0	0	0	1	0	0	0	0	0	0	0	0	0	0	0
6	0	0	1	0	1	1	0	0	0	0	0	0	0	0	0	0	0	0
7	0	0	0	0	0	0	0	0	0	1	0	0	0	0	0	0	0	0
8	0	0	0	0	0	0	0	0	0	0	1	0	0	0	0	0	1	1
9	1	0	0	0	0	0	0	1	0	0	0	0	0	0	0	0	0	0
10	0	0	0	0	1	0	0	0	1	0	0	1	1	0	1	0	1	1
11	0	0	0	0	0	0	0	0	0	0	1	0	1	0	0	0	0	0
12	0	0	0	0	0	0	0	0	0	0	1	1	0	0	0	0	0	0
13	0	0	0	0	0	0	0	0	0	0	0	0	0	0	1	1	0	0
14	0	0	0	0	0	0	0	0	0	0	1	0	0	1	0	1	0	0
15	0	0	0	0	0	0	0	0	0	0	0	0	0	1	1	0	0	0
16	0	0	0	0	0	0	0	0	1	0	1	0	0	0	0	0	0	1
17	0	0	0	0	0	0	0	0	1	0	1	0	0	0	0	0	1	0

Id	Definition of Functional Areas	
0	Logistics-2 (Temporary Stowage)	Working Area
1	Maintenance-1 (Computer) / EVA-2 (EVA Computer/Data)	
2	Maintenance-2 (Work Surface) / Logistics-1 (Work Surface) / EVA-1 (Suit Testing)	
3	Mission Planning-2 (Computer/Command) / Spacecraft Monitoring	
4	Group Social-1 (Open Area) / Mission Planning-3 (Training)	
5	Medical-1 (Computer)	Service Area
6	Medical-3 (Medical Care)	
7	Human Waste-1 (Waste Collection)	
8	Human Waste-2 (Cleansing) / Hygiene-1 (Cleansing)	
9	Waste Management	
10	Group Social-2 (Table) / Meal Consumption / Mission Planning-1 (Table)	Relaxation Area
11	Meal Preparation-1 (Food Prep)	
12	Meal Preparation-2 (Work Surface)	
13	Exercise-1 (Cycle Ergometer)	
14	Exercise-2 (Treadmill)	
15	Exercise-3 (Resistive Device)	
16	Private Habitation-1 (Work Surface) / Medical-2 (Ambulatory Care)	
17	Private Habitation-2 (Sleep & Relaxation) / Hygiene-2 (Non-Cleansing)	

Figure 114. The adjacency matrix for the third design methodology implementation.

After developing the adjacency matrices, they must be analyzed with Social Network Analysis (SNA) and Label Propagation Approach (LPA) to evaluate spaces and connections between them to assist habitation layout and form generation phases in the generative design processes. During the analysis phase, the Python environment uses the NetworkX module to perform SNA and LPA. Since the Python syntax used in this chapter was looked at in detail in Chapter 4, only a short explanation will be given along with the syntax.

Python's built-in libraries must be installed before the script can do tasks such as reading and editing data, creating and analyzing networks, identifying communities within networks, and displaying data. The pandas library in Python is used to read the habitation matrix. Defining the syntax of SNA and LPA algorithms as a function is necessary for generalizing the method to other matrices. Using the pandas package to transform the data into a data frame and the .iloc method to select values from the matrix, the function may be used repeatedly with different matrices with only a few changes to the source code.

To create a social network, we use the methods from the NetworkX package to the matrix data. The functional spaces are represented as network nodes, and the links between them are represented by edges, which can be colored and scaled to reflect the importance of the connections between them. Labeling the data based on the Excel data is necessary for displaying the results with the appropriate functional area labels following the workflow. Each index number in the matrix is accompanied by the name of an area, which we provided in the first row of the data frame.

Following this, the syntax lines of SNA are written to execute the analysis. Each node's centrality in a network can be calculated with just a few short lines of code using NetworkX's in-built functions. The produced values are standardized to a range of 0–1 so that the methods used to calculate betweenness, closeness, and eigenvector centralities can be compared across nodes with certainty.

Community detection is the next step in network analysis. Its goal is to reveal a complex network's structure, behavior, dynamics, and organization by locating distinct clusters of nodes (entities) that are similar to one another but different from others. The Label Propagation Algorithms (LPA), a semi-supervised machine learning approach, is used to detect communities in the generated network during the SNA process

The results of the SNA and LPA algorithms are exported as Gephi-compatible gexf files to view the findings in Gephi, network visualization, and exploration tool. In addition, the matplotlib python package permits exporting the resulting network graph as a png file. The findings and analyses will be extracted from Gephi to present them in a tabular format, and the network graph illustrated using the matplotlib library will be utilized to depict detected communities in the social network of matrices.

The steps can be executed in Python with the help of the code block that is provided following. In the preceding pages, we will also present the results obtained for the three matrices after they were evaluated using the SNA and LPA algorithms.

```
[1] import pandas as pd
[2] from operator import itemgetter
[3] import networkx as nx
[4] from networkx.algorithms.community.label_propagation import label_propagation_communities
[5] import matplotlib.pyplot as plt
[6] from matplotlib.pyplot import figure, text

[7] data=pd.read_excel("Habitation Matrix.xlsx")

[8] def Habitation_Analysis():
[9]     habitation_df=data.iloc[: , 1:]
[10]    habitation_matrix=habitation_df.values
[11]    habitation_graph=nx.from_numpy_matrix(habitation_matrix)
[12]    pos = nx.spring_layout(habitation_graph)
[13]    d = dict(habitation_graph.degree)
[14]    nx.draw(habitation_graph, pos=pos,node_color='lightgray', edge_color='darkgray',
[15]            with_labels=True,
[16]            node_size=[d[k]*260 for k in d])
[17]    label_keys=list(habitation_df.index.values)
[18]    label_values=list(habitation_df.head())
[19]    label = {}
[20]    for key in label_keys:
[21]        for value in label_values:
[22]            label[key] = value
[23]            label_values.remove(value)
[24]            break
[25]    habitation_graph = nx.relabel_nodes(habitation_graph, label)
[26]    degree_dict = dict(habitation_graph.degree(habitation_graph.nodes()))
[27]    nx.set_node_attributes(habitation_graph, degree_dict, 'Degree')
[28]    betweenness_dict = nx.betweenness_centrality(habitation_graph)
[29]    nx.set_node_attributes(habitation_graph, betweenness_dict, 'Betweenness Centrality')
[30]    closeness_dict = nx.closeness_centrality(habitation_graph)
[31]    nx.set_node_attributes(habitation_graph, closeness_dict, 'Closeness Centrality')
[32]    eigenvector_dict = nx.eigenvector_centrality(habitation_graph)
[33]    nx.set_node_attributes(habitation_graph, eigenvector_dict, 'Eigenvector Centrality')
[34]    communities = label_propagation_communities(habitation_graph)
[35]    community_label = {}
[36]    for i,a in enumerate(communities):
[37]        for name in a:
[38]            community_label[name] = i
[39]    nx.set_node_attributes(habitation_graph, community_label, 'Community Label')
[40]    nx.write_gexf(habitation_graph, ' Habitation _Quaker_network.gexf')

[41] Habitation_Analysis()
[42] plt.savefig("Habitation _Analysis.png", dpi=600, bbox_inches='tight')
[43] plt.show()
```

7.1.2.Findings of network analysis and community detection

Following the execution of the previously presented Python syntax, network analysis and community detection results reveal insightful information about defined habitation adjacency matrices that may be used to enhance habitation design phases. In this section, each matrix's findings will be examined separately to determine their respective habitation typology.

Table 22 displays the findings of SNA implementation for the first adjacency matrix, which reveals that spaces with IDs 4 and 10, which are mission-related and relaxation-related common spaces, have the highest degree of measures due to their eight interactions with other spaces. While space ID 10 has the highest betweenness and closeness centrality due to its position in the network, space ID 4 has the highest eigenvector centrality, indicating that its nearby nodes are also critical spaces in the network. In addition, space with ID 2, which functions as a workspace, logistics center, and suit testing location, has a high degree and centrality metrics compared to the other network nodes. In addition, the medical care space with ID 6 and the garbage collection space with ID 7 has a high degree of proximity and eigenvector centrality in the functional scenario of the first matrix due to their functional integration as service areas with other spaces. The treadmill space with ID 14 as an exercise area is established as a connection point for the other exercise areas in the matrix, which explains why its centrality measures are higher than others. The room with ID 16, which works as a private workplace and ambulatory care, is another significant network node in terms of its degree and closeness centrality. Degree and centrality measures are lowest for spaces with IDs 3, 5, and 17, which only have a single connection to other spaces. That means they are reachable from a single location and the most private locations on the network.

Table 22. The SNA findings for the first habitation adjacency matrix.

Id	Label	Degree	Betweenness Centrality	Closeness Centrality	Eigenvector Centrality	Community Label
4	Group Social-1 (Open Area) / Mission Planning-3 (Training)	8	0.331863	0.586207	0.477358	0
10	Group Social-2 (Table) / Meal Consumption / Mission Planning-1 (Table)	8	0.576471	0.653846	0.445829	1
2	Maintenance-2 (Work Surface) / Logistics-1 (Work Surface) / EVA-1 (Suit Testing)	5	0.038971	0.435897	0.336461	0
6	Medical-3 (Medical Care)	4	0.137255	0.5	0.300704	0
7	Human Waste-1 (Waste Collection)	4	0.106863	0.5	0.312119	0
14	Exercise-2 (Treadmill)	4	0.220588	0.472222	0.165442	1
16	Private Habitation-1 (Work Surface) / Medical-2 (Ambulatory Care)	4	0.128676	0.472222	0.187787	1
0	Logistics-2 (Temporary Stowage)	3	0.023039	0.404762	0.211149	0
12	Meal Preparation-2 (Work Surface)	3	0.007353	0.435897	0.175362	1
1	Maintenance-1 (Computer) / EVA-2 (EVA Computer/Data)	2	0	0.386364	0.18431	0
8	Human Waste-2 (Cleansing) / Hygiene-1 (Cleansing)	2	0	0.459459	0.20908	1
9	Waste Management	2	0.002451	0.354167	0.118507	0
11	Meal Preparation-1 (Food Prep)	2	0	0.414634	0.140686	1
13	Exercise-1 (Cycle Ergometer)	2	0	0.333333	0.04844	1
15	Exercise-3 (Resistive Device)	2	0	0.333333	0.04844	1
3	Mission Planning-2 (Computer/Command) / Spacecraft Monitoring	1	0	0.377778	0.10811	0
5	Medical-1 (Computer)	1	0	0.34	0.068102	0
17	Private Habitation-2 (Sleep & Relaxation) / Hygiene-2 (Non-Cleansing)	1	0	0.326923	0.04253	1

In addition to SNA results, the conclusion of the community detection algorithm for the first matrix revealed the segmentation of functional areas within the network. As depicted in Figure 115, the network consists of two discrete communities that can be partitioned to serve as independent functional zones in the first habitation matrix.

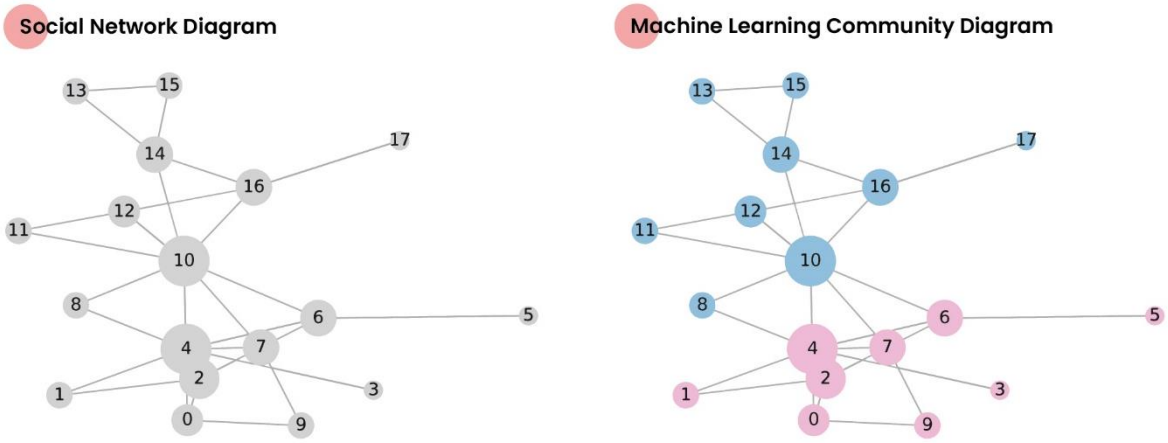

Figure 115. The community detection results for the first habitation adjacency matrix.

To automate design decisions for habitation typology, we suggest employing detected communities as floor areas of habitation while reserving the inner connections of spaces within detected communities. In the generative design environment, each community's network is generated as a diagrammatic floor plan to create a two-story habitation typology. Additionally, the total floor area is automatically computed based on the corresponding areas in each community, and the floor height is determined by the highest height requirement in each community.

Table 23 presents the results of the SNA for the second habitation adjacency matrix, which reveals that space with ID 10 has the highest degree with eleven connections to other nodes, as well as the highest ranking in all types of centrality measures, indicating that it is a key and hub node in the network. The other key node in the network is in the space with ID 4, which has eight connections to other spaces. Its betweenness centrality is much lower than that of the space with ID 10, but it is still the second-highest betweenness measure in the network. Its closeness and eigenvector measures show that it is accessible from other spaces and has important neighbors in the network. The space with ID 2 ranks third in the degree analysis, with seven links to other spaces, and its closeness and eigenvector values indicate that its position in the network is significant. The space with ID 16 in this network, which acts as a private space for working and ambulatory care, is linked to five other spaces and has a high degree of closeness centrality. Both the degree and centrality measures are lowest for the spaces with ids 5 and 17, which have only a single connection. The medical area's computer room is designated ID 5, whereas the sleeping, relaxing, and cleaning areas are designated ID 7. They provide the highest level of privacy in the network.

Table 23. The SNA findings for the second habitation adjacency matrix.

Id	Label	Degree	Betweenness Centrality	Closeness Centrality	Eigenvector Centrality	Community Label
10	Group Social-2 (Table) / Meal Consumption / Mission Planning-1 (Table)	11	0.604902	0.73913	0.493393	2
4	Group Social-1 (Open Area) / Mission Planning-3 (Training)	8	0.214706	0.62963	0.382708	1
2	Maintenance-2 (Work Surface) / Logistics-1 (Work Surface) / EVA-1 (Suit Testing)	7	0.115441	0.607143	0.365744	1
16	Private Habitation-1 (Work Surface) / Medical-2 (Ambulatory Care)	5	0.117647	0.5	0.227364	2
6	Medical-3 (Medical Care)	4	0.117647	0.53125	0.244492	1
7	Human Waste-1 (Waste Collection)	4	0.083088	0.53125	0.251131	1
13	Exercise-1 (Cycle Ergometer)	4	0	0.485714	0.220481	2
14	Exercise-2 (Treadmill)	4	0	0.485714	0.220481	2
15	Exercise-3 (Resistive Device)	4	0	0.485714	0.220481	2
0	Logistics-2 (Temporary Stowage)	4	0.030882	0.435897	0.177675	0
8	Human Waste-2 (Cleansing) / Hygiene-1 (Cleansing)	3	0	0.5	0.235686	1
11	Meal Preparation-1 (Food Prep)	2	0	0.447368	0.115574	2
12	Meal Preparation-2 (Work Surface)	2	0	0.447368	0.115574	2
3	Mission Planning-2 (Computer/Command) / Spacecraft Monitoring	2	0	0.414634	0.106353	0
1	Maintenance-1 (Computer) / EVA-2 (EVA Computer/Data)	2	0	0.404762	0.142046	1
9	Waste Management	2	0.002451	0.377778	0.081381	0
5	Medical-1 (Computer)	1	0	0.354167	0.046401	1
17	Private Habitation-2 (Sleep & Relaxation) / Hygiene-2 (Non-Cleansing)	1	0	0.34	0.043151	2

The conclusion of the community detection algorithm for the second matrix also showed how the network was broken into functional areas. As indicated in Figure 116, the network consists of three distinct communities that can be partitioned to serve as separate functional zones in the second habitation matrix. The first community in the second habitation matrix comprises spaces with IDs 0, 3, and 9, which are logistics, command, monitoring, and waste management areas. While the second community includes spaces with IDs 1, 2, 4, 5, 6, 7, and 8, which are areas for maintenance, mission planning, medical, cleansing, and waste collection, the third community consists of spaces with IDs from 10 to 17, which are for meal preparation and consumption, exercise, and private work and relaxation spaces. It is possible to create a three-story habitation typology with corresponding areas of function in each community if the network for each community is established in the generative design environment as a diagrammatic floor plan.

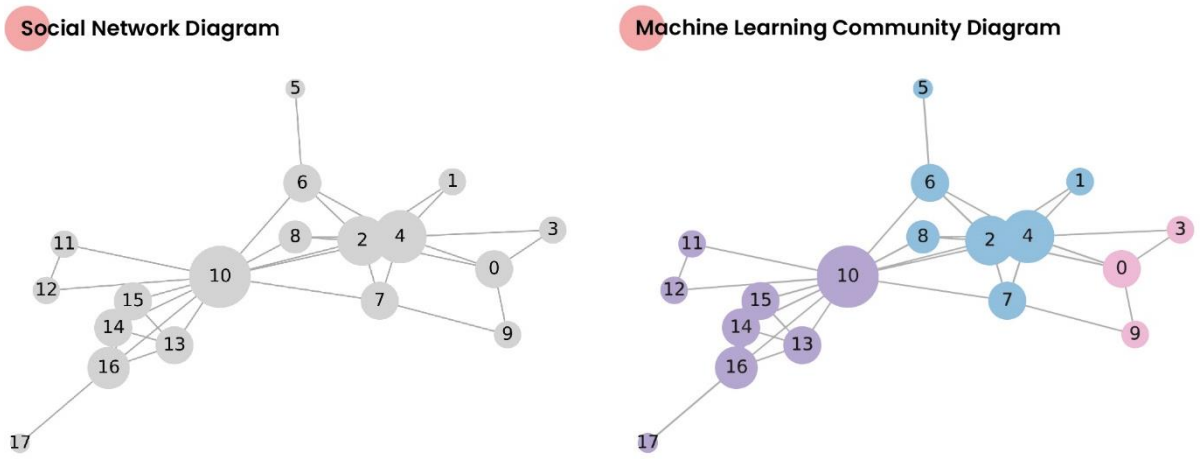

Figure 116. The community detection results for the second habitation adjacency matrix.

As can be seen in Table 24, the SNA for the third habitation adjacency matrix reveals that space with ID 10 has the highest degree of connectivity with seven connections to other nodes and the highest ranking in all types of centrality measures, indicating that it is a vital and significant connector node in the network. The other key node in the network is in the space with ID 2, which has five connections to other spaces. Its centrality measures are lower than the space with ID 4, which has three connections to other spaces. The space with ID 4 as a common area for missions has the second highest betweenness and closeness measures, and the spaces with IDs 8, 16, and 17 as hygiene and private working and relaxing spaces have the second highest eigenvector centralities. The medical space with ID 6 in this network is connected to three other spaces and has the third highest degree of closeness centrality. The space with ID 7 has the lowest degree and centrality measures because it only has one connection and is used to collect waste.

Table 24. The SNA findings for the third habitation adjacency matrix.

Id	Label	Degree	Betweenness Centrality	Closeness Centrality	Eigenvector Centrality	Community Label
10	Group Social-2 (Table) / Meal Consumption / Mission Planning-1 (Table)	7	0.683824	0.472222	0.569952	2
2	Maintenance-2 (Work Surface) / Logistics-1 (Work Surface) / EVA-1 (Suit Testing)	5	0.485294	0.425	0.1455	1
4	Group Social-1 (Open Area) / Mission Planning-3 (Training)	3	0.529412	0.472222	0.235954	1
6	Medical-3 (Medical Care)	3	0.117647	0.386364	0.117487	1
8	Human Waste-2 (Cleansing) / Hygiene-1 (Cleansing)	3	0	0.34	0.372489	2
14	Exercise-2 (Treadmill)	3	0.220588	0.354167	0.208039	3
16	Private Habitation-1 (Work Surface) / Medical-2 (Ambulatory Care)	3	0	0.34	0.372489	2
17	Private Habitation-2 (Sleep & Relaxation) / Hygiene-2 (Non-Cleansing)	3	0	0.34	0.372489	2
0	Logistics-2 (Temporary Stowage)	2	0.220588	0.326923	0.045158	0
1	Maintenance-1 (Computer) / EVA-2 (EVA Computer/Data)	2	0	0.309091	0.05751	1
3	Mission Planning-2 (Computer/Command) / Spacecraft Monitoring	2	0	0.309091	0.05751	1
9	Waste Management	2	0.117647	0.257576	0.013909	0
11	Meal Preparation-1 (Food Prep)	2	0	0.333333	0.225267	2
12	Meal Preparation-2 (Work Surface)	2	0	0.333333	0.225267	2
13	Exercise-1 (Cycle Ergometer)	2	0	0.269841	0.082225	3
15	Exercise-3 (Resistive Device)	2	0	0.269841	0.082225	3
5	Medical-1 (Computer)	1	0	0.283333	0.033282	1
7	Human Waste-1 (Waste Collection)	1	0	0.207317	0.00394	0

The conclusion of the community detection algorithms for the third matrix also indicated the network's functional area categorization (see Figure 117). The network consists of four distinct communities, corresponding to distinct functional zones in the third habitation matrix. The first community in the third habitation matrix consists of logistics, waste collection, and waste management spaces with IDs 0, 7, and 9, respectively. In the second community, areas with IDs 1, 2, 3, 4, 5, and 6 are designated for maintenance, mission planning, and medical care. In the third community, areas with IDs 8, 10, 11, 12, 16, and 17 are used for hygiene, meal preparation, and consumption, and private habitation spaces for work and relaxation. The exercise areas with IDs 13, 14, and 15 are indicated in the fourth community. Assuming the network for each community is established as a diagrammatic floor plan in the generative design environment, it is possible to develop a four-story habitation typology with corresponding functional zones.

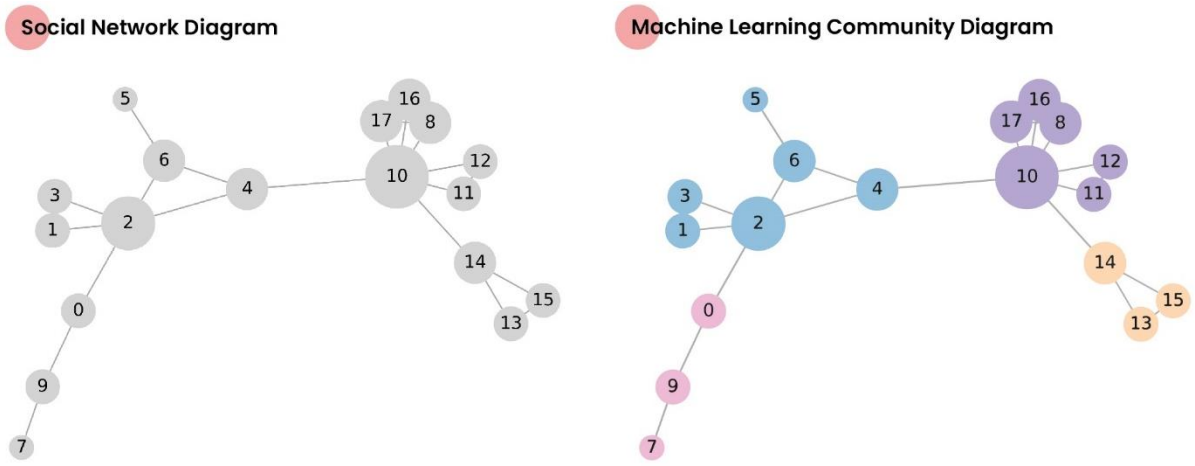

Figure 117. The community detection results for the third habitation adjacency matrix.

7.1.3. Conclusion of the habitation typology decision methodology

The results of SNA analysis reveal the most critical spaces in the habitation adjacency matrices, specifically the hub or key locations, those areas that play a significant role in sustaining the operation of many other activities. Additionally, the analyses identify the most communal and private spaces for design considerations throughout the phase of habitation layout planning. Additionally, the analyses identify the most communal and private spaces for design considerations throughout the phase of habitation layout planning.

The data from the execution of the community detection algorithm for three distinct habitation adjacency matrices reveals that functional communities in a functional network may differ because of defined relations via adjacency matrices. However, the community detection algorithm provides possible results for each case to group functions following the scenario defined with adjacency matrices. It specifies distinct communities for different functional configurations in matrices. Therefore, it is proposed that the communities within the networks be used to define habitation floor plans for three different habitation typologies with two, three, and four floors.

7.2. Habitation Plan and Form Generation via Generative Design

This section aims to define habitation layouts for the adjacency matrices created and explored in the previous section and to create the forms of habitable volumes for generating habitation shells in the following phases.

Using volume and height data for a 4-crew habitation from the research of Stromgren et al. in 2020 and community network data from the last section, the floor plans of three habitation matrices will be generated using space syntax and physics simulation tools with a Voronoi pattern algorithm. First, the space-syntax phases and their corresponding algorithms will be shown, followed by a demonstration of the reasoning of physics simulations using the Kangaroo Physics engine simulation

tools. Following the conclusion of the simulation, the Voronoi approach will be used to shape early design representations of habitation floor plans. In this research study, the executive design level of habitation layouts is not a focus. Therefore, the generated preliminary layouts will not be investigated for further details, but their floor boundaries will be employed to generate a lofted form to describe an autonomous form-generating process. The process will generate two-, three-, and four-story habitation forms using an algorithmic methodological approach. The preliminary forms of habitations will be used for establishing dual habitable shells.

7.2.1. Methodology

Syntactic, a generative space-syntax tool, develops the best-integrated functional configuration based on specified architectural requirements. A diagram depicting a floor plan based on space syntax analysis begins with the design of a connectivity diagram corresponding to the floor plan. Using the algorithm depicted in Figure 118, the architectural requirements obtained from Stromgren et al. for a 4-crew habitation in 2020 will be imported into the generative design environment as architectural requirements.

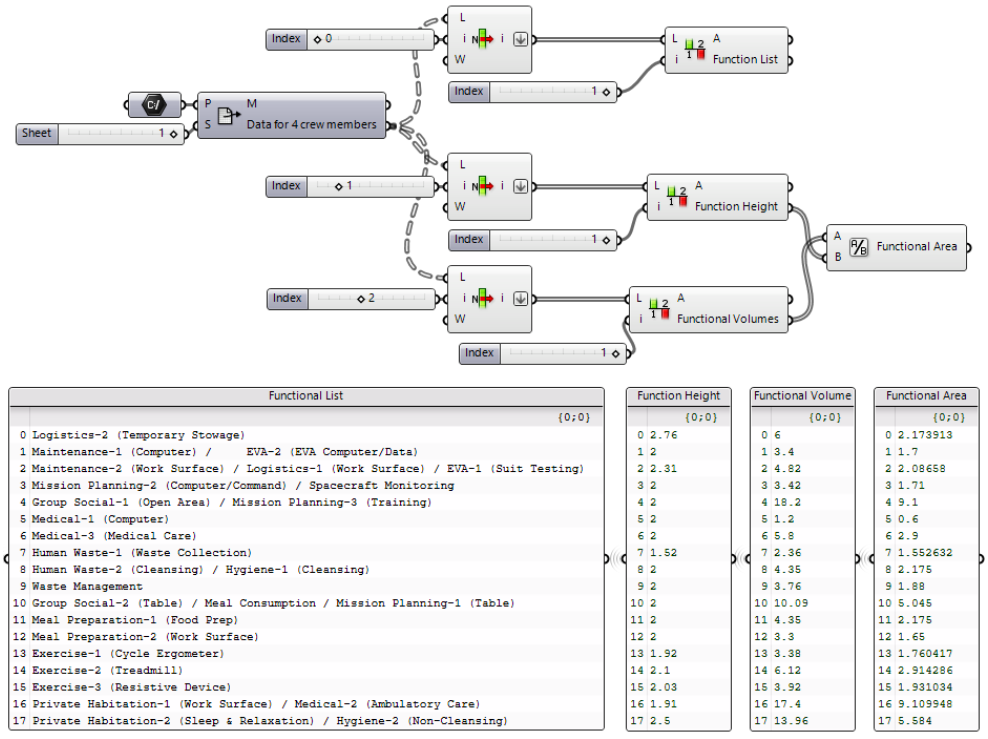

Figure 118. Data importing grasshopper algorithm.

Each architectural requirement will be represented by one point out of 18 points that will be created randomly. These points serve as the center points of the functional spaces defined by the designer. Then, designers connect the points they consider should be directly related using lines. According to the community networks of each habitation matrix, the proposed habitation design methodology constructs the connection lines between points. These connection lines will eventually

result in establishing rooms with direct access to one another. In the last stage, points, lines, area labels, and associated values are input parameters for the "Graph from Nodes and Links" component to construct the connection diagram. The created connectivity diagram generates the community network's associated bubble diagram. Figure 119 depicts the algorithm for generating the connectivity diagram of the first matrix's initial community network.

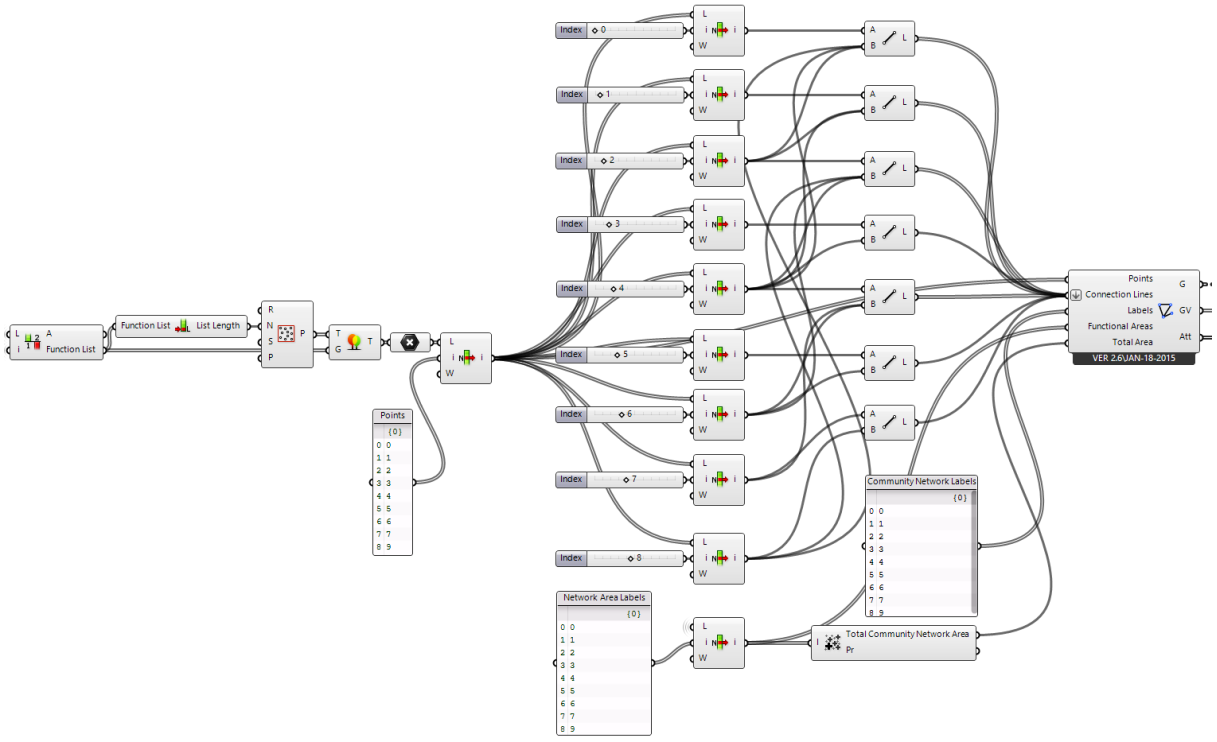

Figure 119. The connectivity diagram algorithm for the first community network in the first adjacency matrix.

As shown in Figure 120, generated connectivity diagrams are used as input data to define force-directed bubble diagrams of floor plans to find the most integrated and homogeneous layout output with space-syntax theory.

The next step is the transformation of bubble diagrams into preliminary floor plans to create a pressure-vessel form morphology to develop a habitation based on human factors. Circles generated from the space-syntax diagram can be considered a surface area of each functional zone. However, The created space-syntax diagram contains gaps and overlapping areas and lacks a barrier defining the habitation site to maximize the integrated layout while minimizing the total area. Shape-finding methodologies must be modified to transform the resulting bubble diagram into an operational floor plan.

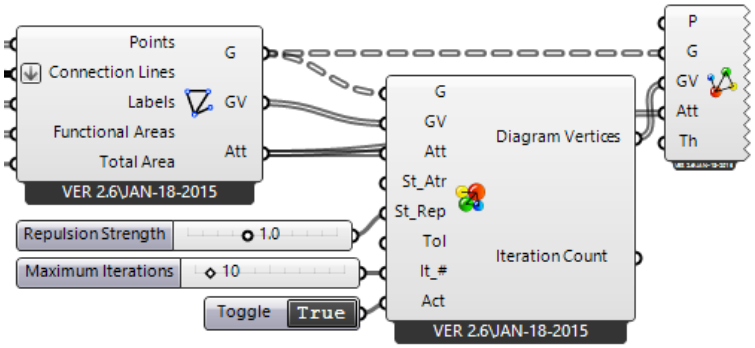

Figure 120. The parametric algorithm for bubble diagram generation.

The initial objective of converting a diagram to a habitation layout is to demonstrate a method for employing collision simulation methods in conjunction with geometric modifications that preserve the diagram's tangency characteristic to generate more precise habitation diagrams for the layout design process.

The Kangaroo physics engine enables designers to customize collision simulation to address physical phenomena. This project defines collision objects using circles from the bubble diagram and generated network lines. The network lines will pull the circles smoothly to converge, and circles will collide until they finally stop moving to create more homogenous diagrams to fit into a boundary definition. The lengths of the network lines are minimized to limit each circle's movable area and preserve the spatial relations between circles.

Figure 121 demonstrates that the center points of the circles in the bubble diagram are defined as inputs of the Collider component to generate collision circles with the corresponding radius values, and the network lines that have been defined with the same relationships as the adjacency matrix for relocated points are imported into collision simulation via the Length component to maintain the adjacency relationships in the diagram and to use the lengths of connection lines as a pulsing factor. In addition, the center points of the bubble diagram are used as input for the OnPlane component to maintain the points' position on the XY plane.

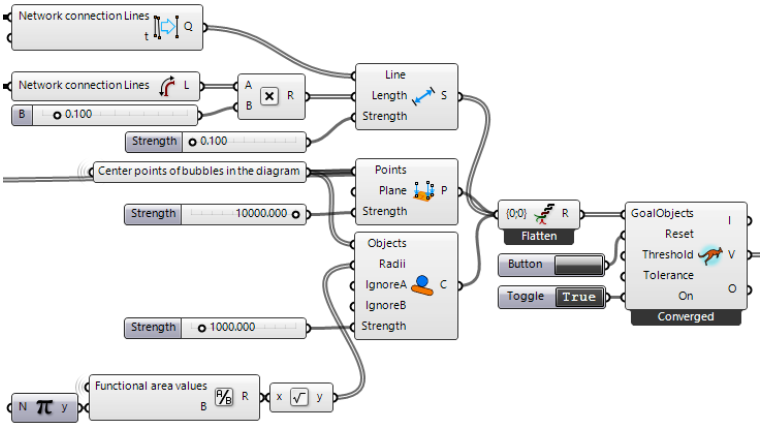

Figure 121. Parametric algorithm for the collision simulation in the habitation design methodology.

Following the completion of the collision simulation, the relocated circles must be turned into a preliminary floor plan with pressure-vessel geometrical considerations. The case studies studied in the fifth chapter use a circular floor typology to meet the inner volume pressurization requirements and to accommodate the low atmospheric pressure of Mars, which is why we recommended defining circular floor designs. The total area of functional spaces within the same community network will decide the circular area of floor designs. The bubbles generated by the collision simulation will be adjusted to fit within the circular boundary with the corresponding area. This step's objective is not to create well-solved floor plans, as this may be accomplished in traditional approaches if there is sufficient floor space. Instead, the objective is to develop a holistic strategy for habitation design.

In the subsequent phase of the methodology, a superimposition algorithm is used to align the centers of circular boundary curves and the group of functional bubbles to execute a Voronoi pattern tool that generates a representation of bubbles as a Voronoi pattern within the bounding box of the circular floor area. The Voronoi pattern depicts the relationship between a set of points on a plane in two dimensions. Each point corresponds to a region known as a Voronoi cell; the distance between the points specifies that. The area occupied by each point diminishes as the distance between them decreases. After generating a Voronoi pattern in the bounding rectangle of the circular floor area, a trimming operation is executed to obtain Voronoi segmentation within the circular floor area. Implementing the algorithm in Figure 122 separates a floor plan's functional spaces.

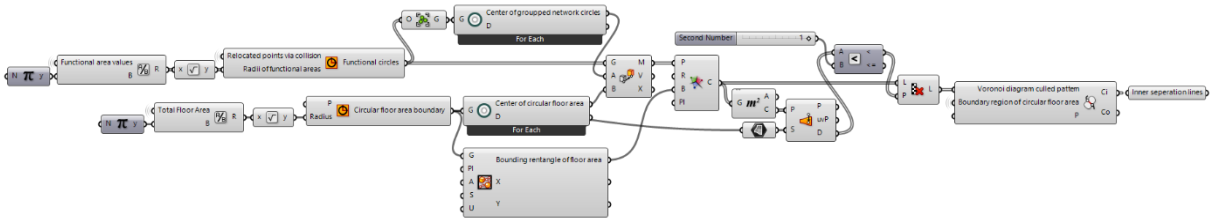

Figure 122. An algorithm for converting collusion bubbles into Voronoi-separated preliminary floor layouts.

The resultant geometries of Voronoi-separated preliminary floor plans are aligned in the z direction with the floor heights using data from Stromgren et al. (2020). The floor thickness is set as 20 centimeters, and the floor height is calculated based on the functional space with the highest height requirement in the corresponding floor plan. The alignment of floor plans is conducted generatively to create a lofted geometry using the circular boundaries of floor plans. The lofted form of the habitation is revealed as a result of a generatively conducted process. The adjacency matrix is used to create a social network graph which is used to detect the community number in the network of a floor plan to specify the floor number of a habitation; the number and area values of corresponding spaces in the community define the total circular area of a floor plan. The generated circular floor plans are aligned from bottom to top following operational, privacy, and crew health considerations.

After aligning the boundary curves of the floor plans and the habitation's top curve, which is made by scaling the boundary curve of the top floor plan by 50% in the x and y directions to narrow the top of the habitation form to reduce the risks of the additive construction process, limit direct light from the top, and increase structural stability, the curves are put into the loft tool to create a lofted habitable volume as a preliminary habitation. The algorithm depicted in Figure 123 is the loft-generating algorithm for the first adjacency matrix.

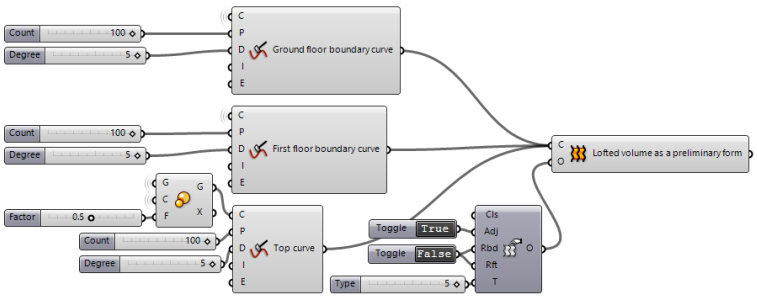

Figure 123. Form generation via loft algorithm for the first adjacency matrix.

7.2.2. Results for layout and form generation phases

This section shows the layout and form generation processes for three predefined adjacency matrices. Following the previously described methods, two-, three-, and four-story habitation forms are generated at a preliminary level. Figure 124 depicts the outcomes of the initial adjacency matrix, which consists of two communities. Each community's data is incorporated into the generative layout design process. First, space-syntax diagrams are constructed, and then bubble diagrams are utilized to simulate collision simulations to reduce overlapping spaces and produce more consistent diagram illustrations. Then, the centers of grouped circles and the whole circular area are overlapped to conduct a Voronoi algorithm using the relocated circle centers. As a result, preliminary floor designs based on Voronoi are developed as functional spaces. The resulting floor plans are z-aligned from their center points with the maximum height requirement of corresponding spaces in each community, and a three-dimensional geometry as a two-story preliminary habitation form is generated for further investigation.

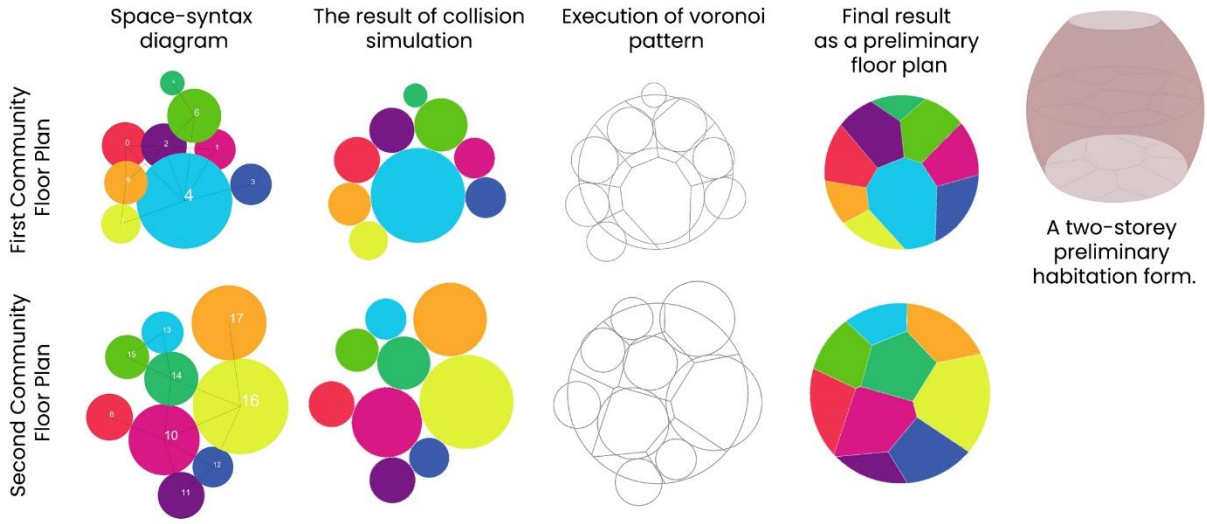

Figure 124. The layout and form generation results for the first adjacency matrix

The second adjacency matrix's design and development processes are illustrated in Figure 125. Using the same iterative method, a three-story habitation form is created. The data from each community is used to create the bubble diagrams. By simulating collisions, bubble diagrams can lessen the amount of overlapped space and provide more uniform diagram depictions. A Voronoi approach is applied to adjacent circles to create preliminary floor plans. The resulting floor plans are then aligned in the z-axis from their respective centers with the maximum height requirement of each community, and a three-dimensional conceptual shape is generated for future study.

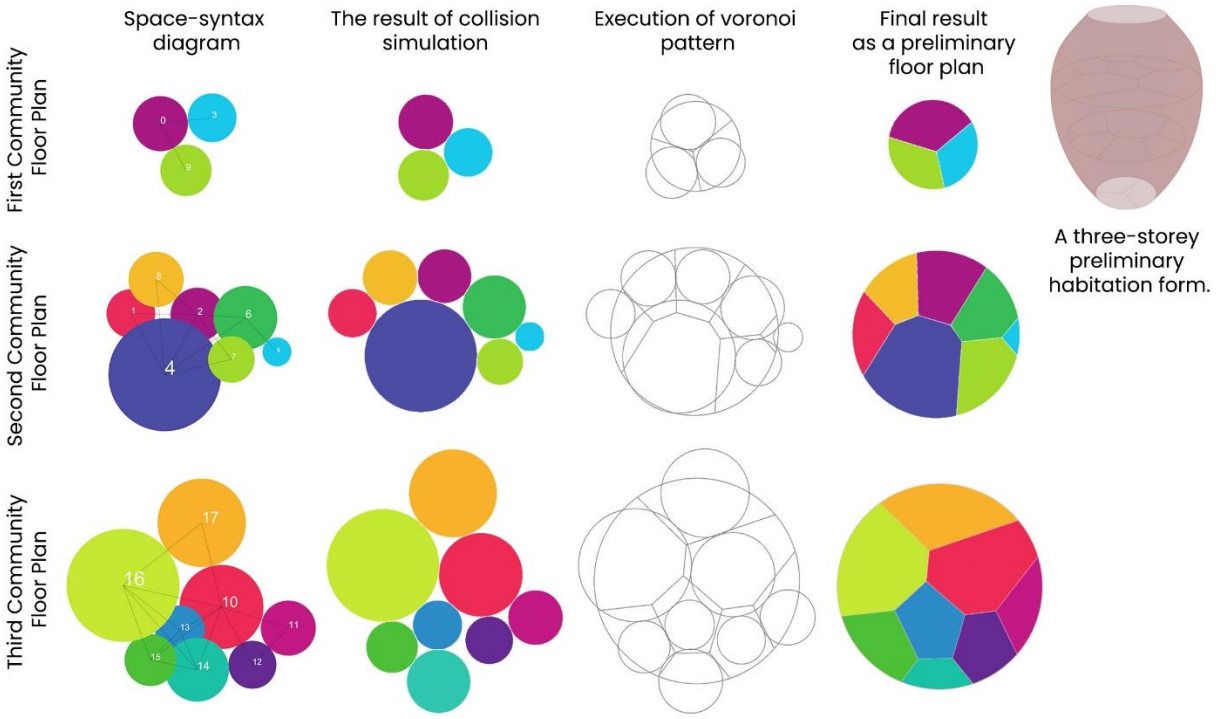

Figure 125. The layout and form generation results for the second adjacency matrix

Figure 126 displays the layout and form generation results for the third adjacency matrix, which has four communities. The same approach is used to develop floor plans for habitation and create a three-dimensional geometry, a four-story preliminary habitation form.

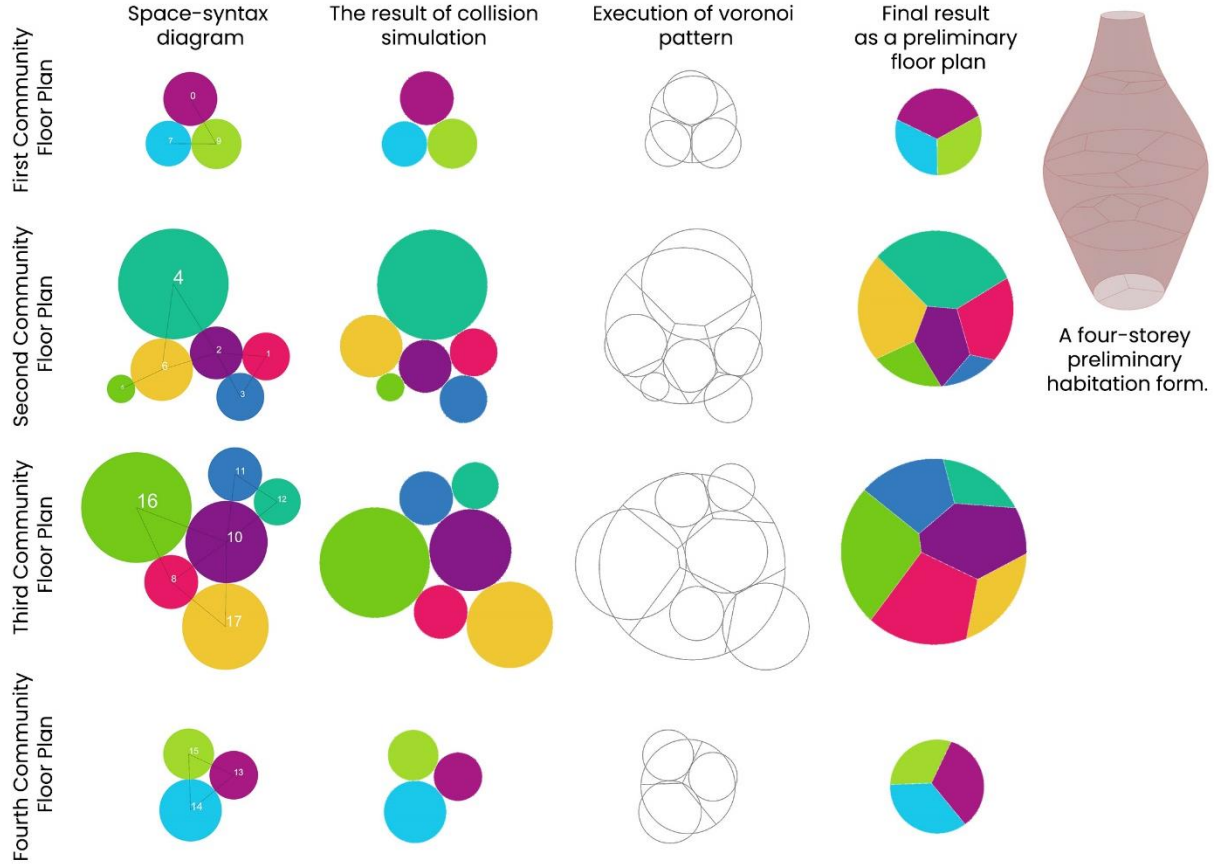

Figure 126. The layout and form generation results for the third adjacency matrix

7.3. Habitation Shell Generation Using Environmental Forces of Mars

Following the development of an initial form for habitation, the next step in the design process is to create the structure's exterior shell. Mars' surface radiation is significantly more than what the human body can withstand, and its atmosphere is far thinner than Earth's. Due to extreme cold and day-to-day and seasonal temperature variations, the planet is inhospitable for even an instant. Seasonal changes on Mars' surface also cause dust storms. The crew's safety is paramount, so the habitat's design should prioritize crew security.

The fifth chapter explores the basic concepts underlying the 3D-printed Mars habitation projects submitted to NASA. Both the Mars Ice House and the Marsha appear to have a double-shell structure, with the latter offering additional insulation from the environment. The additional volume between the shells not only spreads light to the lowest level of habitation but also offers additional security against external threats and could be utilized as a garden to rest or as a circulation zone to reach the upper floors. The generated preliminary habitation form might be employed as the inhabited interior of a dual habitation shell like Marsha because it was created according to functional specifications. The crew would then be protected from the dangerous environment of Mars by using the preliminary geometry of inner habitation to make an outer shell.

The design or formulation of the internal volume or its envelope does not require any special considerations for the severe Martian climate, and they can be created from any 3D-printable material. However, the outer layer must provide powerful protection against extreme stress scenarios. So, the next step is to build an outer shell for the habitat using environmental stresses common in Mars' cold climate.

When the inner habitation form is enlarged by 150 cm, the outer shell boundary for the second layer of a dual habitation envelope is established. The space between the habitation layers is proposed to be used as a circulation volume for the installation of stairs created using additive manufacturing techniques; this will also allow for the smooth transmission of daylight from the top to lower levels of the habitation.

The external shell of habitation can be simulated using Karamba3D, considering the environmental factors described in the sixth chapter. During a Mars habitation shell's study and development phase, numerical finite element modeling (FEM) techniques are used to determine how environmental forces affect the shell.

7.3.1. Structural simulation setup in a Mars habitation shell design

A protective shield is critical for crewed missions to Mars to secure humans from the hostile environment. Environmental loads should be included in the design phase to ensure a sustainable design against Mars' extreme conditions. The generated interior volumes should serve as the basis for design generation, ensuring that the habitation is also sustainable for human comfort.

The environmental factors outlined in earlier chapters will be incorporated into a load case-based structural simulation. Karamba3D, a parametric structural engineering tool for finite element calculations to study spatial trusses, frames, and shells, will be implemented in the parametric design environment of Grasshopper, a plug-in for the 3D modeling software Rhinoceros, for the simulation.

The first phase is setting up the support type and positions on the bottom of the geometry. For habitation simulations, the supports must be described as fixed in the XY plane, and their placements must be established using the circumferential points of the base. The MeshToShell (Karamba3D) component is used to obtain mesh vertices, as shown in Figure 127. The obtained mesh vertices are filtered based on their Z-coordination to identify vertices with a value of zero, but the resulting points may be too close together. Therefore, an additional filtering tool (CullDuplicates) is utilized to eliminate duplicated points within 0.1 meters of the other point. As a result of the filtering procedure, twenty-five points are identified as the simulation's support points. The Support (Karamba) component defines the support conditions with six degrees of freedom (dofs), three rotational, and three translational. The six dofs depicted in Figure 127 are fixed to define a static result.

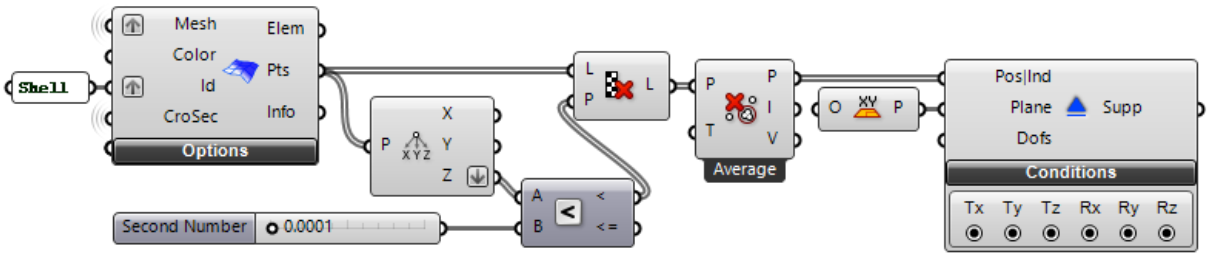

Figure 127. Fixed-support point definition algorithm.

The next step in structural modeling is the definition of environmental forces as load instances. Initially, the Karamba3D Load tool is used to define the gravity of Mars. As a default setting in Karamba3D, the gravity value indicates the gravity of the Earth as -1.00. While Earth's gravity is roughly 10 m/s^2, Mars' gravity contributes an acceleration of approximately 3.71 m/s^2 (van Ellen, 2018). As shown in Figure 128, gravity is defined as load case 0 with a value of 0.371 and a negative direction in the Z coordination plane.

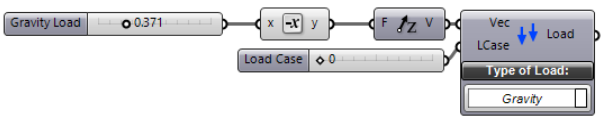

Figure 128. The load definition algorithm for the gravity on Mars via Karamba3D.

The second environmental load case to define is the atmospheric pressure of Mars, which is 600 Pa on average. As depicted in Figure 129, the atmospheric force, load case 1, is described with a value of 0.6 kN/m^2 as point loads on the mesh surface with a global orientation in the negative direction in the Z coordination plane.

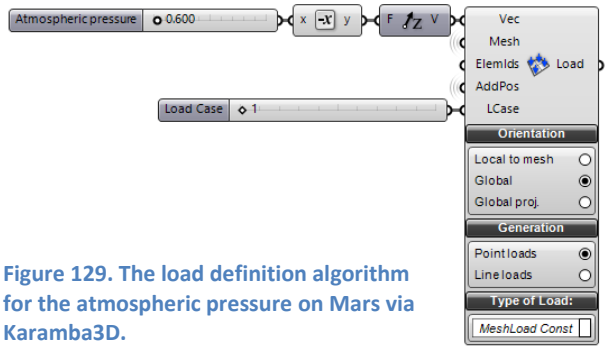

Figure 129. The load definition algorithm for the atmospheric pressure on Mars via Karamba3D.

The next load case seen in Figure 130 is defined as load case 2, which is the internal pressure of the Mars habitat. NASA suggests a minimum internal pressure of 52.67 kPa for everyday operations on Mars (Park et al., 2020). Load case 2 is defined with a 52.67 kN/m^2 value as point loads on the mesh surface with a global orientation in the positive direction in the Z coordination plane.

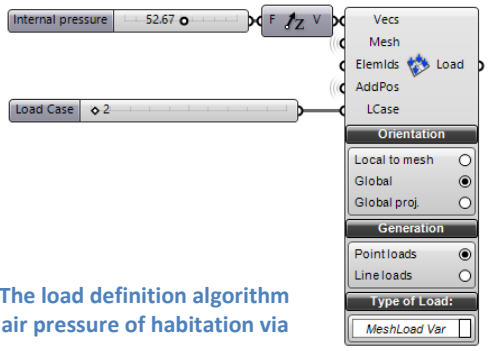

Figure 130. The load definition algorithm for internal air pressure of habitation via Karamba3D.

As indicated in the third chapter, Mars has reported wind speeds of up to 30 meters per second (Miscio, 2018), and the equation for dynamic pressure reveals that the maximal wind pressure on the surface of Mars is 9 Pa (9 N/m^2). The wind load, load case 3, as seen in Figure 131, is defined in the Y direction with a 0.009 kN/m^2 magnitude as a point load with a local orientation to the mesh surface.

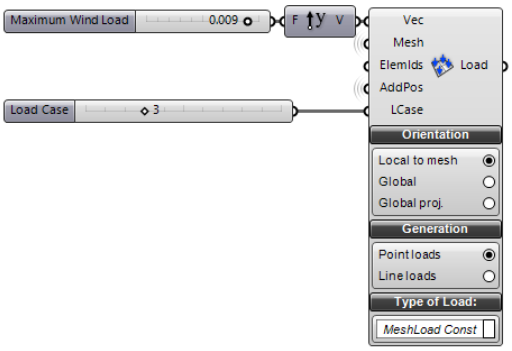

Figure 131. The load definition algorithm for wind pressure on Mars via Karamba3D.

In addition, the algorithms outlined in Figure 132 for the temperature loads are calculated independently for the lowest, average, and highest surface temperatures on Mars. The habitation is assumed to have a temperature of 25 °C. The habitat should feature a "shirt-sleeve environment," a term used in aircraft design to characterize the inside of an airplane in which no unique clothing is required.

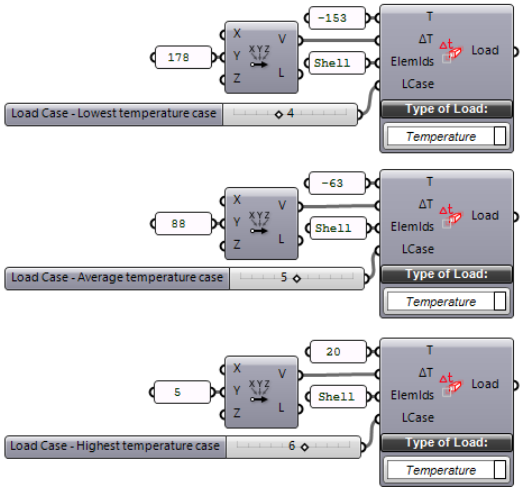

Figure 132. The load definition algorithms for temperature fluctuations on Mars via Karamba3D.

At the south pole of Mars, the lowest temperature recorded is -153 °C, resulting in a 178 °C temperature differential between the interior and exterior of the habitat. The average surface temperature of Mars is -63 °C, and even with average weather, there is an 88-degree temperature difference between the interior and exterior of the habitat. On the other side, the highest temperature ever recorded on Mars is 20°C at the planet's equator, and a location on the equator may provide thermal convenience for habitation construction, but water and ice resources become distant. Moreover, this temperature value does not persist for an extended period. The explained temperature variations are incorporated into the design process as load cases 4, 5, and 6 for the minimum, average, and maximum surface temperatures on Mars, respectively.

As was previously mentioned, the most significant ground velocity associated with seismic events is 1.2 x 10^{-5} meters per second. Mars' seismic activity can be factored into designs by being expressed as a percentage of the earth's gravitational effects. The magnitudes of earthquake shaking are expressed as a fraction of the force of gravity (% g) (USGS, 2022). The largest Marsquake yet recorded may have generated an acceleration of up to 12x10^{-4} cm/sec^{-2} relative to the acceleration of gravity. Thus, the magnitude of the shaking force is only 12.10^{-4}/980 g, or 0.0000012245 g, or 0.00012245% g, which is extremely low and should not be considered throughout the design process. However, the simulation includes the largest marsquake, load case 7, as seen in Figure 133, which has a magnitude of 0.0012 g in the X and Y directions.

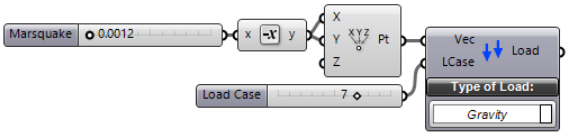

Figure 133. The load definition algorithm for Marsquakes on Mars via Karamba3D.

After defining environmental load cases, we must identify an in-situ material as the external habitation shell's construction material. Invented by Wan, Wendner, and Cusatis (2016), Martian concrete is a one-of-a-kind material for on-site construction. As Mars has always been a "planet rich in sulfur," it is composed of synthetic Martian soil material and molten sulfur. As depicted in Figure 134, Karamba3D specifies the features of sulfur concrete as a construction material.

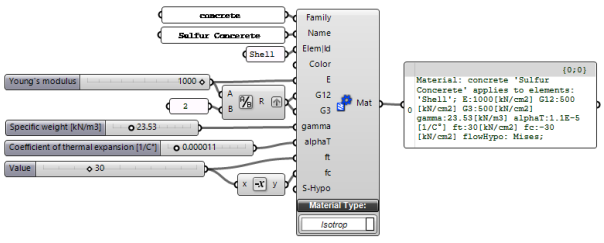

Figure 134. The material definition algorithm for Martian concrete via Karamba3D.

Specifying a shell construction is not complete unless the cross-sections are defined in addition to the materials. According to our research, any structures or bases in which astronauts live should have a radiation protection factor of at least 91.67 percent. Using the radiation shield calculation from the third chapter and a protection factor of 91.67 percent, we determine that a shield made of Martian regolith would need to be at least 60.99 centimeters thick to give appropriate

radiation protection. If we want to create an Earth-like habitat for Mars explorers, we need to estimate the necessary shell thickness with average annual radiation of 3.6 mSv across Mars' solar cycle, yielding a protection factor of 99.4 percent against 600 mSv for a Mars surface mission. Based on the results of the calculations, a regolith shell thickness of 125.59 centimeters would be enough protection against daily radiation levels similar to those on Earth.

To protect the crew from the high radiation levels on Mars' surface, we used the Shell Var component of Karamba3D, as shown in Figure 135, to provide a varied shell thickness for each face of the mesh if necessary. The thickness of the shell is defined by a range between 60.99 and 125.59 centimeters to provide minimum and maximum requirements as design parameters. As a result, the simulation will determine whether the shell's thickness is reduced or increased, and the resulting shell will be optimum in terms of radiation shielding and structural safety.

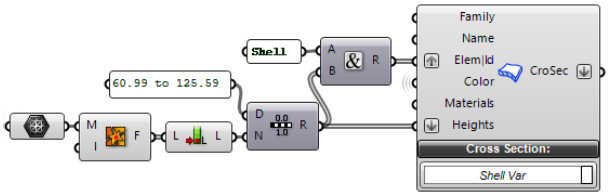

Figure 135. The variable shell thickness definition algorithm for a habitation on Mars via Karamba3D.

The final stage in executing a simulation is constructing a simulation model using the specified settings as input parameters for the Assemble Model component of Karamba3D, as seen in Figure 136. The output of this component is the simulation model, which may be analyzed using the Analyze tool in Karamba3D. Additionally, ModelView and ShellView are two tools that can be employed to plot an analyzed model. While ModelView allows the designer to examine the current state of a model by plotting the scale of deformation, reactions, loads, supports, etc., ShellView enables the designer to examine the current state of a shell structure by displaying the analysis results, such as cross-section, thickness, utilization, and displacement, etc.

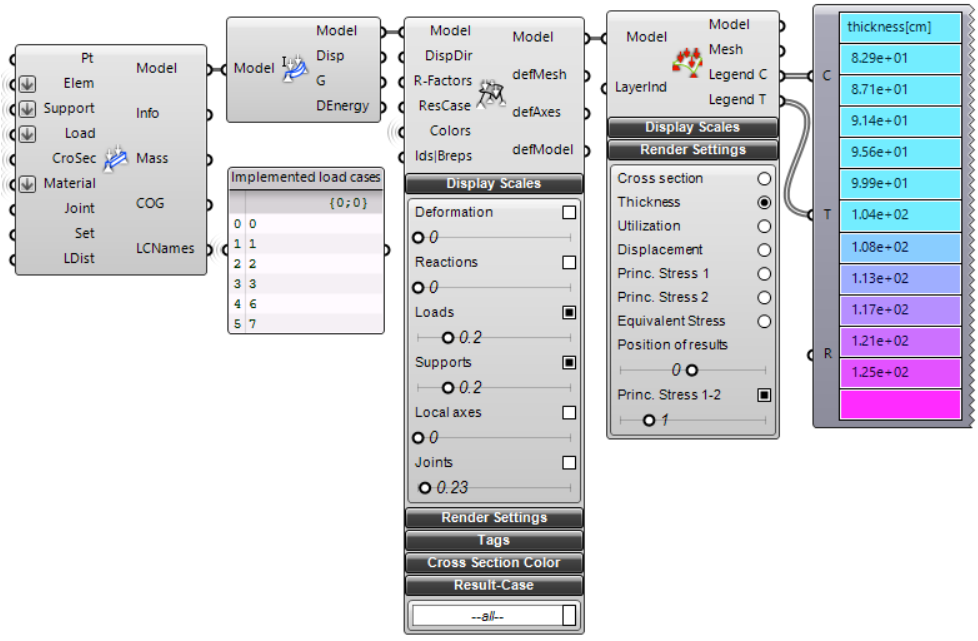

Figure 136. The algorithm to execute and plot the structural simulation analysis.

7.3.2. The structural simulation results for Martian habitation shells

This section will discuss and demonstrate the findings of the simulation study conducted at 25°C indoors and -153°C, -63°C, and +20°C outdoors utilizing the specified structural forces. The simulation results of the habitations under gravity (load case 0), atmospheric pressure (load case 1), internal air pressure (load case 2), maximum wind pressure (load case 3), and marsquake (load case 7) loads for three external thermal loads at -153°C (load case 4), -63°C (load case 5), and +20 °C (load case 6) are depicted in the figures. For defined load cases, the resulting shell thickness, utilization ratio (the ratio between tensile or compressive strength and the material's comparative stress in each face of the shell), and displacement for each of the three habitation shells will be shown with additional data obtained from the simulations to demonstrate the influence of environmental forces. The results will help us understand how the shells change and respond to external forces at the three temperatures.

As shown in Figure 137, the first adjacency matrix-generated habitation is a two-story vertically oriented habitation with a 5.86 m inner height and a 6.09 m external shell height. Its circular habitable ground and first-floor areas are 23.70 m^2 and 32.35 m^2, respectively. Its shell thickness ranges from 82.9 cm at the base to 125 cm at the top of the habitation. The shell is displaced by 0.002674 cm due to gravity (load case 0), 0.00016 cm due to atmospheric pressure (load case 1), 0.014013 cm due to internal air pressure (load case 2), $4.1476x10^{-6}$ cm due to maximum wind pressure (load case 3), and 0.000043 cm due to a Marsquake (load case 7).

The thermal load at -153°C (load case 4) causes a significant amount of elastic energy change, equal to 4463.77 kNm, and it causes 1.299352 cm displacement on the shell. At the same temperature, the bottom of the shell has a utilization ratio of 10.5%, whereas the top of the habitation has a utilization ratio of -6.9%. The maximum displacement occurs at the top of the shell with an approximately 1.29-centimeter shell displacement.

A thermal load at -63 °C (load case 5) results in an elastic energy change of 760.47 kNm and a shell displacement of 0.550309 cm. At the same temperature, the utilization ratio is 4.5% at the base of the shell and -3.4% at the peak of the habitation shell. The maximum displacement occurs at the top of the shell with an approximately 0.54-centimeter shell displacement.

The thermal load displacement at +20°C (load case 6) is 0.141924 cm, and the elastic energy change is 75.84 kNm. At this temperature, the shell's midsection reveals the highest percentage of shell utilization (1.3%), while the upper and lower levels display the lowest rate (0.6%). At around 0.152 centimeters, the most significant shell displacement occurs towards the shell's apex.

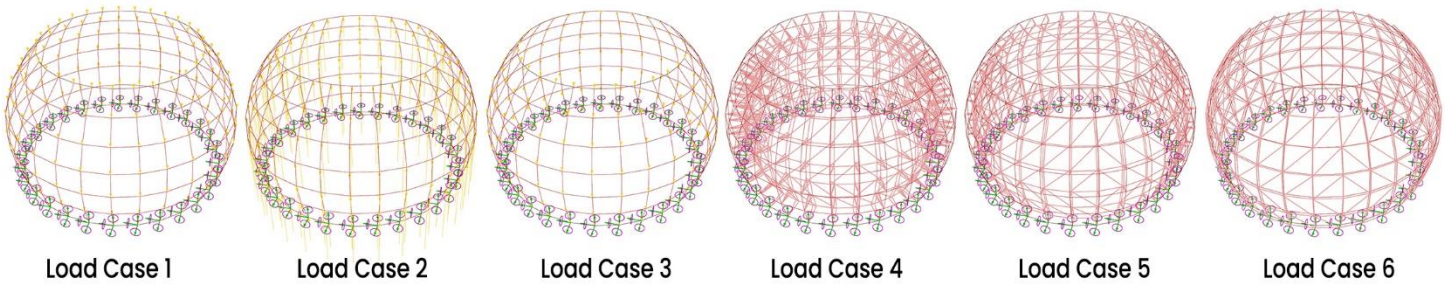

Simulation results | T : -153 °C; ΔT: +178 °C

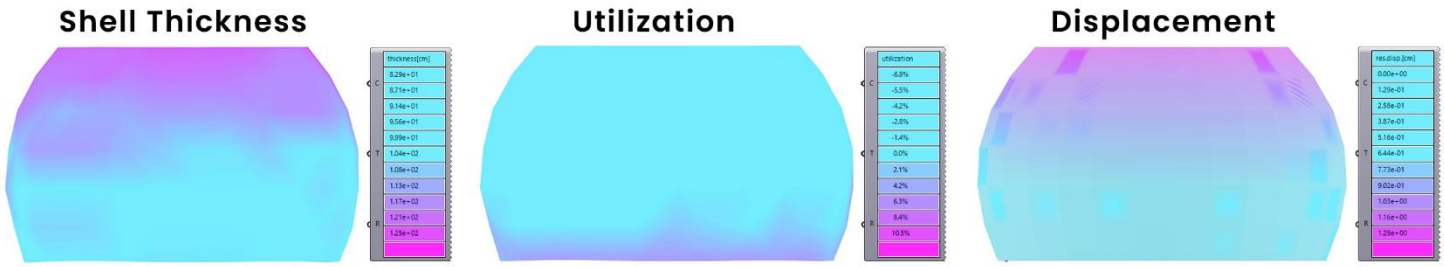

Simulation results | T : -63 °C; ΔT: +88 °C

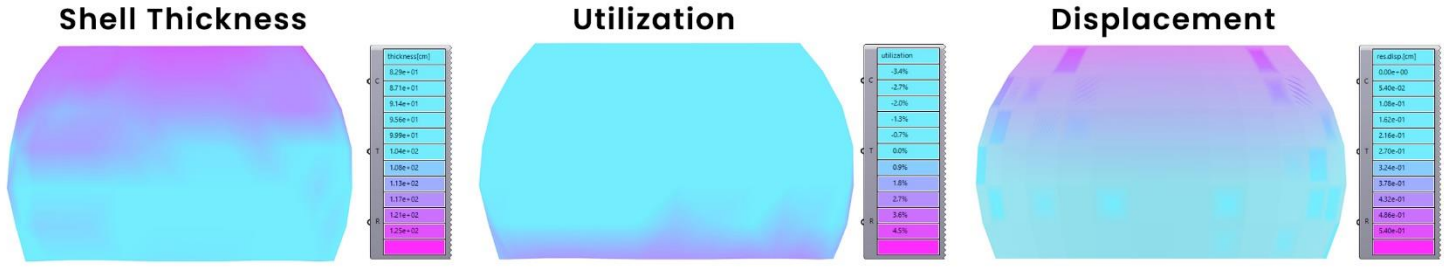

Simulation results | T : +20 °C; ΔT: +5 °C

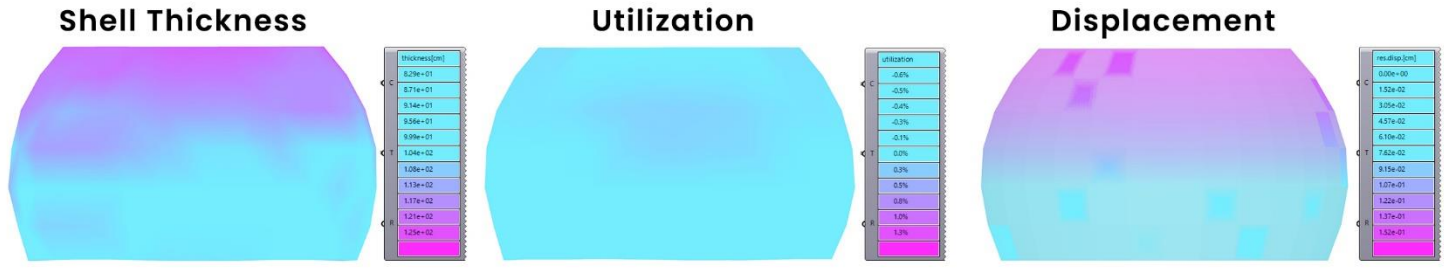

Figure 137. The simulation results and illustration of first adjacency matrix-generated habitation

The habitation formed by the second adjacency matrix is displayed in Figure 138. The habitation is a three-story, vertically oriented structure with an interior height of 8.37 meters and an exterior shell height of 9.0 meters. The ground floor is 5.77 m^2, the first floor is 20.12 m^2, and the second floor is 30.17 m^2. The shell's thickness ranges from 82.6 cm at its base to 125 cm at its apex. Gravity (load case 0) causes a displacement of 0.00629 cm, air pressure (load case 1) causes a displacement of 0.00038 cm, internal air pressure (load case 2) causes a displacement of 0.033393 cm, maximum wind pressure (load case 3) causes a displacement of 0.00002 cm, and a marsquake (load case 4) causes a displacement of 0.000211 cm (load case 7).

In load case 4, the shell deflects 1.451386 cm when subjected to a thermal load at -153 °C, resulting in a change in elastic energy of 6654.57 kNm. At the same temperature, the utilization ratio is 10.6% at the base of the habitation and -6.6% at the top. The shell is displaced by approximately 1.42 cm at its highest point.

The elastic energy change for a thermal load at -63 °C (load case 5) is 1132.47 kNm, while the shell displacement is 0.613569 cm. The utilization ratio at the base of the habitation shell is 4.6% and -3.3% at the top. There is a displacement of approximately 0.6 cm at the highest point of the shell.

The thermal load displacement at +20°C (load case 6) is 0.160456 cm, and the elastic energy change is 113.30 kNm. At this temperature, the center of the shell has the highest rate of shell utilization (1.2%), while the top and bottom have the lowest (-0.9%). Approximately 0.16 centimeters of shell displacement occurs at the shell's top.

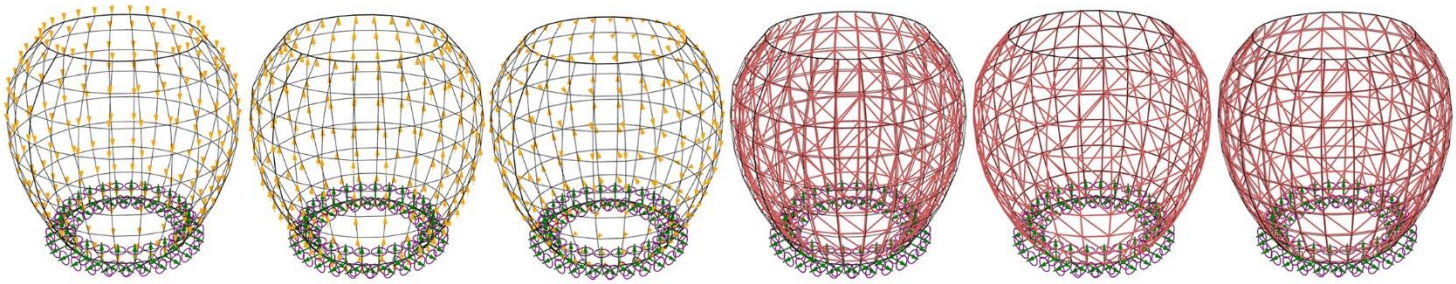

Simulation results | T : -153 °C; ΔT: +178 °C

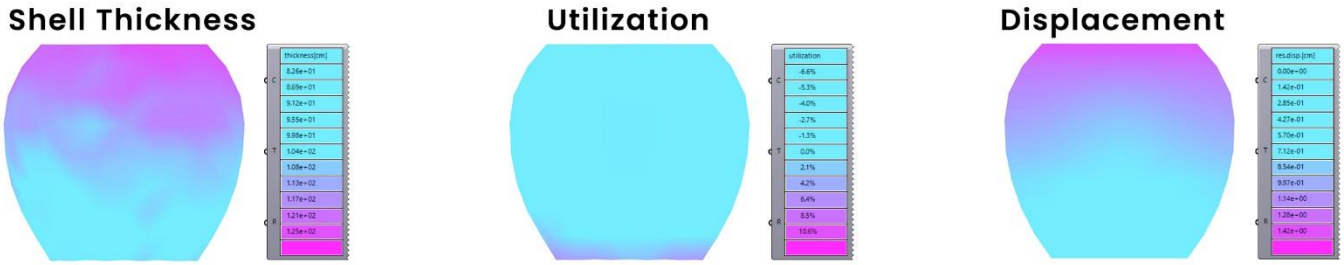

Simulation results | T : -63 °C; ΔT: +88 °C

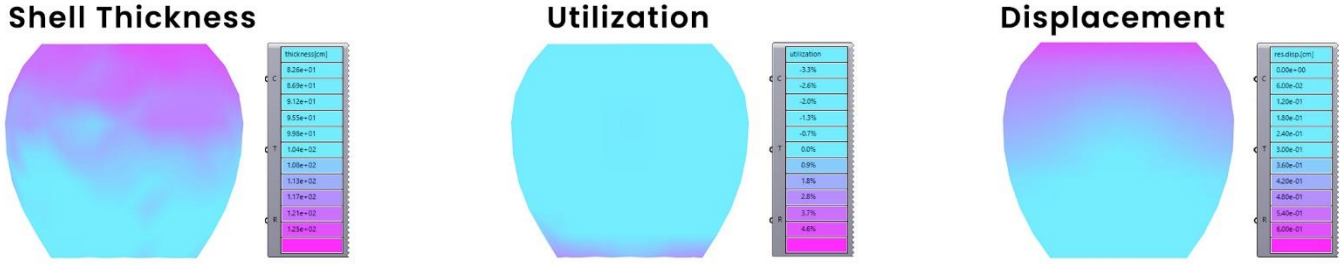

Simulation results | T : +20 °C; ΔT: +5 °C

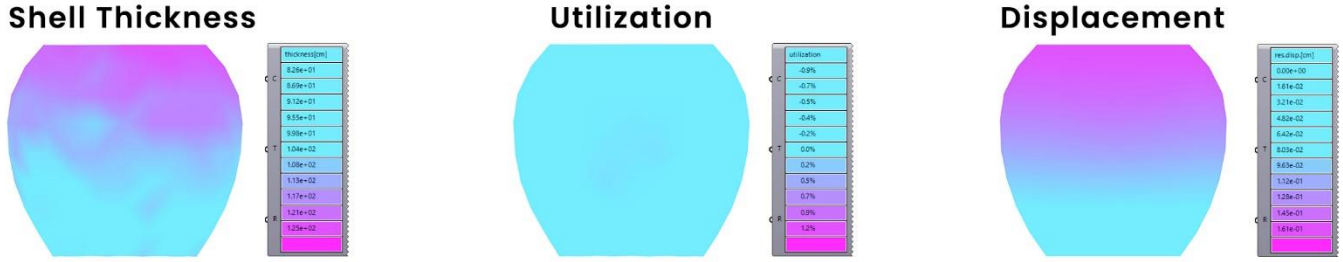

Figure 138. The simulation results and illustration of second adjacency matrix-generated habitation.

Figure 139 shows the habitation created via the third adjacency matrix. The structure has four floors, is vertically orientated, and has an outer shell height of 11.0 meters and an interior height of 10.47 meters. The ground floor is 5.60 m^2, the first floor is 18.10 m^2, the second floor is 25.74 m^2, and the third floor is 6.60 m^2. The shell's thickness ranges from 82.6 cm at its base to 125 cm at its apex. A displacement of 0.007088 cm is caused by gravity (load case 0), 0.00043 cm is caused by air pressure (load case 1), 0.037783 cm is caused by internal air pressure (load case 2), 0.000026 cm is caused by maximum wind pressure (load case 3), and 0.000292 cm is caused by a marsquake (load case 7).

In load case 4, when the shell is exposed to a thermal load at -153 °C, it deflects 1.654788 cm, causing a change in elastic energy of 7025.04 kNm. At the same temperature, the utilization ratio is 10.0% at the base and -5.8% at the top of the habitation. At its highest point, the shell is displaced by 1.62 cm.

Thermal load at -63 ° Celsius (load case 5) results in an elastic energy change of 1195.06 kNm and a shell displacement of 0.688257 cm. At its lowest point, the habitation shell's utilization ratio is 4.4%, while it falls to -2.6% at its highest point. At the shell's highest point, there is a displacement of about 0.656 cm.

At +20°C (load case 6), the thermal load displacement is 0.204953 cm, and the elastic energy change is 119.46 kNm. The rate of shell utilization is highest in the center of the shell (1.3%) and lowest in the top and bottom (-0.5%) at this temperature. The shell's top experiences a displacement of about 0.235 centimeters.

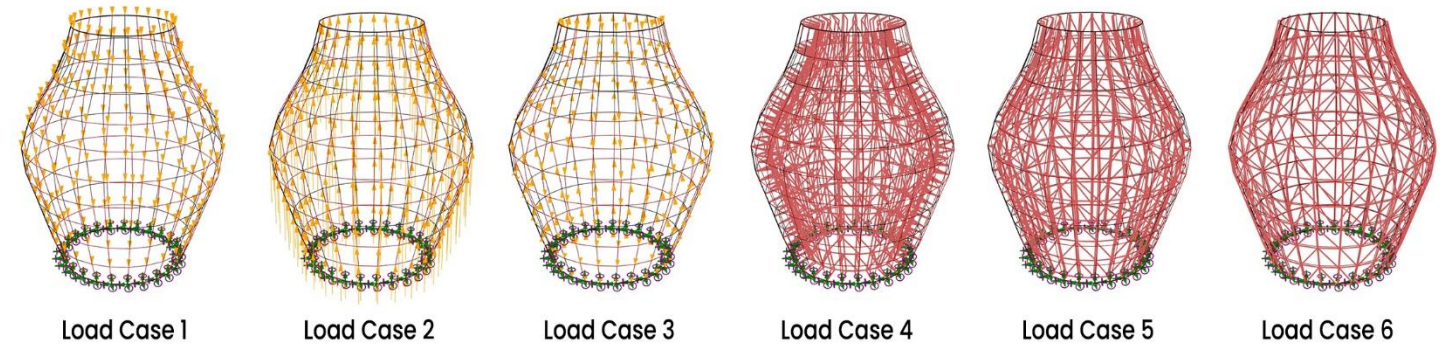

Simulation results | T : -153 °C; ΔT: +178 °C

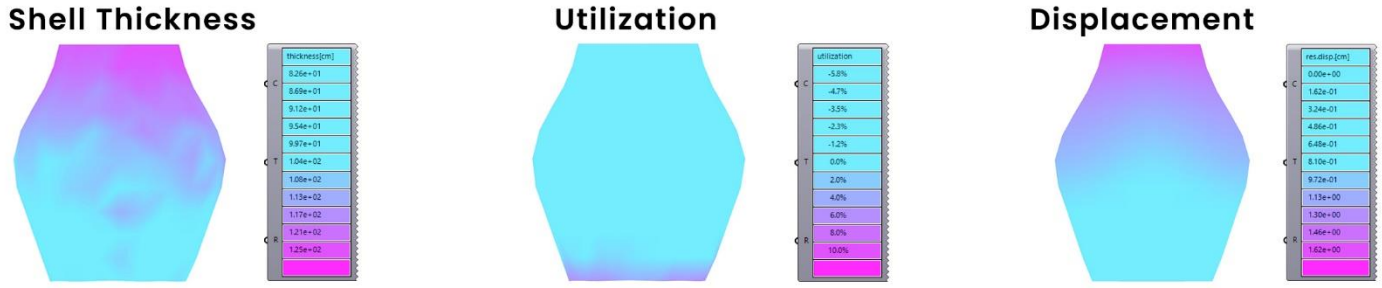

Simulation results | T : -63 °C; ΔT: +88 °C

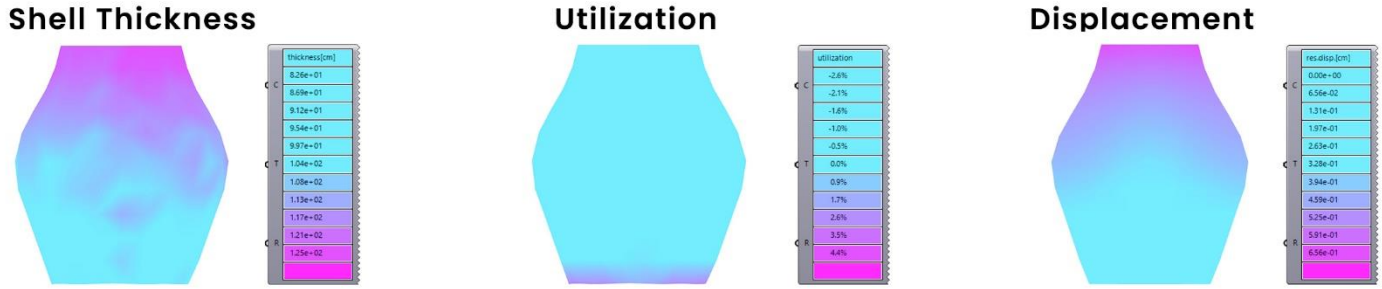

Simulation results | T : +20 °C; ΔT: +5 °C

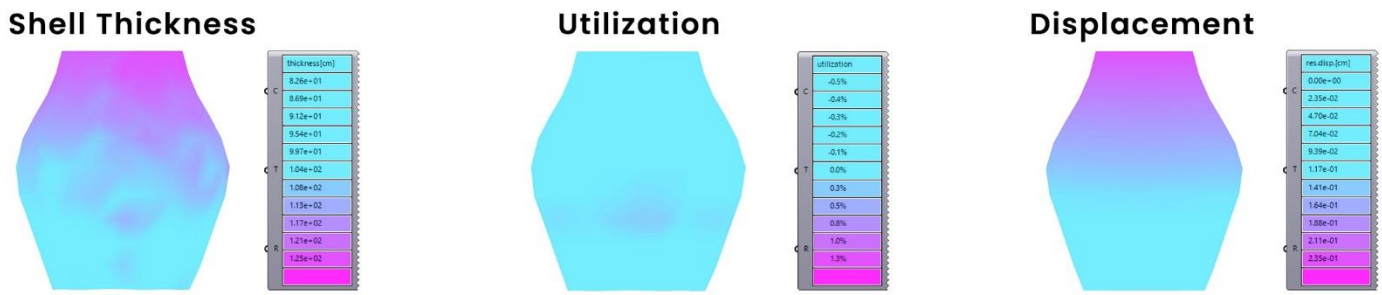

Figure 139. The simulation results and illustration of third adjacency matrix-generated habitation.

7.3.3. Further validation of design methodology

This dissertation attempted to describe in many ways the context, necessity, and data utilized to establish the proposed methodology for developing a self-validated design process. Chapter 7's design studies were the most extensive in this regard, and they demonstrated in detail the consequences of generative, multi-objective, simulation-based habitation design approaches. Chapter 6 outlines the theories and tools necessary to implement the suggested design process and their respective guiding principles. The case studies in Chapter 5 were another major attempt to demonstrate the design requirements of a Mars habitation using NASA-validated design projects, and the chapter's conclusion was used to support the proposed design methodology. In Chapter 4, actual Mars analog habitations are analyzed using social network analysis and label propagation approaches to reveal their functional design considerations within measurable scientific measures. The conclusion of this chapter is utilized to develop adjacency matrices of studied design projects in Chapter 7. In Chapter 3, each environmental parameter on Mars is explained to formulate them as design parameters for projects conducted in Chapter 7. The site selection studies of three different institutions are reviewed and superimposed to determine the optimal location for a Mars settlement.

The design workflow alternatives for transforming the design proposals into actual implementations require additional research and testing. The easiest way to test a design methodology is to implement it in a real-world design issue; therefore, a sub-scaled habitation model developed with the suggested methodology might be constructed using a material that mimics the in-situ resources of the Mars surface. For this kind of investigation, multidisciplinary teams are required.

7.4. The Conclusion of Habitation Design Methodology

This study describes an autonomous design methodology for designing habitation solutions for Mars' extremely harsh environment using generative design tools and data science methodologies. A new design methodology for habitation in harsh environments has been established to optimize functionality and feasibility in response to the many design phases and design requirements of each particular habitation project of the future.

A literature-based research study assesses the physical requirements for an extraterrestrial habitat. Based on the findings of the fourth chapter, the collected requirements are used to establish three adjacency matrices for habitation plans. The defined matrices are examined using Social Network Analysis (SNA) in the Python environment, and the relations between spaces are reinterpreted considering the analysis to establish viable adjacency relations. A block of Python algorithm for conducting graph data science methodologies generates network representations of matrices following SNA analysis to reveal insightful information from network diagrams. The Label Propagation Approach (LPA) is conducted as a semi-supervised ML approach using a community detection

algorithm. Network graphs are subdivided into smaller sections known as communities. A community consists of spaces with the same label assigned to each space by the ML algorithm. Three investigated matrices revealed two, three, and four communities after completing the community detection approach. These communal areas are considered functional spaces on a floor plan and should be planned on the same floor. The communities are used to build space-syntax diagrams at the start of the habitation design process, and floor layouts are generated when a space-syntax diagram configuration, a physics simulation, and a Voronoi pattern definition have been implemented. The research objectives of the thesis did not include the plan generation process; however, the definition of the floor area was sufficient to continue with the design of a long-term habitation because the plan configuration could be implemented using conventional design methods and was not directly relevant to the automation of long-term habitation construction. After floor plans are generated, their boundary curves are used as floor areas to construct a lofted preliminary habitation form by aligning the curves along the Z-axis. The created preliminary form is offset by 1.5 m to provide a dual habitation shell, with the inner layer defining the envelope of habitable space and the outer layer defining the protective shell of inhabited volume. When openings are defined on the outer shell, the space between layers is proposed as a vertical circulation area to reach the top levels and a volume to spread natural light to lower floors. Afterward, the environmental forces specified in the third chapter are included in the generative design process using a structural simulation tool to create a habitation shell resistant to the extreme conditions of Mars to protect future explorers in the missions. The six chapters described the integration of environmental forces into the generative design process. However, micrometeoroid impact was excluded from this study because it is neither a continuous nor a constant design element. The predicted properties of a micrometeoroid for a structural simulation were described in the third chapter, but a meteoroid that is larger, denser, and faster than anticipated cannot be solved as a design problem to include in the design process. After the design process, the effects of environmental forces on habitation shells are displayed and explained to disclose their implications for diverse design instances.

As a result, the defined design methodology is successfully implemented for three specific cases, but the methodology requires additional research into factors such as making openings on the shell with structural durability and radiation in mind; providing natural light for the habitable volume; sound insulation; the use of color; implementing the methodology by utilizing different in-situ materials, and defining additive construction phases with an executive plan.

08 th Chapter
FINDINGS AND CONCLUSION

This section reviews the original research questions, describes our findings and achievements, evaluates the limitations of the proposed design methodologies, explains the significance of our conclusions, and speculates on possible future research directions.

This dissertation has developed novel methods that combine data science, a machine learning algorithm, and generative design methodologies to enable multi-objective investigation during the early phases of Mars habitation design. It first suggests using graph data science methodologies to optimize the adjacency matrix of habitation layouts and then justifies the need to integrate a semi-supervised machine learning algorithm to make typology decisions using a label propagation approach. The developed design methodology suggests employing structural simulations with environmental forces as structural loads to produce habitation shells through a self-generation process. It finishes with implementation examples of novel design methodology, describing it in detail to expose the effects of environmental influences on different habitation shell analyses. This chapter concludes with a summary of contributions, a discussion of outstanding issues, and some final comments.

8.1. Questions of research and dissertation objectives

This dissertation is organized on the following question:

How can architects use the environmental design process to design a space-resilient equilibrium between competing quantitative objectives to develop a fully autonomous design strategy for a Martian habitation concept?

The interdisciplinarity of this problem needs an in-depth examination of the design approach and the required data as design criteria. The fundamental objective of this dissertation is to develop theoretical and methodological approaches that, when combined, generate a habitation definition that is highly functional in the extreme Martian environment, is responsive to defined data, and is simulated through a collaborative, organic, data-driven creative process using environmental data and a computer.

8.2. Summary of Contributions

In this section, the significance of the findings within the context of the research question is highlighted by presenting a summary of the dissertation's contributions to space architecture literature, habitation design implementations, and other research studies relevant to the scope of environmental design problems.

8.2.1. A review study of space missions

The dissertation covers a comprehensive literature review of space exploration missions and plans from the past to the present to clarify the background of Mars habitation and the need for a future mission. The study summarizes the critical space missions, organizes this overview chronologically, reviews the technological advances that space technologies have illustrated over the past decades, and outlines the additional technological advancements that will be required for future space exploration missions.

8.2.2. Adaptation of Mars conditions into quantifiable parameters

The dissertation examines the environmental data on Mars as revealed by planetary exploration missions. Defining data gives background information for a hypothetical site on Mars to convert harsh environmental circumstances into design parameters and define which environmental factors must be simulated to develop a space-resilient habitation. The dissertation describes in depth how each environmental factor can be simulated as a design parameter for the contexts of Mars.

8.2.3. The optimal location on Mars for a surface settlement

The dissertation describes three alternative methodologies for establishing the criteria for selecting a landing and research site on Mars' surface for a future crewed mission. This study provides an overview of NASA's site selection workshop series for the 2020 Mars rover landing, as well as a research study on plant-based site selection from Wageningen University & Research (WUR), an ice mapping methodology from the Subsurface Water Ice Mapping (SWIM) team at The Planetary Science Institute (PSI), and a research study from MIT on the development of software tools that can assimilate large quantities of geologic and obliquity data. The conducted superimposition study revealed that Mawrth Vallis is the optimal landing location for a long-term crewed surface mission based on latitude, altitude, landforms, distance from ice reserves, and plant friendliness to cultivate local foods.

8.2.4. Analysis of Mars analog habitations by using SNA

The dissertation reviewed analog missions conducted to study the habitability of Mars and examined the habitation plans of seven Mars analog missions by employing data science methodologies to reveal valuable facts about their layout configurations. Analysis of habitation plans using Social Network Analysis (SNA) measures and Label Propagation Approach (LPA) as a semi-supervised machine learning algorithm are presented in the study, which concludes with the research findings of data science approaches in order to provide a layout design guideline illustration for a space-resilient habitation.

8.2.5. Assessment of 3D-printed Mars habitation proposals

The dissertation examines the four winning habitation projects of NASA's 3D-Printed Habitat Challenge to formulate the design, construction, and technology requirements for a Mars habitat based on their design principles. As a result of the analysis, eight design specifications for a space-resilient habitation design are outlined in an assessment report. The thesis study's fundamental reasoning and contents to explain a novel design methodology are based on the specified design requirements, which have been discovered and examined by employing state-of-the-art case studies for habitation design methodologies.

8.2.6. Integration of graph data science into the layout design

The dissertation integrated Social Network Analysis (SNA) measurements into functional connection analysis of three predefined habitation layout adjacency matrices to evaluate the positions of each space within the predefined matrices. A node represents each functional space in the matrices, and the edges between the nodes indicate the relationships between the nodes according to the adjacency matrices, generating an undirected network graph suitable for SNA analysis. Once graphs are analyzed via SNA, the degree and centrality measures of each space in the networks are revealed to make any necessary modifications to the adjacency matrices. The novel method enables the analysis of operational planning decisions employing scientific metrics to maximize the functionality of a layout configuration.

8.2.7. Typology decisions via a machine-learning algorithm

This dissertation presents a novel methodology for defining a habitation's floor number, functional spaces on each floor, and habitation typology by incorporating The Label Propagation Approach (LPA) into the early design process. Using a community detection algorithm from the NetworkX Python module and a semi-synchronous label propagation algorithm (a semi-supervised machine learning technique that needs only a network representation and no other data) to find

functional nodes in a network graph that belong to the same community, the deployed machine learning methods divide the functional networks of floor plans into communities in which the functional spaces needed to be configured together. When the interconnections between communities predefined by adjacency matrices are preserved, the generated communities are offered as functional configurations of floor plans. So, the community detection method defines the functional relationships in a floor plan, the floor number as a community number in a network, and the type of habitation project defined by the floor number.

8.2.8. A structural simulation setup with Mars' environmental forces

The dissertation describes a unified structural simulation setup for Mars' environmental conditions, including gravity, atmospheric pressure, the internal pressure of Mars habitation, maximum wind pressure, thermal loads for minimum, average, and highest exterior temperature for a 25 °C interior habitation temperature, and the effect of the largest Marsquake (though it can be negligible). Karamba3D's structural analysis tools are executed with the Grasshopper user interface to integrate the structural requirement of the habitation into the design phases. The presented structural modeling configuration is the most comprehensive simulation strategy for a Mars habitation described in the literature.

8.2.9. Design implementations with a novel design methodology

The dissertation demonstrates the advanced design implementations of three different habitation projects using a novel machine learning-aided generative design methodology. This methodology is defined by the convergence of SNA, LPA, and generative design approaches. While the implemented projects outline the habitation design phases step by step within a generative design environment, they also reveal a detailed explanation of the design methodology to indicate weaknesses, strengths and lacking sections for further research studies. Future research attempts may benefit from using this knowledge to help guide their direction.

8.2.10. Understanding of Mars' effects on a shell structure

Protection from Mars' harsh environment is the main challenge of any surface exploration mission requiring a crew. Understanding the impact of environmental extremes on a structure to research habitation design is vital for developing space habitation technologies. The simulation findings demonstrate the most significant or negligible environmental forces for Mars's surface habitation. In addition, the simulations of environmental factors for various design instances and their results make a multidisciplinary problem comparative, responsive, and manageable for designers.

8.3. Remaining questions and Future Work

A machine-learning-aided habitation design process aims to outline a scientific design methodology that considers human factors, design and construction automation, and Mars environmental forces. While this methodology successfully implements some aspects of design solutions, it has some errors that need to be considered to improve the design proposal's design cycle and detail level. The following problems need to be developed with more advanced methodologies and tools.

The selection of the site is the first obstacle in the design of a habitable environment, as many factors must be considered, such as the proximity of water or ice, the availability of construction materials, the shape of the terrain, the average temperature, the annual wind speed, the amount of sunlight, etc. To accurately incorporate terrain, in-situ resources, and local environmental conditions into design simulations, it is necessary to identify and assess several locations that are ideal for human settlements. The alternative allows for the selection of materials or formulation of a composition that considers the environment's characteristics.

The second problem is using an inappropriate construction material or insufficiently defining a material composition for additive manufacturing. While Mars conditions have been experienced, they are still a matter of data; hence, the created simulant materials are conducted on Earth conditions, but their mechanical behaviors need to be tested under the real-life conditions of Mars. There may be a high failure rate associated with the chosen construction material.

The design process should be initiated independently after selecting the construction site and materials. Data science approaches, which we suggest, can be used to determine the typology of habitation and its functional requirements, such as determining essential spaces and examining the relationships between them via social network analysis or a connectivity diagram. However, additional automation is needed to define relationships between spaces in a more complicated habitation like a station. The relationship between spaces can be taught to a decision-maker algorithm, like a self-learning system or piece of software, so that it can make better decisions with each cycle.

After defining functional relations, the next step is to develop an executive interior layout that meets the needs of operations while maintaining the previously established functional connections between spaces and considering human considerations.

The definition of internal circulation poses a significant threat to the implementation of the methodology. The proposed approach recommends implementing circulation directly from room to room without a corridor or between the two layers of the dual habitation shell. Contrasting with the first case, where there must always be unrestricted and open mobility between spaces, the second case has stairs confined to a small area that can be influenced by thermal expansion. The design

approach of circulation zones around functional spaces, indicated in the designs of Marsha and X-House V2, is followed; however, there is a risk of failure due to the volumetric change of the shell because of extreme temperature fluctuations.

The result of the form generation is modeled as a shell structure and analyzed using extreme load definitions. The output value of shell thickness may have a significant impact on the lifespan of a structure. Studying the relationship between habitation form and material characteristics is necessary to create an optimal shell thickness that should give an acceptable protection level under extreme conditions while boosting the structure's durability.

The final part involves simulating the additive construction process of the habitation and then implementing it automatically. It is essential to justify a habitation's design from the preliminary stages through construction if it has a detrimental impact on the construction process.

8.4. Discussion and Conclusion

We have chosen to develop and apply a scientific methodology to assess the problem statement and focus on the area between simulation and acquired data. The ideal approach for gaining knowledge about a location like Mars, where the environmental hazards are too extreme to test a habitation in the context without study and implementation, is to conduct comprehensive simulations, regardless of how precisely they resemble actual circumstances. A research methodology would provide evidence to support the argument that a comprehensive analog and simulation might generate reliable knowledge about the actual parameters on Mars to design a habitation for these circumstances. Integration of data from missions and simulations can decrease some risks associated with executing a surface habitation design and construction. The simulation for a habitation design process may be executed under the most realistic settings achievable using scientific data as design parameters. Without using environmental data from previous studies and space missions to conduct a structural simulation, it would be impossible to investigate the problem in this dissertation. Even if the assumptions of human psychology and comfort in a future Mars settlement are based on verifiable data gathered from such as the International Space Station, they will never be regarded as proper knowledge when applied to Mars. We also employ simulated knowledge to explain the studied design generations in our investigation's conclusions.

References

AISpaceFactory. (2018). *Marsha - AI Spacefactory's Mars Habitat*. https://www.aispacefactory.com/marsha

Akhtar, N. (2014). Social network analysis tools. *2014 Fourth International Conference on Communication Systems and Network Technologies*, 388–392.

Akhtar, N., & Ahamad, M. V. (2021). Graph tools for social network analysis. In *Research Anthology on Digital Transformation, Organizational Change, and the Impact of Remote Work* (pp. 485–500). IGI Global.

Akhtar, N., Javed, H., & Sengar, G. (2013). Analysis of Facebook social network. *2013 5th International Conference and Computational Intelligence and Communication Networks*, 451–454.

al Husseini, A. M., Alvarez Sanchez, L., Antonakopoulos, K., Apeldoorn, J. J., Ashford Jr, K. L., Atabay, K. D., & Langston, S. (2009). *Access Mars: Assessing Cave Capabilities Establishing Specific Solutions*.

Alexiadis, A., Alberini, F., & Meyer, M. E. (2017). Geopolymers from lunar and Martian soil simulants. *Advances in Space Research*, *59*(1), 490–495.

Alfaris, A. A. F. (2009). *The Evolutionary Design Model (EDM) for the design of complex engineered systems: Masdar City as a case study*. Massachusetts Institute of Technology.

Alfonseca, M., & Ortega, A. (2000). Representation of some cellular automata by means of equivalent L Systems. *Complexity International*, *7*, 1–16.

Allen, C. C. (1998). Bricks and ceramics. *Using in Situ Resources for Construction of Planetary Outposts*, 1.

Allen, C. S., Burnett, R., Charles, J., Cucinotta, F., Fullerton, R., Goodman, J. R., Griffith Sr, A. D., Kosmo, J. J., Perchonok, M., & Railsback, J. (2003). *Guidelines and capabilities for designing human missions*.

Andrew, A. G., Karen, F., & Johnson. (2021). *NASA's InSight Reveals the Deep Interior of Mars*. NASA Jet Propulsion Laboratory. https://www.nasa.gov/feature/jpl/nasa-s-insight-reveals-the-deep-interior-of-mars

Andringa, J. M., Easter, R. W., Gray, A. A., Lamassoure, E. S., & Mungas, G. S. (2005). Mars human precursor mission concepts for the decade 2010-2020. *2005 IEEE Aerospace Conference*, 191–201.

Anyszka, R., Bielinski, D., Imiela, M., Szajerski, P., Pawlica, J., Walendziak, R., & Sicinski, M. (2016). *Sulfur Concrete – Promising Material for Space-Structures Building*.

Bagrow, J. P., & Bollt, E. M. (2005). Local method for detecting communities. *Physical Review E*, *72*(4), 46108.

Banerdt, W. B., Smrekar, S. E., Banfield, D., Giardini, D., Golombek, M., Johnson, C. L., Lognonné, P., Spiga, A., Spohn, T., & Perrin, C. (2020). Initial results from the InSight mission on Mars. *Nature Geoscience*, *13*(3), 183–189.

Baratoux, D., Samuel, H., Michaut, C., Toplis, M. J., Monnereau, M., Wieczorek, M., Garcia, R., & Kurita, K. (2014). Petrological constraints on the density of the Martian crust. *Journal of Geophysical Research: Planets*, *119*(7), 1707–1727.

Barlow, N. (2014). Mars: An introduction to its interior, surface and atmosphere. *Mars: An Introduction to Its Interior*.

Barlow, N. G. (2013). 3 Terrestrial Planets. *Planets, Stars and Stellar Systems*, 3111.

Bassingthwaighte, T. (2017). *The Design of Habitats for the Long-Term Health of Inhabitants in the Extreme Environments of Earth and Outer Space*. University of Hawaii at Manoa.

Bastian, M., Heymann, S., & Jacomy, M. (2009). Gephi: an open source software for exploring and manipulating networks. *Proceedings of the International AAAI Conference on Web and Social Media*, *3*(1), 361–362.

Basu, S., Richardson, M. I., & Wilson, R. J. (2004). Simulation of the Martian dust cycle with the GFDL Mars GCM. *Journal of Geophysical Research: Planets*, *109*(E11).

Becker, R. (2021). Is there Life on Mars? Where is the Proof. *Journal of Astrobiology*, *7*, 38–75.

Beish, J. D. (2002). Mars: The opposition cycle of Mars. *Journal of the Association of Lunar and Planetary Observers, the Strolling Astronomer*, *44*(4), 44–45.

Bell, J. F., McSween, H. Y., Crisp, J. A., Morris, R. v, Murchie, S. L., Bridges, N. T., Johnson, J. R., Britt, D. T., Golombek, M. P., Moore, H. J., Ghosh, A., Bishop, J. L., Anderson, R. C., Brückner, J., Economou, T., Greenwood, J. P., Gunnlaugsson, H. P., Hargraves, R. M., Hviid, S. F., … Soderblom, L. A. (2000). Mineralogic and compositional properties of Martian soil and dust: Results from Mars Pathfinder. *Journal of Geophysical Research*, *105*, 1721–1755.

Bell, M. (1999). *Micrometeoroid Protection*. NASA Jet Propulsion Laboratory. https://llis.nasa.gov/lesson/705

Belton, Michael J.S., Malin, Michael C., and Carr, Michael H.. "Mars" *Encyclopedia Britannica*, 2 Sep. 2022, https://www.britannica.com/place/Mars-planet. Accessed 6 November 2022.

Benaroya, H. (2018). *Building habitats on the moon: engineering approaches to lunar settlements*. Springer.

Benaroya, H., Bernold, L., & Chua, K. M. (2002). Engineering, design and construction of lunar bases. *Journal of Aerospace Engineering*, *15*(2), 33–45.

Benton, M., Kutter, B., Bamford, R., Bingham, B., Todd, T., & Stafford-Allen, R. (2012). Conceptual space vehicle architecture for human exploration of mars, with artificial gravity and mini-magnetosphere crew radiation shield. *AIAA SPACE 2012 Conference & Exposition*, 5114.

Berlinski, D. (2001). *The advent of the algorithm: the 300-year journey from an idea to the computer*. Houghton Mifflin Harcourt.

Binsted, K. A., & Hunter, J. B. (2013). HI-SEAS (Hawaii Space Exploration Analog and Simulation, hi-seas. org) as an opportunity for long-duration instrument/protocol testing and verification. *Analog Sites for Mars Missions II: Past, Present and Future Missions to Mars*, *1738*, 4044.

Binsted, K., Kobrick, R. L., Griofa, M. Ó., Bishop, S., & Lapierre, J. (2010). Human factors research as part of a Mars exploration analogue mission on Devon Island. *Planetary and Space Science*, *58*(7–8), 994–1006.

Biswal M, M. K., & Annavarapu, R. N. (2019). *Chronology of Mars Exploration Missions*. https://doi.org/10.13140/RG.2.2.36435.22560

Biswal M, M. K., & Annavarapu, R. N. (2021). Human Mars Exploration and Expedition Challenges. *AIAA Scitech 2021 Forum*, 628.

Black, M. (1956). *The Exploration of Mars*. JSTOR.

Blondel, V. D., Guillaume, J.-L., Lambiotte, R., & Lefebvre, E. (2008). Fast unfolding of communities in large networks. *Journal of Statistical Mechanics: Theory and Experiment*, *2008*(10), P10008.

Bloomberg, J. J., Reschke, M. F., Clement, G. R., Mulavara, A. P., & Taylor, L. C. (2015). *Risk of impaired control of spacecraft/associated systems and decreased mobility due to vestibular/sensorimotor alterations associated with space flight*.

Bogdahn, C., Breaum, A., Breum, H., Larsen, H., Løvenskjold, M., & Kristiansen, T.-H. (2019). *In-situ Habitat Design on Mars*.

Bolonkin, A. A. (2009). Artificial environments on Mars. In *Mars* (pp. 599–625). Springer.

Bonabeau, E., Dorigo, M., Theraulaz, G., & Theraulaz, G. (1999a). *Swarm intelligence: from natural to artificial systems* (Issue 1). Oxford university press.

Bonabeau, E., Dorigo, M., Theraulaz, G., & Theraulaz, G. (1999b). *Swarm intelligence: from natural to artificial systems* (Issue 1). Oxford university press.

Bonacich, P. (1972). Technique for analyzing overlapping memberships. *Sociological Methodology*, *4*, 176–185.

Bonacich, P. (2007). Some unique properties of eigenvector centrality. *Social Networks*, *29*(4), 555–564.

Bosoi, C. R., & Rose, C. F. (2009). Identifying the direct effects of ammonia on the brain. *Metabolic Brain Disease*, *24*(1), 95–102.

Brady, D. A., Robinson, J. A., Costello, K. A., Ruttley, T. M., Dansberry, B. E., Thumm, T., Panjwani, S., Cohen, L., Marcil, I., & Schoen, A. (2018). Updated Benefits for Humanity from the International Space Station. *International Astronautical Congress (IAC)*, *JSC-E-DAA-TN61292*.

Bryman, A., & Hardy, M. A. (2004). *Handbook of data analysis*. Sage.

Burke, A., & Tierney, T. (2012). *Network practices: new strategies in architecture and design*. Chronicle Books.

Burry, J., Felicetti, P., Tang, J., Burry, M., & Xie, M. (2005). Dynamical structural modeling: a collaborative design exploration. *International Journal of Architectural Computing*, *3*(1), 27–42.

Caldas, L., & Rocha, J. (2001). *A generative design system applied to Sizaís school of architecture at Oporto*.

Canadian Space Agency. (2021). *The Artemis missions: humanity's return to the Moon*. https://www.asc-csa.gc.ca/eng/astronomy/moon-exploration/artemis-missions.asp

Catling, D. C. (2014). Mars atmosphere: History and surface interactions. In *Encyclopedia of the solar system* (pp. 343–357). Elsevier.

Celani, G., Beirão, J. N., Duarte, J. P., & Vaz, C. (2011). *Optimizing the "characteristic structure": Combining shape grammars and genetic algorithms to generate urban patterns*.

Center for Nondestructive Evaluation. (2022). *Transmitted Intensity and Linear Attenuation Coefficient*. IOWA State University. https://www.nde-ed.org/Physics/X-Ray/radmatinteraction.xhtml

Chaillou, S. (2020). *IA & ARCHITECTURE* (Vol. 9). Pavillon de l'Arsenal.

Chancellor, J., Scott, G., & Sutton, J. (2014). Space Radiation: The Number One Risk to Astronaut Health beyond Low Earth Orbit. *Life : Open Access Journal*, *4*, 491–510. https://doi.org/10.3390/life4030491

Christensen, P. R., Jakosky, B. M., Kieffer, H. H., Malin, M. C., McSween, H. Y., Nealson, K., Mehall, G. L., Silverman, S. H., Ferry, S., Caplinger, M., & Ravine, M. (2004). The Thermal Emission Imaging System (THEMIS) for the Mars 2001 Odyssey Mission. *Space Science Reviews*, *110*(1), 85–130. https://doi.org/10.1023/B:SPAC.0000021008.16305.94

Cichan, T., Bailey, S. A., Norris, S. D., Chambers, R. P., & Ehrlich, J. W. (2016). *Mars Base Camp*.

Clarke, J. D. A. (2002). An Australian Mars Analogue Research Station (MARSOZ)-A Proposal. *Mars Society Australia Inc. May*.

Clauset, A., Newman, M. E. J., & Moore, C. (2004). Finding community structure in very large networks. *Physical Review E*, *70*(6), 66111.

Coates, P., Derix, C., Krakhofer, I. S. P., & Karanouh, A. (2005). *Generating architectural spatial configurations. Two approaches using Voronoi tessellations and particle systems*.

Cohen, M. (2015). *First Mars Habitat Architecture*. https://doi.org/10.2514/6.2015-4517

Connors, M. M., Harrison, A. A., & Akins, F. R. (2005). *Living aloft : human requirements for extended spaceflight*. University Press of the Pacific.

Crowley, I. F., & Trudeau, J. R. (2011). *Wernher von Braun*.

Crusan, J. C., Smith, R. M., Craig, D. A., Caram, J. M., Guidi, J., Gates, M., Krezel, J. M., & Herrmann, N. B. (2018). Deep space gateway concept: Extending human presence into cislunar space. *2018 IEEE Aerospace Conference*, 1–10.

Cusack, S., Ferrone, K., Kramer, W. V., Garvin, C., Palaia, J., & Shiro, B. (2009). Flashline Mars Arctic Research Station (FMARS) 2009 Expedition Crew Perspectives. *SpaceOps 2010 Conference Delivering on the Dream Hosted by NASA Marshall Space Flight Center and Organized by AIAA*, 2258.

Daga, A. W., Allen, C., Battler, M. M., Burke, J. D., Crawford, I. A., Léveillé, R. J., Simon, S. B., & Tan, L. T. (2009). Lunar and martian lava tube exploration as part of an overall scientific survey. *Annual Meeting of the Lunar Exploration Analysis Group*, *1515*, 15.

Dai, M.-L., & Ozawa, K. (1997). Texture synthesis by L-systems. *Image and Vision Computing*, *15*(3), 197–204.

Davis, G., Montes, C., & Eklund, S. (2017). Preparation of lunar regolith based geopolymer cement under heat and vacuum. *Advances in Space Research*, *59*(7), 1872–1885.

Day, D. (2004). Aiming for Mars, Grounded on Earth. *The Space Review*.

Denis, F., de Temmerman, N., & Rammer, Y. (2017). The potential of graph theories to assess buildings' disassembly and components' reuse: How building information modelling (BIM) and social network analysis (SNA) metrics might help Design for Disassembly (DfD)? *HISER International Conference: Advances in Recycling and Management of Construction and Demolition Waste*, 123–128.

Derényi, I., Palla, G., & Vicsek, T. (2005). Clique percolation in random networks. *Physical Review Letters*, *94*(16), 160202.

Deuss, M., Deleuran, A. H., Bouaziz, S., Deng, B., Piker, D., & Pauly, M. (2015). ShapeOp—a robust and extensible geometric modelling paradigm. In *Modelling Behaviour* (pp. 505–515). Springer.

Do, S., Owens, A., Ho, K., Schreiner, S., & de Weck, O. (2016). An independent assessment of the technical feasibility of the Mars One mission plan–Updated analysis. *Acta Astronautica*, *120*, 192–228.

Dovey, K., & Dickson, S. (2002). Architecture and Freedom? Programmatic Innovation in the work of Koolhaas/OMA. *Journal of Architectural Education*, *56*(1), 5–13.

DRAKE, B. (1990). Alternative lunar mission strategies. *Space Programs and Technologies Conference*, 3846.

Drake, B. G. (1998). *Reference mission version 3.0: addendum to the human exploration of Mars: the reference mission of the NASA Mars exploration study team*. National Aeronautics and Space Administration, Lyndon B. Johnson Space Center.

Drake, B. G., Hoffman, S. J., & Beaty, D. W. (2010). Human exploration of Mars, Design Reference Architecture 5.0. *2010 IEEE Aerospace Conference*, 1–24. https://doi.org/10.1109/AERO.2010.5446736

Duarte, J. P. (2001). *Customizing mass housing: a discursive grammar for Siza's Malagueira houses*.

Dunbar, B. (2021a). *Explore Moon to Mars*. NASA. https://www.nasa.gov/topics/moon-to-mars/overview

Dunbar, B. (2021b). *Moon to Mars Overview*. 8 June. https://www.nasa.gov/topics/moon-to-mars/overview

Dunbar, B. (2022). *James Webb Space Telescope*. National Aeronautics and Space Administration. https://www.nasa.gov/webbfirstimages

Dyke, S. J., Marais, K., Bilionis, I., Werfel, J., & Malla, R. (2021). Strategies for the design and operation of resilient extraterrestrial habitats. *Sensors and Smart Structures Technologies for Civil, Mechanical, and Aerospace Systems 2021*, *11591*, 1159105.

Dyson, G. (2002). *Project Orion: The True Story of the Atomic Spaceship*. American Association of Physics Teachers.

Edgett, K. S., Butler, B. J., Zimbelman, J. R., & Hamilton, V. E. (1997). Geologic context of the Mars radar "Stealth" region in southwestern Tharsis. *Journal of Geophysical Research: Planets*, *102*(E9), 21545–21567.

Egor, G., Sven, S., Martin, D., & Reinhard, K. (2020). Computer-aided approach to public buildings floor plan generation. Magnetizing floor plan generator. *Procedia Manufacturing*, *44*, 132–139.

Ehresmann, B., Hassler, D. M., Zeitlin, C., Guo, J., Köhler, J., Wimmer-Schweingruber, R. F., Appel, J. K., Brinza, D. E., Rafkin, S. C. R., & Böttcher, S. I. (2016). Charged particle spectra measured during the transit to Mars with the Mars Science Laboratory Radiation Assessment Detector (MSL/RAD). *Life Sciences in Space Research*, *10*, 29–37.

Ehresmann, B., Zeitlin, C., Hassler, D. M., Wimmer-Schweingruber, R. F., Böhm, E., Böttcher, S., Brinza, D. E., Burmeister, S., Guo, J., & Köhler, J. (2014). Charged particle spectra obtained with the Mars Science Laboratory Radiation Assessment Detector (MSL/RAD) on the surface of Mars. *Journal of Geophysical Research: Planets*, *119*(3), 468–479.

El-Khaldi, M. M. S. (2007). *Mapping boundaries of generative systems for design synthesis*. Massachusetts Institute Of Technology.

English, N. (2018). *The Astronomical Legacy of Asaph Hall BT - Chronicling the Golden Age of Astronomy: A History of Visual Observing from Harriot to Moore* (N. English, Ed.; pp. 321–327). Springer International Publishing. https://doi.org/10.1007/978-3-319-97707-2_20

Farmer, C. B., Davies, D. W., Holland, A. L., Laporte, D. D., & Doms, P. E. (1977). Mars: Water vapor observations from the Viking orbiters. *Journal of Geophysical Research*, *82*, 4225–4248.

Fasoulaki, E. (2008). *Integrated design: A generative multi-performative design approach*. Massachusetts Institute of Technology.

Feynman, J., & Gabriel, S. B. (2000). On space weather consequences and predictions. *Journal of Geophysical Research: Space Physics*, *105*(A5), 10543–10564.

Fincher, W., & Boduch, M. (2009). *Standards of human comfort: relative and absolute*.

Fisher, J. A., Richardson, M. I., Newman, C. E., Szwast, M. A., Graf, C., Basu, S., Ewald, S. P., Toigo, A. D., & Wilson, R. J. (2005). A survey of Martian dust devil activity using Mars Global Surveyor Mars Orbiter Camera images. *Journal of Geophysical Research: Planets*, *110*(E3).

Fogg, M. J. (1998). Terraforming Mars: A review of current research. *Advances in Space Research*, *22*(3), 415–420.

Forget, F. (2009). The present and past climates of planet Mars. *EPJ Web of Conferences*, *1*. https://doi.org/10.1140/epjconf/e2009-0924-9

Frazer, J. (1995). *An evolutionary architecture*.

Freeman, L. C. (1977). A set of measures of centrality based on betweenness. *Sociometry*, 35–41.

Garcia, M. (2022). *Visitors to the Station by Country*. National Aeronautics and Space Administration. https://www.nasa.gov/feature/visitors-to-the-station-by-country/

Garcia-Chevesich, P. , Bendek, E. , Pizarro, R. , Valdes-Pineda, R. , Gonzalez, D. , Bown, H. , Martínez, E. and Gonzalez, L. (2017). Weathering Processes on Martian Craters: Implications on Recurring Slope Lineae and the Location of Liquid Water. *Open Journal of Modern Hydrology*, *7*, 245–256. https://doi.org/https://doi.org/10.4236/ojmh.2017.74014

Giardini, D., Lognonné, P., Banerdt, W. B., Pike, W. T., Christensen, U., Ceylan, S., Clinton, J. F., van Driel, M., Stähler, S. C., Böse, M., Garcia, R. F., Khan, A., Panning, M., Perrin, C., Banfield, D., Beucler, E., Charalambous, C., Euchner, F., Horleston, A., … Yana, C. (2020). The seismicity of Mars. *Nature Geoscience*, *13*(3), 205–212. https://doi.org/10.1038/s41561-020-0539-8

Gibney, E. (2016). Europe's first Mars rover gets funding—despite crash of test craft. *Nature News*, *540*(7632), 177.

GLOBAL TIMES. (2019). *Mars base opens in desert*. https://www.globaltimes.cn/content/1146426.shtml

Golombek, M. P., Haldemann, A. F. C., Forsberg-Taylor, N. K., DiMaggio, E. N., Schroeder, R. D., Jakosky, B. M., Mellon, M. T., & Matijevic, J. R. (2003). Rock size-frequency distributions on Mars and implications for Mars Exploration Rover landing safety and operations. *Journal of Geophysical Research: Planets*, *108*(E12).

GOURDOUKIS, D. (2016). *Protocol Architecture*. ARISTOTLE UNIVERSITY OF THESSALONIKI.

Grant, J., Golombek, M., Wilson Purdy, S., Farley, K., Williford, K., & Chen, A. (2018). The science process for selecting the landing site for the 2020 Mars rover. *Planetary and Space Science*, *164*. https://doi.org/10.1016/j.pss.2018.07.001

Greeley, R., Whelley, P. L., Arvidson, R. E., Cabrol, N. A., Foley, D. J., Franklin, B. J., Geissler, P. G., Golombek, M. P., Kuzmin, R. O., & Landis, G. A. (2006). Active dust devils in Gusev crater, Mars: observations from the Mars exploration rover spirit. *Journal of Geophysical Research: Planets*, *111*(E12).

Griebel, H. S., Knuth, S., Landgraf, M., Kalkum, F., & Hettmer, M. (2002). The Mars Society Balloon Probe Mission. *IAF Abstracts, 34th COSPAR Scientific Assembly*, 694.

Groemer, G., Gruber, S., Uebermasser, S., Soucek, A., Lalla, E. A., Lousada, J., Sams, S., Sejkora, N., Garnitschnig, S., & Sattler, B. (2020). The AMADEE-18 Mars analog expedition in the Dhofar region of Oman. *Astrobiology*, *20*(11), 1276–1286.

Guo, J., Zeitlin, C., Wimmer-Schweingruber, R. F., Hassler, D. M., Posner, A., Heber, B., Köhler, J., Rafkin, S., Ehresmann, B., & Appel, J. K. (2015). Variations of dose rate observed by MSL/RAD in transit to Mars. *Astronomy & Astrophysics*, *577*, A58.

Guo, J., Zeitlin, C., Wimmer-Schweingruber, R. F., Rafkin, S., Hassler, D. M., Posner, A., Heber, B., Köhler, J., Ehresmann, B., & Appel, J. K. (2015). Modeling the variations of dose rate measured by RAD during the first MSL Martian year: 2012–2014. *The Astrophysical Journal*, *810*(1), 24.

Haberle, McKay, C., Cabrol, N., Grin, E., Schaeffer, J., Zent, A., & Quinn, R. (2001). On the Possibility of Liquid Water on Present Day Mars. *Journal of Geophysical Research*, *106*, 23,317-323,326. https://doi.org/10.1029/2000JE001360

Hagberg, A., Schult, D., & Swart, P. (2009). *Exploring network structure, dynamics, and function*. Scipy.

Halatsch, J., Kunze, A., & Schmitt, G. (2008). Using shape grammars for master planning. In *Design Computing and Cognition'08* (pp. 655–673). Springer.

Hall, N. (2021). *Mars Atmosphere Model*. National Aeronautics and Space Administration. https://www.grc.nasa.gov/www/k-12/airplane/atmosmrm.html

Hall, T. W. (1999). Artificial Gravity and the Architecture of Orbital Habitats. *Journal of the British Interplanetary Society*, *52*(7–8), 290–300.

Hanel, R., Conrath, B., Hovis, W., Kunde, V., Lowman, P., Maguire, W., Pearl, J., Pirraglia, J., Prabhakara, C., Schlachman, B., Levin, G., Straat, P., & Burke, T. (1972). Investigation of the

Martian environment by infrared spectroscopy on Mariner 9. *Icarus*, *17*(2), 423–442. https://doi.org/https://doi.org/10.1016/0019-1035(72)90009-7

Hansmeyer, M. (2003). *L-System in Architecture: Nature's and Processes as Generators of Architectural Design*.

Harada, M., Witkin, A., & Baraff, D. (1995). Interactive physically-based manipulation of discrete/continuous models. *Proceedings of the 22nd Annual Conference on Computer Graphics and Interactive Techniques*, 199–208.

Harmon, J. K., Arvidson, R. E., Guinness, E. A., Campbell, B. A., & Slade, M. A. (1999). Mars mapping with delay-Doppler radar. *Journal of Geophysical Research: Planets*, *104*(E6), 14065–14089.

Harrison, A. A. (2010). Humanizing outer space: architecture, habitability, and behavioral health. *Acta Astronautica*, *66*(5), 890–896. https://doi.org/https://doi.org/10.1016/j.actaastro.2009.09.008

Harvey, B. (2007a). First plans. *Russian Planetary Exploration: History, Development, Legacy, Prospects*, 17–42.

Harvey, B. (2007b). Returning to the planets? *Russian Planetary Exploration: History, Development, Legacy, Prospects*, 291–323.

Hassler, D. M., Zeitlin, C., Wimmer-Schweingruber, R. F., Ehresmann, B., Rafkin, S., Eigenbrode, J. L., Brinza, D. E., Weigle, G., Böttcher, S., & Böhm, E. (2014). Mars' surface radiation environment measured with the Mars Science Laboratory's Curiosity rover. *Science*, *343*(6169), 1244797.

Häuplik-Meusburger, S., & Bannova, O. (2016). *Space Architecture Education for Engineers and Architects*. Springer International Publishing. https://doi.org/10.1007/978-3-319-19279-6

Häuplik-Meusburger, S., Binsted, K., & Bassingthwaighte, T. (2017). *Habitability studies and full scale simulation research: preliminary themes following HISEAS mission IV*.

Head, J. W., Marchant, D. R., & Kreslavsky, M. A. (2008). Formation of gullies on Mars: Link to recent climate history and insolation microenvironments implicate surface water flow origin. *Proceedings of the National Academy of Sciences*, *105*, 13258–13263.

Heinicke, C., & Arnhof, M. (2021). A review of existing analog habitats and lessons for future lunar and Martian habitats. *REACH*, *21*, 100038.

Heldmann, J. L., Stoker, C. R., Gonzales, A., McKay, C. P., Davila, A., Glass, B. J., Lemke, L. L., Paulsen, G., Willson, D., & Zacny, K. (2017). Red Dragon drill missions to Mars. *Acta Astronautica*, *141*, 79–88.

Heldmann, J., Toon, O., Pollard, W., Mellon, M., Pitlick, J., McKay, C., & Andersen, D. (2005). Formation of Martian Gullies by the Action of Liquid Water Flowing Under Current Martian Environmental Conditions. *J Geophys Res*, *110*. https://doi.org/10.1029/2004JE002261

HI-SEAS. (n.d.). *The Hawai'i Space Exploration Analog and Simulation*. Retrieved January 7, 2022, from https://www.hi-seas.org/about-hi-seas

Hoffman, N. (2002). Active Polar Gullies on Mars and the Role of Carbon Dioxide. *Astrobiology*, *2*, 313–323. https://doi.org/10.1089/153110702762027899

Holmberg, D. (2010). Radiation protection in space. *Umeå University*.

Holubec, K., & Connolly, J. (2010). *NASA Space Flight Human-System Standard Human Factors, Habitability, and Environmental Health*.

Hubbard, G. S., Naderi, F. M., & Garvin, J. B. (2002). Following the water, the new program for Mars exploration. *Acta Astronautica*, *51*(1–9), 337–350.

Hyde, R., Ishikawa, M., & Wood, L. (1990). *Mars in this decade: The great exploration*. Lawrence Livermore National Lab., CA (USA).

ICON Technology. (2022). *MARS DUNE ALPHA*. https://www.iconbuild.com/technology/mars-dune-alpha

Institute of Biomedical Problems (IMBP). (n.d.). *The main purpose of 520-day isolation*. Retrieved January 7, 2022, from http://mars500.imbp.ru/en/520_about.html

Janssen, F., & Houben, R. W. G. (2013). Reinforced ice structures. *Eindhoven University of Technology (262 Pp.)*.

Jean-Marc, S., & Richard, H. (n.d.). *REVISITING MARS SEMI-DIRECT*.

Johnson, S. W., Rohloff, K. J., Whitmire, J. N., Pyrz, A. P., Ullrich, G. W., & Lee, D. G. (1971). The lunar regolith as a site for an astronomical observatory. *Space Technology and Science*, 1059.

Johnson-Freese, J. (2017). Build on the outer space treaty. *Nature*, *550*(7675), 182–184.

Kading, B., & Straub, J. (2015). Utilizing in-situ resources and 3D printing structures for a manned Mars mission. *Acta Astronautica*, *107*, 317–326.

Kahre, M. A., Murphy, J. R., & Haberle, R. M. (2006). Modeling the Martian dust cycle and surface dust reservoirs with the NASA Ames general circulation model. *Journal of Geophysical Research: Planets*, *111*(E6).

Kanas, N., & Manzey, D. (2008). *Space psychology and psychiatry*.

Karatekin, Ö., van Hove, B., Ferri, F., Aboudan, A., & Colombatti, G. (2018). Reconstruction of the Mars atmosphere using the flight data from ExoMars Schiaparelli's instrumented heat shield and radio communications. *European Planetary Science Congress*, EPSC2018-1211.

Kennedy, K. (2017). *Space Architecture & Systems Architecting*.

Kilian, A., & Ochsendorf, J. (2005). Particle-spring systems for structural form finding. *Journal of the International Association for Shell and Spatial Structures*, *46*(2), 77–84.

Kim, M. H. Y., Thibeault, S. A., Wilson, J. W., Simonsen, L. C., Heilbronn, L., Chang, K., Kiefer, R. L., Weakley, J. A., & Maahs, H. G. (2000). Development and testing of in situ materials for human exploration of Mars. *High Performance Polymers*, *12*(1), 13–26.

Knight, T. (2000). Introduction to shape grammars. *Lecture Notes Presented at the MIT, MIT/Miyagi Workshop*.

Köhler, J., Zeitlin, C., Ehresmann, B., Wimmer-Schweingruber, R. F., Hassler, D. M., Reitz, G., Brinza, D. E., Weigle, G., Appel, J., & Böttcher, S. (2014). Measurements of the neutron spectrum on the Martian surface with MSL/RAD. *Journal of Geophysical Research: Planets*, *119*(3), 594–603.

Kolarevic, B. (2003a). Digital morphogenesis. *Architecture in the Digital Age: Design and Manufacturing*, 12–28.

Kolarevic, B. (2003b). Information master builders. *Architecture in the Digital Age: Design and Manufacturing*, *59*.

Kolarevik, B. (2003). Digital production/fabrication. *Digital Technology & Architecture–White Paper ACADIA*, *4*.

Kolb, K. J., Pelletier, J. D., & McEwen, A. S. (2010). Modeling the formation of bright slope deposits associated with gullies in Hale Crater, Mars: Implications for recent liquid water. *icarus*, *205*(1), 113–137. https://doi.org/10.1016/j.icarus.2009.09.009

Koning, H., & Eizenberg, J. (1981). The language of the prairie: Frank Lloyd Wright's prairie houses. *Environment and Planning B: Planning and Design*, *8*(3), 295–323.

Kozikoğlu, N., & ÇEBİ, P. D. (2015). Thinking and designing with the idea of network in architecture. *A| Z ITU Journal of the Faculty of Architecture*, *12*(3), 71–87.

Krawczyk, R. J. (2002a). *Architectural interpretation of cellular automata*.

Krawczyk, R. J. (2002b). *Experiments in architectural form generation using cellular automata*.

Kunz, J. C., Christiansen, T. R., Cohen, G. P., Jin, Y., & Levitt, R. E. (1998). The virtual design team. *Communications of the ACM*, *41*(11), 84–91.

Lai, J.-Y., Neduncheran, A., Uppalapati, S., Arunan, S., Creech, J., Gamal, H., Potrivitu, G. C., & Rivolta, A. (2018). Proposal for a Floating Habitat Design for Manned Missions to Venus. *69th International Astronautical Congress (IAC 2018)*, 1–5.

Lam, Z., & King, S. A. (2005). Simulating tree growth based on internal and environmental factors. *Proceedings of the 3rd International Conference on Computer Graphics and Interactive Techniques in Australasia and South East Asia*, 99–107.

Landau, E. (2019). *How the Webb Telescope Will Explore Mars*. NASA. https://www.nasa.gov/feature/how-the-webb-telescope-will-explore-mars

Landis, G. A. (n.d.). *Footsteps to Mars*.

Larson, W. J., & Pranke, L. K. (1999). *Human Spacecraft Mission Analysis and Design*. McGraw-Hill Primis Custom Publishing, New York.

Lauro, S. E., Pettinelli, E., Caprarelli, G., Guallini, L., Rossi, A. P., Mattei, E., Cosciotti, B., Cicchetti, A., Soldovieri, F., & Cartacci, M. (2021). Multiple subglacial water bodies below the south pole of Mars unveiled by new MARSIS data. *Nature Astronomy*, *5*(1), 63–70.

Lazcano, A., & Bada, J. L. (2008). Stanley L. Miller (1930–2007): reflections and remembrances. *Origins of Life and Evolution of Biospheres*, *38*(5), 373–381.

Lee, A. G., Mader, T. H., Gibson, C. R., & Tarver, W. (2017). Space flight–associated neuro-ocular syndrome. *JAMA Ophthalmology*, *135*(9), 992–994.

Lele, A. (2014). *Mars Missions: Past, Present and Future BT - Mission Mars: India's Quest for the Red Planet* (A. Lele, Ed.; pp. 85–92). Springer India. https://doi.org/10.1007/978-81-322-1521-9_7

Leovy, C. (2001). Weather and climate on Mars. *Nature*, *412*(6843), 245–249.

Li, J., Chen, Y., & Lin, Y. (2010). Research on traffic layout based on social network analysis. *2010 2nd International Conference on Education Technology and Computer*, *1*, V1-284.

Li, Y., Song, Z., Ding, Y., Xin, Y., Wu, T., Su, T., He, R., Tai, F., & Lian, Z. (2016). Effects of formaldehyde exposure on anxiety-like and depression-like behavior, cognition, central levels of glucocorticoid receptor and tyrosine hydroxylase in mice. *Chemosphere*, *144*, 2004–2012.

Lim, G., & Herrmann, J. W. (n.d.). NASA-STD-3001, Space Flight Human-System Standard and the Human Integration Design Handbook.

Lima, M. (2011). Visual complexity. *Source: Http://Www. Visualcomplexity. Com*.

Lin, T. D. (1985). Concrete for lunar base construction. *Lunar Bases and Space Activities of the 21st Century*, 381.

Lin, T. D., Love, H., & Stark, D. (1992). Physical properties of concrete made with Apollo 16 lunar soil sample. *NASA. Johnson Space Center, The Second Conference on Lunar Bases and Space Activities of the 21st Century, Volume 2*.

Lindenmayer, A., & Rozenberg, G. (1972). Developmental systems and languages. *Proceedings of the Fourth Annual ACM Symposium on Theory of Computing*, 214–221.

Litaker, H. L., & Howard, R. L. (2022, March). Viability of Small Dimension Crew Quarters for Surface Habitation. In 2022 IEEE Aerospace Conference (AERO) (pp. 1-13). IEEE.

MACKENZIE, B. (1989). Building Mars habitats using local materials. *The Case for Mars III: Strategies for Exploration- General Interest and Overview(A 90-16651 05-12). San Diego, CA, Univelt, Inc., 1989,*.

Macy, M. W., & Willer, R. (2002). From factors to actors: Computational sociology and agent-based modeling. *Annual Review of Sociology*, 143–166.

Mahaffy, P. R., Stern, J. C., Franz, H. B., Stalport, F., Eigenbrode, J., Blake, D. F., Conrad, P., Steele, A., & McAdam, A. C. (2010). Field and Laboratory Studies of Samples from the Bockfjord Volcanic Complex in the 2009 Arctic Mars Analog Svalbard Expedition. *Astrobiology Science Conference 2010: Evolution and Life: Surviving Catastrophes and Extremes on Earth and Beyond*, *1538*, 5306.

Maher, M. lou, Smith, G., & Gero, J. S. (2003). *DESIGN AGENTS IN 3D VIRTUALWORLDS*.

Mahoney, E. (2016). *Deep Space Habitation Overview*. National Aeronautics and Space Administration. https://www.nasa.gov/deep-space-habitation/overview/

Majeed, S., Uzair, M., Qamar, U., & Farooq, A. (2020). Social Network Analysis Visualization Tools: A Comparative Review. *2020 IEEE 23rd International Multitopic Conference (INMIC)*, 1–6. https://doi.org/10.1109/INMIC50486.2020.9318162

Malin, M., & Edgett, K. (2000). Evidence for Recent Groundwater Seepage and Surface Runoff on Mars. *Science (New York, N.Y.)*, *288*, 2330–2335. https://doi.org/10.1126/science.288.5475.2330

Malin, M., Edgett, K., Posiolova, L., McColley, S., & Noe Dobrea, E. (2006). Present-Day Impact Cratering Rate and Contemporary Gully Activity on Mars. *Science (New York, N.Y.)*, *314*, 1573–1577. https://doi.org/10.1126/science.1135156

Mankins, J. C. (1995). Technology readiness levels. *White Paper, April*, *6*(1995), 1995.

Marano, G. C., Pasin, U., Sardone, L., & SpA, O. W. (2021). *Generative Modelling and Artificial Intelligence for Structural Optimization of a Large Span Structure*.

Mark, E. (2007). *Simulating dynamic forces in design with special effects tools*.

Mark, E., Gross, M., & Goldschmidt, G. (2008). *A perspective on computer aided design after four decades*.

Mars Institute. (2020). *Haughton-Mars Project (HMP)*. https://www.marsinstitute.no/hmp

Mars, K. (2021). *NASA'S CHAPEA (Crew Health and Performance Exploration Analog) & Mars Dune Alpha Habitat*. NASA CHAPEA. https://www.nasa.gov/chapea/habitat

Mars Society. (2022). *European Mars Analogue Research Station*. http://www.euromars.org/

Marshall-Goebel, K., Damani, R., & Bershad, E. M. (2019). Brain physiological response and adaptation during spaceflight. *Neurosurgery*, *85*(5), E815–E821.

Martínez, G. M., & Renno, N. O. (2013). Water and Brines on Mars: Current Evidence and Implications for MSL. *Space Science Reviews*, *175*(1), 29–51. https://doi.org/10.1007/s11214-012-9956-3

Masson-Delmotte, V., P. Zhai, A. Pirani, S. L., Connors, C. Péan, S. Berger, N. Caud, Y. Chen, L. Goldfarb, M.I. Gomis, M. Huang, K. Leitzell, E. Lonnoy, J. B. R., & Matthews, T.K. Maycock, T. Waterfield, O. Yelekçi, R. Yu, and B. Z. (eds.). (2021). *IPCC, 2021: Climate Change 2021: The Physical Science Basis. Contribution of Working Group I to the Sixth Assessment Report of the Intergovernmental Panel on Climate Change*.

Mcewen, A., Ojha, L., Dundas, C., Mattson, S., Byrne, S., Wray, J., Cull-Hearth, S., Thomas, N., & Gulick, V. (2011). Seasonal Flows on Warm Martian Slopes. *Science (New York, N.Y.)*, *333*, 740–743. https://doi.org/10.1126/science.1204816

McKenna-Lawlor, S., Gonçalves, P., Keating, A., Reitz, G., & Matthiä, D. (2012). Overview of energetic particle hazards during prospective manned missions to Mars. *Planetary and Space Science*, *63*, 123–132.

McLane III, J. C. (2006). 'Spirit of the Lone Eagle': An Audacious Program for a Manned Mars Landing. *Sp. Rev.[Online]. Available Online at: Http://Www. Thespacereview. Com/Article/669/1.[Accessed: 12-Mar-2016]*.

McSween, H., Wyatt, M., Gellert, R., F., B., Morris, R., Herkenhoff, K., Crumpler, L., Milam, K. A., Stockstill-Cahill, K., Tornabene, L., Arvidson, R., Bartlett, P., Blaney, D., Cabrol, N., Christensen, P., Clark, B., Crisp, J. A., des Marais, D., Economou, T., & Zipfel, J. (2006). Characterization and petrologic interpretation of olivine-rich basalts at Gusev Crater, Mars. *Journal of Geophysical Research*, *111*. https://doi.org/10.1029/2005JE002477

McSween, H. Y.; Murchie, S. L.; Crisp, J. A.; Bridges, N. T.; Anderson, R. C.; Britt, D. T.; Bruckner, J.; Dreibus, G.; Economou, T.; Ghosh, A.; Golombek, M. P.; Greenwood, J. P.; Johnson, J. R.; Moore, H. J.; Morris, R. V.; Parker, T. J.; Rieder, R.; Sin, H. (1998). Chemical, Multispectral, and Textural Constraints on the Composition and Origin of Rocks at the Mars Pathfinder Landing Site. *Journal of Geophysical Research*. https://trs.jpl.nasa.gov/handle/2014/20152

Meek, T. T., Vaniman, D. T., Blake, R. D., & Godbole, M. J. (1987). Sintering of lunar soil simulants using 2.45 GHz microwave radiation. *Lunar and Planetary Science Conference*, *18*.

MENDEL, W. W. (1993). INTERNATIONAL MARS MISSION (FROM THE 1991 INTERNATIONAL SPACE UNIVERSITY (ISU) DESIGN PROJECT) f. *Acta Astronautica*, *29*(9), 70–704.

Messerschmid, E., & Bertrand, R. (2013). *Space stations: systems and utilization*. Springer Science & Business Media.

Messina, P., Vennemann, D., & Gardini, B. (2005). The european space agency exploration programme aurora. *1st Space Exploration Conference: Continuing the Voyage of Discovery*, 2518.

Milliken, R., Grotzinger, J., & Thomson, B. (2010). Paleoclimate of Mars as captured by the stratigraphic record in Gale Crater. *Geophysical Research Letters*, *37*. https://doi.org/10.1029/2009GL041870

Miscio, E. (2018). *Development of atmosphere and altimeter models for Mars mission simulation and integration in dSPACE real-time environment*. Politecnico di Torino.

Mitchell, T. (1997). *Machine learning* (Vol. 1, Issue 9). McGraw-hill New York.

Monclar, R. S., Oliveira, J., de Faria, F. F., Ventura, L., de Souza, J. M., & Campos, M. L. M. (2011). Using social networks analysis for collaboration and team formation identification. *Proceedings of the 2011 15th International Conference on Computer Supported Cooperative Work in Design (CSCWD)*, 562–569.

Moore, H. J., & Jakosky, B. M. (1989). Viking landing sites, remote-sensing observations, and physical properties of Martian surface materials. *Icarus*, *81*(1), 164–184. https://doi.org/https://doi.org/10.1016/0019-1035(89)90132-2

Moore, P. (1997). *Maraldi, Giacomo Filippo (1665–1729) BT - Encyclopedia of Planetary Science* (p. 427). Springer Netherlands. https://doi.org/10.1007/1-4020-4520-4_235

Morris, M., Ciardullo, C., Lents, K., Montes, J., Rudakevych, O., Sono, M., Sono, Y., & Yashar, M. (2016a). *Mars Ice House: Using the Physics of Phase Change in 3D Printing a Habitat with H2O*.

Morris, M., Ciardullo, C., Lents, K., Montes, J., Rudakevych, O., Sono, M., Sono, Y., & Yashar, M. (2016b). *Mars Ice House: Using the Physics of Phase Change in 3D Printing a Habitat with H2O*. https://doi.org/10.2514/6.2016-5528

Morris, M., Ciardullo, C., Lents, K., Montes, J., Rudakevych, O., Sono, M., Sono, Y., & Yashar, M. (2016c, September 13). Mars Ice House: Using the Physics of Phase Change in 3D Printing a Habitat with H2O. *AIAA SPACE 2016*. https://doi.org/10.2514/6.2016-5528

Morris, R., Klingelhoefer, G., Schröder, C., Rodionov, D., Yen, A., Ming, D., de Souza, P., Fleischer, I., Wdowiak, T., Gellert, R., Bernhardt, B., Evlanov, E., Zubkov, B., Foh, J., Bonnes, U., Kankeleit, E., Guetlich, P., Renz, F., Squyres, S., & Arvidson, R. (2006). Mössbauer mineralogy of rock, soil, and dust at Gusev Crater, Mars: Spirit's journey through weakly altered olivine basalt on the Plains and pervasively altered basalt in the Columbia Hills. *Journal of Geophysical Research*, *111*, 1–28. https://doi.org/10.1029/2005JE002584

Morris, R. v, Golden, D. C., Bell, J. F., Shelfer, T. D., Scheinost, A. C., Hinman, N. W., Furniss, G. M., Mertzman, S. A., Bishop, J. L., Ming, D. W., Allen, C. C., & Britt, D. T. (2000). Mineralogy, composition, and alteration of Mars Pathfinder rocks and soils: Evidence from multispectral, elemental, and magnetic data on terrestrial analogue, SNC meteorite, and Pathfinder samples. *Journal of Geophysical Research*, *105*, 1757–1817.

Mueller, R. P., Prater, T. J., Roman, M., Edmunson, J. E., Fiske, M. R., & Carrato, P. (2019). NASA centennial challenge: three dimensional (3D) printed habitat, phase 3. *70th International Astronautical Congress (IAC)*, *KSC-E-DAA-TN74064*.

Mueller, R. P., Sibille, L., Hintze, P. E., Lippitt, T. C., Mantovani, J. G., Nugent, M. W., & Townsend, I. I. (2014). Additive construction using basalt regolith fines. In *Earth and Space 2014* (pp. 394–403).

Muhleman, D. O., Grossman, A. W., & Butler, B. J. (1995). Radar investigation of Mars, Mercury, and Titan. *Annual Review of Earth and Planetary Sciences*, *23*(1), 337–374.

Müller, P., Wonka, P., Haegler, S., Ulmer, A., & van Gool, L. (2006). Procedural modeling of buildings. In *ACM SIGGRAPH 2006 Papers* (pp. 614–623).

Musselwhite, D., Swindle, T., & Lunine, J. (2001). Liquid CO2 breakout and the formation of recent small gullies on Mars. *Geophysical Research Letters*, *28*, 1283–1285. https://doi.org/10.1029/2000GL012496

Myers, R. L., & Myers, R. L. (2006). *The basics of physics*. Greenwood Publishing Group.

NASA. (2010). *Science Instruments*. NASA Jet Propulsion Laboratory, California Institute of Technology. https://mars.nasa.gov/mgs/mission/sc_instruments.html

NASA. (2015). *NASA's Journey to Mars: Pioneering Next Steps in Space Exploration.* National Aeronautics and Space Administration Washington, DC.

NASA. (2021a). *Historical Log*. NASA Science Mars Exploration Program. https://mars.nasa.gov/mars-exploration/missions/historical-log/

NASA. (2021b). *Mars Facts*. NASA Science Mars Exploration Program. https://mars.nasa.gov/all-about-mars/facts/

NASA. (2021c). *MARS The Red Planet*. NASA Science Solar System Exploration. https://solarsystem.nasa.gov/planets/mars/in-depth/

NASA. (2021d). *NASA Spinoff*. NASA Technology Transfer Program. https://spinoff.nasa.gov/

NASA. (2022). *About Webb Orbit*. JAMES WEBB SPACE TELESCOPE, GODDARD SPACE FLIGHT CENTER. https://webb.nasa.gov/content/about/orbit.html

NASA Jet Propulsion Laboratory. (2022). *NASA's InSight Records Monster Quake on Mars*. California Institute of Technology. https://www.jpl.nasa.gov/news/nasas-insight-records-monster-quake-on-mars

NASA Science. (2018). *Mars Orbiter Mission*. Solar System Exploration. https://solarsystem.nasa.gov/missions/mars-orbiter-mission/in-depth/

NASA Science. (2019). *InSight (Discovery Mission)*. MARS Exploration Program. https://mars.nasa.gov/mars-exploration/missions/insight/

NASA Science. (2022a). *2001 Mars Odyssey*. MARS Exploration Program. https://mars.nasa.gov/mars-exploration/missions/odyssey/

NASA Science. (2022b). *ExoMars 2016 Mission (ESA/Roscosmos)*. MARS Exploration Program. https://mars.nasa.gov/mars-exploration/missions/esa-exomars-2016-tgo/

NASA Science. (2022c). *For Scientists: Landing Site Selection*. MARS 2020 Mission Perseverance Rover. https://mars.nasa.gov/mars2020/mission/science/for-scientists/landing-site-selection/

NASA Science. (2022d). *Mars Atmospheric and Volatile EvolutioN*. MARS Exploration Program. https://mars.nasa.gov/mars-exploration/missions/maven/

NASA Science. (2022e). *Mars Express (ESA)*. MARS Exploration Program. https://mars.nasa.gov/mars-exploration/missions/express/

NASA Science. (2022f). *Mars Reconnaissance Orbiter*. MARS Exploration Program. https://mars.nasa.gov/mars-exploration/missions/mars-reconnaissance-orbiter/

NASA Science. (2022g). *Mars Science Laboratory*. MARS Exploration Program. https://mars.nasa.gov/mars-exploration/missions/mars-science-laboratory/

NASA Science. (2022h). *Perseverance Rover's Landing Site: Jezero Crater*. MARS 2020 Mission Perseverance Rover. https://mars.nasa.gov/mars2020/mission/science/landing-site/

NASA Science. (2022i). *Picking a Landing Site for NASA's Mars 2020 Rover*. MARS 2020 Mission Perseverance Rover. https://mars.nasa.gov/mars2020/timeline/prelaunch/landing-site-selection/eight-potential-sites/

National Air and Space Museum. (2021). *MAJOR LANDFORMS*. Smithsonian National Air and Space Museum. https://airandspace.si.edu/exhibitions/exploring-the-planets/online/solar-system/mars/surface/major-landforms.cfm

Nazari-Sharabian, M., Aghababaei, M., Karakouzian, M., & Karami, M. (2020). Water on Mars—A Literature Review. *Galaxies*, *8*(2). https://doi.org/10.3390/galaxies8020040

Nelson, M. (2015). Mars water discoveries - Implications for finding ancient and current life. *Life Sciences in Space Research*, *7*. https://doi.org/10.1016/j.lssr.2015.10.006

Nikle, A., Boyce, P., Greene, J. K., & Pyle, S. (n.d.). *Inspiration Mars: Team JASPer*.

Nisztuk, M., & Myszkowski, P. B. (2019). Hybrid evolutionary algorithm applied to automated floor plan generation. *International Journal of Architectural Computing*, *17*(3), 260–283.

Nourian, P. (2016). *Configraphics: Graph theoretical methods for design and analysis of spatial configurations*.

Nourian, P., Rezvani, S., & Sariyildiz, S. (2013). *Designing with Space Syntax A configurative approach to architectural layout, proposing a computational methodology*.

Olson, J., Craig, D., & center, N. A. and S. Administration. L. research. (2011). *NASA's Analog Missions: Paving the Way for Space Exploration*. National Aeronautics and Space Administration.

Ortiz, A. R., Rygalov, V. Y., & León, P. de. (2015). *Radiation Protection Strategy Development for Mars Surface Exploration*.

Osburg, J. (2002). *An interdisciplinary approach to the conceptual design of inhabited space systems*.

Oxman, R. (2008). Performance-based design: current practices and research issues. *International Journal of Architectural Computing*, *6*(1), 1–17.

Palubicki, W., Horel, K., Longay, S., Runions, A., Lane, B., Měch, R., & Prusinkiewicz, P. (2009). Self-organizing tree models for image synthesis. *ACM Transactions On Graphics (TOG)*, *28*(3), 1–10.

Parish, Y. I. H., & Müller, P. (2001). Procedural modeling of cities. *Proceedings of the 28th Annual Conference on Computer Graphics and Interactive Techniques*, 301–308.

Park, K. (2020). *Structural Consideration in Additive Manufacturing of Concrete as Part of NASA's Centennial 3D Printed Mars Habitat Challenge*. Pennsylvania State University.

Park, K., Memari, A., Nazarian, S., Duarte, J., & Hojati, M. (2020, June). *Structural Analysis of Full-Scale and Sub-Scale Structure for Digitally Designed Martian Habitat*.

Pascal Lee. (2017). *NASA Haughton-Mars Project: New Partnership on Mars Drone Application Research*. SETI INSTITUTE. https://www.seti.org/press-release/nasa-haughton-mars-project-new-partnership-mars-drone-application-research

Pedraza, J. M. (2013). *Going to the 'moon' without leaving campus*. https://www1.und.edu/features/2013/10/ndx-planetary-exploration-system.cfm

Pedraza, J. M. (2018). *UND Space Studies launches fifth "Mars" mission with physician aboard*. http://blogs.und.edu/uletter/2018/05/und-space-studies-launches-fifth-mars-mission-with-physician-aboard/

Petrenko, V. F., & Whitworth, R. W. (1999). *Physics of ice*. OUP Oxford.

Petrovic, J. J. (2003). Review mechanical properties of ice and snow. *Journal of Materials Science*, *38*(1), 1–6.

Picardi, G., Plaut, J. J., Biccari, D., Bombaci, O., Calabrese, D., Cartacci, M., Cicchetti, A., Clifford, S. M., Edenhofer, P., & Farrell, W. M. (2005). Radar soundings of the subsurface of Mars. *Science*, *310*(5756), 1925–1928.

Piker, D. (2013). Kangaroo: form finding with computational physics. *Architectural Design*, *83*(2), 136–137.

Platoff, A. M. (1999). *Eyes on the red planet: Human Mars mission planning, 1952-1970*. University of Houston-Clear Lake.

Pletser, V., Lognonne, P., Diament, M., & Dehant, V. (2009). Subsurface water detection on Mars by astronauts using a seismic refraction method: Tests during a manned Mars mission simulation. *Acta Astronautica*, *64*(4), 457–466. https://doi.org/https://doi.org/10.1016/j.actaastro.2008.07.005

Portree, D. S. F. (2001). *Humans to Mars: Fifty years of mission planning, 1950-2000* (Issue 20). National Aeronautics and Space Administration.

Potter, S. (2018). NASA Finds Ancient Organic Material, Mysterious Methane on Mars. *Retrieved December*, *11*, 2019.

Powers, R. M. (2017). *The World's First Spaceship Shuttle*. Stackpole Books.

Preisinger, C. (2013). Linking structure and parametric geometry. *Architectural Design*, *83*(2), 110–113.

Price, H., Hawkins, A., & Radcliffe, T. (2009). Austere human missions to Mars. *AIAA SPACE 2009 Conference & Exposition*, 6685.

Prusinkiewicz, P., Hammel, M., Hanan, J., & Mech, R. (1996). L-systems: from the theory to visual models of plants. *Proceedings of the 2nd CSIRO Symposium on Computational Challenges in Life Sciences*, *3*, 1–32.

Putzig, N. (2020). *SWIM Overview*. The Planetary Science Institute. https://swim.psi.edu/about.php?section=overview

Putzig, N. E., Morgan, G. A., Sizemore, H. G., Baker, D. M. H., Petersen, E. I., Pathare, A., Dundas, C. M., Bramson, A. M., Courville, S. W. W., & Perry, M. (2021). Mapping Ice Resources on Mars. *AGU Fall Meeting 2021*.

R. Gellert, R. Rieder, J. Brückner, B. C. Clark, G. Dreibus, G. Klingelhöfer, G. Lugmair, D. W. Ming, H. Wänke, A. Yen, J. Zipfel, S. W. S. (2006). Alpha Particle X-Ray Spectrometer (APXS): Results from Gusev crater and calibration report. *Journal of Geophysical Research: Planets*, *111*(E2). https://doi.org/https://doi.org/10.1029/2005JE002555

Raftery, M., Cooke, D., Hopkins, J., & Hufenbach, B. (2013). An affordable mission to Mars. *64th International Astronautical Congress, IAC-13, A5, 4-D2. 8.4*.

Raghavan, U. N., Albert, R., & Kumara, S. (2007). Near linear time algorithm to detect community structures in large-scale networks. *Physical Review E*, *76*(3), 36106.

Ramkissoon, N. K., Pearson, V. K., Schwenzer, S. P., Schröder, C., Kirnbauer, T., Wood, D., Seidel, R. G. W., Miller, M. A., & Olsson-Francis, K. (2019). New simulants for martian regolith: controlling iron variability. *Planetary and Space Science*, *179*, 104722.

Rask, J., Vercoutere, W., Navarro, B. J., & Krause, A. (2008). Space Faring: The Radiation Challenge. *Nasa, Module*, *3*(8), 9.

Reilly, C. (2020). *This 3D-printed Mars habitat could be your new home in space - CNET*. Cnet. https://www.cnet.com/pictures/this-3d-printed-mars-habitat-could-be-your-new-home-in-space-marsha-ai-spacefactory/

Research in Svalbard Database. (2011). *ARCTIC MARS ANALOG SVALBARD EXPEDITION (AMASE)*. https://www.researchinsvalbard.no/project/6482

Rieder, R., Economou, T., Wanke, H., Turkevich, A., Crisp, J., Bruckner, J., ... & McSween Jr, H. Y. (1997). The chemical composition of Martian soil and rocks returned by the mobile alpha proton X-ray spectrometer: Preliminary results from the X-ray mode. *Science*, *278*(5344), 1771-1774.

Rodmann, J., Miller, A., Bunte, K. D., & Millinger, M. (2019). Micrometeoroid Impact Risk Assessment for Interplanetary Missions. *Orbital Debris Conference*.

Rojdev, K., Moore, J., Piatek, I., & Calvert, D. (2015). Systems Engineering Lessons Learned for Class D Missions. In *AIAA SPACE 2015 Conference and Exposition* (p. 4676).

Rollock, A. E., & Klaus, D. M. (2022). Defining and characterizing self-awareness and self-sufficiency for deep space habitats. *Acta Astronautica*.

Roman, M. C., Eberly, E. A., Mueller, R. P., & Deutsch, S. (2016). NASA centennial challenge: Three dimensional (3D) printed habitat. In *Earth and Space 2016: Engineering for Extreme Environments* (pp. 333–342). American Society of Civil Engineers Reston, VA.

Roman, M., Yashar, M., Fiske, M., Nazarian, S., Adams, A., Boyd, P., Bentley, M., & Ballard, J. (2020). *3D-printing lunar and martian habitats and the potential applications for additive construction*.

Royal Belgian Institute for Space Aeronomy. (2021). *Mars climate, important temperature difference between day and night*. Royal Belgian Institute for Space Aeronomy. https://www.aeronomie.be/en/encyclopedia/mars-climate-important-temperature-difference-between-day-and-night

Rubin, A. E., & Grossman, J. N. (2010). Meteorite and meteoroid: New comprehensive definitions. *Meteoritics & Planetary Science*, *45*(1), 114–122.

Rubinstein, H., Abramovich, R. S., Shikar, A., Zagai, M., Nevenzal, H., & Finzi, Y. (2019). The 2019 analog Mars mission season at the Desert Mars analog ramon station. *Conference: 70th International Astronautical Congress (IAC-19), Washington, DC*.

Rubinstein, H., Sorek-Abramovich, R., Shikar, A., Zagai, M., Nevenzal, H., Finzi, Y., Babad, A., Yair, Y., Mauda, S., & Porat, Y. (2019). Mars analogs at Ramon crater region: D-MARS. *Lunar and Planetary Science Conference*, *2132*, 2813.

Salge, C., Lipski, C., Mahlmann, T., & Mathiak, B. (2008). Using genetically optimized artificial intelligence to improve gameplaying fun for strategical games. *Proceedings of the 2008 ACM SIGGRAPH Symposium on Video Games*, 7–14.

Salotti, J.-M. (2011). 2-4-2 Concept for manned missions to Mars. *2-4-2 Concept for Manned Missions to Mars*, 1–5.

Schindler, K. (2016). *Lowell Observatory*. Arcadia Publishing.

Schlacht, I. (2012). *SPACE HABITABILITY. Integrating Human Factors into the Design Process to Enhance Habitability in Long Duration Missions*. https://doi.org/10.14279/depositonce-3093

Schofield, J., Barnes, J., Crisp, D., Haberle, R., Larsen, S., Magalhaes, J. A., Murphy, J., Seiff, A., & Wilson, G. (1998). The Mars Pathfinder Atmospheric Structure Investigation (ASI/MET) Meteorological Experiment. *Science (New York, N.Y.)*, *278*, 1752–1758. https://doi.org/10.1126/science.278.5344.1752

Schofield, J. T., Barnes, J. R., Crisp, D., Haberle, R. M., Larsen, S., Magalhaes, J. A., Murphy, J. R., Seiff, A., & Wilson, G. (1997). The Mars Pathfinder atmospheric structure investigation/meteorology (ASI/MET) experiment. *Science*, *278*(5344), 1752–1758.

Schulson, E. M. (1999). The structure and mechanical behavior of ice. *Jom*, *51*(2), 21–27.

Schultz, R. A. (1993). Brittle strength of basaltic rock masses with applications to Venus. *Journal of Geophysical Research: Planets*, *98*(E6), 10883–10895.

Scott, W. R., & Davis, G. F. (2015). *Organizations and organizing: Rational, natural and open systems perspectives*. Routledge.

Sejkora, N., Sams, S., & Groemer, G. (2018). Geodata workflow for the AMADEE-18 Mars analog mission. *European Planetary Science Congress*, EPSC2018-442.

Seu, R., Biccari, D., Orosei, R., Lorenzoni, L. v, Phillips, R. J., Marinangeli, L., Picardi, G., Masdea, A., & Zampolini, E. (2004). SHARAD: The MRO 2005 shallow radar. *Planetary and Space Science*, *52*(1–3), 157–166.

Shekhtman, L. (2019). *With Mars Methane Mystery Unsolved, Curiosity Serves Scientists a New One: Oxygen*. NASA. https://www.nasa.gov/feature/goddard/2019/with-mars-methane-mystery-unsolved-curiosity-serves-scientists-a-new-one-oxygen

Shukla, R. K., & Deshmukh, D. B. (2016). A review on role of CAD/CAM in designing for skill development. *Int. J. Res. Eng. Sci. Technol.*, *1*(June 2015).

Shunk, G. K., Gomez, X. R., & Averesch, N. J. H. (2020). A self-replicating radiation-shield for human deep-space exploration: Radiotrophic Fungi can attenuate ionizing radiation aboard the international space station. *BioRxiv*.

Simon, J. (2019). *Evolving Floorplans*. https://www.joelsimon.net/evo_floorplans.html

Simpson, R. A., Harmon, J. K., Zisk, S. H., Thompson, T. W., & Muhleman, D. O. (1992). Radar determination of Mars surface properties. *Mars*, 652–685.

Singh, H., & Sharma, R. (2012). Role of adjacency matrix & adjacency list in graph theory. *International Journal of Computers & Technology*, *3*(1), 179–183.

Sklar, S. T., & Rupert, S. M. (2004). A FIELD METHODOLOGY APPROACH BETWEEN AN EARTH-BASED REMOTE SCIENCE TEAM AND A PLANETARY-BASED FIELD CREW. *Proceedings of the 7th International Mars Society Convention*.

Smith, A. R. (1984). Plants, fractals, and formal languages. *ACM SIGGRAPH Computer Graphics*, *18*(3), 1–10.

Smith, D. E., Zuber, M. T., Frey, H. v, Garvin, J. B., Head, J. W., Muhleman, D. O., Pettengill, G. H., Phillips, R. J., Solomon, S. C., & Zwally, H. J. (2001). Mars Orbiter Laser Altimeter: Experiment summary after the first year of global mapping of Mars. *Journal of Geophysical Research: Planets*, *106*(E10), 23689–23722.

Smith, M., Craig, D., Herrmann, N., Mahoney, E., Krezel, J., McIntyre, N., & Goodliff, K. (2020). The artemis program: An overview of nasa's activities to return humans to the moon. *2020 IEEE Aerospace Conference*, 1–10.

Squyres, S. W., Arvidson, R., Bell, J., Brückner, J., Cabrol, N., Calvin, W., Carr, M., Christensen, P. R., Clark, B. C., Crumpler, L., des Marais, D., D'Uston, C., Economou, T., Farmer, J., Farrand, W., Folkner, W., Golombek, M., Gorevan, S., Grant, J., & Yen, A. (2004). The Spirit Rover's Athena Science Investigation at Gusev Crater, Mars. *Science (New York, N.Y.)*, *305*, 794–799. https://doi.org/10.1126/science.1100194

Squyres, S. W., Arvidson, R. E., Bell, J. F., Brückner, J., Cabrol, N. A., Calvin, W. M., Carr, M. H., Christensen, P. R., Clark, B. C., Crumpler, L. S., Marais, D. J. des, d'Uston, C., Economou, T., Farmer, J. D., Farrand, W. H., Folkner, W. M., Golombek, M. P., Gorevan, S., Grant, J. A., … Yen, A. S. (2004). The Opportunity Rover's Athena Science Investigation at Meridiani Planum, Mars. *Science*, *306*, 1698–1703.

Steele, A., Amundsen, H. E. F., Fogel, M., Benning, L., Schmitz, N., Conrad, P., Younse, P., & Backes, P. (2011). The Arctic Mars Analogue Svalbard Expedition (AMASE) 2010. *Lunar and Planetary Science Conference*, *1608*, 1588.

Stiny, G., & Gips, J. (1978). *Algorithmic aesthetics: computer models for criticism and design in the arts*. Univ of California Press.

Stooke, P. J. (Ed.). (2012). Chronological sequence of missions and events. In *The International Atlas of Mars Exploration: The First Five Decades: Volume 1: 1953 to 2003* (Vol. 1, pp. 1–324). Cambridge University Press. https://doi.org/DOI: undefined

Strauss, D. (1997). The Planet Mars: A History of Observation and Discovery by William Sheehan. *Isis*, *88*.

Strauss, S. (2004). Extravehicular mobility unit training suit symptom study report. *Johnson Space Center, Houston, TX*.

Stromgren, C., Burke, C., Cho, J., Rucker, M. A., & Garcia-Robles, M. (2020). Defining the Required Net Habitable Volume for Long-Duration Exploration Missions. In *ASCEND 2020* (p. 4032).

Sumini, V., & Mueller, C. (2017). Structural challenges for space architecture. *Structure Magazine*, 42–45.

Suzuki, S. (2020). *TOPOLOGY-DRIVEN FORM-FINDING*.

Swarmer, T. M., Anderson, L., & León, P. de. (2014). *Performance review of a pressurized inflatable lunar habitat integrated with an electric rover and pressurized analog planetary suits during an initial ten day simulation*.

Szalapaj, P. (2001). Parametric propagation of form. *Architecture Week*, *19*.

Szantai, A., Audouard, J., Forget, F., Olsen, K. S., Gondet, B., Millour, E., Madeleine, J.-B., Pottier, A., Langevin, Y., & Bibring, J.-P. (2021). Martian cloud climatology and life cycle extracted from Mars Express OMEGA spectral images. *Icarus*, *353*, 114101.

Tafforin, C. (2013). The Mars-500 crew in daily life activities: an ethological study. *Acta Astronautica*, *91*, 69–76.

Tanaka, K. L., Coles, K. S., & Christensen, P. R. (Eds.). (2019). Syrtis Major (MC-13). In *The Atlas of Mars: Mapping its Geography and Geology* (pp. 136–139). Cambridge University Press. https://doi.org/DOI: 10.1017/9781139567428.018

Tatarewicz, J. N. (2009). The "Vision for Space Exploration" of President George W. Bush, space science, and US space policy. *Futures*, *41*(8), 531–540.

The European Space Agency. (n.d.-a). *Mars500 Crew*. Retrieved January 7, 2022, from https://www.esa.int/Science_Exploration/Human_and_Robotic_Exploration/Mars500/Mars500_crew

The European Space Agency. (n.d.-b). *Mars500 Quick Facts*. Retrieved January 7, 2022, from https://www.esa.int/Science_Exploration/Human_and_Robotic_Exploration/Mars500/Mars500_quick_facts

The European Space Agency. (n.d.-c). *The isolation facility*. Retrieved January 7, 2022, from https://www.esa.int/Science_Exploration/Human_and_Robotic_Exploration/Mars500/The_isolation_facility

The European Space Agency. (2021). *Comparing Webb and Hubble*. https://www.esa.int/ESA_Multimedia/Images/2021/06/Comparing_Webb_and_Hubble

The European Space Agency. (2022). *WEBB*. https://www.esa.int/Science_Exploration/Space_Science/Webb

The Mars Society. (2017). *The Flashline Mars Arctic Research Station*. http://fmars.marssociety.org/about-the-fmars/

The Mars Society. (2022). *The Mars Desert Research Station*. http://mdrs.marssociety.org/

The Planeraty Society. (2021). *Every Mission to Mars, Ever*. https://www.planetary.org/space-missions/every-mars-mission

The Planetary Science Institute. (2021). *SWIM 2.0 Data Products and Results*. Subsurface Water Ice Mapping. https://swim.psi.edu/SWIM2Products.php

The Planetary Society. (2022). *Tianwen-1 and Zhurong, China's Mars orbiter and rover*. https://www.planetary.org/space-missions/tianwen-1

The U.S. Nuclear Regulatory Commission. (2011). *ML11229A721 - 0751 - H122 - Basic Health Physics - 32 - Shielding Radiation*. https://www.nrc.gov/docs/ML1122/ML11229A721.pdf

Theraulaz, G., & Bonabeau, E. (1995). Modelling the collective building of complex architectures in social insects with lattice swarms. *Journal of Theoretical Biology*, *177*(4), 381–400.

Tomkins, A. G., Genge, M. J., Tait, A. W., Alkemade, S. L., Langendam, A. D., Perry, P. P., & Wilson, S. A. (2019). High survivability of micrometeorites on Mars: sites with enhanced availability of limiting nutrients. *Journal of Geophysical Research: Planets*, *124*(7), 1802–1818.

Turner, F. J., & Verhoogen, J. (1960). Igneous and metamorphic rocks. *New York*.

UAE Space Agency. (2022). *Emirates Mars Mission*. https://www.emiratesmarsmission.ae/

USGS. (2022). *Earthquake Hazard Program*. https://earthquake.usgs.gov/learn/glossary/?term=G or g

Valle, G., Zipay, J., Litteken, D., Christiansen, E., & Jones, T. (2019). *System Integration Comparison Between Inflatable and Metallic Spacecraft Structures*. 1–14. https://doi.org/10.1109/AERO.2019.8742000

van Ellen, L. (2018). *Building on Mars - Master thesis*.

van Helden, A. (1994). Telescopes and authority from Galileo to Cassini. *Osiris*, *9*, 8–29.

Veritas, B. (2010). Ice characteristics and ice/structure interactions. *Guidance Note NI*, *565*.

von Braun, W., & White, H. J. (1953). *The Mars Project*. University of Illinois Press.

Wamelink, W. (2018). *The ideal settlement site on Mars - hotspots if you asked a crop*. Wageningen University & Research. https://www.wur.nl/en/newsarticle/The-ideal-settlement-site-on-Mars-hotspots-if-you-asked-a-crop.htm

Wan, L., Wendner, R., & Cusatis, G. (2016). A novel material for in situ construction on Mars: experiments and numerical simulations. *Construction and Building Materials*, *120*, 222–231. https://doi.org/https://doi.org/10.1016/j.conbuildmat.2016.05.046

Ward, B. (2013). *Dr. Space: The Life of Wernher von Braun*. Naval Institute Press.

Watters, T. R., Leuschen, C. J., Plaut, J. J., Picardi, G., Safaeinili, A., Clifford, S. M., Farrell, W. M., Ivanov, A. B., Phillips, R. J., & Stofan, E. R. (2006). MARSIS radar sounder evidence of buried basins in the northern lowlands of Mars. *Nature*, *444*(7121), 905–908.

Werkheiser, M. J., Dunn, J., Snyder, M. P., Edmunson, J., Cooper, K., & Johnston, M. M. (2014, August 4). 3D Printing In Zero-G ISS Technology Demonstration. *AIAA SPACE 2014 Conference and Exposition*. https://doi.org/10.2514/6.2014-4470

Whiting, Melanie; Abadie, L. (2019). *5 Hazards of Human Spaceflight*. National Aeronautics and Space Administration. https://www.nasa.gov/hrp/5-hazards-of-human-spaceflight

Wilkinson, S., Musil, J., Dierckx, J., Gallou, I., & de Kestelier, X. (2016). Concept design of an outpost for mars using autonomous additive swarm construction. *Acta Futura*, *10*, 121–129.

Williamson, M.-C., Hipkin, V., Lebeuf, M., & Berinstain, A. (2007). Exploration Architecture Validation Through Analog Missions-A Canadian Perspective. *LEAG Workshop on Enabling Exploration: The Lunar Outpost and Beyond*, *1371*, 3044.

Willson, D., Clarke, J. D. A., & Murphy, G. (2005). MARS-OZ: a design for a Simulated Mars Base in the Australian Outback. *Journal of the British Interplanetary Society*, *58*(9–10), 282–293.

Woodbury, R. (2010). *Elements of parametric design*. Taylor and Francis.

Woolford, B., & Mount, F. (2006). *Human Factors Lessons Learned on the International Space Station*.

Wordsworth, R. D. (2016). The Climate of Early Mars. *Annual Review of Earth and Planetary Sciences*, *44*(1), 381–408. https://doi.org/10.1146/annurev-earth-060115-012355

Wordsworth, R., Kerber, L., Pierrehumbert, R., Forget, F., & Head, J. (2015). Comparison of "warm and wet" and "cold and icy" scenarios for early Mars in a 3D climate model: Warm and Wet vs. Cold and Icy Early Mars. *Journal of Geophysical Research: Planets*, *120*. https://doi.org/10.1002/2015JE004787

Wu, Z., Li, T., Zhang, X., Li, J., & Cui, J. (2020). Dust tides and rapid meridional motions in the Martian atmosphere during major dust storms. *Nature Communications*, *11*(1), 1–10.

Xinhua. (2006, July 20). Roundup: China to develop deep space exploration in five years. *People's Daily Online*. http://en.people.cn/200607/20/eng20060720_284801.html

Yashar, M. (2022). *Mars X-House: Winner of NASA's Phase 3 3D-Printed Habitat Challenge in Final Design*. https://www.melodieyashar.com/marsxhouse/

Yashar, M., Ciardullo, C., Morris, M., Pailes-Friedman, R., Moses, R., & Case, D. (2019). *Mars X-House: Design Principles for an Autonomously 3D- Printed ISRU Surface Habitat*.

YEĞEN, E. C. E. (2019). *AN INQUIRY OF SPACE ARCHITECTURE: DESIGN CONSIDERATIONS AND DESIGN PROCESS*. MIDDLE EAST TECHNICAL UNIVERSITY.

Zeitlin, C., Hassler, D. M., Cucinotta, F. A., Ehresmann, B., Wimmer-Schweingruber, R. F., Brinza, D. E., Kang, S., Weigle, G., Böttcher, S., & Böhm, E. (2013). Measurements of energetic particle radiation in transit to Mars on the Mars Science Laboratory. *Science*, *340*(6136), 1080–1084.

Zelenkauskaite, A., Bessis, N., Sotiriadis, S., & Asimakopoulou, E. (2012). Interconnectedness of complex systems of internet of things through social network analysis for disaster management. *2012 Fourth International Conference on Intelligent Networking and Collaborative Systems*, 503–508.

Zhang, M. (2010). Social network analysis: History, concepts, and research. In *Handbook of social network technologies and applications* (pp. 3–21). Springer.

Zubrin, R., Baker, D., & Gwynne, O. (1991). Mars direct-a simple, robust, and cost effective architecture for the space exploration initiative. *29th Aerospace Sciences Meeting*, 329.

Zubrin, R. M., & Baker, D. A. (1992). Mars direct: Humans to the red planet by 1999. *Acta Astronautica*, *26*(12), 899–912.

Zubrin, R., & Weaver, D. (1993). Practical methods for near-term piloted Mars missions. *29th Joint Propulsion Conference and Exhibit*, 2089.

DOCTORAL THESIS

POLITECNICO
MILANO